# Intensity error sensing in the active control of free field sound radiation

Robert Koehler

Department of Mechanical Engineering

Adelaide University

South Australia 5005

Australia

*A thesis accepted in fulfillment of the requirements*

*for the degree of PhD in Mechanical Engineering*

*on the 28th of September 2001*

This page intentionally contains only this sentence.

# Abstract

The annoyance of low frequency tonal noise, such as from electrical transformers, has long since been recognised, with many examples of passive and active noise control being applied on transformers and other sources that radiate into a free space. Passive techniques have been found to be ineffective at low frequencies, requiring very heavy materials which are impractical due to maintenance and ventilation requirements as well as cost. Active noise control may be the answer to solving such noise problems. However, as yet very few practical active noise control implementations exist.

This thesis describes by theory and experiment, the effectiveness of an alternate error sensing strategy suitable for the control of general free field sound radiation problems, namely active intensity. While active intensity sensing is not new (Sommerfeldt and Nashif (1994), Swanson (1994), Reichard et al. (1995), Kang and Kim (1997), Qiu et al. (1998), Berry et al. (1999) and Li (2000)), simulations of their performance have led to mixed results. In this research, active intensity error sensing has been rigorously analysed:

1. in the near and far field of the disturbance source.
2. to determine its ability to lead to global control via sound power attenuation.
3. in a real control system.

The performance of active intensity error sensors were evaluated both analytically and experimentally in progressively more complex environments to identify their capabilities and limitations. It was found that active intensity error sensors would, in general, globally attenuate the noise by the same amount that would be achieved using traditional pressure error sensors. Active intensity sensors were found to outperform pressure sensors in a region behind the control source. When active intensity sensors were located between the primary disturbance and the control source the active intensity error criterion is no longer positive definite and global increases in sound levels are observed.

The results of this work could be applied to the active control of the fundamental frequency of transformer noise where the wavelength of the noise is large with respect to the physical dimensions of the transformer.

# Statement of originality

To the best of my knowledge, except where otherwise referenced and cited, everything that is presented in this thesis is my own original work and has not been presented previously for the award of any other degree or diploma in any University. I consent that this thesis be made available for loan and photocopying.

Robert Koehler.

This page intentionally contains only this sentence.

# Acknowledgments

This thesis would not exist without the help and invaluable support of a great many people. I would like to acknowledge the efforts of all of those people who have helped to shape this thesis. Many thanks to my parents Carmen and Joe Borowski and Willy Köhler, who encouraged me to work hard and pursue my mathematical and scientific interests from an early age, and made many sacrifices to ensure I received a good education.

I would like to thank Dr Scott D. Snyder for his outstanding supervision, endless advice and encouragement. Without his direction and guidance, this thesis would most likely never have been completed. The author would also like to thank Professor Colin H. Hansen and Dr Anthony C. Zander for their contributions and enlightening discussions. To Dr Colin D. Kestell, Dr Ben S. Cazzolato, Dr Carl Q. Howard, Dr Xiaojun Qiu and Dr Xun Li, for all of their discussions, advice and friendship. I am also grateful to Silvio De Ieso, Derek Franklin and George Osborne for all their help in operating and repairing the equipment and to Ron Jager and Anthony Sherry for helping to lug the transformer in and out of the anechoic chamber.

Finally I would like to express my gratitude to Nicole for her endless encouragement, support and patience in the preparation of this thesis.

This thesis is dedicated to the loving memory of my father Willy Köhler.

This page intentionally contains only this sentence.

# Contents

This page intentionally contains only this sentence.

# List of Figures

This page intentionally contains only this sentence.

# List of Tables

# Chapter 1

# Introduction

Free field sound radiation is a problem in many practical settings. For example, many common problems are related to excessive levels of noise in residential areas adjacent to industrial and commercial zones. While residents are usually far enough away from the noise source to not sustain any hearing damage, there is an inherent annoyance in exposure to this type of industrial noise (Bies and Hansen (1996)). Some free field noise problems are directly related to the health of employees such as in a noisy manufacturing environment. There are also maritime military problems, such as radiation from surface and submerged vessels.

While quantifying the potential for damage to hearing through exposure to noise levels is a very complicated subject unto itself, it has been shown in a number of studies that hearing loss is related to the type of noise, the exposure time and age (Beranek (1988)). It has even been shown to be related to race and sex (Royster et al. (1980)). Standards exist in almost every country today which set limits on the level of exposure and allowed exposure time (ISO-1999 (1990), AS2107 (1987), INCE (1987)).

Strict enforcement of noise emission control laws is becoming more common and as such, ignoring the health of employees, or the annoyance of local residents, can now cost commercial enterprises through litigation and fines. It is quite usual for no design consideration to have

been given to the noise emissions of machinery, including large scale electrical transformers installed in residential zones. As such, in situ noise control of these free field sources becomes necessary. High frequency noise (above 1kHz) may be satisfactorily addressed by passive means, the longer wavelengths associated with low frequencies, however, means that effective damping materials would have to be impractically large and massive. Passive noise control is therefore not commonly a practical solution for low frequency free field noise, where ventilation considerations may be a problem. Large downtimes for the installation of passive barriers and enclosures around the offending machinery is also unacceptable when the continued operation of the machinery is critical.

## 1.1 Historical background

The best engineering solution for particular low frequency noise problems may be "active noise control" (ANC), the introduction of a secondary "cancelling" sound field that leads to a reduction in overall levels. The concept is not new; in fact it is almost 70 years old. Many authors (Nelson and Elliott (1992), Ffowcs Williams (1984), Warnaka (1982), Guicking (1990)) give credit to the German physicist Paul Lueg, who filed a patent in 1933 (Lueg (1936)). However, work by de Heering (1993) and Guicking (1993) has produced evidence that a French researcher by the name Henri Coanda was the first to submit a patent application on the subject in 1932 (Coanda (1934)). While neither patented system was realisable at the time, both Coanda and Lueg clearly proposed the basis of ANC. Lueg in fact suggested that a transducer in the path of a noise source could be used to generate a secondary, canceling noise (Figure 1.1).

Electronics was in its relative infancy when Coanda and Lueg first published their patents on active noise control and little research was done in the 20 years that followed. Conover (1956), was the first researcher to actually apply active noise control to a free field noise source. In his experiments Conover manually adjusted the gain and phase of a signal fed to a control

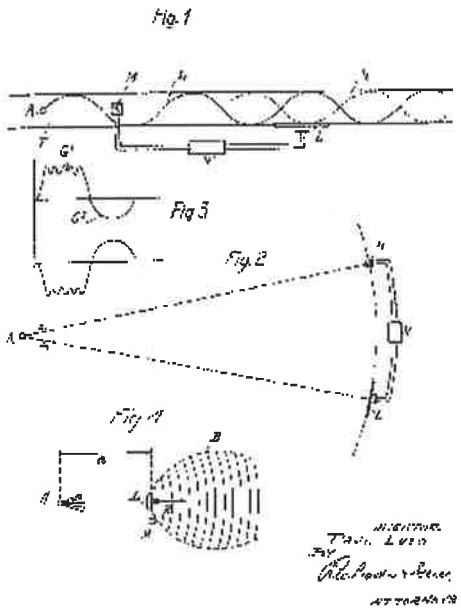


*Figure 1.1: Lueg's 1936 patent application.*

speaker located close to a transformer, and was able to demonstrate that significant far field sound attenuation at a single tone was achievable.

The next body of research into active noise control came from Olson and May (1953) see Figure 1.2, where a real feedback control system consisting of a single microphone and a single speaker being driven by an amplifier, whose input signal was adjusted so as to be 180° out of phase with the error signal from the microphone. Olson and May suggested possible uses for the device in the headrest of the seats in aircraft and automobiles. Olson (1956) published further applications including active headsets and even active vibration control of machinery. Some of these suggestions have been (or are close to being) commercially realised today.

Now a field of immense interest, active noise control is detailed comprehensively in a number of well known publications (Nelson and Elliott (1992), Tokhi and Leitch (1992), Fuller and Elliot (1996), Kuo and Morgan (1996) and Hansen and Snyder (1997)). There have also been many overviews published including Warnaka (1982), Ffowcs Williams (1984), Angevine (1995), Hansen (1997), Berkman and Bender (1997), Tokhi (1997), Kestell and Hansen (1998) and Elliott (1999).

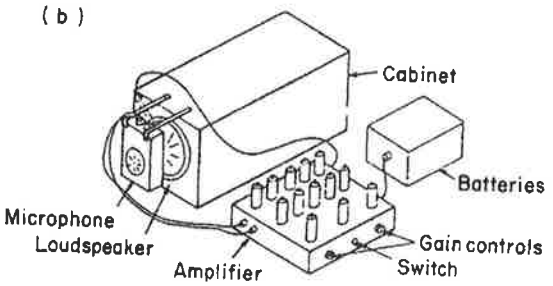


*(a) Olson's control setup*

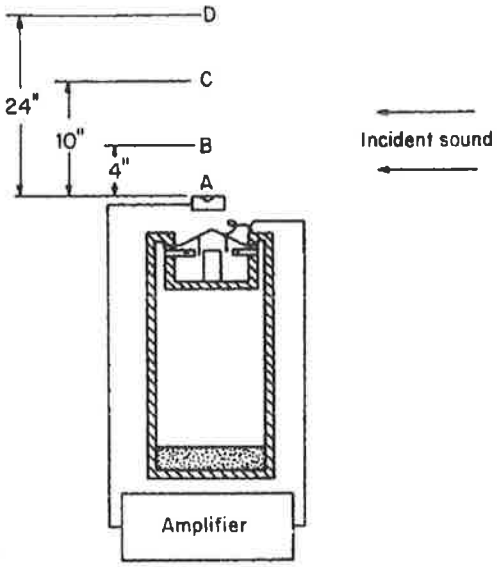


*(b) Section view of Olson's sound absorber*

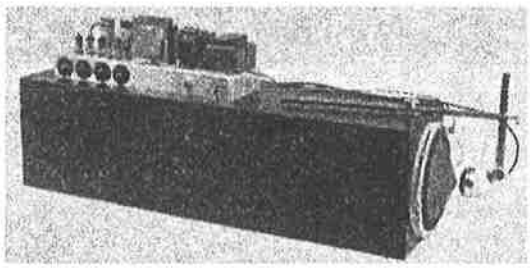

*(c) Olson's original sound absorber*

*Figure 1.2: Olson's original sound absorber design.*

## 1.2 Objective

Low frequency free field tonal sound radiation from vibrating structures, such as electrical transformers, is an ideal target for adaptive feedforward active noise control. The objective of this research is to design and evaluate a practical active noise control strategy for globally reducing the sound radiated from a vibrating structure. It will be shown that actively controlling the noise by employing an energy-based, acoustic intensity sensing strategy does not necessarily lead to better global results than traditional pressure sensing. As stated, reducing the noise globally is the objective and it is the hypothesis of this thesis that this can be satisfied, by a single control source separated from the primary source by less than a tenth of a wavelength, and a single near field pressure sensor. It is found that despite the direct relationship between the acoustic intensity and the acoustic power radiated by a source radiating uniformly in all directions, traditional pressure sensing can lead to as good as if not better global attenuation.

## 1.3 Scope

The practical implementation of ANC to the control of free field sound radiation combines many fields of acoustic research, all of which are considered in the following chapters. This thesis commences with a review of the most recent and relevant published literature, which addresses:

- active noise control of free field sound radiation using pressure error sensors,
- related work suggesting alternate sensing strategies,
- previous attempts at using active intensity error sensors,
- active control of vibration to attenuate sound,
- identification of gaps in current knowledge concerning intensity sensing.

The literature review identified active intensity error sensors to be a possibly better alternative to the use of traditional pressure error sensors. A simplistic monopole radiation problem was re-analysed and experimental results were acquired which validate previous theoretical work. The use of active intensity error sensors and their performance as compared to traditional pressure sensors was developed and tested using a number of simplistic models of increasing environmental complexity. Each model was then experimentally validated and the results discussed. Finally, the active intensity error sensors were evaluated on a small electrical transformer. Following the results and conclusions, a direction for future research is suggested.

# Chapter 2

# Literature review

## 2.1 Why do this research?

The work in this thesis is concerned with the active control of free field sound radiation. Free field sound radiation problems have been the target of many active noise control researchers in the past (Conover (1956), Angevine (1981), McLoughlin et al. (1994), ADTP (1997), Berry et al. (1999)), and will continue to be of interest in the foreseeable future. It is an area with significant potential for practical application, as well as being an area which still requires significant strides in methodology of approach before this potential can be realised.

Given the decades of past work, why should it be that the active control of free field sound radiation still requires much research before it is truly viable in practical application? There are several reasons, each related to the underlying physics associated with free space sound fields.

Free space sound fields are very complicated, and can span great distances. Further, many practical sound sources of interest are large as compared to the wavelength of sound. Consider the radiation of the 400Hz harmonic by a transformer with a typical dimension of 6 metres.

Of course, free space sound fields are not unique in this characteristic; consider even the low frequency interior sound field in a commercial airliner. However, what is particular to free space sound problems is the high degree of sound pressure amplitude decay over distance. This arises from the sound field being able to spread in an unbounded fashion as it travels away from the sound source.

To understand why this is such a problem, consider that for an active noise control system to be able to provide global sound attenuation, the controlling sound sources must be able to mimic the unwanted sound field amplitude with high fidelity, and simply invert phase. If this is the case, then the principle of superposition implies that the two sound fields will "cancel".

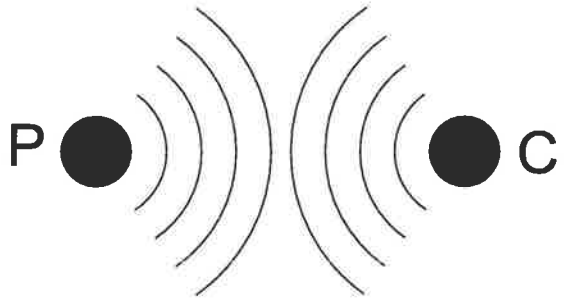


*Figure 2.1: Primary and control monopole sources in free space.*

An enclosed sound field is dominated not by the direct acoustic radiation from a source, but by the reverberant sound field which results from multiple reflections from the enclosure boundaries. Below the Schroeder frequency (Pierce (1989)), the sound field inside such an enclosure can be described in terms of the acoustic mode shapes of the enclosure. A control source placed anywhere within the enclosure is able to excite the modes to differing degrees. This is a resulting fundamental property from the reverberant nature of low modal density enclosed sound fields; a mode is excited through the reinforcement of certain reflected waves until a resonant condition is achieved. The bottom line result is that the control source can produce a high-fidelity copy of the primary source-excited sound field from a wide variety of locations in the enclosure. Consider now the case of two monopole sources in free space. Referring to Figure 2.1, the monopole source on the left is the primary source, and the one on the right is the control source. Here there are no boundaries for the sound field to reflect off, and hence there

is no reverberant field. The free sound field is defined by the direct sound field. To achieve appreciable total sound power attenuation in free space, say of the order of 10dB or more, the sources must be less than 1/10 wavelength apart (Nelson and Elliott (1986)). If a 100Hz tone were the aim of control, this would mean a separation distance of less than approximately 300mm. At a wavelength of $\lambda/2$, the expected sound power reduction is theoretically 0dB and hence active control with only one control sound source is not feasible.

Why is there such a dramatic difference between the enclosed and free space sound field results? Or, in terms of performance alone, why do the free space sound field results roll off so quickly? The answer lies in the fundamental physics: because of the spatial decay of the sound pressure in the free field, which diminishes at 6dB per doubling of the distance from the source, it quickly becomes impossible for a single control source to mimic the unwanted sound field with high fidelity as the separation distance increases. See Figure 2.2.

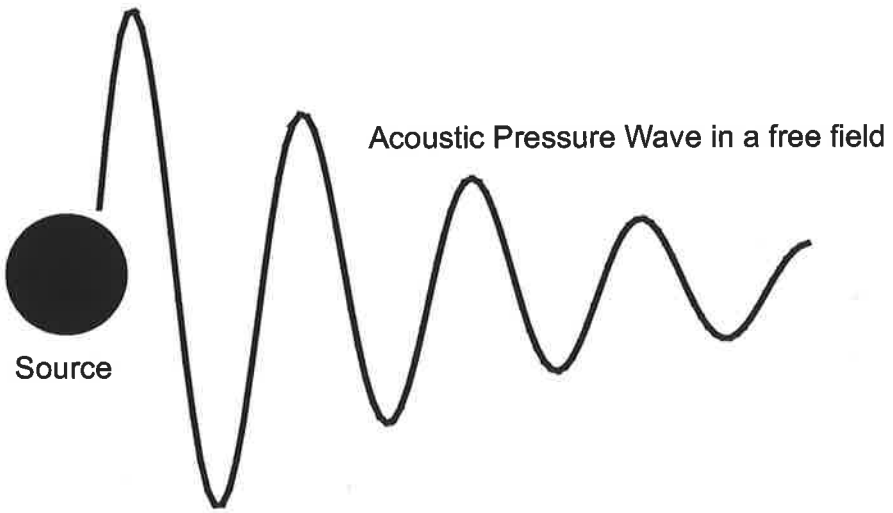


*Figure 2.2: Free space sound field decay at 6dB per doubling of the distance from the source.*

This result can be improved marginally through the addition of more sources, but only marginally (Thornton (1988), Nelson and Elliott (1992)). The same line of explanation applies to controlling free field radiation from "large" sound sources, such as transformers. A single control source can only attenuate sound radiated from the structure in its immediate vicinity. The implication is that large structures require large numbers of control sources.

Given the above description, it is straightforward to surmise that the many noise problems of practical interest will require a great many sound sources to solve. These controlling sound sources must completely surround the source of unwanted noise (Magiante and Vian (1977), Magiante (1977), Jessel (1979), Jessel and Angevine (1980)) and be numerous enough to be a good approximation of a continuous source. Applying this idea to the case of a large electrical transformer, it quickly becomes apparent that the required number of sources can be in the hundreds.

Where there are hundreds of sound sources, it can be assumed that there are hundreds of sensors (assuming that the control system has some feedback mechanism). There are many problems which quickly present themselves: how to process so many signals, where to place the sensors, what the sensors should be measuring, etc. It is the answer to these questions that is the topic of the work to be presented in this thesis.

## 2.2 The current situation

As mentioned, free space active control problems often involve very complicated sound fields, which can span great distances. The traditional approach to free space noise control, the erection of physical barriers, can be inhibitive, both in terms of cost and equipment and access. They can also be very inflexible to changes in the sound field/sound source.

Since Lord Rayleigh published his treatise on the theory of sound in the late 1870's (Rayleigh (1887)), acoustics has enjoyed a steady growth in research. Rayleigh's was the first modern scientific work on the theory of acoustics, and has since led to a greater understanding of sound, how it is produced and transmitted and its effect on humans. Today it is realised that sound is a double-edged sword, bringing enjoyment to some, such as through "music", and annoyance to others, who do not wish to hear it. A factory owner may enjoy hearing the noise of machines on the factory floor, as it means money is being made. However, the workers exposed to that

factory noise may feel entirely differently about the sound, and may even suffer permanent hearing loss. A great deal of research looking at how much sound exposure leads to hearing damage has been undertaken. Legislation has been imposed by various governmental bodies, restricting sounds of differing types to certain levels, thus limiting the potential to annoy and minimising the health risk. The field of noise control has been the spinoff of these activities.

The impetus for attenuating low frequency free space sound has arisen largely from a need to reduce the acoustic emission of many industrial components which are placed in close proximity to domestic dwellings, components such as transformers and industrial stacks. However, an understanding of the mechanisms involved in minimising the low frequency noise transmitted to a receiver by a free space noise source is of interest across a wide spectrum of problems.

Of particular relevance to the work to be presented here is acoustic radiation which is dominated by tonal components. Many practical noise sources are predominantly tonal or narrowband radiators, with industrial (rotating) machines providing the underlying excitation (fans, compressors, pumps and turbines, electric motors, generators and gearboxes are all examples of common rotating machinery). These devices are not necessarily poorly designed, or suffer a fault that causes sound to be radiated. Simply by their rotary nature they can induce periodic excitations which find their way into the acoustic media, usually air. How to stop this from happening, or at least how to stop the resulting acoustic wave from traveling to where it is unwanted, is the essence of free space noise control.

Put simply, passive control involves two potential approaches to solving the noise problem: put a wall between the receiver and the noise source, or else put a box over the source. In the first of these options, the installation of a wall or barrier, the aim is to re-direct the acoustic power flow away from whatever is behind the barrier. To be effective at this, the barrier must be constructed from a "heavy" material. Technically, this means the material must have a high surface density. The result of a high surface density is to reflect the acoustic energy away from the observer. Therefore, the sound field on the observer side of the barrier is due entirely to sound field diffraction over the top and around the sides of the barrier. The extent

of the sound pressure reduction at the observer is a function of the geometry and surface density of the barrier. Assuming that the barrier is of sufficient surface density, the height and width of the barrier determine the degree of attenuation achievable. While calculation of the exact attenuation levels on the observer side is complicated and will vary from installation to installation, a reasonable sized wall usually provides something of the order of 10dB of attenuation. Attenuation levels of 20dB or more are almost impossible with a simple barrier (Snyder (1999)).

The second method of building a box or an enclosure around a sound source, aims to provide global sound attenuation by reducing the flow of energy into the acoustic field. If the sound waves are trapped within the enclosure, then how does sound get out? The answer is through vibration. The sound field generated by the sound source shakes the boundary of the enclosure and the vibrating enclosure re-radiates to the acoustic field. The effectiveness of a particular enclosure at attenuating the sound level is determined by the mechanical impedance of the enclosure (which measures the resistance to vibratory excitation). Generally a mechanical structure is easier to shake at low frequencies than high frequencies. Hence in general, enclosures do a better job at providing attenuation at high frequencies than at low frequencies.

Active control has been researched as an alternative to passive techniques of attacking free space noise control problems. The density of the materials required in enclosures and barriers to make passive control work increases with decreasing frequency. So that at low frequencies, the weight, and cost of the bulky materials makes a passive approach inefficient. The components of an active noise control system, the sensors, actuators and electronics system often add relatively little weight to the target system. Active control also works best at low frequencies, making it an inviting solution to free space noise control problems.

Traditionally, acoustic pressure has been used as the physical variable measured by the "error sensor", which measures the residual sound field after active control has been applied. The main reason for using pressure error sensors is that they are cheap and easy to use. Some types of electret microphones cost as little as a few tens of cents and can measure sound pressure

to an acceptable level of accuracy. Although pressure error sensing is prevalent, the results achieved with them have been mixed (see for example Angevine (1981) and Zalas and Tichy (1984)). Research conducted by Angevine on the active control of tonal transformer noise in the laboratory demonstrated that global control is achievable (Angevine (1981)). Other research on the active control of aircraft cabin noise at propeller blade pass frequencies has shown that pressure sensing leads to localised control (Zalas and Tichy (1984)). It has been suggested that sensing some measure of the total radiated sound power (Deffayet and Nelson (1988), Cunefare and Koopmann (1991a), Cunefare and Koopmann (1991b)) might lead to global control. In the active control of enclosed sound fields, Sun et al. (1998) derived a theoretical criterion for a sensing system to achieve global control in terms of structural modes. In the control of free space tonal noise, active acoustic intensity measured at a point is a measure of the sound power radiated through an elemental area. If the sound field is relatively uniform, then the active intensity measured at a single point is to a good approximation a measure of the sound power. The notion is that by implementing intensity-based sensors, it may be possible to improve the performance of systems actively controlling free space tonal noise. The work presented here will analyse the performance of active intensity sensors, and compare it to results obtained using traditional pressure sensors.

## 2.3 ANC systems

### 2.3.1 What does an active noise control system consist of?

Active noise control is, in general, an electronically facilitated manipulation of an acoustical environment through the use of transducers. It can be separated into two parts: the physical control system, which consists of the acoustical environment and the transducers which couple it to the electronics, and the electronic control system. See Figure 2.3.

There are two common control arrangements used in active noise control system implementa-

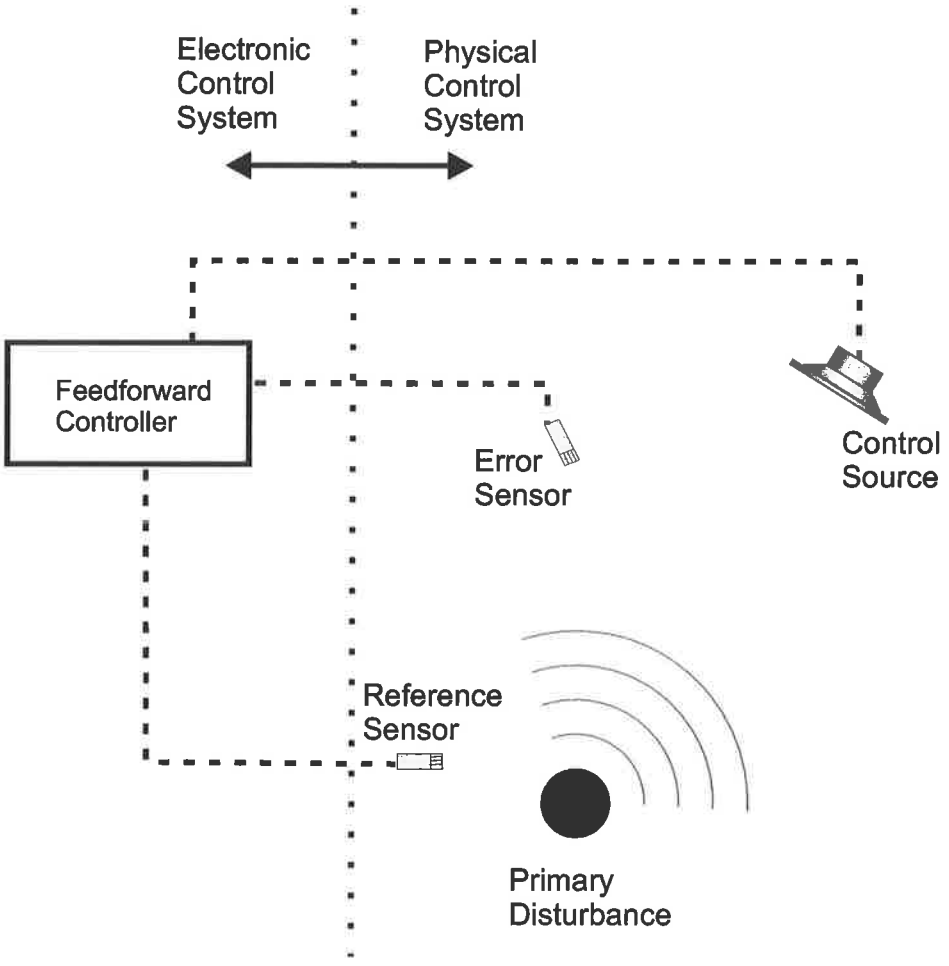


*Figure 2.3: Feedforward control system is comprised of two parts, the "physical" control system (actuators and sensors) and the "electronic" control system.*

tion; feedforward and feedback. It is also possible to combine these.

The basic differences between the two approaches are well-known in the control community. Referring to Figure 2.4, a feedforward system requires some *a priori* measurement of an impending disturbance, and then manipulates the physical environment to alter the response of the system to the input (usually through insertion of a transmission zero in the response). A feedback system alters the dynamic response of the system *in general*, by altering pole locations. In the active control of tonal noise, feedforward control is the most common (Elliott and Nelson (1993)). Feedforward control systems use a "reference signal", correlated with the primary noise source, filtering the signal to drive the actuators at an amplitude and phase appropriate for attenuating the system response to the input. Feedforward active control systems are often made adaptive, where the filter characteristics are adjusted on-line to achieve optimality in some specified sense; commonly, minimisation of the mean square value of the error signal measurements is what is desired. For most of the adaptive algorithms, the reference signal must be linearly correlated with the error signal for this type of control system to work. A reference signal can usually be extracted from tonal noise sources, such as by indirectly sensing some quantity such as revolutions per minute if the source is a rotating machine. Alternatively, if no access to the physical source of the disturbance is available, then directly measuring the sound pressure field close to the source, or vibration distribution on the source, may be sufficient. These direct reference signals can then be filtered to extract the tonal components of interest.

As mentioned, the majority of practical feedforward active control systems use an algorithm to optimise the control characteristics via changing the filter weights used to derive the control signal from the reference signal. The algorithm often calculates the current filter weights based upon previous values and the results of a search scheme which aims to minimise the mean square value of the error signal. The particular search scheme employed is usually a gradient based, steepest descent scheme (Widrow and Stearns (1985)), meaning that the algorithm uses the gradient of the error to determine the next set of filter weights to arrive at the minimum in

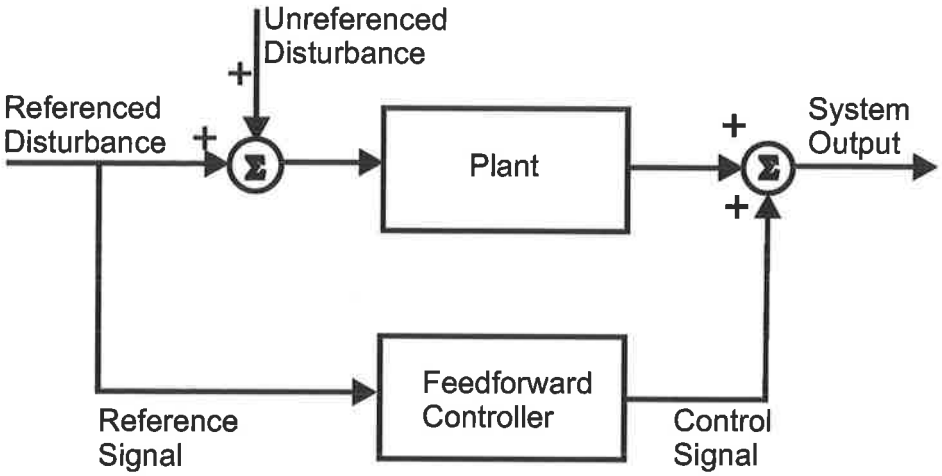


*Figure 2.4: Basic feedforward control system arrangement.*

the least number of iterations. The selection of algorithm and algorithm parameters influences the convergence rate and stability of the system (Haykin (1986)). The most common search algorithm is a variant of the least mean squared (LMS) algorithm (Widrow and Stearns (1985), Haykin (1986)). The LMS algorithm uses the least mean squared error as an estimate of the actual error, and hence develops a simple expression for the gradient.

Figure 2.5 shows the signal flow in a typical feedforward active noise control system. A reference sensor, which feeds off the primary acoustic disturbance, is fed through a control filter and sent to a control source. The weights of the control filter are adjusted by an LMS algorithm. The algorithm calculates the new weights from the old weights plus the product of the error signal and a filtered reference (filtered though a cancellation path transfer function CPTF) signal. The cancellation path transfer function model is required to account for the presence of a transfer function between the control output, via the control source and error signal inputs via the error sensor.

In the active control of sound in free space, there are two basic actuator or control transducer options. One is sound sources, such as speakers or horns to induce a controlling acoustic field. The other is vibration actuation, such as via shakers or piezoceramic exciters to directly modify the vibration distribution which creates the acoustic field. The focus of the research

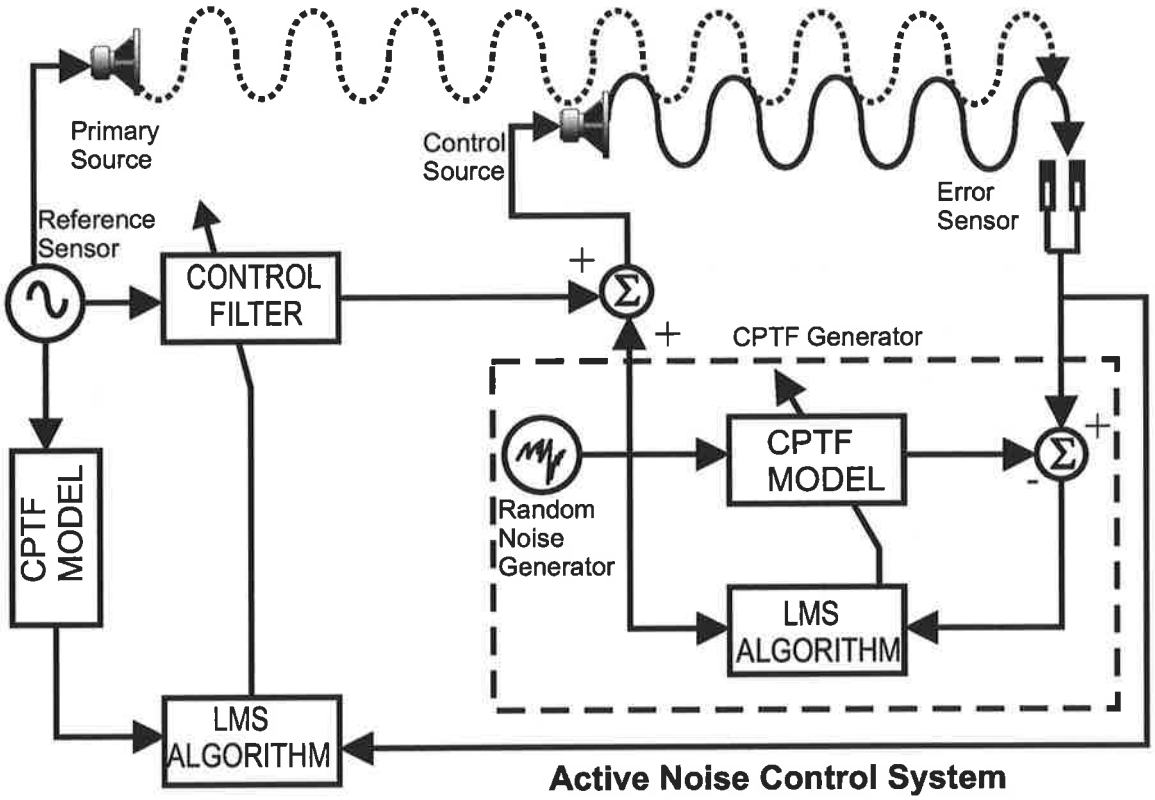


*Figure 2.5: Block diagram of a general active noise control system employing a filtered-X LMS algorithm.*

presented here is principally acoustic control of the primary noise, where the actuators used to propagate the control signals are speakers. However, vibration control sources will also be tested on more complicated primary noise generating structures.

There are two sensing requirements in a feedforward control system, reference signal sensing and error sensing. The reference sensing system will not be considered here. The sensing system used to produce the error signal, the difference between the measured primary sound field and the measured control sound field, is what is of interest in the work presented here.

### 2.3.2 Performance of an ANC system

There are four critical success factors in the implementation of an active noise control system (Hansen et al. (1999), Snyder (1999)). To design an optimal active noise control system, these four points need to be addressed in the given hierarchical order of importance. Figure 2.6 shows the hierarchy of critical success factors.

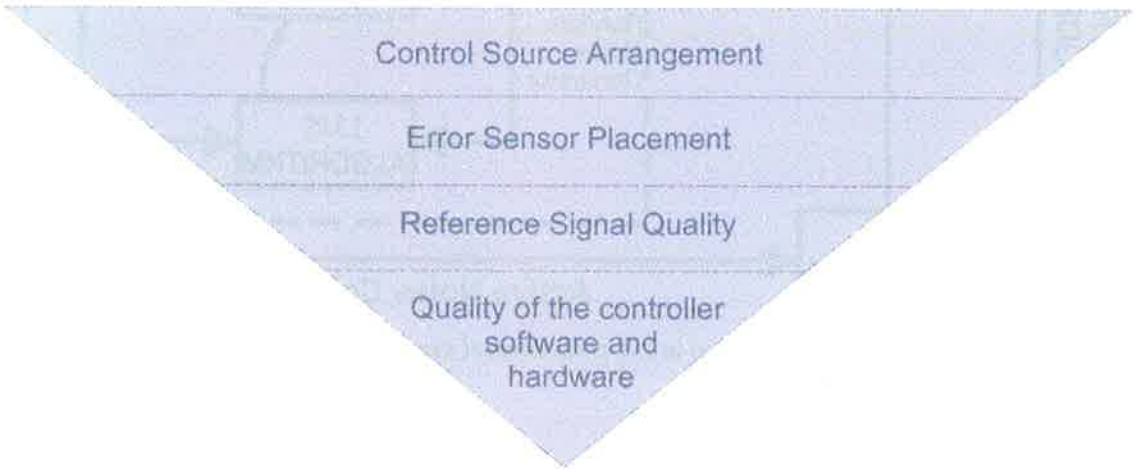


*Figure 2.6: The hierarchy of factors that affect the performance of an active noise control system.*

Given any primary disturbance, it is possible to calculate the maximum achievable acoustic power attenuation given a set of control source locations (Hansen and Snyder (1997)). Hence the control source arrangement sets an upper limit on how much global sound attenuation can be achieved. Nelson and Elliott (1986), have shown that with control of a monopole primary

sound field by a single monopole control source, the maximum power attenuation is a function of the distance separating the sources.

Error sensor placement and sensing strategy determine how close to the upper limit on global sound attenuation (set by the control source arrangement) the given system can come. The control source arrangement is optimally dictated by the maximum power attenuation, which occurs when the total sound power is minimised. Unfortunately, sensing *power* is not usually practical, and therefore it is necessary to use other sensing methods to approximate sound power. It is this approximation that limits the sound attenuation with a particular sensing strategy. Of particular relevance to the work presented here is a comparison of the results obtained with pressure error sensing to that achievable with an intensity-based error sensing strategy.

The coherence between the reference signal and the error signal, which is inherently the coherence between the cancelling sound field and the unwanted sound field, sets a limit upon the performance of the "electronic" part of the control system. The coherence must be very high for high levels of sound cancellation to be achieved. If there were perfect correlation between the error signal and the reference signal, then sound cancellation would be possible up to the limit set by the error sensor type and placement. Deviations from this ideal limit the performance (Ross (1982)).

The quality of the electronic control system finally determines how much cancellation at the error sensors actually occurs, given the constraints placed by the signal coherence, sensor type, placement and control source location (Snyder et al. (2001)). Of issue here is the dynamic range of the controller and the word size if it is digital signal processor (DSP). Other controller properties which influence the performance of the control system include the sample rate of the analogue to digital and digital to analogue converters and the processor speed of the DSP, which determine the time delay associated with processing the transducer signals. The algorithm mentioned previously, is also of importance. The LMS algorithm as mentioned has specific properties such as rate of convergence which influences the time delay of the con-

troller as a whole and stability which determines whether the controller can adapt to changes in the physical conditions, such as temperature and wind.

The work presented here, in the overall context above, is concerned with the analysis of two error sensing strategies whose optimal implementation may lead to global control of tonal free field sound fields.

## 2.4 Error sensors

The error sensor is used to measure some physical variable which acts as a performance measure of the active control system. The objective of the control system is to minimise this performance measure. The choice of variable, such as pressure or vibration, determines to what extent the unwanted disturbance is measured and altered. The number of sensors employed and their location also influences the degree of attenuation.

Traditionally, free space active control systems use pressure sensors that are in the acoustic far field. This reflects the goal of these active control systems to reduce the far field sound radiation from a source. Due to the fundamental physics of the system, measurements provided by far field pressure sensors often suffer from long acoustic delays and poor signal to noise ratios (Qiu et al. (1998)). Placement of pressure sensors in the near field has been less common than far field placement, primarily due to concerns of having the measurement dominated by the evanescent component of the sound field; reducing the evanescent component may not have an impact upon the far field result. For the idealised case of monopole primary and control sources, the power attenuation accompanying the minimisation of the acoustic pressure at a single (error) point in space varies from a maximum level of $\Delta W$, achieved when attenuating pressure at any point on a line roughly centred between the sources (biased towards the control source) to zero power attenuation, or even increased total power when the pressure is minimised at a point very close to either of the sources (Hansen and Snyder (1997)).

It is of interest to analyse other error sensor types and to ascertain whether they can improve upon the performance currently possible with the use of pressure error sensors. Of particular interest here is previous research on acoustic pressure sensing and other energy based sensing strategies such as active intensity in the active control of free field sound. There are two reasons for this. Firstly, intuitively, acoustic intensity is directly related to sound power and so minimisation of intensity may offer some performance advantages. Secondly, active intensity can be measured in the near field of a sound source. This may offer some system stability and noise advantages.

## 2.5 Pressure error sensors

### 2.5.1 Single pressure sensors

#### 2.5.1.1 Active suppression of free field monopole radiation

Work by Nelson and Elliott (1992) has confirmed the intuitive result, that it is possible to completely cancel the pressure at any point in a monopole source-excited free field by means of active control using an additional monopole source. The work also demonstrated that acoustic pressure minimisation at a point will not necessarily produce the desired by-product of global sound attenuation. Although the sound pressure at the sensor location could be made zero, the sound pressure at other locations can actually increase. It is important to note that it is not *physically* impossible to achieve global sound attenuation with the given primary/control source arrangement. It is simply the inappropriate selection of the error sensing strategy or location which leads to sub-optimal performance.

#### 2.5.1.2 Active suppression of free field structural radiation

One of the first attempts at free field active noise control was made by Conover in 1956 (Conover (1956)). His work presented the results of a manual active control attempt on an in situ transformer. Conover used a single speaker, relatively close to the transformer, and a far field error sensor to control a number of harmonics of the 60Hz fundamental frequency and in particular the 120Hz transformer noise tone. He manually adjusted the gain and phase of the control signal to the speaker until he achieved the maximum pressure reduction his equipment allowed for at the desired frequency. The results indicated a reduction in the far field sound pressure of up to 10dB.

Some practical testing was done by Kido and Onoda (1972), on an in-service power transformer. They tested 1, 2 and 3 far field pressure sensors and control speakers to control a 100Hz tone. The control speakers were located on the transformer. For the single pressure sensor and single control speaker arrangement the attenuation varied, with some locations being as high as 20dB. However, in other locations the sound field actually increased by 10dB.

This work was extended to multiple control sources by Hesselmann (1978). Hesselmann also tested a transformer, but in an anechoic chamber with a rigid floor. In order to improve the signal to noise ratio, the transformer was fed with a slightly higher (20%) than normal input voltage of 480 Volts, which increased the sound pressure level. The results indicated that 10 to 20dB of sound pressure reduction (in all directions) on one side of the transformer is possible when attempting to attenuate a 100Hz tone. Two control speakers were positioned on the transformer tank to form a longitudinal quadrupole in conjunction with the primary noise source (which is a poor radiator at low frequencies). The control signals were manually tuned to be directly out of phase with the primary sound field. The sound pressure level was measured radially up to 8 metres from the transformer tank. The results showed that in the near field (less than a half a wavelength) the sound pressure actually increases over that of the primary tone only. However at distances further than half the wavelength the sound pressure

is attenuated up to 30dB.

At around the same time, Ross (1978) attempted to simultaneously control three tones at 100, 200 and 300Hz respectively, using Conover's setup of a single pressure sensor and control source to attenuate the noise from two adjacent transformers. The control speaker was positioned directly in front of the transformers and the pressure sensor was placed in an office building approximately 20 metres away. The far field noise at 100Hz was globally reduced by at least 10dB, and at particular locations inside the room, by up to 20dB. It was found that the higher frequency tones could only be locally controlled. The method of initiating control was again manual. The three tones were first extracted via band-pass filters, then three variable gain and phase shifters were manually adjusted on each filtered signal and then the results were recombined and fed to the control source.

More recently Berge et al. (1987) tested a free field active control system on a transformer, paying particular attention to how it performs under changing environmental conditions and across a 40°arc. The control was achieved using a feedforward control system. A single pressure error sensor which was 36 metres from a single control source was used to control 100 and 200Hz tones. The control source was again placed very close to the transformer. In this work, the control system was tested at different times of the day. The results showed great variability, clearly demonstrating the localised control phenomenon. The author was at a loss to explain the unimpressive results.

More recently again Pan et al. (1992) (see Figure 2.7) investigated the active control of particular structural modes which were radiating sound from a rectangular plate in an infinite baffle. They used a single far field pressure error sensor and a single acoustic control source located at approximately a hundredth of a wavelength ($\frac{2\lambda}{100}$) from the plate. The sound radiating structural mode attenuated was the (2,2) mode at 338Hz, and they showed that global attenuation was possible on average by 10dB.

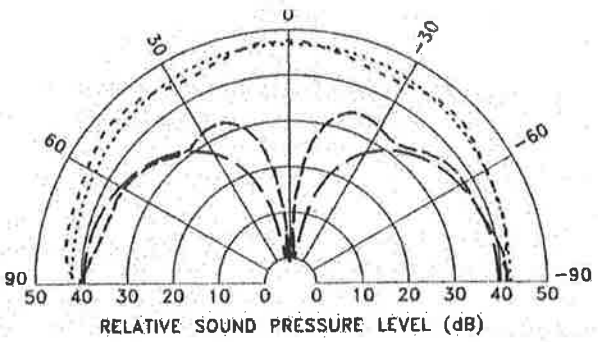


*(a) Acoustic control*

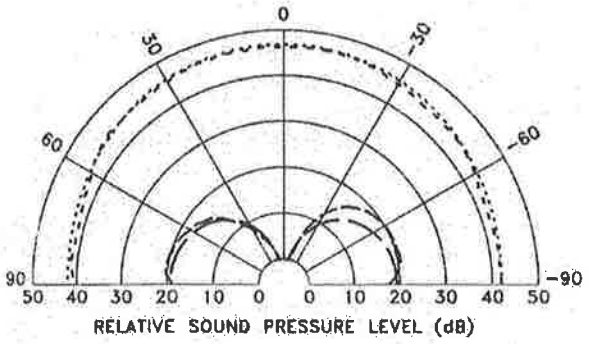


*(b) Vibration control*

*Figure 2.7: Acoustic and vibration control of a simply supported rectangular steel plate excited at the plate centre at 338Hz. acoustic monopole source separation distance $2\lambda/100$ and vibration control source location $(x,z) = (0,-70)mm$. after Pan et al. (1992).*

## 2.5.2 Multiple pressure sensors

### 2.5.2.1 Active suppression of free field monopole radiation

The work of Nelson and Elliott (Eghtesadi and Leventhall (1982), Nelson and Elliott (1986), Nelson et al. (1987c), Nelson and Elliott (1992)), has demonstrated that for a single monopole primary and monopole control source, there is a global optimum for the minimisation of the total source power output. If a sensor existed that could exactly measure the total sound power from the sources, then this global optimal control could theoretically be achieved. The sound power could be measured by an infinite (practically a large) number of far field pressure sensors. The problem with this lies in practical problems dealing with large number of sensor systems. Nelson and Elliott demonstrated the extent of far field control achievable with multiple pressure sensors at various source separation distances for a single monopole primary controlled by a single monopole control source. With a maximum of 4 far field pressure sensors at $\lambda/8$ separation distance, the maximum achievable power attenuation was 7.2dB, and when minimising the sum of the 4 far field pressure measurements, the power attenuation was 6.5dB. Further work by Thornton (Thornton (1988)), suggests that negligible further reductions in power output were produced by increasing the number of sensors from 4 to 20.

Elliott et al. (1991), analysed multiple free field monopole primary and control sources, when the primary array is all in-phase and the total power output is minimised, the power output of all the secondary sources are found to be exactly zero. If the power absorption of the secondary source array is maximised, the net power output of the primary source array can either be reduced or increased. Snyder and Tanaka (1993b) extended this analysis to a baffled monopole, and a duct and showed that under optimal conditions the power output of the control sources is zero.

Martin and Roure (1998) attempted to globally attenuate tonal noise radiated by a dipole primary source. They employed two groups of 3 loudspeakers, located 1 metre on either side of the primary dipole. A genetic algorithm was used to select the best 7 error sensor locations

from a total of 210 considered. For the 100Hz tone, 15.6dB of global attenuation was predicted numerically and 11.3dB was achieved in practice. At the 200Hz tone, the global attenuation predicted numerically (16.2dB) more closely matched that achieved in practice (16.6dB) and at 300Hz, the global attenuation numerically predicted is 10.4dB and experimentally it was 10.1dB.

#### 2.5.2.2 Active suppression of free field structural radiation

Work by Magiante and Jessel (Magiante and Vian (1977), Magiante (1977), Jessel and Angevine (1980), Jessel (1979)), showed that global attenuation of a primary noise source of any shape and size and emitting any noise spectrum is possible if a control field can be induced on a continuous surface enclosing the primary source. This means that the sound field would be completely cancelled and quiet for any observer outside the surface. To achieve Magiante and Jessel's global control, infinitely many discrete sources would be needed to generate the continuous surface mentioned above. Magiante performed some computer simulations (Magiante (1977)) and studied single and cardioid acoustic control sources. He concluded that attenuation improves as the number of control sources increases, the attenuation decreases as the frequency increases. He stated that if a "sufficient" number of sources are employed, then significant attenuation is possible, everywhere in the far field.

In the early 1980's Angevine (Jessel and Angevine (1980), Angevine (1981)), undertook experiments with a model of a transformer in an anechoic chamber. The frequencies investigated were 125, 250 and 500Hz. 26 speaker pairs were fixed to the ends of a small cylinder, acting as the control sources, in what the author termed a tripole arrangement. The separation distance of all the tripoles to the model transformer was 0.5 metres, which for the three frequencies is $2\lambda/10$, $4\lambda/10$ and $7\lambda/10$. Each tripole had a dedicated pressure sensor positioned at 0.5 metres from the tripole, and 1 metre away from the model transformer. The 125Hz tone (separation distance $2\lambda/10$) was attenuated by up to 16dB globally, and with 8dB attenuation at 250Hz (separation distance $4\lambda/10$). Another intuitive result confirmed in this work was that as

the number of tripoles employed increased, the amount of global attenuation increased. This confirms the theory put forward by Magiante and Jessel.

As mentioned previously work by Kido and Onoda (1972) (see Figure 2.8) also tested multiple far field pressure sensors. This latter research was conducted on an in-service electrical transformer, with up to 3 control speakers located on the transformer tank and 3 error microphones located close together in the far field. This sensor arrangement with multiple error microphones compactly located yielded a larger region of attenuation than was had with just a single error microphone.

Kempton (1976), was the first to publish the need for control sources to be located very close to the primary disturbance, in order that the interference field does not get too complicated with intermixed regions of attenuation and amplification. He proposed that a limited number of low order multipoles from an expansion of the primary sound field, located close to the primary sound source, could cancel the sound field in the far field. Work by Williams (1983) showed that the decomposition of acoustic radiation of complex structures in terms of a series expansion is possible. Koopmann et al. (1989), Song et al. (1991b), Song et al. (1991a), Qiu et al. (1999) showed that equivalent multipole sources could be obtained by a superposition method of reconstructing complicated sound fields. Martin and Roure (1997) applied this principle by optimising the control source locations using a spherical harmonic expansion of the primary field. Following up this work Martin and Roure (1998) analysed error sensor locations. In this work, 210 error sensor locations were analysed located on the tip of a hemisphere 3 metres in radius, with a genetic algorithm used to select the 10 best sensor locations. Using 8 speakers arranged around a 20kV transformer in an anechoic chamber and the 10 error sensors, tones up to 200Hz were globally attenuated by up to 11dB.

Bolton et al. (1995) investigated multipole acoustic control sources and reported mixed results. Lower order multipoles could give rise to better sound power attenuation than higher order ones. These results were confirmed experimentally by Beauvilain et al. (2000). Qiu and Hansen (2000) reported on the basis of simulations that multipoles would not appreciably

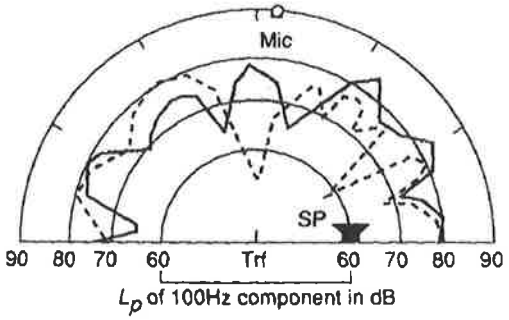


*(a) 1 far-field error microphone, 1 collocated control source*

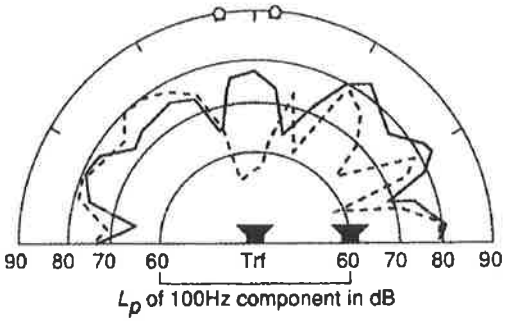


*(b) 2 far-field error microphones, 2 collocated control sources*

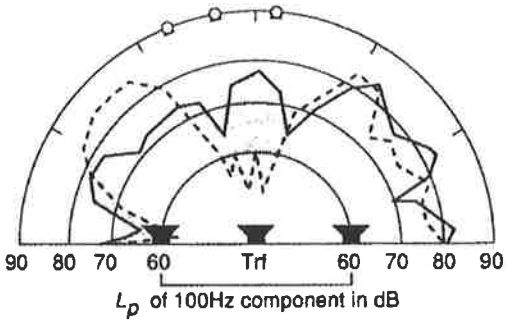


*(c) 3 far-field error microphones, 3 collocated control sources*

*Figure 2.8: Results of control of 100Hz tone from an in-service transformer, after Kido and Onoda (1972).*

improve the performance of active noise control systems deploying these as acoustic control sources.

An analysis of the sound power attenuation has been done by Nelson and Elliott (1986) and Nelson et al. (1987c). Hansen and Snyder (1997) furthered this work, looking at the performance of pressure sensors in minimising the sound power. The results of these analyses on monopole radiation showed that pressure sensors could indeed produce noticeable power reductions at small source separation distances ($d < \frac{\lambda}{10}$), when located optimally. The optimal sensor location is between the primary and control sources and in the far field. As mentioned previously in Section 2.4 the pressure sensor location that generated the greatest power attenuation, was found to be between the primary and secondary monopole sources. It was situated just off centre nearer the secondary source side. If, however, the sensor is suboptimally located, then the results can be very different. If the sensor is placed directly in front of the primary source, the resultant power attenuation is negligible. Also when positioned directly adjacent to the secondary source the power attenuation is almost zero. It should be noted that these works considered only monopole sources and hence near field effects were not present.

### 2.5.3 Conclusions

It can be summarised that when employing traditional pressure error sensors, the results can be mixed. Increasing number of sensors does not necessarily lead to global attenuation. The efficiency of an active noise control system is restricted by the control source type selection and placement. Sensor placement is clearly crucial to a successful active noise control system design.

## 2.6 Related work suggesting other sensing strategies

In an effort to improve active noise control system performance, a range of alternative error sensing strategies have been put forward in recent years. There has been a transition from pressure sensed error criteria to energy-based criteria, such as energy density in the active control of enclosed sound fields (Sommerfeldt and Nashif (1991), Sommerfeldt and Nashif (1992), Nashif and Sommerfeldt (1992), Sommerfeldt and Nashif (1994), Sommerfeldt and Parkins (1994), Sommerfeldt et al. (1995), Park and Sommerfeldt (1996), Park and Sommerfeldt (1997),Parkins et al. (2000b), Clark (1995)). In an enclosed field the notion is that by minimising the acoustic energy rather than just the pressure at a point, there is a better chance of achieving optimal levels of global disturbance attenuation. Similarly, in free field sound radiation, sensing strategies such as modal filtering by shaped sensors, or active intensity sensing, aim to produce an accurate measure of the sound power whilst minimising the number of sensors. This is supported by the work of Deffayet and Nelson (1988) in free space control of far field radiation from a simply supported rectangular plate.

Cunefare and Koopmann (1991b), Cunefare and Koopmann (1991a) simulated minimising the sound power from 3D structures based on a Helmholtz integral equation approach, using acoustic control sources, and found that optimal control (sound power attenuation) does not guarantee global pressure attenuation. The result extends what is known about the power attenuation and global control of monopole radiators (Nelson and Elliott (1986)). Giordano (1993) undertook experiments on a 3D box sound source, attempting to validate the approach described in Cunefare and Koopmann (1991b) and Cunefare and Koopmann (1991a). The box had 4 speakers embedded into its top and was excited at the resonance of one of its sides (1,1) structural mode by an internal electrodynamic shaker. By the Helmholtz integral technique the control strengths to be applied to those speakers were calculated in an iterative process until the values agreed with numerical simulations. The sound power was then numerically minimised and it resulted in a 10dB reduction in the sound power, with far field pressure attenuation ranging from 8dB to 19dB. In the work of Giordano (1993), no mention is made of any areas

in which the pressure increased.

## 2.7 Enclosed sound fields

A great deal of research effort has been directed at the active control of enclosed sound fields, driven largely by the need for lightweight control of low frequency sound in aircraft cabins. One of the early experiments was undertaken by Zalas and Tichy (1984) who described the zone of control when using pressure sensors inside an aircraft cabin to be the size of a grape fruit. Returning to more fundamental geometries Bullmore et al. (1987), Elliott et al. (1987), Elliott and Nelson (1987), Elliott et al. (1988), Nelson et al. (1987a,b), Snyder and Hansen (1994a), Snyder and Hansen (1994b), Doelman (1989) investigated simple enclosed sound fields, with a number of acoustic control sources and a number of error sensors measuring pressure and potential energy. It was found that when pressure sensors were placed at some locations inside the enclosures, such as where acoustic modes have zero pressure, performance was poor. Sound attenuation improved spatially by implementing a potential energy sensing strategy. An energy based sensing strategy does not suffer from the acoustic modal null points which a pressure sensing strategy has. Curtis et al. (1990) concluded that in enclosed fields, an energy sensing strategy is better.

Returning to enclosures of a complex geometry, Bullmore et al. (1990), Elliott et al. (1989, 1990), Pope (1990a,b), Pope et al. (1983, 1987a,b), Svensson and Wilberg (1998), Zalas and Tichy (1984), Eatwell (1990), Dorling et al. (1989) have all investigated the problem of sound attenuation in an aircraft cabin, using active and passive techniques. Work has also been done on automotive cabins by Kinoshite and Aoki (1993) and others. This practical research on vehicle cabins has run into the local control problems first discovered by Zalas and Tichy (1984); see Bullmore et al. (1987), Elliott et al. (1987), Elliott and Nelson (1987), Elliott et al. (1988), Nelson et al. (1987b), Nelson et al. (1987a). To exploit this localised control problem, researchers have developed active headsets where local control is quite an acceptable option.

These were first proposed by Olson and May (1953), Olson (1956) and are now a commercial reality (Sallowayetal and Millar (1996), Johanson and Winberg (1997)). Standard passive ear mufflers provide on the order of 20dB of attenuation, and active headsets can improve upon this in the low frequency range by another 10dB (Johanson and Winberg (1997)). In a similar vein, research on virtual sensing strategies (Garcia-Bonito et al. (1997), Garcia-Bonito and Elliott (1995a,b), Kestell (2000), Kestell and Hansen (1998), Kestell et al. (2000)) relies on improving the zone of control near the ear by predicting and cancelling the sound pressure at the ear with a control system installed in the headrest of a vehicle, as first described by Olson and May (1953), Olson (1956). It has been found that virtual sensors, employing greater than 2 pressure microphones, improve the region over which sound attenuation is achieved in enclosed sound fields (Garcia-Bonito et al. (1997), Garcia-Bonito and Elliott (1995a,b), Kestell (2000), Kestell and Hansen (1998), Kestell et al. (2000)). They also enjoy other benefits over headsets, such as improved hygiene and less risk of attenuating warning signals which are crucial to the passengers (Kestell (2000)).

The problem of *airborne* noise transmission into an enclosure such as an aircraft or automobile cabin and its active control by structural sensing has also been recognised (Snyder and Tanaka (1993a), Cazzolato and Hansen (1998), Cazzolato (1999b)). Snyder and Tanaka (1993a) examined a coupled enclosure and shaped sensors to sense an orthogonal group of structural modes that contribute to a potential energy error signal, based on the structural modes. It was found that only a few eigenvectors of the potential energy performance measure need to be measured by shaped sensors in order to achieve near optimal control. Cazzolato and Hansen (1998), Cazzolato (1999b) investigated minimising acoustic potential energy by minimising the "radiation modes", which are orthogonal with respect to the global potential energy in the active control of sound transmission into an enclosure by structural sensing. Good attenuation was reported for relatively few sensors.

Sommerfeldt and Nashif (1991), Sommerfeldt and Nashif (1992), Nashif and Sommerfeldt (1992), Sommerfeldt and Nashif (1994), Sommerfeldt and Parkins (1994), Sommerfeldt et al.

(1995), Park and Sommerfeldt (1996), Park and Sommerfeldt (1997), Parkins et al. (2000b), Clark (1995) have reported further investigations into the use of an energy-based error criterion in the active control of noise in enclosures. These researchers have analysed and implemented energy density sensing, which overcomes observability problems described by Kang and Kim (1995). Cazzolato and Hansen (2000b), Cazzolato and Hansen (2000a), Parkins et al. (2000a), have investigated the errors in 1D, and 3D energy density probes for enclosed fields. These works have shown the potential for improved attenuation when using energy density sensors over traditional pressure and potential energy sensors.

A number of error sensing strategies for active control of duct noise including: pressure, power and potential energy were investigated by Curtis et al. (1990), Zander and Hansen (1993), Zander (1994) . The use of energy based sensing strategies often led to better global attenuation. Work by Sommerfeldt and Nashif (1994) noted that in general an acoustic intensity cost function is not positive definite. They also theorised that in a duct, placing acoustic intensity error sensors between the primary sound source and the control source would lead to negative intensity. They concluded that in order for an acoustic intensity error criterion to be effective, the transducers in such a system would need to be arranged in such a way so that the intensity from the primary and control sources is always positive. Swanson (1994) performed a simulation of intensity error sensing in a duct, in which the practical implementation in the time and frequency domain is discussed. Intensity error sensing improved the wide-band performance and robustness. Reichard et al. (1995) reported on some experimental results of a frequency domain filtered-x feedforward control system minimising the acoustic intensity in a duct. A single acoustic intensity sensor was positioned downstream of the single control source. Up to 20dB pressure attenuation was observed downstream of the control source. Intensity and pressure error sensing in an open ended duct is compared in work by Kang and Kim (1997). Intensity error sensors were found to perform well at all locations along the duct, whereas pressure sensors do not work as well closer to the primary noise (Kang and Kim (1997)).

In short, there have been many demonstrations of the value of energy sensing in enclosed

spaces. This in part provides the stimulus for the research described in this thesis, looking at the application of energy-based sensing in free space noise problems.

## 2.8 Active intensity error sensors

As mentioned in the active control of enclosed sound fields, some authors (Sommerfeldt and Nashif (1994), Swanson (1994), Reichard et al. (1995) and Kang and Kim (1997)) have analysed acoustic intensity error sensors in 1-dimensional ducts and found that they improve upon the attenuation achieved with pressure sensors.

### 2.8.1 Single active intensity sensors

#### 2.8.1.1 Active suppression of free field monopole radiation

It has been suggested that a suitable measure of the performance of active control is the total radiated acoustic power. Optimising the error sensor type and location for the case of a single monopole primary source and a single monopole control source has been considered by Hansen and Snyder (1997) and Qiu et al. (1998). Hansen and Snyder (1997) first considered the acoustic power attenuation as a function of error sensor placement. The work centred on considering a traditional pressure sensor and showed the optimal near field error sensor location to be in-between the two monopole sources, but slightly closer to the control source for a source separation distance of $\lambda/10$. Qiu et al. (1998) extended the work of Hansen and Snyder (1997) by considering alternate error sensor types in the near field including active intensity, potential energy, kinetic energy and energy density sensors and sensor numbers also at a source separation distance of $\lambda/10$. The theme of both these works was the consideration of the acoustic power attenuation as a function of error sensor placement.

The work of Qiu et al. (1998) concluded that single pressure sensors were not as good as single active intensity sensors when the sensor is placed behind the control source. They confirmed the intuitive result that in the far field, active intensity sensing is equal to pressure sensing as the far field intensity is directly proportional to the squared pressure. This work is important in the context of this thesis, as it presents the starting point for a more detailed and thorough investigation.

#### 2.8.1.2 Active suppression of free field structural radiation

Currently no known research has been completed on analysing the performance of a single intensity sensor in the active control of free field structural radiation. This thesis will present work to fill this gap in knowledge of free field active noise control sensing strategies.

### 2.8.2 Multiple active intensity sensors

#### 2.8.2.1 Active suppression of free field monopole radiation

Qiu et al. (1998) found that if a circle of error sensors positioned at a radius $\lambda/8$ is setup around the primary source with a control source separation distance of $\lambda/10$, by increasing the number of error sensors the active intensity remains slightly better than pressure, however the level of power attenuation does not change. If the sensor circle is arranged in the far field then there is no difference between results achieved with active intensity sensors and pressure sensors. Again, as the sensor number is increased the level of power attenuation does not change.

#### 2.8.2.2 Active suppression of free field structural radiation

Work done by Berry et al. (1999), has considered the attenuation of the acoustic field generated by single plate vibration modes. The work was restricted to simulations of a simply supported

rectangular plate in an infinite baffle, controlled by multiple control sources and sensed by multiple active intensity sensors and pressure sensors. The error sensors were arranged such that they were located in the near field and setup in a regular grid of $3 \times 3$ sensors $3\lambda/20$ behind a grid of $2 \times 2$ control sources at $\lambda/20$ from the plate. The (1,1) plate mode (resonant frequency 283Hz) was excited off resonance at 100Hz. The results showed that when minimising the squared pressure at the error sensor location, a total sound power attenuation of 18dB could be achieved, while minimisation of the active intensities gives a slightly better result of 20dB. The results were indicative of global far field attenuation of the sound field. The author found that intensity minimisation, similar to pressure minimisation, suffers from a rapid decrease of the control performance when the sensors are positioned near to the sources, and attributed this to the signed nature of the cost function. Similar results were obtained with the (3,1) mode. Berry concluded that near field sound intensity minimisation does not in general provide significant improvements as compared to near field squared pressure minimisation, because the sum of the intensities can be driven to large and negative values after control.

## 2.9 Controlling vibration to attenuate sound

Active vibration control is the reduction of structural vibration levels, either locally or globally through the introduction of secondary control forces and minimisation of a predetermined error criteria. When active vibration control (AVC) is used to attenuate the sound radiation from a vibrating structure, the process is called active structural acoustic control (ASAC). The earliest work found on active vibration control was performed in the USSR in the 60's, Knyasev and Tartakovskii (1967), and mid 80's, Vyalyshev et al. (1986) on a beam and a panel. Their work included both experimental and theoretical analysis of the problem. These earliest attempts used single electrodynamic control actuators and minimised the signal from a single accelerometer.

Meirovitch and Baruh (1985), Lee and Moon (1990) were the first to note that a large number of sensors would be necessary to obtain a measure of the vibration distribution of a primary radiating structure. They suggested modal filtering as a means to keep the number of actuators and sensors low, therefore minimising the hardware requirements for a controller. They suggested that by attempting to minimise only certain structural modes, which contributed the most to the sound power, the number of sensors could be reduced.

At the beginning of the 1990s Fuller (1990), Metcalf et al. (1992), undertook experiments on the active control of vibrations from a circular baffled plate with point force control shakers, by minimising the total radiated acoustic power. They showed that using acoustic error sensors produced better results than vibration sensors on the plate. Work by Pan et al. (1992), tested ASAC on a simply supported rectangular plate in an infinite baffle. They minimised the far field sound pressure with a single error sensor. Both a single acoustic source and single vibration source were employed, and the sound directivity was plotted before and after control (see Figure 2.7). They investigated both sound pressure and sound power error criteria. It is noted that the plate modal velocity components are adjusted to produce far field sound control, either by decreasing their amplitudes and or by changing the temporal phases of the plate modes. They found that vibration control led to better global attenuation than did acoustic sources when controlling the (3,1) structural mode. Since these fundamental works, the research into active control of sound radiated from vibrating structures has split.

The research has splintered off into, firstly, a search for novel ways of actuating a vibrating structure. Fuller et al. (1991) investigated AVC on a simply supported rectangular plate in an infinite baffle using a single PZT (Lead Zirconate Titanate) piezoceramic control source and a single far field error sensor, and showed that global attenuation can be achieved. Wang et al. (1991a), extended the work by Fuller on a simply supported rectangular plate in an infinite baffle to multiple control sources. Multiple PZT control sources and point force control sources (point force shakers) were tested experimentally. It was noted that point force shakers produced the best results, but it was noted that PZT actuators have practical advantages in

terms of space savings and weatherability. Sound power was used as the cost function. They described an "optimal process" as having been used to derive the control signals, but no mention is made of how this is achieved or how it minimised the sound power. They found that as the number of actuators is increased so is the sound power attenuation. Wang et al. (1991b), examined AVC with multiple PZT actuators on a rectangular plate in a baffle and concluded that ASAC with more control sources is more effective as the effects of modal spillover reduce. It was found that the location and number of actuators significantly affects the amount of sound attenuation. It was theorised that broad-band control can be achieved with enough actuators. Wang and Fuller (1991) also calculated the intensity and pressure distribution in front of a rectangular plate in an infinite baffle, before and after control through a single PZT actuator.

Dimitriadis et al. (1991), theoretically analysed PZT actuators, they suggested that it might be possible to shape PZT actuators to excite particular structural modes, similar to PVDF (Polyvinylidene Fluoride) shaped sensors. Sung and Jan (1997), investigated ASAC on a clamped rectangular plate with PZT control sources. They analysed theoretically the bending moments that PZTs induced on the plate and validated the results experimentally. Research by Tanaka and Kikushima (1999a) seems to confirm the notion that PZT actuators perform worse than traditional point force electrodynamic actuators. They showed that carefully selected point vibration sensor and actuator placement can lead to better results than distributed sensors and actuators. Tanaka and Kikushima (1999a) experimented on a rectangular plate and demonstrated that modal spillover can be overcome by grouping the structural modes into odd/even and so on (Tanaka and Kikushima (1999b)). Work by Brennan et al. (1999) has made a comparison 5 different structural control actuators, including PZT and electrodynamic.

Secondly, the research has splintered off into a search for a novel sensor implementation. The emphasis of most of this research is on PVDF shaped sensors. Some of the earliest work on PVDFs was done by Clark and Fuller (1991) and Clark and Fuller (1992b), who compared 2 PVDF shaped sensors with up to 3 microphone error sensors, while employing 3 PZT control

sources. The modal amplitudes were measure before and after control was applied. For the plate excited on resonance, it was found that increasing the number of control sources only marginally improved the sound attenuation. For the plate excited off resonance, increasing the number of control sources resulted in appreciable improvement in sound attenuation. Later work by the author (Clark and Fuller (1992d)) used an optimisation algorithm to select optimal error sensor and control actuator locations. They tested this with a single microphone and a single PVDF error sensor. The results showed that both pressure microphone and PVDF error sensors produced near optimal results.

The bulk of research into PVDFs has focused on their use to measure particular structural modes (Clark and Fuller (1993)). However Charette et al. (1998), described a technique to use PVDF sensors to measure the volume displacement of a source. PVDF volume displacement sensors were investigated for plate radiation. Work by Rossetti and Norris (1996) considered a comparison of structural control and acoustic control actuators. At low frequencies the structural actuators outperformed the acoustic control actuators. At higher frequencies the performance of structural and acoustic control actuators were found to be similar. In the work by Rossetti and Norris (1996), a combination of pressure microphones and accelerometers were used as error sensors. They found that a combination gave good attenuation across a broad range of frequencies.

Not all vibration sensors are based on PVDFs. Maillard and Fuller (1998) tested two sensing approaches, firstly an accelerometer array used to estimate the far field sound pressure, and secondly an accelerometer array used to estimate the net volume acceleration of the plate. The results showed that the structural estimate of the far field sound pressure leads to better sound attenuation. Schwenk et al. (1994) and Audrain et al. (2000) considered minimisation of the structural intensity, measured by an array of accelerometers, in the active control of vibrations in a beam.

Finally, the research has splintered off into a search for an optimal sensing strategy. In sensing structural modes, early researchers found that the control system hardware that they had at

the time would cope poorly with the large numbers of sensors necessary to calculate them (Meirovitch and Baruh (1985), Lee and Moon (1990)). As such the idea of reducing the number of inputs to the control system by selecting a reduced number of sensor signals (modal filtering) which give a measure of some global quantity such as acoustic power (Meirovitch and Baruh (1985), Lee and Moon (1990), Morgan (1991), Snyder and Tanaka (1993a), Elliott and Johnson (1993), Snyder et al. (1995b), Snyder et al. (1996), Berry (1999)).

Work by Clark and Fuller (1992c) demonstrated that properly selected PVDF distributed sensors should only sense those components that contribute significantly to the far field sound radiation. Clark and Fuller (1992a) also compared PVDF shaped sensors with pressure microphone error sensors, employing multiple PZT control sources. It was noted that far field attenuation is achieved when the supersonic wavenumber components are reduced. They suggested that the k-transform could be used as an error criterion. Similarly work by Masson et al. (1998) reported the use of a wavelet approach to active structural acoustic control.

Work by Naghshineh and Koopermann (1992) on active vibration control on a beam, attempted to minimise the total radiated sound power. Naghshineh and Koopermann (1993), also investigated the sound power minimisation of large vibrating structures. A modal filtering strategy was employed for a clamped beam case study producing good far field attenuation.

Tanaka et al. (1996a) performed research on the sensing of power modes (or modes that contribute most to the radiated sound power). They then minimised the sound power as approximated by these power modes. Snyder and Tanaka (1993a) showed that by deriving an orthogonal set of structural modes which contribute to the error criterion, a reduced number of sensors is produced. Continuing along this vein of research Snyder et al. (1995a), Tanaka et al. (1996b), looked at smart sensors made from PVDF. This enabled modal filtering (Snyder et al. (1993)) to be done, thereby choosing those structural modes which contribute most to the radiated sound power and concentrating on controlling them.

Similar methods of reducing the number of inputs in a modal filter have been investigated

by Gibbs et al. (2000). Their approach applied a radiation modal expansion to the primary vibrating structure.

Reduction of sound power radiated from a rectangular plate in an infinite baffle was experimentally tested by Tan and Hird (1997) using different control methods: PD control, Cross-correlation method, Inverse operational amplifier method. The results produced showed good broad-band attenuation. However it was noted that a feedforward adaptive control system would be necessary in practice because the tested systems could not be accurately modelled to the degree needed by a feedback approach.

More recently Berkhoff (2000) and Snyder et al. (2001) have proposed acoustic-based modal filtering. These works considered the decomposition of many acoustic pressure measurements into a small set which is directly related to a global error criterion such as acoustic power.

## 2.10 Algorithms for the placement of sensors and actuators

Numerous authors, and most recently Baek and Elliott (2000), have emphasised the importance of transducer placement in the active control of enclosed fields. To this end there has been a great deal of research activity directed at finding the optimal location of sensors and actuators (Baek and Elliott (1993), Baek (1993), Tsahalis et al. (1993), Katsikas et al. (1993), Ruckman and Fuller (1993), Zimmermann (1993), Wang (1993), Benzaria and Martin (1994), Wang et al. (1994), Baek and Elliott (1995), Baek and Elliott (1995), Ruckman and Fuller (1995), Manolas et al. (1996), Wang (1996), Pottie and Botteldooren (1996), Simpson and Hansen (1996), Sergent and Duhamel (1997), Naghshineh et al. (1998), Hansen et al. (1999)).

Multiregression for acoustic sensor and actuator location was investigated as early as Snyder et al. (1991b). Genetic algorithms were explored by Baek and Elliott (1993), Baek (1993), Tsahalis et al. (1993), Katsikas et al. (1993), Wang (1993), Zimmermann (1993), Baek and Elliott (1995), Manolas et al. (1996), Wang (1996), Pottie and Botteldooren (1996), Simpson

and Hansen (1996), Hansen et al. (1999). An annealing algorithm was investigated by Wang et al. (1994), Baek and Elliott (1995). A successive quadratic programming algorithm and finite difference gradient technique (subset selection) was conducted on a plate by Ruckman and Fuller (1993), Ruckman and Fuller (1995). A QR subset selection method was analysed by Naghshineh et al. (1998). Also various minimum/maximum methods have been researched by Benzaria and Martin (1994), Sergent and Duhamel (1997). Benzaria and Martin (1994) used an interpolation method and gradient algorithm to locate acoustic control sources.

In the active control of enclosed sound fields and active vibration control, sensor placement is often optimised for best modal extraction and identification, Baruh and Chloe (1990), Kammer and Yao (1994), Lim (1993), Liu and Tasker (1995), Obinata and Doki (1993), Yao et al. (1993).

Martin and Roure (1997), Martin and Roure (1998) optimised the control source locations by a spherical harmonics expansion of the primary field and error sensor locations by a genetic algorithm, producing very good results.

A problem with many of these search methods is that they rely on a knowledge of the modal characteristics of the structure/enclosure. Also, since all these methods essentially rely on trial and error they are all fairly computationally intensive.

## 2.11 Other sensing and actuating methods

Many new sensors and actuators are being developed which is hoped will lead to better sound attenuation performance. Fuller (1997) gives an overview of the different sensors/actuators PVDF shaped sensors, PZT actuators and sensors, active skin actuators. Active tile actuators were investigated by Johnson (1996) and Johnson and Elliot (1997). These actuators are designed to cover a vibrating structure and each tile element is actuated to negate the vibration produced by the structure. Active control using smart foam was first developed by Guigou and

Fuller (1998) and active skin by Johnson and Fuller (2000). These actuators function similar to active tiles, by covering the region of the structure which is radiating the sound, and cancelling the vibration. In some circumstances it is not the desire to improve control performance that directs the design of new actuating/sensing systems, but the environmental conditions under which the actuators and sensors need to operate. Li et al. (1997) analysed a curved-panel control source design, which unlike traditional speakers is weather-proof. In the commercial active transformer control system by Quiet Power (ADTP (1997)) weather proofed error microphones and control speakers (Brungardt et al. (1997)) were developed. Their design used PZT and tuned acoustic actuators and electret microphones in the far field. Garcia-Bonito et al. (1998), Kim and Jones (1991) have shown that due to the low power output from PZT shakers, a higher output shaker is necessary to efficiently actuate large structures and they have developed PZT actuators with larger displacement. AURA shakers (Cazzolato (1999a)), designed for use in the computer gaming industry are worn on the backs of players of 3D games to simulate being shot by applying impulse forces on the players back. These shakers were found to be useful for active control of transformer noise, as they produced a large displacement and could be tuned to a desired frequency and be double or triple mounted. The theory of 'perfect' active control put forth by Magiante and Vian (1977), Magiante (1977), Jessel (1979), of a continuous control source completely surrounding the primary disturbance, has not been achievable because no such continuous source exists. However work by Heydt et al. (2000) on electrostrictive polymer film loudspeakers has shown that a continuous "wall" acoustic actuator can be constructed. At present they have a poor response at low frequencies and would not be useful for active noise control. Strain sensing in the active control of structural radiation by Masson et al. (1997), is another alternative to traditional acoustic (microphone) sensors. Although like PZT, strain sensors are a semi-permanent attachment to the structure, so placement has to be optimised. Kim and Brennan (2000) found that point force actuators are good at controlling plate-dominated modes while an acoustic source is effective in controlling cavity-dominated modes, in the active control of sound transmission into enclosed spaces. Constans and Belegundu (1998) did simulations minimising the sound power from vibrating shell struc-

tures, by applying optimally located point masses to alter the structural mode shapes which contribute most to the sound power.

## 2.12 Gaps in current knowledge

Many laboratory demonstrations of active control, using acoustic and vibration transducers have been done. However, very few practical implementations exist. While a lot of focus has been given to transducer type and location, no definitive "best approach" has emerged. There are numerous researchers that imply better results with "power" or "energy", but almost no application in free space. Work by Qiu et al. (1998) has investigated the optimal active intensity error sensor placement in terms of minimum acoustic power in the active control of monopole sound radiation and has identified regions where active intensity error sensors perform better than traditional pressure error sensors. When a sum of active intensities error criterion is employed, Qiu et al. (1998) described a condition for which the sum of active intensities cost function is guaranteed to be positive. However this fundamental work was restricted to active control of an idealised monopole sound source. Berry et al. (1999) extended the work of Qiu et al. (1998), and considered arrays of 9, 48 and 432 active intensity error sensors in the active control of sound radiation from single structural modes of a simply supported rectangular steel plate in an infinite baffle. The error sensors were located away from the plate and behind the arrays of 4 and 12 acoustic control sources near the location identified by Qiu et al. (1998) as being where active intensity error sensors outperform pressure error sensors in the active control of a monopole sound source. The plate model Berry employed consisted of the single structural modes: (1,1) excited on resonance, (1,3) excited on and off resonance. Berry stated a similar condition to that arrived at by Qiu et al. (1998), for guaranteeing that the sum of active intensities cost function produces a minimum. Neither of these fundamental works were able to explain the poor performance of active intensity error sensors. It has been shown (Thornton (1988) and Nelson and Elliott (1992)) that a single acoustic control monopole source located

suitably close to a primary monopole source source ($< \lambda/12$), with a single far field pressure error sensor can lead to global attenuation. Further work by Pan et al. (1992) has confirmed this for the active control of a harmonically excited simply supported rectangular steel plate in an infinite baffle, where the separation distance between the plate and the control source was $2\lambda/100$. It is therefore important to analyse the performance of a single error sensor in the active control of more realistic structures whereas previous research has avoided this. Given the described practical benefits of employing active intensity error sensors in the near field, it is important to consider single active intensity error sensors and compare their performance to pressure error sensors in a broad range of free space noise control problems.

This page intentionally contains only this sentence.

# Chapter 3

# Active suppression of a single monopole primary source by a single monopole control source

## 3.1 Introduction


*Figure 3.1: Thesis Flow chart.*

While the literature review in Chapter 2 concluded that the active control of a single monopole primary source by a single monopole control source, employing both pressure and active intensity error sensing strategies has been done by Qiu et al. (1998), it also highlighted that in certain regions active intensity error sensors give marginally better power attenuation performance than pressure error sensors. In order to form a basis for a comparison between traditional pressure error sensors and active intensity error sensors, this fundamental work will be

revisited. Figure 3.1 outlines the steps in the process of examining active intensity error sensing. Chapter 3 considers the case of active control a monopole source by a single monopole control source. Chapters 4 and 5 consider the case of a monopole source located on an infinite baffle and a simply supported rectangular steel plate respectively. Chapter 6 analyses the practical case of a small electrical transformer on a hard floor in an anechoic chamber. Finally Chapter 7 draws conclusions and discusses possible future work.

## 3.2 Theory

### 3.2.1 Introduction

The purpose of the control source is to attenuate the sound field produced by the primary source. The chosen method of assessing the level of attenuation is to analyse the sound power attenuation. It has been noted by Cunefare and Koopmann (1991b,a), that minimising the sound power does not necessarily lead to global control. However it does guarantee that the average far field sound pressure has been reduced.

In order to initially assess, in simulation, the potential of intensity-based error sensing as part of a feedforward active noise control system implementation in free space, the problem of controlling acoustic radiation from one monopole source via the introduction of a second monopole source will be considered. This arrangement is illustrated in Figure 3.2. The monopole radiation problem has been used in fundamental studies in the past, for assessing limits on acoustic power attenuation (Nelson and Elliott (1992)), the potential of acoustic pressure error sensing (Nelson and Elliott (1992)), for studies directed at optimising error sensor placement (Hansen and Snyder (1997), Qiu et al. (1998)), and for studies of acoustic intensity error sensing (Qiu et al. (1998)). Results from some of these previous studies will be used here for comparison.

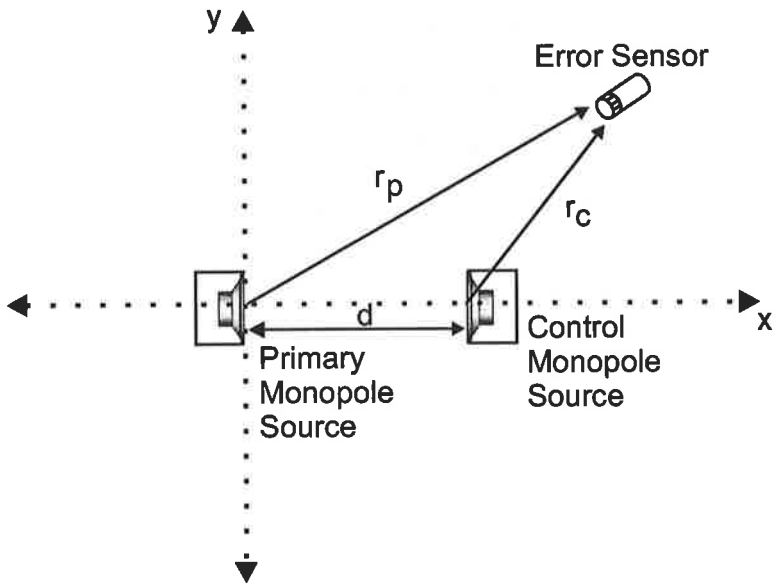


*Figure 3.2: Single monopole primary source and a single monopole control source arrangement.*

Assessment of the quality of error sensing strategies for the monopole radiation problem requires several steps:

Step 1: Calculation of the acoustic power output of the primary monopole source in the absence of control.

Step 2: Calculation of the maximum possible acoustic power attenuation for the given control source arrangement.

Step 3: Calculation of the control source volume velocity that will minimise the error criteria of interest (acoustic pressure at a point in space, acoustic intensity at a point in space, etc) for the given error sensing arrangement.

Step 4: Calculation of the total acoustic power output of the primary + control source arrangement using the control source volume velocity from step 3, followed by the acoustic power attenuation through comparison with the original (primary only) acoustic power output.

Step 5: Comparison of the attenuation in step 4 with the maximum possible attenuation for the given control source arrangement calculated in step 2. This will provide some assessment of the efficiency of the error sensing strategy.

### 3.2.2 Minimising the total sound power

Consider a single monopole source, radiating unwanted tonal noise at frequency $\omega$. This source is called the primary monopole source. Consider now a second monopole source, separated from the primary source by a distance $d$, which is to act as the control source.

The acoustic power output of a monopole source radiating into free space is given by Nelson and Elliott (1992)

$$W = \frac{1}{2}|q|^2 \frac{\omega^2 \rho}{4\pi c} \tag{3.1}$$

where $q$ is the source strength, $\omega$ is the angular frequency of the source, $\rho$ is the density of the acoustic medium and $c$ is the speed of sound in that medium. It is assumed that there is no fluid loading acting on the monopole.

The total acoustic power output of the two monopole arrangement (primary + control) can be expressed as a quadratic (Nelson and Elliott (1992), Hansen and Snyder (1997)) function of the control source strength $q_c$ given by

$$W = A_W |q_c|^2 + q_c^* b_W + b_W^* q_c + c_W \tag{3.2}$$

where $\mathbf{X}^*$denotes the complex conjugate of $\mathbf{X}$, $A_W = Z_0/2$, $b_W = \frac{1}{2} Z_0 q_p \frac{sinkd}{kd}$, $c_W = \frac{1}{2} Z_0 |q_p|^2$, $Z_0 = \frac{\omega^2 \rho}{4\pi c}$, $q_c$ and $q_p$ are the control and primary source strengths respectively, $k$ is the wave number and $d$ is the separation distance between the sources. The assumption made is that acoustic reciprocity between a monopole source and an error sensor location exists. As $A_W$ is positive definite, this expression has a unique minimum (Nelson and Elliott (1992), Adby

and Dempster (1974), Nelson et al. (1987c), Noble (1969), Haykin (1986), Huang and Chen (1989), Bellman (1960)). A derivation of this can be found in Appendix E. The optimal control source strength is given by

$$q_{c,opt} = -A_W^{-1} b_W = -q_p \frac{\sin kd}{kd} \tag{3.3}$$

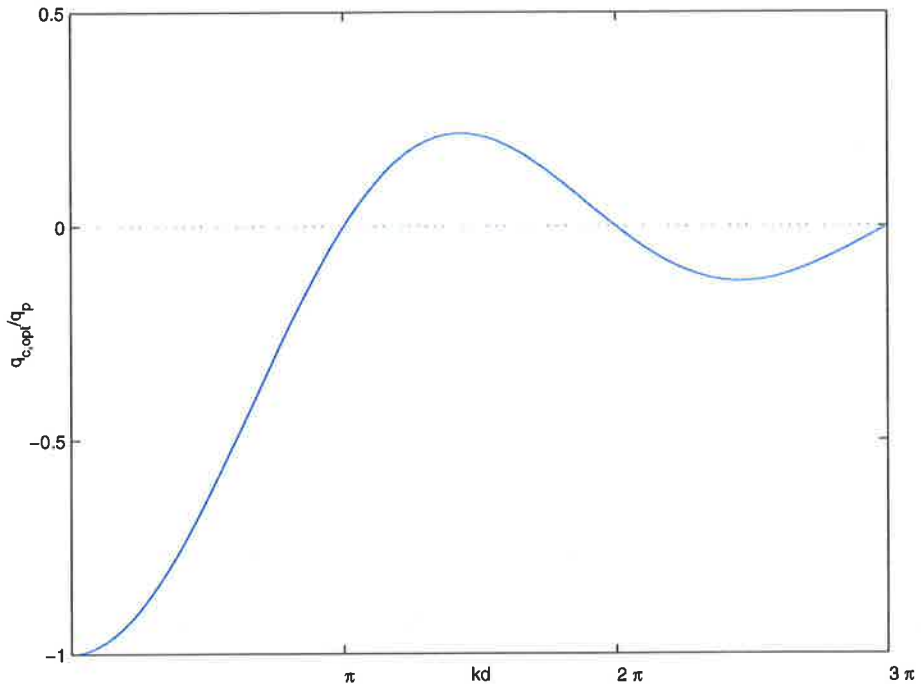


*Figure 3.3: Optimal control source strength $q_{c,opt}$ relative to the primary source strength $q_p$ as a function of the separation distance $d$ at a particular wavenumber $k$. After Nelson and Elliott (1992).*

Figure 3.3 shows the optimal control source strength as a function of the separation distance $d$ at a particular wavenumber $k$. Substituting this result into the quadratic expression and normalising in terms of the uncontrolled acoustic power output, the maximum possible acoustic power attenuation is found to be:

$$\frac{W_p}{W_{min}} = 1 - \left(\frac{\sin kd}{kd}\right)^2 \tag{3.4}$$

where $W_{min}$ is the acoustic power when the optimal control source strength is applied and $W_p$ is the acoustic power of the primary source acting alone, as shown in Figure 3.4.

Hence if appreciable power attenuation of a monopole primary source is desired then a monopole

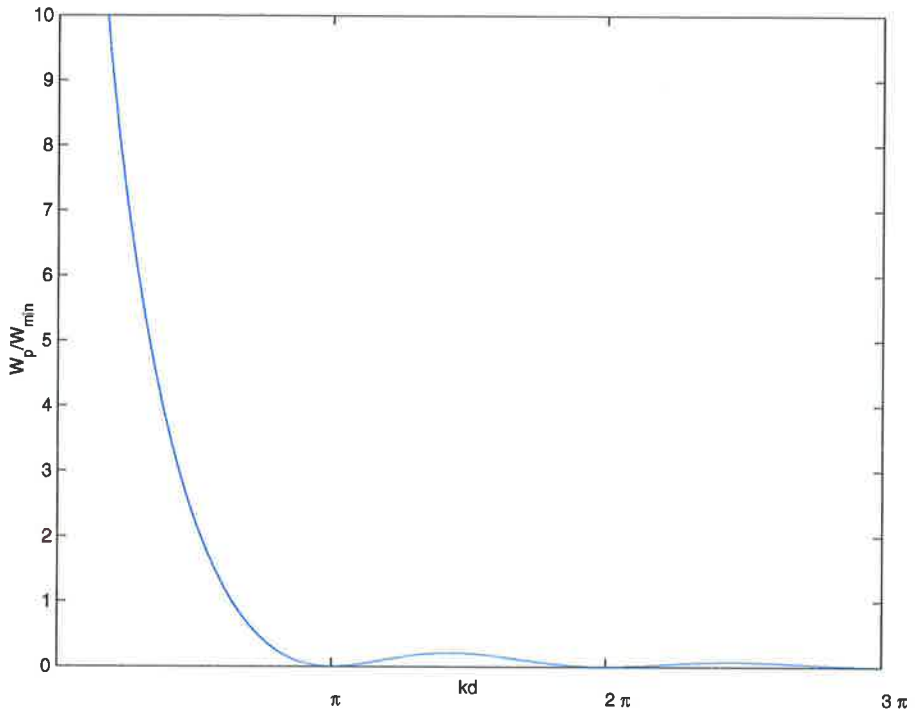


*Figure 3.4: Optimal power attenuation $W_p/W_{min}(dB)$ as a function of the separation distance $d$ at a particular wavenumber $k$. After Nelson and Elliott (1992).*

control source would need to be located within $\lambda/2$ (corresponding to $kd = \pi$ in Figure 3.4). At a separation distance of $d = \lambda/10$ the level of power attenuation is 9.8dB. This computed level of power attenuation sets an upper limit on the global control achievable with a single source.

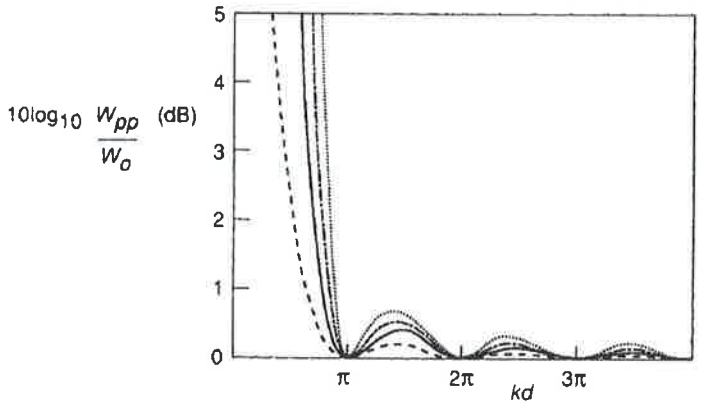


*Figure 3.5: Optimal power attenuation as a function of the separation distance $d$ at a particular wavenumber $k$ for: ––one; –two ; –·– three ; ···four; control sources. Presented previously by Nelson and Elliott (1992).*

Nelson and Elliott (1992) also showed (see Figure 3.5) that by increasing the number of monopole control sources up to 4, the separation distance necessary to obtain appreciable power attenuation is still $\lambda/2$. Work by Nelson and Elliott (1992) also investigated analytically minimising the squared pressure at a single far field location (equivalent to a single pressure error sensor in the far field) when controlling a single primary monopole source with a single monopole control source. They found that when the far field pressure minimisation point is in line with the primary and control sources, then the separation distance to ensure power attenuation must be less than $d = \lambda/6$. When the pressure is minimised at right angles to a line passing through the primary and control sources, then the necessary separation distance is increased to $d = \lambda/3$. The previously noted problems with sensing the pressure in the far field in practice, make the results demonstrated by Nelson and Elliott (1992) difficult to realise. It was shown again analytically by Hansen (1997) and Qiu et al. (1998) that power attenuation is in fact possible with pressure sensing in the near field. The work here is concerned with comparing the performance of active noise control when minimising squared acoustic pressure at a point in space against the performance when minimising acoustic intensity at a point in space.

### 3.2.3 Minimising pressure

Considering minimisation of acoustic pressure first, the squared acoustic pressure amplitude at a point $\mathbf{r}$ (described by the vector $\overrightarrow{OE}$ in Figure 3.6) in space is given by the sum of pressures due to the primary and control sources respectively as

$$p_{total}(\mathbf{r}) = p_p(\mathbf{r}) + p_c(\mathbf{r}) \tag{3.5}$$

which can be re-expressed as a quadratic (Nelson and Elliott (1992), Hansen and Snyder (1997)) as

$$|p_{total}|^2 = A_p |q_c|^2 + q_c^* b_p + b_p^* q_c + c_p \tag{3.6}$$

where $A_p = \left(\frac{\omega\rho}{4\pi r_c}\right)^2$, $b_p = \left(\frac{\omega\rho}{4\pi}\right)^2 \frac{1}{r_c r_p} q_p e^{-jk(r_p - r_c)}$, $c_p = \left(\frac{\omega\rho}{4\pi r_p}\right)^2$, $r_p$ and $r_c$ are the distances

between the error sensor location and the primary and control sources, respectively, as shown in Figure 3.6. Again the assumption of acoustic reciprocity is made.

As with radiated acoustic power, because $A_p$ is positive definite, this expression has a unique minimum given by the (pressure) optimal control source strength:

$$q_{c,p} = -A_p^{-1} b_p \tag{3.7}$$

For a derivation of this result see for example Hansen and Snyder (1997). Substituting this result back into the expression for acoustic power given in equation (3.2), and normalising with respect to the uncontrolled acoustic power output, the sound power attenuation that results from minimising squared acoustic pressure amplitude at a point in space is given by

$$\frac{W_p}{W_{min}} = \frac{c_W}{A_w \left| A_p^{-1} b_p \right|^2 - (A_p^{-1} b_p)^* b_W - b_W^* (A_p^{-1} b_p) + c_W} \tag{3.8}$$

### 3.2.4 Minimising active intensity

The total acoustic particle velocity in the direction $\hat{\mathbf{u}}_{total}$ of both sources at an observation point $\mathbf{r}$ (described by the vector $\overrightarrow{OE}$ in Figure 3.6) in the free field is given by the sum of the particle velocities of the primary and control sources given by

$$\mathbf{u}_{total}(\mathbf{r}) = \mathbf{u}_p(\mathbf{r}) + \mathbf{u}_c(\mathbf{r}) \tag{3.9}$$

which can be rewritten as

$$\mathbf{u}_{total}(\mathbf{r}) = u_{total} \hat{\mathbf{u}}_{total} = u_p \hat{\mathbf{u}}_p + u_c \hat{\mathbf{u}}_c \tag{3.10}$$

where the unit vector $\hat{\mathbf{u}}_p$ (which is $\frac{\overrightarrow{PE}}{|\overrightarrow{PE}|}$ as shown in Figure 3.6) is in the radial direction relative to the primary source , $\hat{\mathbf{u}}_c$ (which is $\frac{\overrightarrow{CE}}{|\overrightarrow{CE}|}$ as shown in Figure 3.6) is in the radial direction relative to the control source.

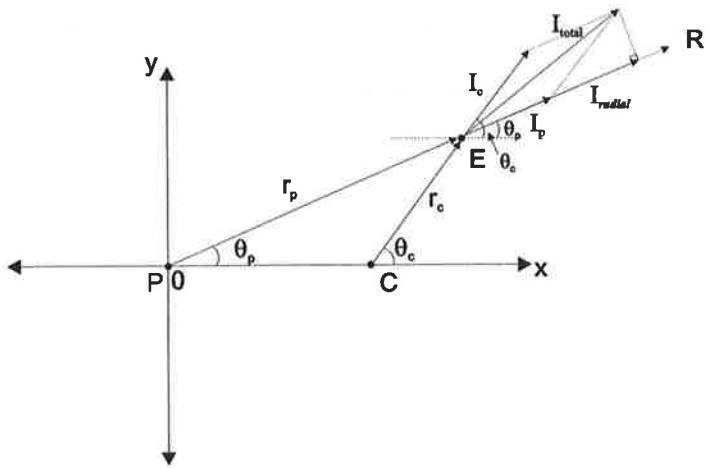


*Figure 3.6: Radial active intensity shown in terms of the it vector components.*

The total active intensity in the direction of $\mathbf{u}_{total}$ is given by

$$\mathbf{I}_{total}(\mathbf{r}) = \frac{1}{2} Re\left\{p^*_{total}(\mathbf{r})\mathbf{u}_{total}(\mathbf{r})\right\} \tag{3.11}$$

It was chosen to minimise the radial (with respect to the primary source, in the same direction as the vector $\mathbf{u}_p$) active intensity, as this is the direction from which all of the primary acoustic energy is coming. It will be shown that the selection of the direction in which the active intensity is minimised (see Figures 3.11 and 3.12) does not significantly alter the results. Hence it is the component of $\mathbf{I}_{total}$ in equation (3.11) in the direction of $\mathbf{I}_p$ henceforth labelled $\mathbf{I}_{radial}$ (as shown in Appendix A) which must be minimised and is given by

$$\mathbf{I}_{radial}(\mathbf{r}) = proj_{\mathbf{I}_{radial}}\mathbf{I}_{total} = (\mathbf{I}_{radial} \bullet \mathbf{I}_{total})\mathbf{I}_{radial} \tag{3.12}$$

The notation $proj_{\mathbf{X}}\mathbf{Y}$ is used to denote the orthogonal projection of vector $\mathbf{Y}$ on vector $\mathbf{X}$. $\mathbf{X} \bullet \mathbf{Y}$ indicates the vector dot product between $\mathbf{X}$ and $\mathbf{Y}$. The direction of positive intensity is defined to be $\hat{\mathbf{u}}_p$. Substituting (3.10) and (3.5) gives

$$\mathbf{I}_{total} = \frac{1}{2} Re\left\{(p^*_p + p^*_c)(\mathbf{u}_p + \mathbf{u}_c)\right\} \tag{3.13}$$

$$= \frac{1}{2} Re\left\{(p^*_p\mathbf{u}_p + p^*_p\mathbf{u}_c + p^*_c\mathbf{u}_p + p^*_c\mathbf{u}_c\right\} \tag{3.14}$$

where $p_p = Z_p(r_p)q_p$ and $p_c = Z_c(r_c)q_c$, $r_p$ is the distance from the primary source to the observation point(error sensor location) and similarly $r_c$ is the distance from the control source to the observation point. $Z_p$ and $Z_c$ both describe the acoustic transfer impedances due to the primary and control sources respectively at the observation point and are given by

$$Z_p(r_p) = \frac{j\omega\rho}{4\pi}\frac{e^{-jkr_p}}{r_p} \tag{3.15}$$

$$Z_c(r_c) = \frac{j\omega\rho}{4\pi}\frac{e^{-jkr_c}}{r_c} \tag{3.16}$$

and where $\mathbf{u}_p = \mathbf{H}_p(r_p)q_p$ and $\mathbf{u}_c = \mathbf{H}_c(r_c)q_c$, where $r_p$ and $r_c$ are defined as before. $\mathbf{H}_p$ and $\mathbf{H}_c$ both describe the acoustic velocity transfer impedances due to the primary and control sources respectively at the observation point $\mathbf{r}$ and are given by

$$\mathbf{H}_p(r_p) = \frac{1}{4\pi}\left(\frac{1}{r_p^2}+\frac{jk}{r_p}\right)e^{-jkr_p}\hat{\mathbf{u}}_p \tag{3.17}$$

$$\mathbf{H}_c(r_c) = \frac{1}{4\pi}\left(\frac{1}{r_c^2}+\frac{jk}{r_c}\right)e^{-jkr_c}\hat{\mathbf{u}}_c \tag{3.18}$$

The active intensity in the direction $\hat{\mathbf{u}}_{total}$ can be re-expressed in a hermitian quadratic form as

$$\mathbf{I}_{total} = \mathbf{A}_I|q_c|^2 + q_c^*\mathbf{b}_I + \mathbf{b}_I^* q_c + \mathbf{c}_I \tag{3.19}$$

where $\mathbf{A}_I = \frac{1}{2}Re\{Z_c^*\mathbf{H}_c\}$ and $\mathbf{b}_I = \frac{1}{4}q_p(\mathbf{H}_c^* Z_p + \mathbf{H}_p Z_c^*)$ and $\mathbf{c}_I = \frac{1}{2}Re\{Z_p^*\mathbf{H}_p\}|q_p|^2$.

As shown in Figure 3.6 the radial active intensity can be written as

$$\mathbf{I}_{radial}(\mathbf{r}) = proj_{\mathbf{I}_{radial}}\mathbf{I}_{total} \tag{3.20}$$

$$= (\mathbf{I}_{radial} \bullet \mathbf{I}_{total})\mathbf{I}_{radial} \tag{3.21}$$

$$= \mathbf{A}_{I_{radial}}|q_c|^2 + q_c^*\mathbf{b}_{I_{radial}} + \mathbf{b}_{I_{radial}}^* q_c + \mathbf{c}_{I_{radial}} \tag{3.22}$$

where $\mathbf{A}_{I_{radial}}$, $\mathbf{b}_{I_{radial}}$ and $\mathbf{c}_{I_{radial}}$ can be written as

$$\mathbf{A}_{I_{radial}} = \frac{1}{2}Re\left\{Z_c^* H_c proj_{\widehat{\mathbf{u}_p}}\widehat{\mathbf{u}}_c\right\} \tag{3.23}$$

$$\mathbf{b}_{I_{radial}} = \frac{1}{4}q_p(H_c^* Z_p proj_{\widehat{\mathbf{u}_p}}\widehat{\mathbf{u}}_{c,0} + Z_c^* H_p \widehat{\mathbf{u}_p}) \tag{3.24}$$

$$\mathbf{c}_{I_{radial}} = \frac{1}{2}Re\left\{Z_p^* H_p\right\}|q_p|^2 \widehat{\mathbf{u}_p} \tag{3.25}$$

where $H_p = \|\mathbf{H}_p\|$, $H_c = \|\mathbf{H}_c\|$ are the complex vector magnitudes of the corresponding vectors describing the velocity transfer impedances.

If the arbitrary definition of positive radial intensity in the direction $\hat{\mathbf{u}}_p$ (see Figure 3.6) is made, then the vector notation for the radial active intensity can be dropped. Consider equation (3.23) for the active intensity of the control source acting on its own $A_{I_{radial}}$. Appendix E shows that provided $A_{I_{radial}}$ is positive, there exists a unique minimum given by the optimal control source strength $q_{c,opt}$. This is not necessarily the case for an active intensity cost function which may be negative at certain locations. The term $proj_{\widehat{\mathbf{u}_p}}\widehat{\mathbf{u}}_c$ which is defined by

$$proj_{\widehat{\mathbf{u}_p}}\widehat{\mathbf{u}}_c = (\widehat{\mathbf{u}}_c \bullet \widehat{\mathbf{u}_p})\widehat{\mathbf{u}_p} \tag{3.26}$$

can at certain error sensor locations be negative, when the dot product $\widehat{\mathbf{u}}_c \bullet \widehat{\mathbf{u}_p}$ is negative, or the angle between $\widehat{\mathbf{u}_p}$ and $\widehat{\mathbf{u}}_c$ is obtuse ($\theta_c > \theta_p$ in Figure 3.6).

Expanding equation (3.23) gives

$$\mathbf{A}_{I_{radial}} = \frac{1}{2}Re\left\{Z_c^* H_c(\widehat{\mathbf{u}}_c \bullet \widehat{\mathbf{u}_p})\widehat{\mathbf{u}_p}\right\} \tag{3.27}$$

$$= \frac{\omega\rho k}{16\pi r_c^2}(\widehat{\mathbf{u}}_c \bullet \widehat{\mathbf{u}_p})\widehat{\mathbf{u}_p} \tag{3.28}$$

If the direction $\widehat{\mathbf{u}_p}$ is taken as being positive, then if the condition $\widehat{\mathbf{u}}_c \bullet \widehat{\mathbf{u}_p} < 0$ is met at a particular error sensor location $\mathbf{r}$, then $A_{I_{radial}} < 0$ and hence there is only a unique maximum exists as derived in Appendix E.

The region where error sensors satisfy the condition that $\hat{\mathbf{u}}_c \bullet \widehat{\mathbf{u}_p} < 0$ can best be illustrated graphically, as shown in Figure 3.7. If $A_{I_{radial}} > 0$ a unique minimum exists or if $A_{I_{radial}} < 0$

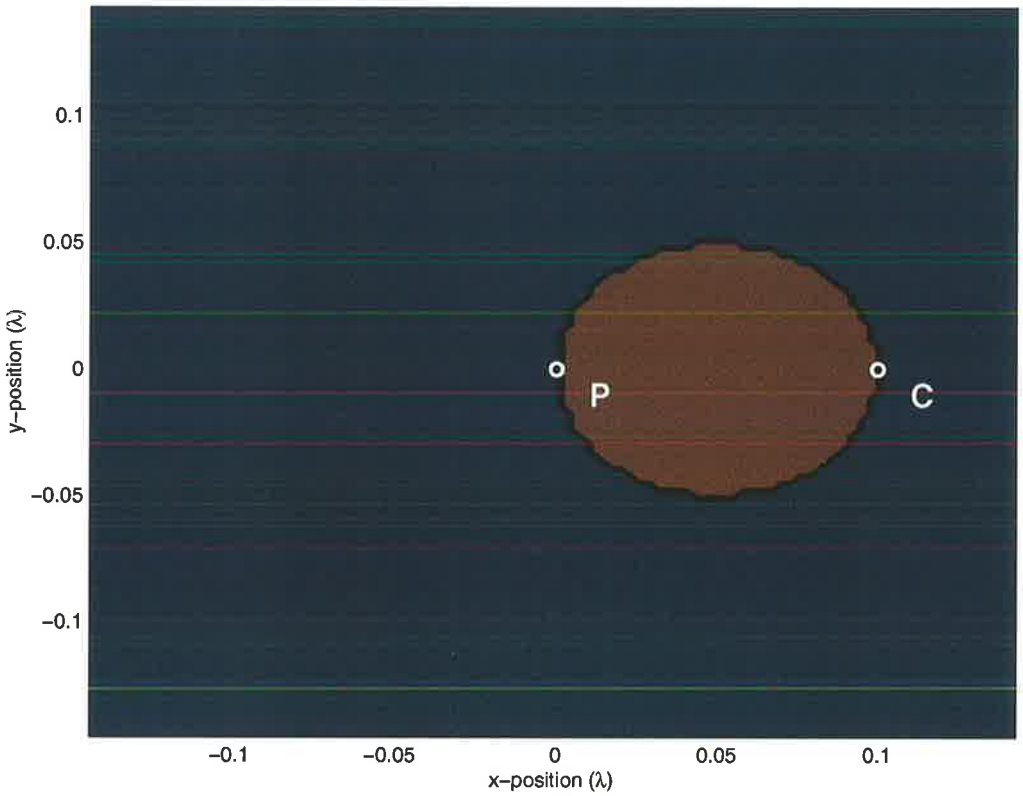


*Figure 3.7: The region (indicated by the colour red) where $A_{I_{radial}} < 0$, and hence the radial active intensity can become negative, leading to an optimal control source strength which maximises the radial active intensity. The blue region indicates the region where $A_{I_{radial}} > 0$ and hence the radial active intensity is positive definite and the optimal control source strength minimises the radial active intensity.*

then a unique maximum exists and in either case the extreme control source strength is given by

$$q_{c,opt} = -A_{I_{radial}}^{-1} b_{I_{radial}} \tag{3.29}$$

Therefore to optimise the radial active intensity at a particular location $\mathbf{r}$ from a primary monopole source by a single control monopole source (3.29) is substituted into (3.22).

The amount of sound power attenuation when the active intensity is minimised at the error sensor location is found by substituting (3.29) into (3.2) giving

$$\frac{W_p}{W_{min}} = \frac{c_{W_f}}{A_{W_f}\left|-\frac{1}{2}A^{-1}_{I_{radial}}(b_{I_{radial}})\right|^2 - (-\frac{1}{2}A^{-1}_{I_{radial}}(b_{I_{radial}}))^* b_{W_f} - b^*_{W_f}(-\frac{1}{2}A^{-1}_{I_{radial}}(b_{I_{radial}})) + c_{W_f}} \tag{3.30}$$

## 3.3 Comparison of power attenuation when minimising pressure and intensity error criterion

As described, the aim of the work presented here is to compare the performance of pressure and intensity error sensing strategies for a simple free space radiation problem. Referring to Figure 3.2, the problem to be studied here has a single monopole control source separated from a single monopole primary source by one-tenth of a wavelength. Using equation (4.17), the maximum possible acoustic power attenuation for this arrangement is 9.8 dB.

Illustrated in Figures 3.8 and 3.9 is the acoustic power attenuation that would result from minimising the square acoustic pressure amplitude at a point in space. While these results have been presented previously by Hansen and Snyder (1997), it is important that they be re-presented here to provide the basis for comparison with intensity error sensing. The results in Figures 3.8 and 3.9 are to different scales: Figure 3.8 depicts results for minimising acoustic pressure at points in space for x,y positions over 3 wavelengths, while Figure 3.9 depicts results over a 0.3 wavelength region. Observe that significant attenuation can be achieved at locations perpendicular to a line joining the sources.

Illustrated in Figures 3.10 and 3.11 are results for the same geometry, but where acoustic intensity is minimised as opposed to square acoustic pressure amplitude. For these results, the acoustic intensity vector is minimised in the radial direction, along a line between the primary and control sources. Comparing Figures 3.8 and 3.10, the results obtained when minimising acoustic intensity at locations distant from the sources are very similar to the acoustic pressure results, this intuitive result (as noted by Qiu et al. (1998)) comes about because the far field

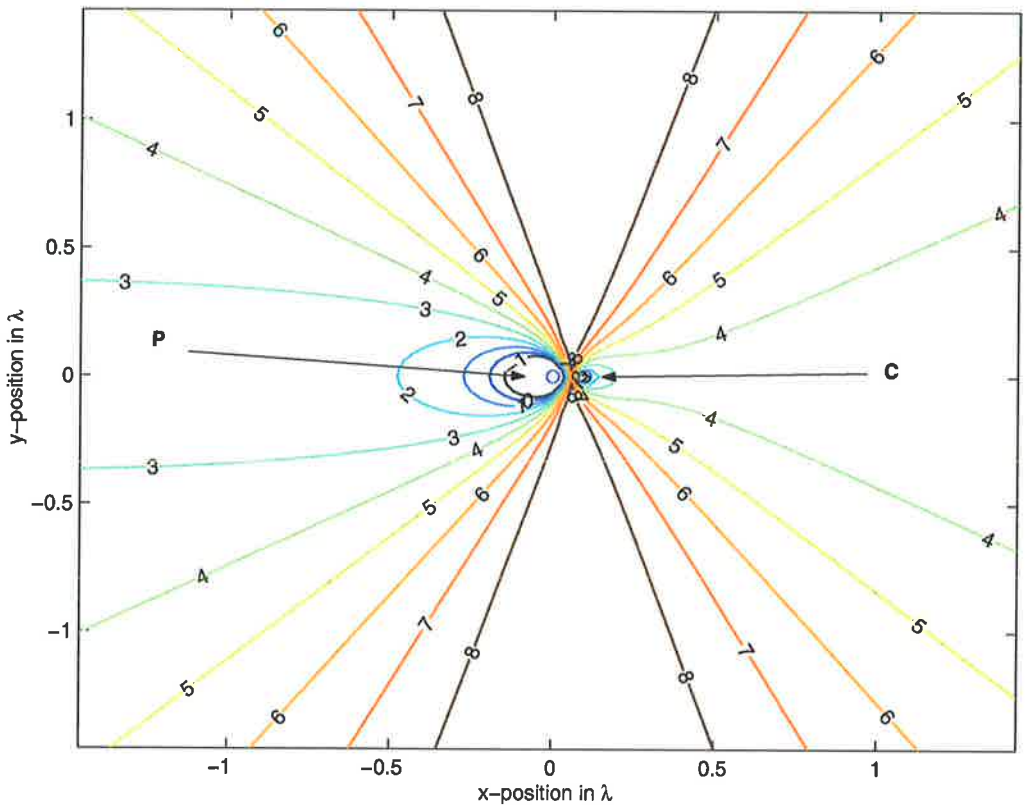


*Figure 3.8: Acoustic power attenuation in dB as a function of pressure error sensor placement, single monopole primary and control sources separated by λ/10 wavelength in far field view. The circle ◯ on the left is the primary monopole source location, and the circle ◯ on the right is the control monopole source location.*

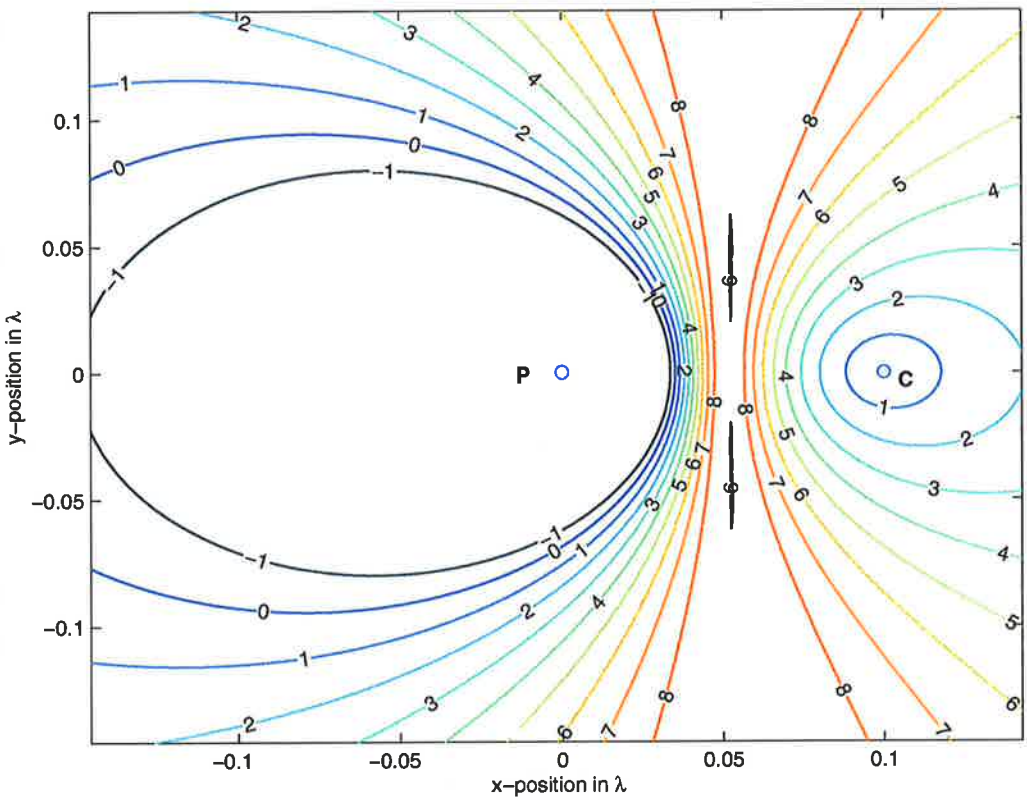


*Figure 3.9: Acoustic power attenuation in dB as a function of pressure error sensor placement, single monopole primary and control sources separated by $\lambda/10$ wavelength in near field view. The circle ○ on the left is the primary monopole source location, and the circle ○ on the right is the control monopole source location.*

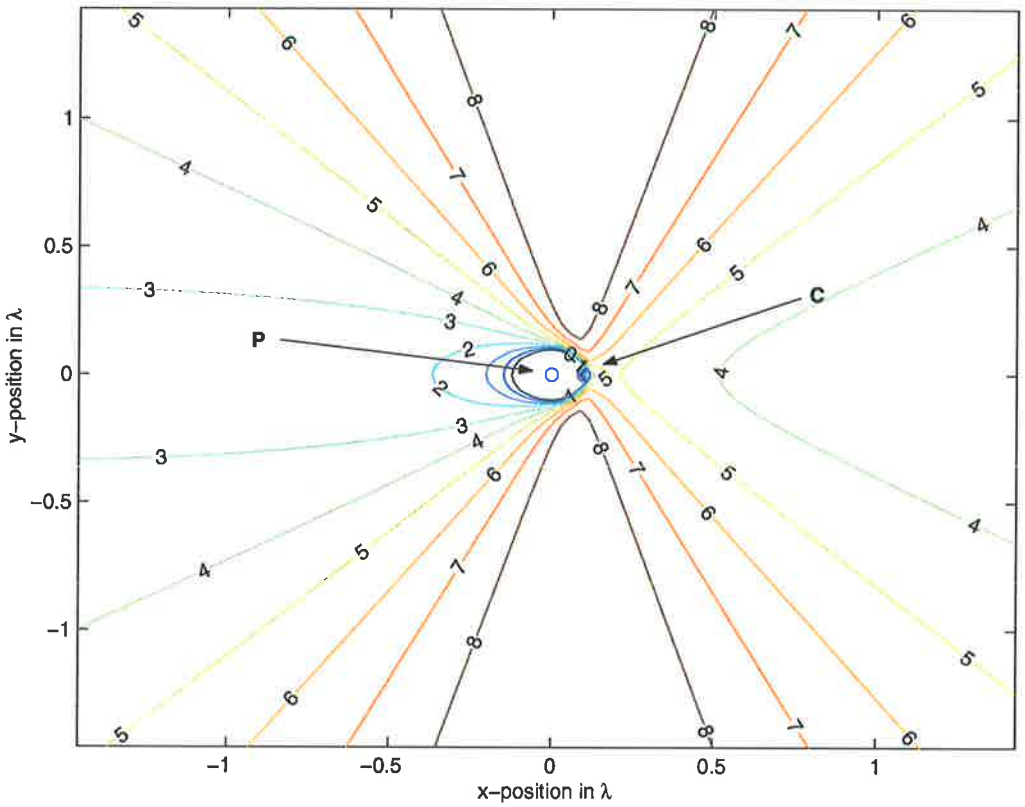


*Figure 3.10: Acoustic power attenuation in dB as a function of radial active intensity error sensor placement (radial with respect to the primary source), single monopole primary and control sources separated by $\lambda/10$ wavelength in far field view. The circle ◯ on the left is the primary monopole source location, and the circle ◯ on the right is the control monopole source location.*

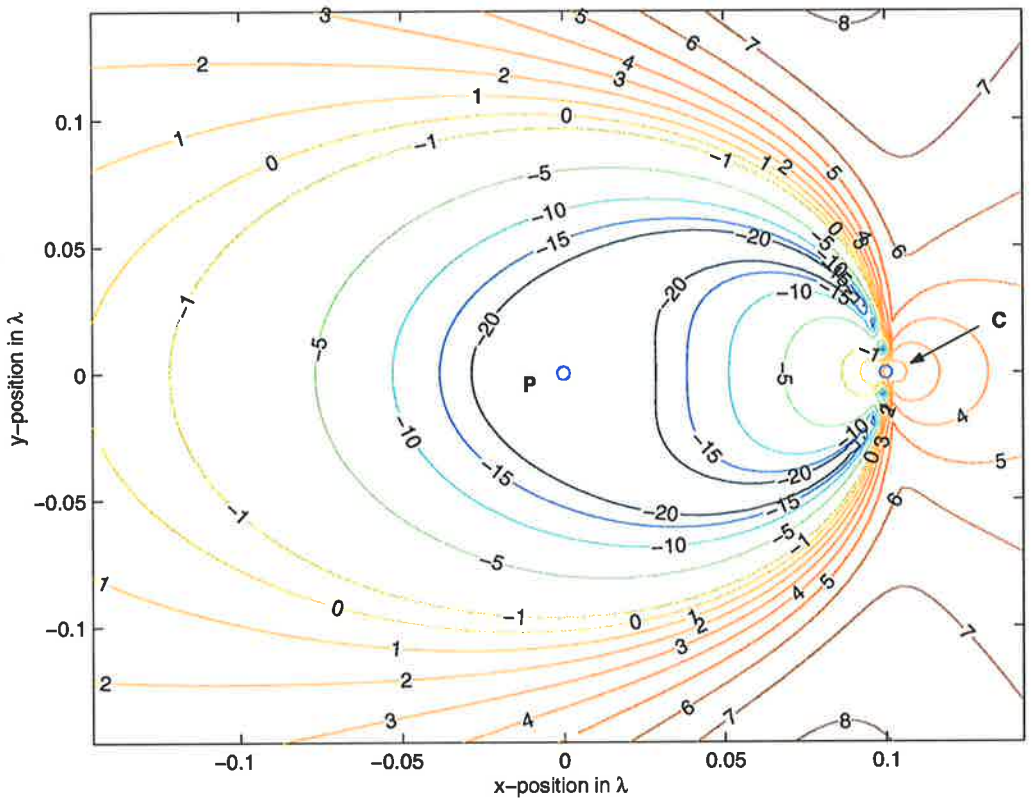


*Figure 3.11: Acoustic power attenuation in dB as a function of radial active intensity error sensor placement (radial with respect to the primary source), single monopole primary and control sources separated by $\lambda/10$ wavelength in near field view. The circle ◯ on the left is the primary monopole source location, and the circle ◯ on the right is the control monopole source location.*

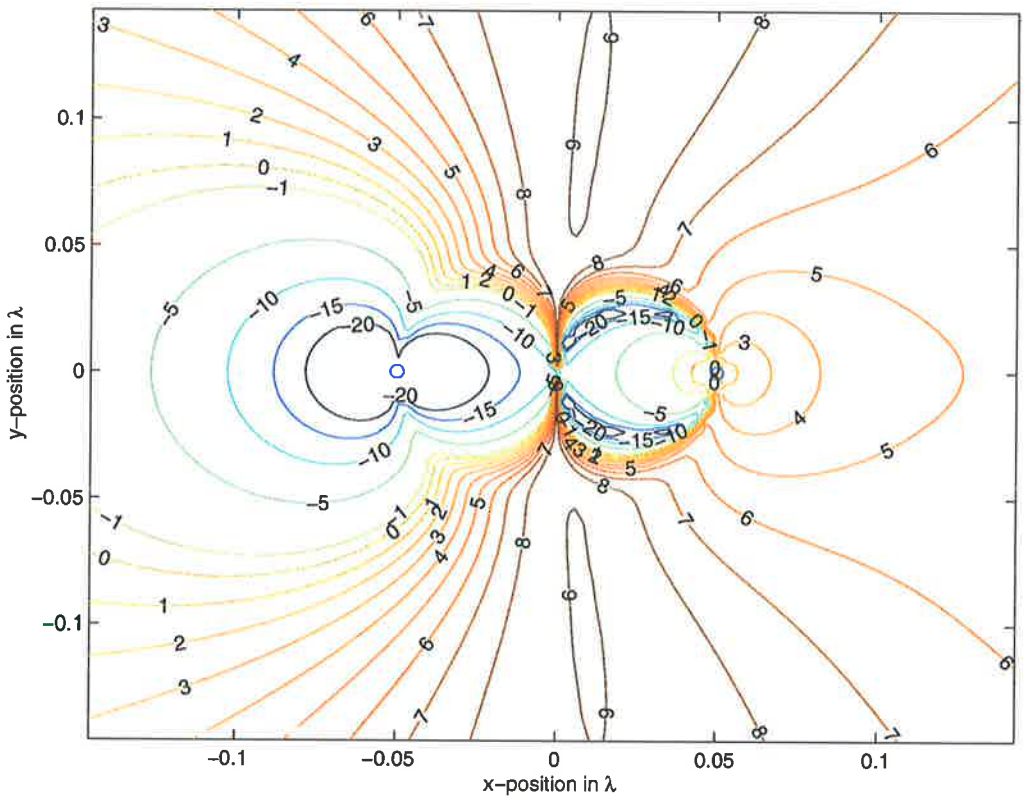


*Figure 3.12: Acoustic power attenuation in dB as a function of the active intensity error sensor placement when the sensor is directed at the midpoint between the primary and control sources, single monopole primary and control sources separated by $\lambda/10$ wavelength in near field view. The circle ◯ on the left is the primary monopole source location, and the circle ◯ on the right is the control monopole source location.*

intensity is directly proportional to the squared pressure. However, when comparing the results in Figures 3.9 and 3.11, it is evident that the results obtained when minimising the error criteria at locations close to the sources are very different. In fact, the acoustic power attenuation that results from minimising acoustic intensity is far worse than when minimising squared acoustic pressure. Note also that the region of poor performance in Figure 3.11 matches the expected result from Figure 3.7. The choice of direction in which the active intensity is minimised (as shown in Figure 3.12) does not affect the distinct region between the primary and control sources where sound power attenuation is negligible.

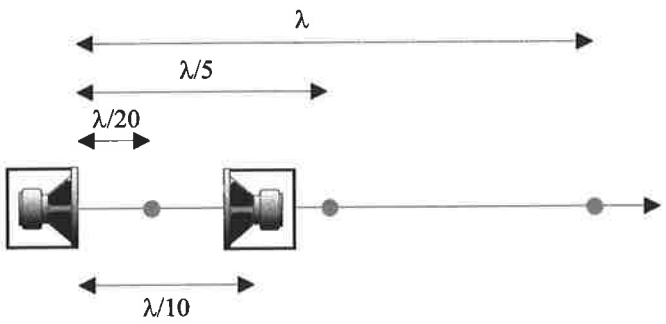


*Figure 3.13: The three sensor locations considered. The red dots indicate the error sensor location.*

As one of the drivers for examining acoustic intensity sensing is the hypothesized ability to place error sensors in the near field of the primary source, this result is particularly bothersome and requires further exploration. Referring back to the five steps outlined at the start of Section 3.2, for an error sensing strategy to be of "high quality", the control source volume velocity that minimises the error criterion of interest, derived in step 3, must be virtually identical to the control source volume velocity that provides maximum acoustic power attenuation, calculated in step 2. Shown in Figures 3.14a and 3.14b are plots of the squared pressure and intensity error criteria evaluated at a location which is λ (see Figure 3.13) from the primary source and directly in front as a function of complex control source volume velocity. Observe that both the pressure and intensity error surfaces have a single minimum, at approximately the same volume velocity, and that these minima are close to volume velocity that is optimal in terms of acoustic power attenuation.

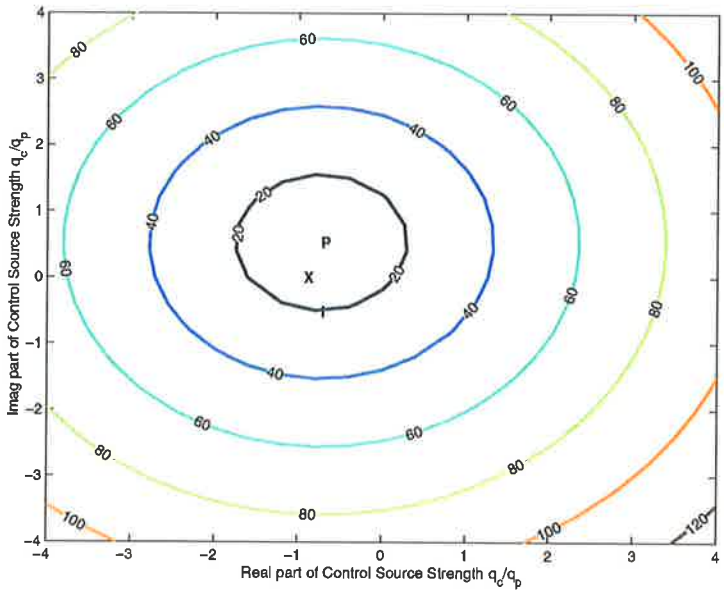


*(a) Pressure amplitude as a function of the real and imaginary parts of the relative control source strength*

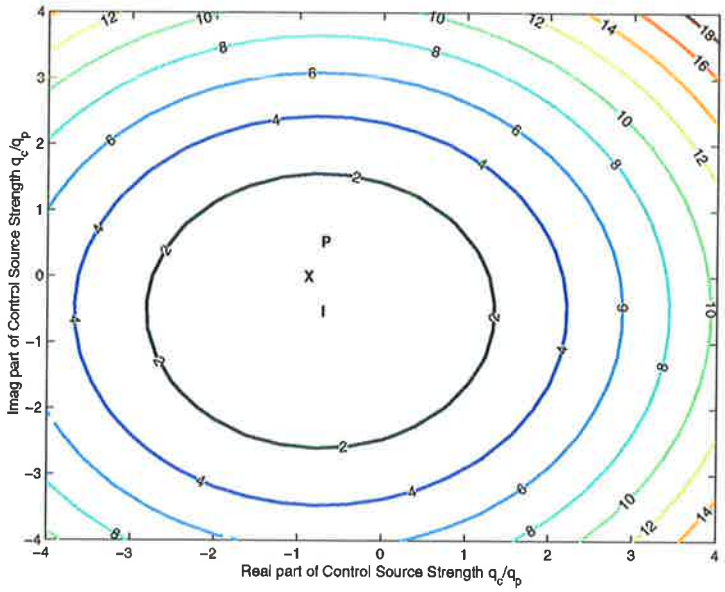


*(b) Radial active intensity as a function of the real and imaginary parts of the relative control source strength*

*Figure 3.14: Squared pressure amplitude and radial active intensity as a function of the real and imaginary parts of the control source strength $q_c$ relative to a unitary primary source strength, at the sensor location $r_e = (\lambda, 0)$. (the calculations are relative to a unitary primary source strength). **X** indicates the optimal control source strength when minimising acoustic power. **P** indicates the optimal control source strength when minimising squared pressure. **I** indicates the optimal control source strength when minimising radial active intensity.*

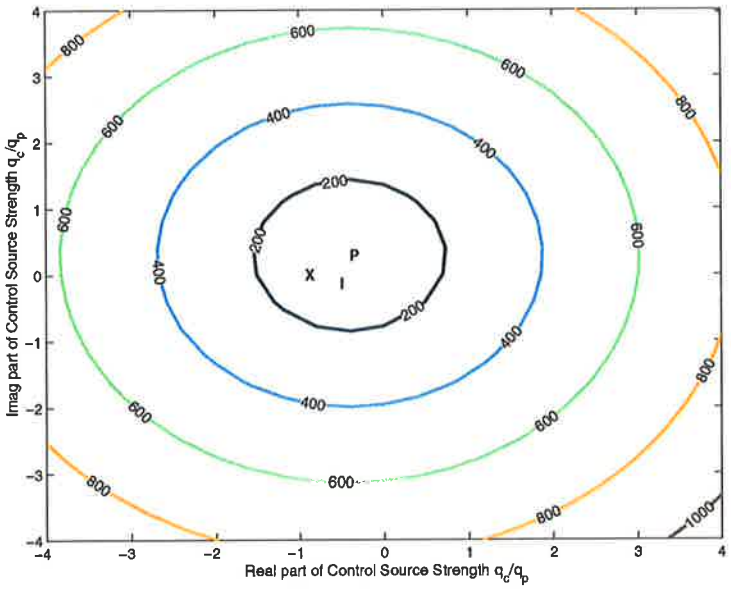


*(a) Pressure amplitude as a function of the real and imaginary parts of the relative control source strength*

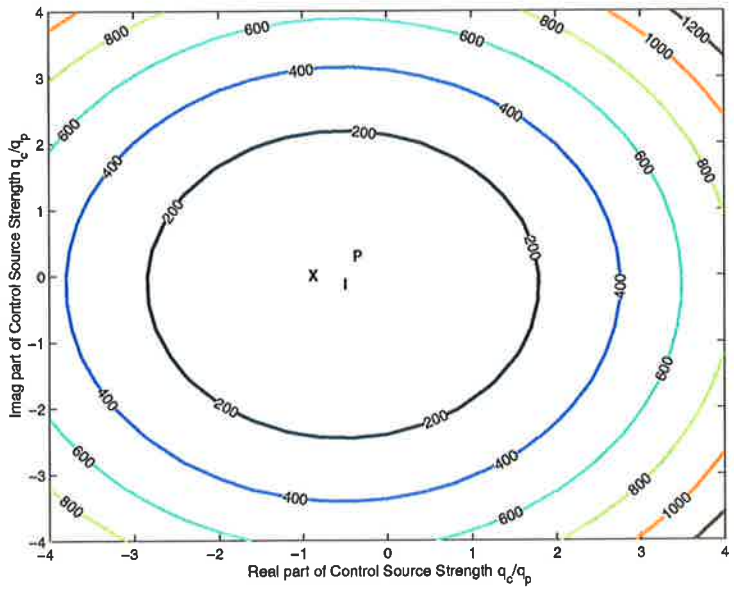


*(b) Radial active intensity as a function of the real and imaginary parts of the relative control source strength*

*Figure 3.15: Pressure amplitude and radial active intensity as a function of the real and imaginary parts of the control source strength $q_c$ relative to a unitary primary source strength, at the sensor location $r_e = (\lambda/5, 0)$. (the calculations are relative to a unitary primary source strength). **X** indicates the optimal control source strength when minimising acoustic power. **P** indicates the optimal control source strength when minimising squared pressure. **I** indicates the optimal control source strength when minimising radial active intensity.*

The result is similar for error sensors located at a position of $\lambda/5$ (see Figure 3.13) from the primary source, just behind the control source, as evident in the error surface plots shown in Figures 3.15a and 3.15b. In this case the intensity minima is slightly closer to the value that will minimise radiated acoustic power than is the pressure minima. Hence at this location acoustic intensity error sensing would produce a superior result, as previously noted in Qiu and Hansen (1997).

The results are very different, however, for an error sensing location of $\lambda/20$ (see Figure 3.13) from the primary source, mid way between the primary and control sources. Referring to Figure 3.16b, observe that with acoustic intensity there is no global minimum. In fact, the point of inflexion is a global maximum.

To examine this result further, consider the results where the imaginary part of the control source volume velocity is equal to zero. The plot of the intensity error surface as a function of (the real part of) control source volume velocity is illustrated in Figure 3.17a.

Observe that there are two points where intensity amplitude becomes zero (actually a locus of infinitely many points where intensity amplitude is zero, see Figure 3.16b): where the control source volume velocity is equal in amplitude and phase to the primary source volume velocity, and where the control source volume velocity is equal in amplitude and opposite in phase to the primary source volume velocity. To explain why there are two locations of zero intensity, the acoustic pressure and particle velocity at the error sensing location are also plotted for this range of control source volume velocities, in Figures 3.17b and 3.17c, respectively. Observe that one of the points of zero intensity corresponds to a point of zero acoustic pressure. The other corresponds to a point of zero acoustic particle velocity. Referring to the plot of sound power attenuation in Figure 3.17d, it is clear that the point corresponding to zero acoustic pressure produces the desired power attenuation, while the point corresponding to zero acoustic particle velocity equates to an increase in total acoustic power output.

It is worthwhile considering these results in terms of active noise control system implementa-

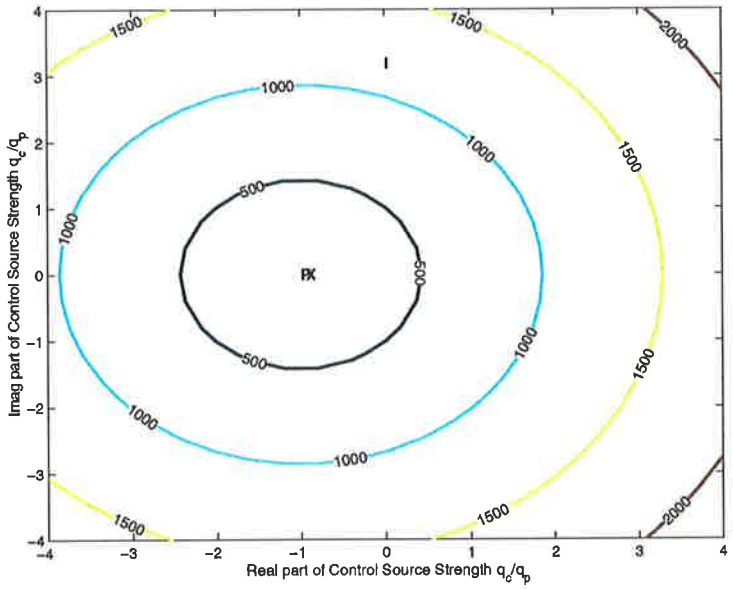


*(a) Pressure amplitude as a function of the real and imaginary parts of the relative control source strength*

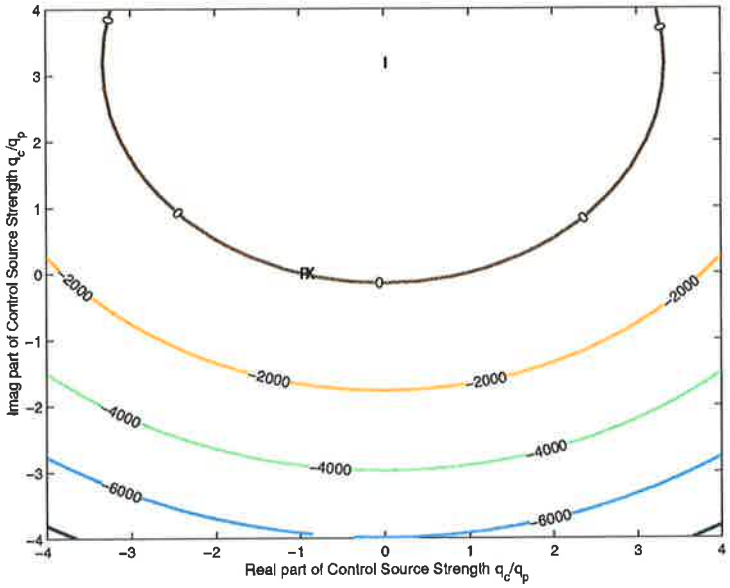


*(b) Radial active intensity as a function of the real and imaginary parts of the relative control source strength*

*Figure 3.16: Pressure amplitude and radial active intensity as a function of the real and imaginary parts of the control source strength $q_c$ relative to a unitary primary source strength, at the sensor location $r_e = (\lambda/20, 0)$. (the calculations are relative to a unitary primary source strength). **X** indicates the optimal control source strength when minimising acoustic power. **P** indicates the optimal control source strength when minimising squared pressure. **I** indicates the optimal control source strength when minimising radial active intensity.*

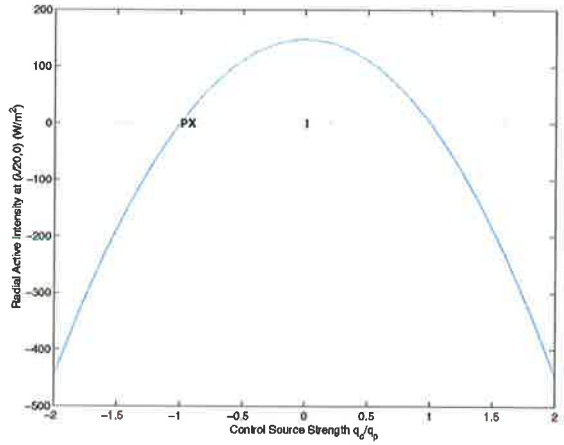


(a) radial active intensity amplitude as a function of relative control source strength

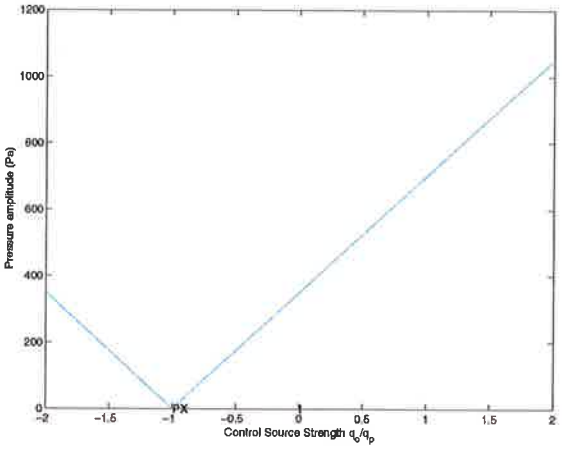


(b) pressure amplitude as a function of relative control source strength

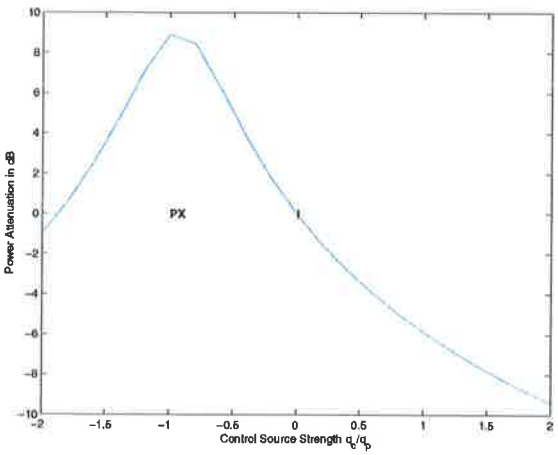


(c) Sound power attenuation in dB as a function of relative control source strength

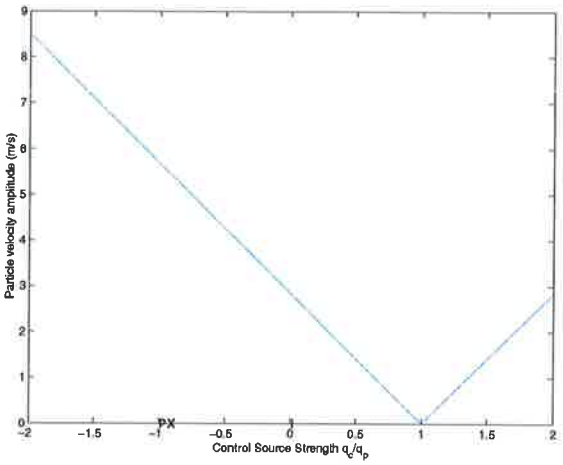


(d) particle velocity amplitude as a function of relative control source strength

*Figure 3.17: Radial active intensity amplitude, Sound power attenuation, pressure amplitude and particle velocity amplitude as a function of the control source strength $q_c$ relative to a unitary primary source strength, at sensor location $r_e = (\lambda/20, 0)$. (the calculations are relative to a unitary primary source strength).* ***X*** *indicates the optimal control source strength when minimising acoustic power.* ***P*** *indicates the optimal control source strength when minimising squared pressure.* ***I*** *indicates the optimal control source strength when minimising radial active intensity.*

tion. First, for the simple monopole example being considered here, there is little difference between the pressure and intensity minimisation results when the sensor is remote from the sources. Second, in some error sensing locations, particularly between the primary and control sources, there is no global minimum in the intensity error surface. Finally, if the error criterion is modified to be intensity amplitude, then there are two points where the error criterion has a zero value: one where acoustic pressure is equal to zero, and one where acoustic particle velocity is equal to zero. The use of a control source volume velocity corresponding to the first of these points yields good sound power attenuation. The use of a control source volume velocity corresponding to the first of these points results in an increase in sound power output.

In short, the use of a sound intensity error criterion for the simple monopole radiation case offers little improvement over the acoustic pressure error criterion at best, and can lead to greatly reduced performance in some sensing locations.

## 3.4 Experimental verification of the acoustic power attenuation of a single monopole primary source and single monopole control source

### 3.4.1 Introduction

Experiments were undertaken to verify several of the key results from the previous simulation study. Referring to Figure 3.18, the experiments were conducted in an anechoic chamber, with a 100Hz sine wave reference signal used as input to both the primary and control speakers. Active control was achieved by manually adjusting the amplitude and phase of the control speaker signal with respect to the primary speaker signal. Tuning was undertaken by visually monitoring either the active intensity or acoustic pressure from the intensity probe on the

signal analyser and adjusting the output so that the active intensity *amplitude* or pressure is minimised. The pressure distribution at a distance of 1.8 metres from the primary source was then measured before and after control. The 1.8 metres radius was the maximum distance allowed by the anechoic room dimensions.

## 3.4.2 Enclosed speaker

### 3.4.2.1 Introduction

In order to model in experiment an acoustic monopole, an enclosed speaker was used (see Figure 3.19). It has been shown (Beranek (1996), Small (1972b), Small (1972a) and Small (1973)) that at low frequencies a speaker can be approximated as a monopole source. The pressure amplitude generated by the enclosed speaker, used in the experiments, was measured radially away from the speaker, and a directivity measurement was made, to verify that it was a suitable model for an acoustic monopole source.

### 3.4.2.2 Enclosed speaker specifications

The enclosed speaker (see Figure 3.21) used consisted of a 110mm SEAS Driver Model number W11CY001. The driver was enclosed in an unported enclosure which consisted of PVC plumbing pipe 165mm in diameter and 200mm long, with a wall thickness of 5mm (see Figure 3.20).

The enclosed speaker has a sensitivity of 86dB/mW and a nominal impedance of 8Ω. The maximum input power was 75Wrms.

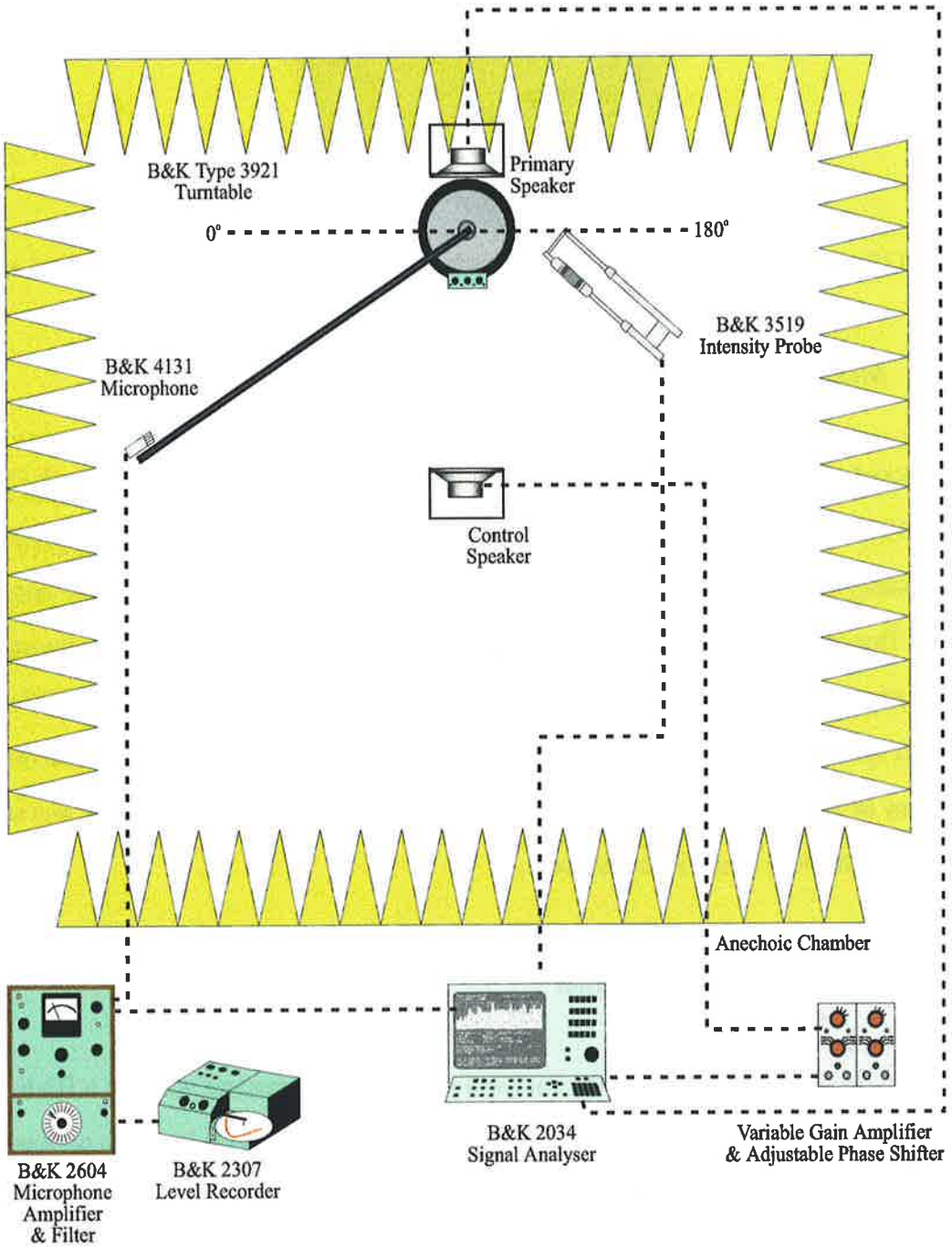


*Figure 3.18: Experimental setup for the measurement of the far field pressure attenuation achieved by active control of 100Hz tonal noise radiated from a monopole primary source and cancelled by a single monopole control source.*

*Figure 3.19: Custom made enclosed speaker, made from 165mm PVC plumbing pipe and a SEAS driver.*

#### 3.4.2.3 Monopole approximation

An enclosed speaker can be modelled as a circular piston in an infinite baffle (Beranek (1996), Small (1972b), Small (1972a) and Small (1973)). It was shown that when the circumference of the piston is less than half the wavelength, the piston behaves essentially like a monopole source. That is at low frequencies (where $ka < \frac{1}{2}$, $k$ being the wave number and $a$ the speaker radius) an enclosed speaker can be considered as a monopole source (Beranek (1996)). The enclosed speaker used in the following experiments has a radius of $a = 55mm$. Driven at a frequency of 100Hz, $ka = 0.1$. As this is much less than 0.5, the enclosed speaker was able to model the behaviour of monopole sources.

#### 3.4.2.4 Radial pressure distribution

The radial pressure distribution of the enclosed speaker was measured with the a B&K Type 4131 condenser microphone starting at the speaker front face, at radial intervals of 50mm. A 3 metre length of 30 by 30mm Aluminum angle section with holes drilled at 50mm intervals to fit the 1/2" B&K Type 4131 condenser microphones was used to measure the pressure transfer function, between the speaker input and the B&K Type 4131 microphone output. The experimental setup is shown in Figure 3.22.

The experiment was conducted in an anechoic chamber (dimensions over wedge tips: 4.79m $\times$

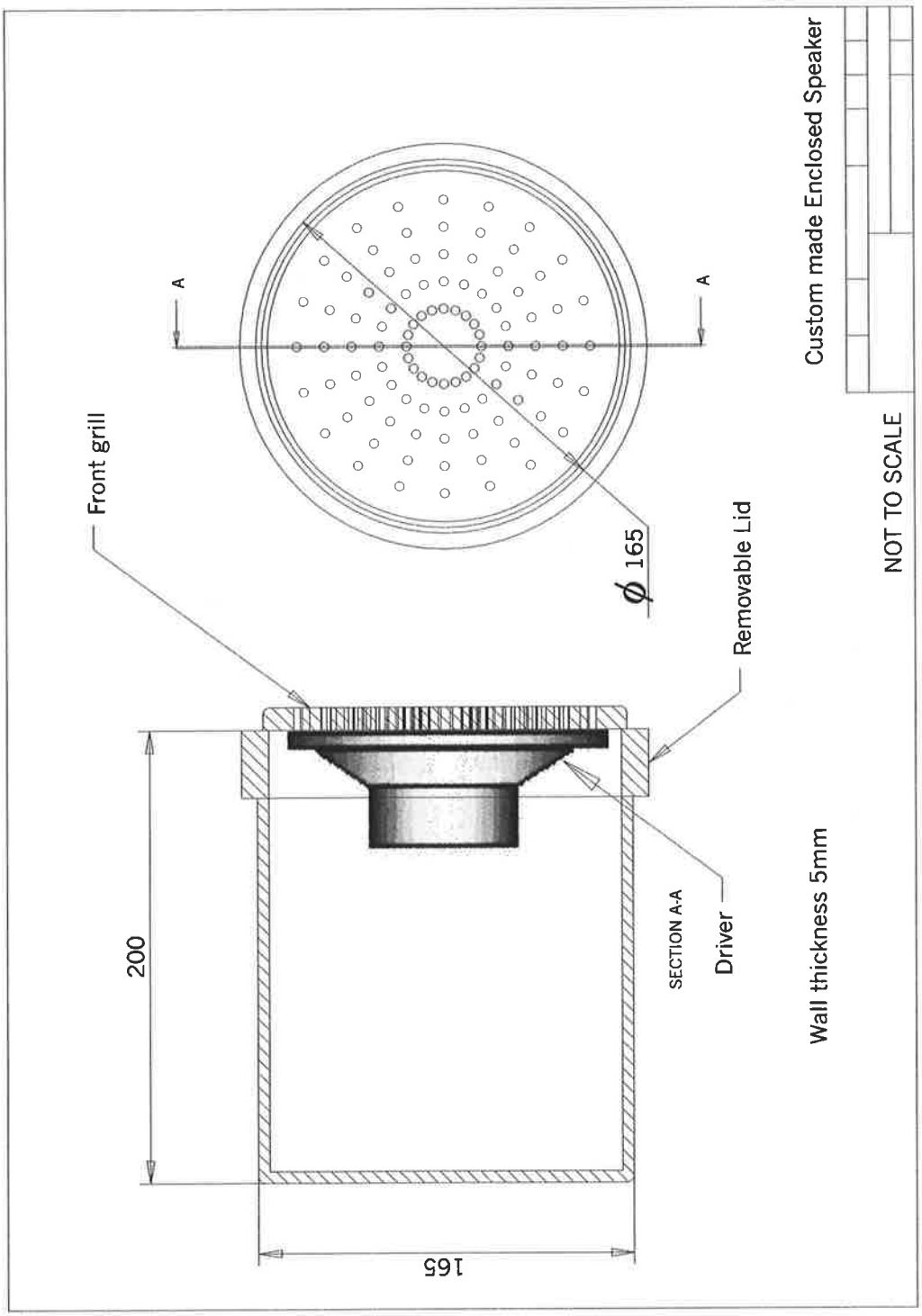


*Figure 3.20: Engineering drawing of custom made enclosed speaker.*

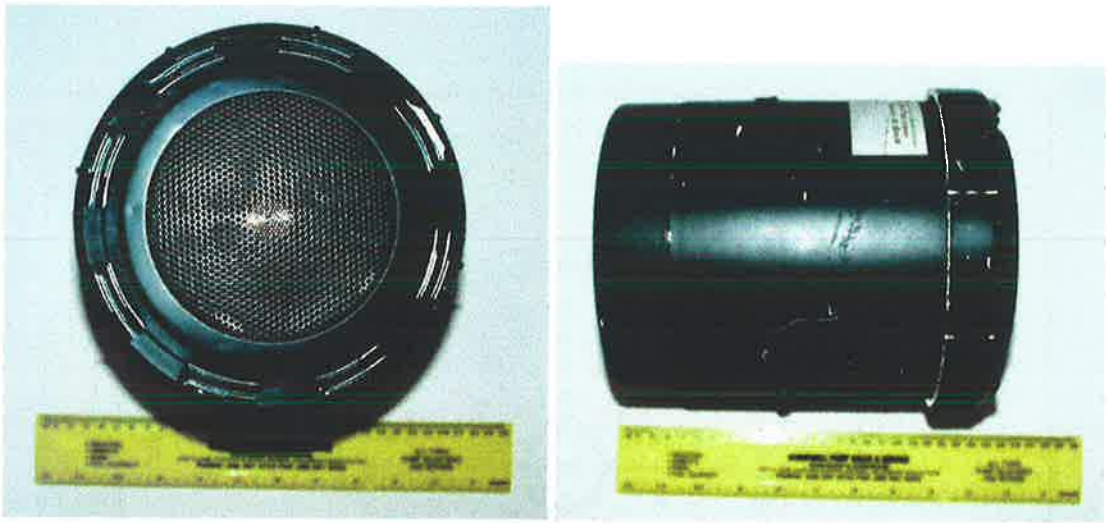

*Figure 3.21: Custom made enclosed speaker, made from 165mm PVC plumbing pipe and a 110mm diameter SEAS driver.*

3.9m × 3.94m) with a lower cut-off frequency of 85Hz. The speaker was driven with random noise and at each 50mm interval location the acoustic signal was measured with the B&K Type 4131 condenser microphone. The Hewlett Packard 35665A Digital Signal Analyser was used to measure the transfer function between the speaker output and the microphone input. 100 linear averages were used in the transfer function measurement. The radial pressure distribution produced is shown in Figure 3.23.

The B&K Type 4131 condenser microphone was not calibrated and hence Figure 3.23 shows the relative pressure amplitude and not the sound pressure level. The objective was to obtain transfer function measurements for the estimation of the optimal sound power attenuation without the construction of a control system, hence calibration of the microphone signal was not done. Very close to the speaker (approximately 50mm) the radial pressure distribution diverges from that of an idealised monopole source because of the near field of the finite sized speaker. At distances greater than 50mm, the enclosed speaker fits the 6dB per doubling of distance characteristic of a monopole source.

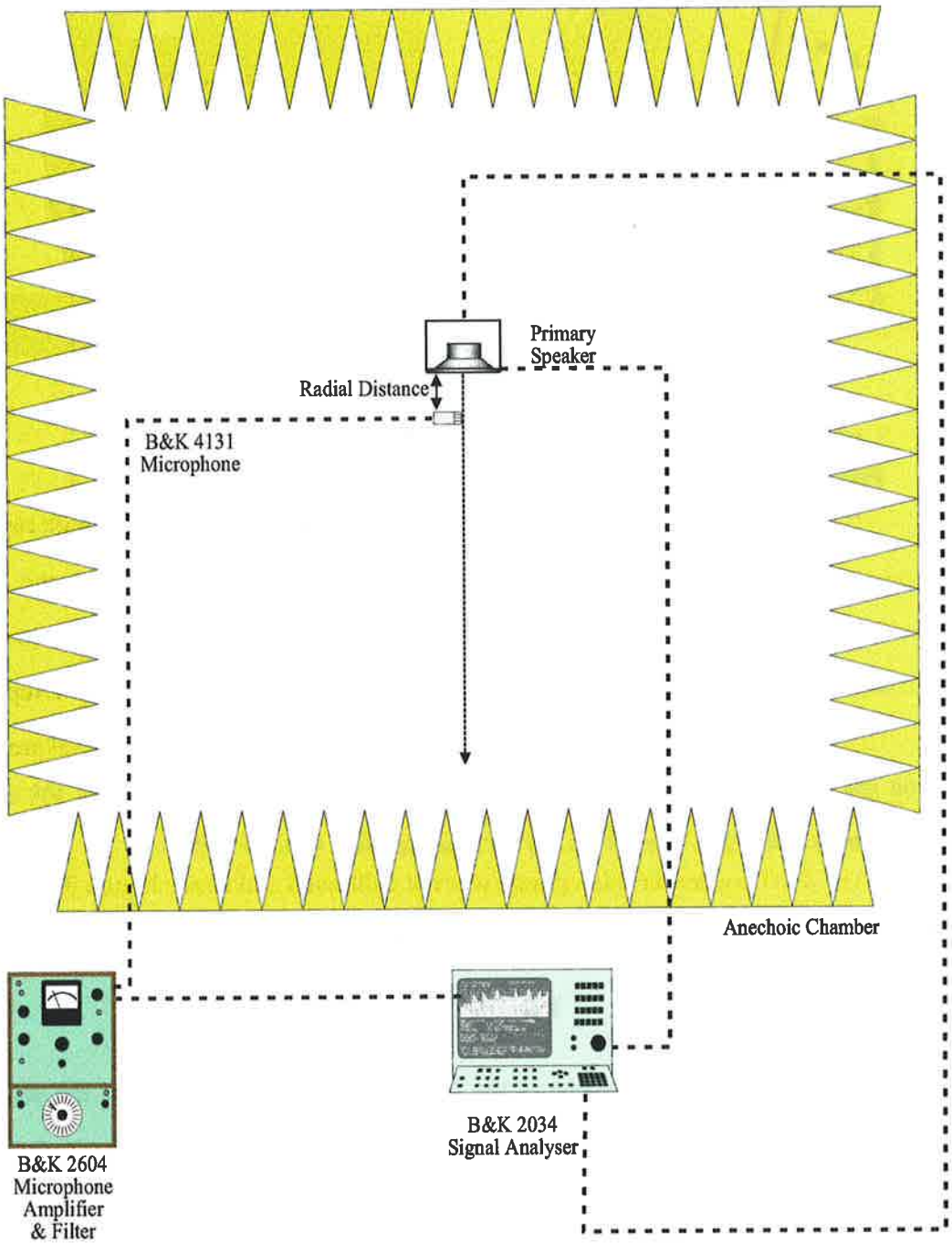


*Figure 3.22: Experimental setup for the measurement of the radial pressure distribution of an enclosed speaker model of a monopole source.*

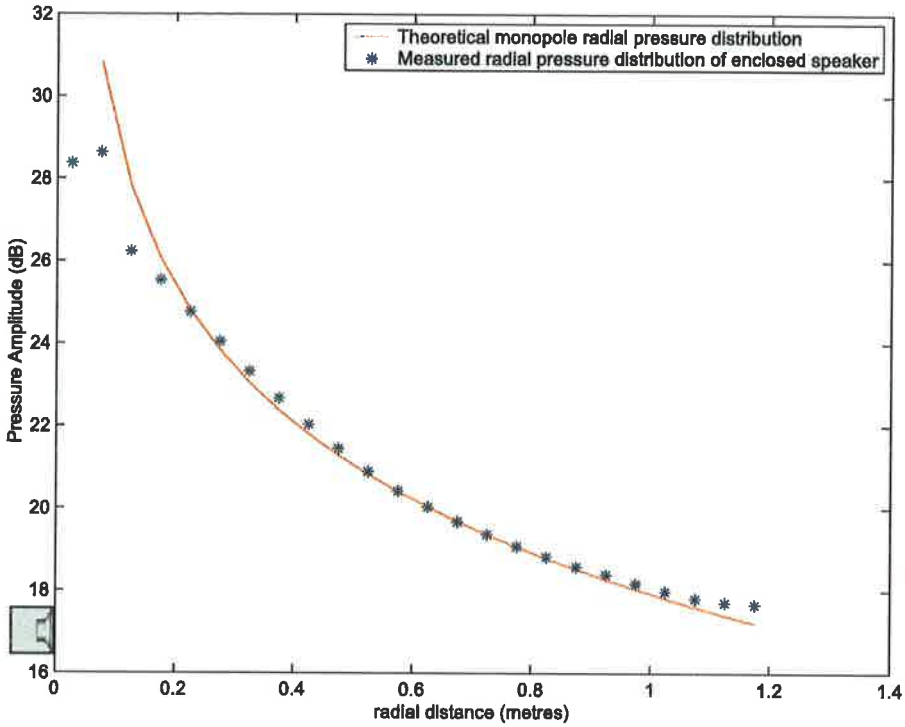


*Figure 3.23: Radial relative pressure distribution of enclosed speaker.*

#### 3.4.2.5 Radial active intensity distribution

Based on the transfer function measurements described in the previous section, the active intensity along a radial line away from the enclosed speaker was calculated.

Consider the active intensity of the monopole source given by

$$\mathbf{I} = \frac{1}{2} Re\{p^* \mathbf{u}\} \tag{3.31}$$

where $p$ is the acoustic pressure at one of the measurement locations and $\mathbf{u}$ is the acoustic particle velocity also at that measurement point. To calculate the active intensity the two-microphone technique described by Kristiansen (1981), Krishnappa and McDougall (1989), Fahy (1995) was used. 24 measurements were made, spaced 50mm apart, in this arrangement the same microphone (B&K Type 4131). Hence there was no phase matching of the microphones necessary. The acoustic pressure amplitude was taken to be the average of two consecutive microphone measurements by

$$p = \frac{p_1 + p_2}{2} \tag{3.32}$$

and the particle velocity is given by (Kristiansen (1981), Krishnappa and McDougall (1989), Fahy (1995)) as

$$\mathbf{u} = \frac{-(p_2 - p_1)}{j\rho\omega d} \tag{3.33}$$

where ρ, ω are defined as before. $d$ is the separation distance between microphone measurements (50mm). $p_1$ and $p_2$ are the acoustic pressure amplitudes at consecutive measurement locations. $d$ was selected to minimise measurement errors (as shown in Appendix C). Using equations (3.32) and (3.33) and substituting them into (3.31) the active intensity can be calculated. Figure 3.24 shows the active intensity as a function of radial distance away from the enclosed speaker.

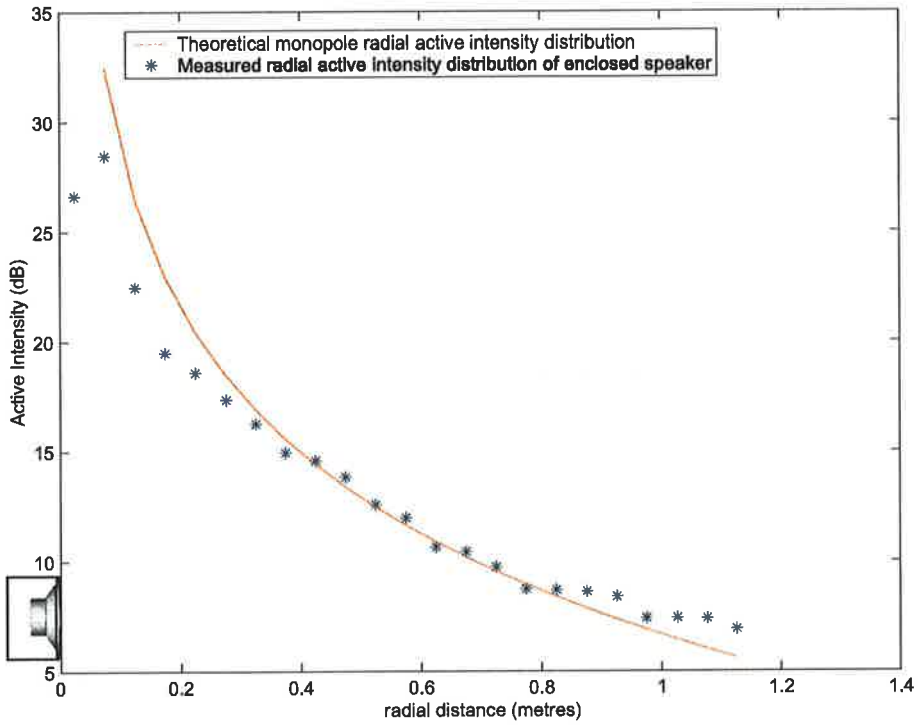


*Figure 3.24: Radial relative active intensity distribution of the enclosed speaker*

It can be seen in Figure 3.24 that the measured relative active intensity does not lie as closely to the theoretical monopole radial active intensity distribution, as the measured pressure to the

theoretical monopole radial pressure distribution shown in Figure 3.23. This is most probably due to errors induced by variations in the separation distance $d$.

#### 3.4.2.6 Enclosed speaker directivity pattern

To further test the accuracy of modelling a monopole source by an enclosed speaker, an experiment was done to measure the directivity of the enclosed speaker. Figure 3.25 shows the setup used. The enclosed speaker was mounted on the floor of the anechoic chamber. On top of the enclosed speaker a B&K Type 3921 Turntable is positioned with a microphone stand and boom (1.8 metres) attached. A B&K Type 4131 condenser microphone is used to measure the produced sound field. A B&K Type 2034 Signal Analyser is used to generate a tone at 100Hz which is fed to the enclosed speaker. The resultant sound field is measure by the B&K Type 4131 condenser microphone which is 1/3 octave band pass filtered in the 100Hz 1/3 octave band. The signal from the filter is fed to a B&K Type 2307 Level Recorder and the signal is plotted on polar plotting paper. The results were scanned into a computer with Corel Trace™. In order to convert the data into a useful electronic format, a number of points were entered into Matlab™ from the traced data. The directivity plot is shown in Figure 3.26. The points entered into Matlab™ are indicated in Figure 3.26 by *. It is noted that the directivity is almost constant, with only slight deviation in radius by approximately 2dB.

#### 3.4.2.7 Enclosed speaker frequency response

The frequency response of the speakers was next measured. Experimental equipment to measure the frequency response of the enclosed speaker was set up as shown in Figure 3.22. The signal generator on the Hewlett Packard 35665A Digital Signal Analyser was used to generate random noise, which was input into the enclosed speaker. A B&K Type 4131 condenser microphone put through a B&K Type 2604 Microphone Amplifier was used to measure the response of the speaker at a distance of 1.8 metres.

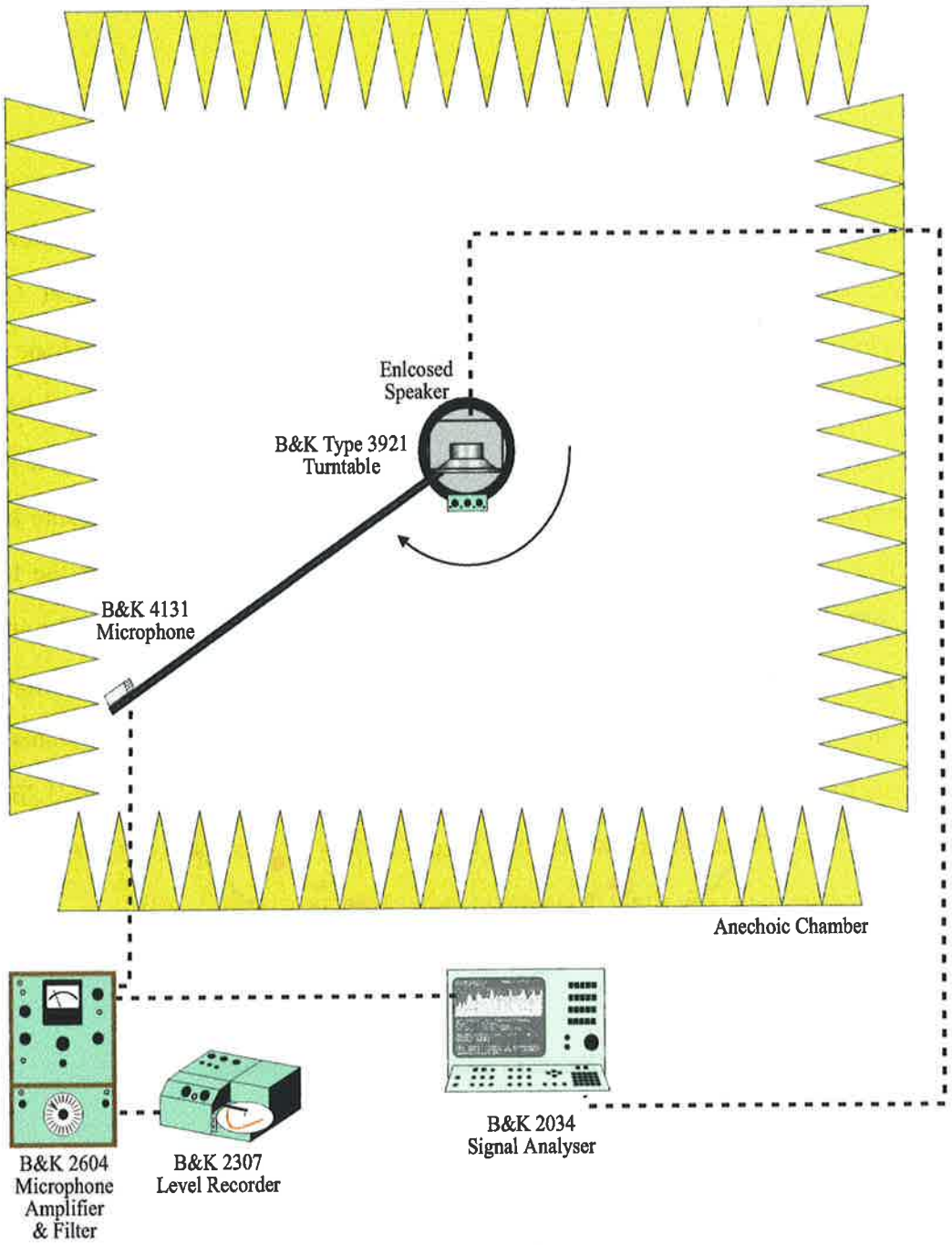


*Figure 3.25: Experimental setup for enclosed speaker.*

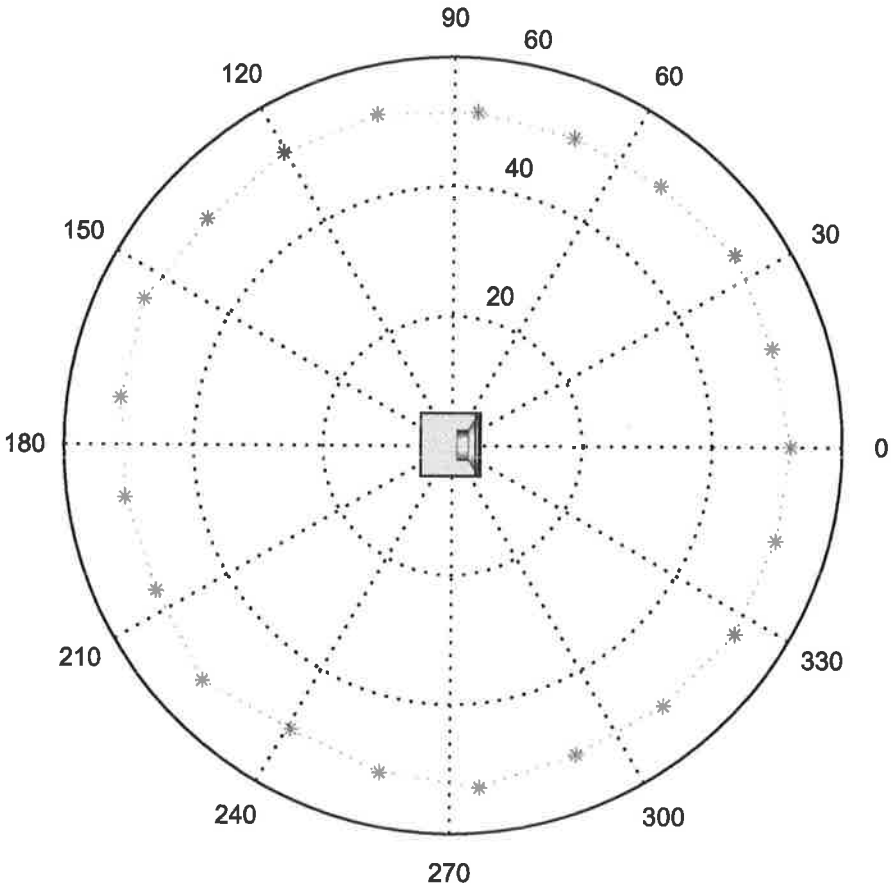


*Figure 3.26: Directivity pattern of enclosed speaker.*

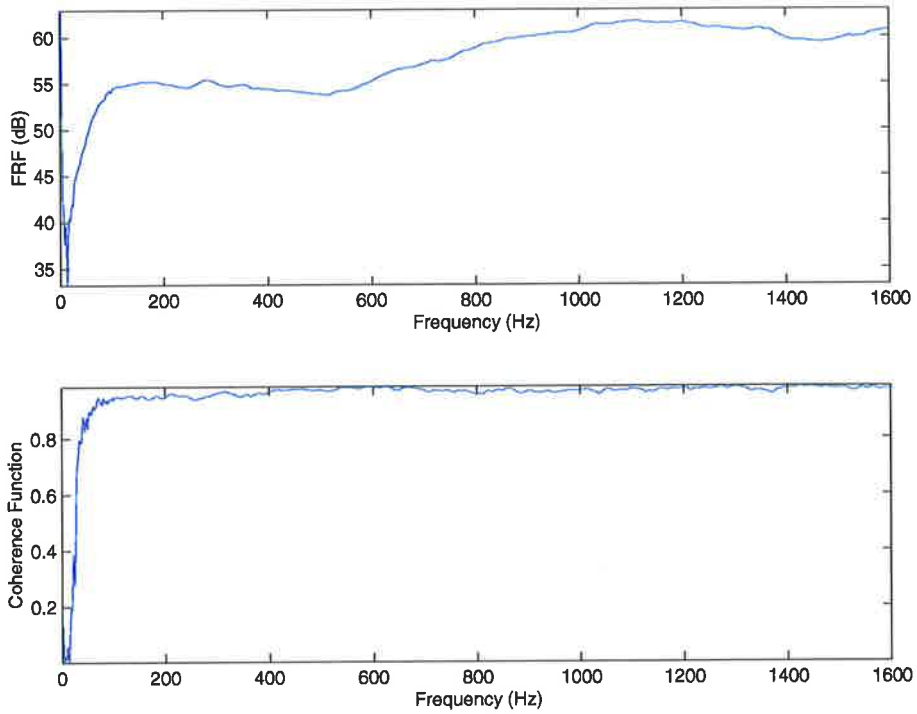


*Figure 3.27: Frequency response function of enclosed speaker and coherence function in the frequency range 0 to 1.6kHz.*

The frequency response and coherence function in the frequency range of 0 to 1600Hz is shown in Figure 3.27. The response is reasonably flat deviating by only approximately 5dB. The coherence function shows good coherence and hence the measurement is reasonably accurate.

Figure 3.28 shows a zoomed view of the frequency range 0 to 300Hz. At the frequency of interest (100Hz), the coherence was 94% and the response is very flat. It can be seen that at frequencies lower than 50Hz the response is rather poor. This is due to the fact that the acoustic cavity (enclosure) couples with the speaker and the cavity acts like an air spring which is quite stiff at low frequencies, resulting in a poor radiation efficiency at these frequencies.

#### 3.4.2.8 Conclusion

The relative radial pressure and active intensity distributions were measured. The radial pressure distribution fell off at approximately 6dB per doubling of distance, indicating monopole

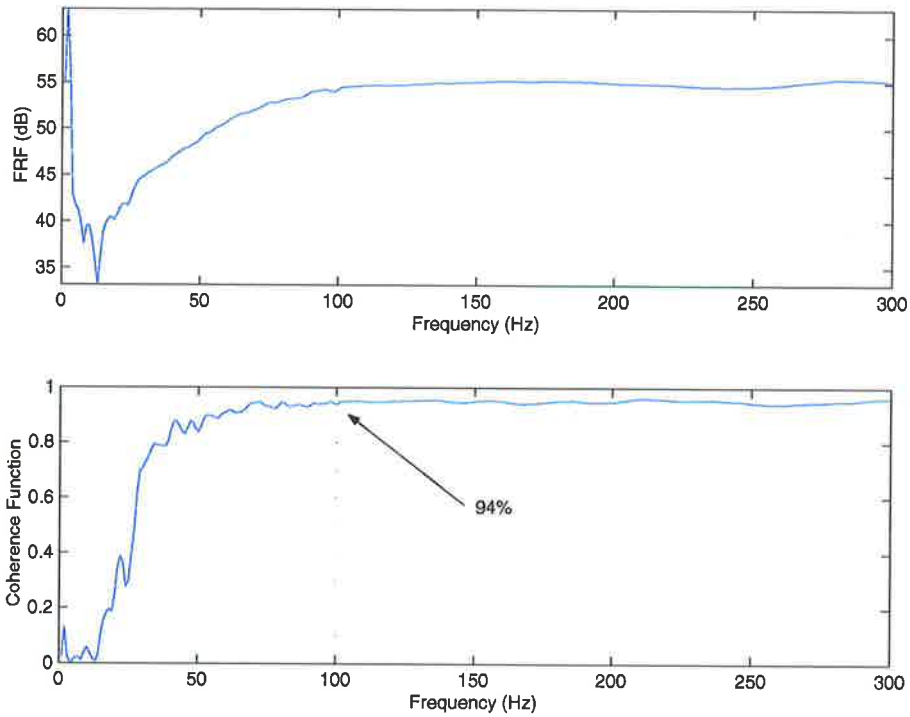


*Figure 3.28: Frequency response function of enclosed speaker and coherence function in the frequency range 0 to 300Hz.*

source behaviour, except very close to the speaker. The directivity of the enclosed speakers was also measured and found to be nearly constant, also indicating monopole behaviour. The frequency response function of the speakers was also measured and found to be reasonably constant above 50Hz. It is therefore concluded that the speakers look like monopoles at low frequencies and are suitable for use in the following experiments.

### 3.4.3 Results

There are two sets of experimental results presented here. The first results employ a transfer function method whereby only the transfer functions between the primary and control source and the error sensors are measured and through quadratic optimisation the optimal attenuation is predicted. Secondly, real control results are presented, where manual control has been used as a working control system capable of handling an intensity error signal was not available at the time that work was done.

#### 3.4.3.1 Measured transfer function method

A technique called the Transfer Function Method has been used by authors such as Baek and Elliott (1993), Baek (1993), Baek and Elliott (1995), Cazzolato and Hansen (1998), Cazzolato (1999b), Li et al. (1999a,b), Kestell (2000), Kestell et al. (2000), Li (2000) to estimate the level of attenuation theoretically achievable with a perfect control system. This method bypasses the need for a real control system, by using transfer function measurements between the primary disturbance and control source and the error sensors and quadratic optimisation theory (Nelson and Elliott (1992)) is used to estimate the level of achievable control. This method can be adapted to include a control signal magnitude and phase error, which simulates more accurately the behaviour of a real control system. It has been previously noted that sound power is difficult to measure in practice. Hence in order to simplify the experimental process, transfer functions between the primary speaker and the error microphone and control speaker and error microphone were measured. The experimental setup is shown in Figure 3.29. Measurement points separated by 50mm were selected. Fahy (1995) has shown that for a frequency of interest of 100Hz a microphone separation distance of 50mm in a p-p type intensity probe arrangement is acceptable.

The primary and control speakers were mounted on stands in an anechoic chamber (dimensions over wedge tips: 4.79m $\times$ 3.9m $\times$ 3.94m) and separated by a distance of $\lambda/10$. The error microphone was moved to 24 locations (spaced 50mm apart) along a radial line passing through both the primary and control sources as shown in Figure 3.29. A Hewlett Packard 35665A Digital Signal Analyser was used to measure the transfer functions. The signal generator on the HP 35665A Digital Signal Analyser was used to drive the primary and control speakers and a B&K Type 4131 condenser microphone put through a B&K Type 2604 Microphone Amplifier which is 1/3 octave band pass filtered in the 100Hz 1/3 octave band was used to measure the response. The primary and control speakers were driven with random noise from the HP 35665A Digital Signal Analyser. 100 linear averages were taken, ensuring that the transfer function was stable.

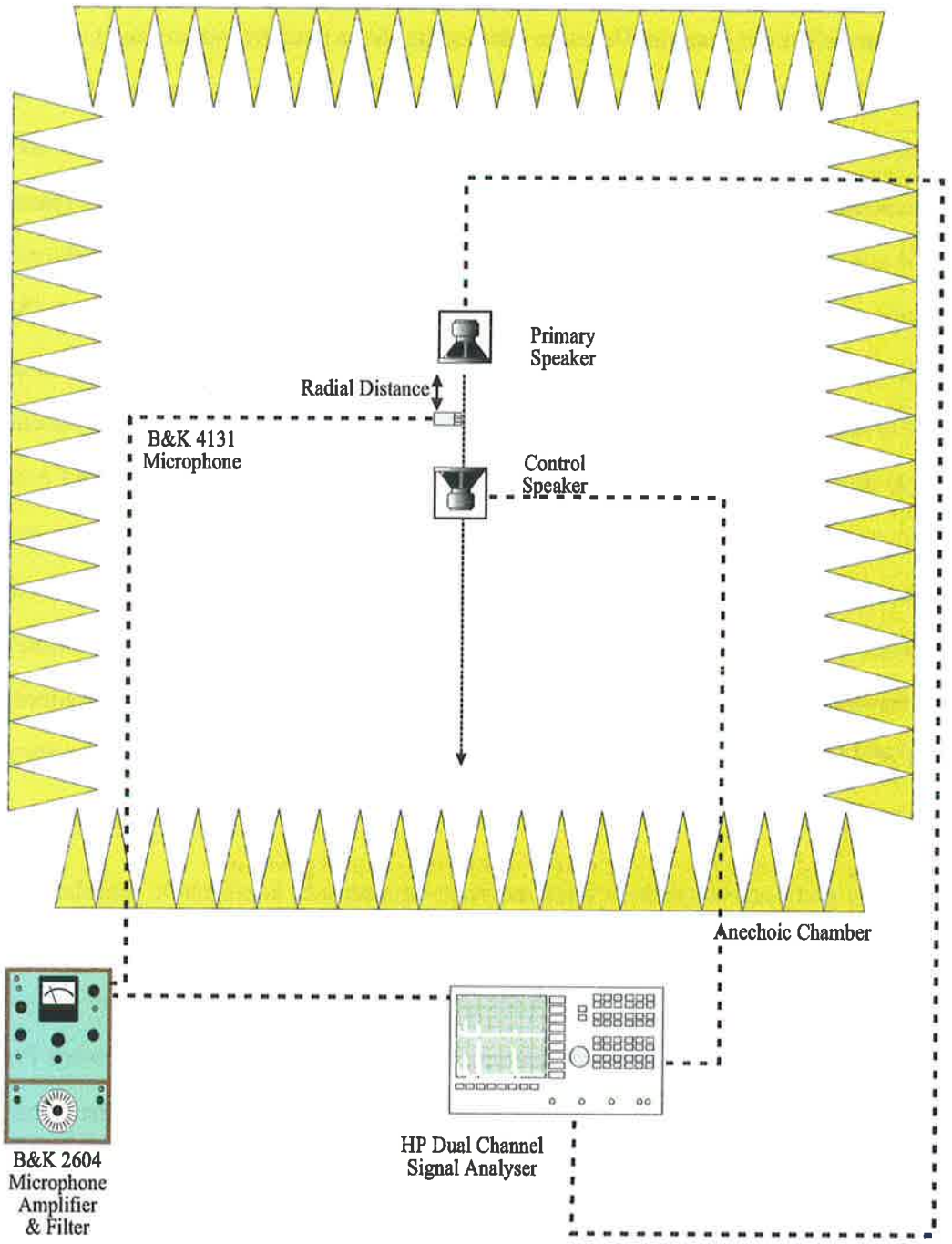


*Figure 3.29: Experimental setup for measurement of the transfer functions between the primary and control speakers and the error microphone. The error microphone was moved to 24 locations separated by 50mm.*

### Sound power estimate

To measure the sound power, the transfer function to 16 far field locations equally spaced on a circle of radius 1.8 metres was also measured.

The power attenuation is given by

$$W_{att} = \frac{W_{before}}{W_{after}} \propto \frac{\sum_{N} |p_{far}|^2_{before}}{\sum_{N} |p_{far}|^2_{after}} \tag{3.34}$$

where the sum is over the $N = 16$ far field transfer function measurement locations. Where

$$p_{far} = Z_{measured} q \tag{3.35}$$

where $Z_{measured}$ is the measured transfer function between the source $q$ (either primary or control) and the far field location.

### Optimal control source strength when minimising sound pressure

The sound pressure transfer function due to the primary and control sources are $Z_p$ and $Z_c$ respectively. The total squared pressure at microphone locations $i$ can be expressed in quadratic form as

$$|p_{total}|^2 = A_p |q_c|^2 + q_c^* b_p + b_p^* q_c + c_p \tag{3.36}$$

where

$$A_p = Z_c^* Z_c \tag{3.37}$$

$$b_p = Z_c^* Z_p q_p \tag{3.38}$$

$$c_p = Z_p^* Z_p \left|q_p\right|^2 \tag{3.39}$$

the optimal control source strength is given by

$$q_{opt,p} = -b_p / A_p \tag{3.40}$$

Substituting equation (3.40) into (3.34), gives the predicted level of power attenuation when the error microphone minimises the squared pressure.

**Optimal control source strength when minimising radial active intensity**

The particle velocity transfer function due to the primary and control sources at the midpoint between microphone locations 1 and 2 in the radial direction are given by

$$\mathbf{H}_p = \frac{-(Z_{p,2} - Z_{p,1})}{jh\omega\rho} \tag{3.41}$$

$$\mathbf{H}_c = \frac{-(Z_{c,2} - Z_{c,1})}{jh\omega\rho} \tag{3.42}$$

where the particle velocity vector is pointing in the radial direction from microphone location 1 towards microphone location 2. The total active intensity in the radial direction can be expressed in quadratic form as

$$\mathbf{I}_{total} = A_I \left|q_c\right|^2 + q_c^* b_I + b_I^* q_c + c_I \tag{3.43}$$

where

$$A_I = \frac{1}{2} Re\{Z_c^* \mathbf{H}_c\} \tag{3.44}$$

$$b_I = \frac{1}{4} q_p (\mathbf{H}_c^* Z_p + \mathbf{H}_p Z_c^*) \tag{3.45}$$

$$c_I = \frac{1}{2} Re\{Z_p^* \mathbf{H}_p\} \left|q_p\right|^2 \tag{3.46}$$

Acoustic reciprocity is assumed. The optimal control source strength is given by

$$q_{opt,I} = -b_I/A_I \tag{3.47}$$

Substituting equation (3.47) into (3.34), gives the predicted level of power attenuation when the error microphone minimises the radial active intensity. The level of sound power attenuation predicted when minimising a sound pressure and radial active intensity cost function is shown in Figure 3.30.

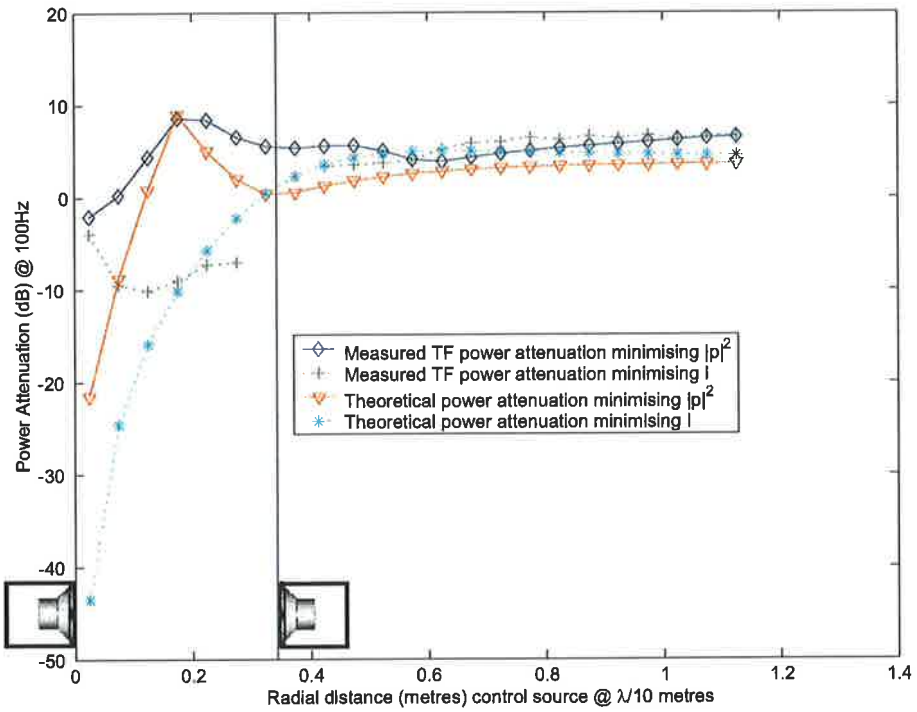


*Figure 3.30: Predicted sound power attenuation using the transfer function technique and theoretically.*

It can be seen that the maximum sound power attenuation is approximately 10dB for this primary and control source configuration (separation distance $d = \lambda/10$). Theoretically there is a predicted maximum sound power attenuation near the midpoint between the primary and control sources when minimising the squared sound pressure. Very close to the primary source the level of power attenuation approaches zero. Close to the control source the power attenuation also drops significantly. However as the radial distance to the error sensor increases so does the level of sound power attenuation. When minimising the active intensity, the theoretically

predicted level of sound power attenuation approaches zero close to the primary source. As the radial distance to the error sensor increases the level of power attenuation increases and becomes significant as the error sensor is moved beyond the control source. The transfer function method results show some discrepancies to that which was predicted theoretically. The results very close to the enclosed speaker sources were affected by a mathematical singularity in the calculations. Also measurements on the transfer function of the enclosed speakers very close to the speaker were inconsistent with a pure monopole source, due to near field effects and measurement error. It is difficult to surmise the exact acoustic centre of the enclosed speaker unit, and hence this impairs the accuracy of the measurements, particularly close to the speaker cone. The dynamic range of the speakers is also a limiting factor on the accuracy of the technique, as can be seen in the results for the minimisation of active intensity very near to the primary source. It can be seen that as the active intensity error sensor is brought close to the primary source the power attenuation is 40dB above that predicted by theory (this is due to the dynamic range of the control system and actuators).

#### 3.4.3.2 Far field pressure distribution

In order to assess the power attenuation of minimising an active intensity cost function over that which is obtained by minimising the squared pressure, control was manually generated through a variable gain amplifier and phase shifter, and the far field (as far away as the dimensions of the anechoic chamber allowed) sound pressure was measured with a microphone attached to a boom and turntable through an arc 180°, before and after control is applied. Figure 3.31 shows the experimental setup. The primary and control sources used were the enclosed pipe speakers described previously. The sources were mounted on stands in an anechoic chamber (dimensions over wedge tips: 4.79m $\times$ 3.9m $\times$ 3.94m) and separated by a distance of $\lambda/10$. A B&K Type 4131 condenser microphone put through a B&K Type 2604 Microphone Amplifier which is 1/3 octave band pass filtered in the 100Hz 1/3 octave band was used to measure the "far field" sound pressure. The B&K Type 4131 condenser microphone was attached

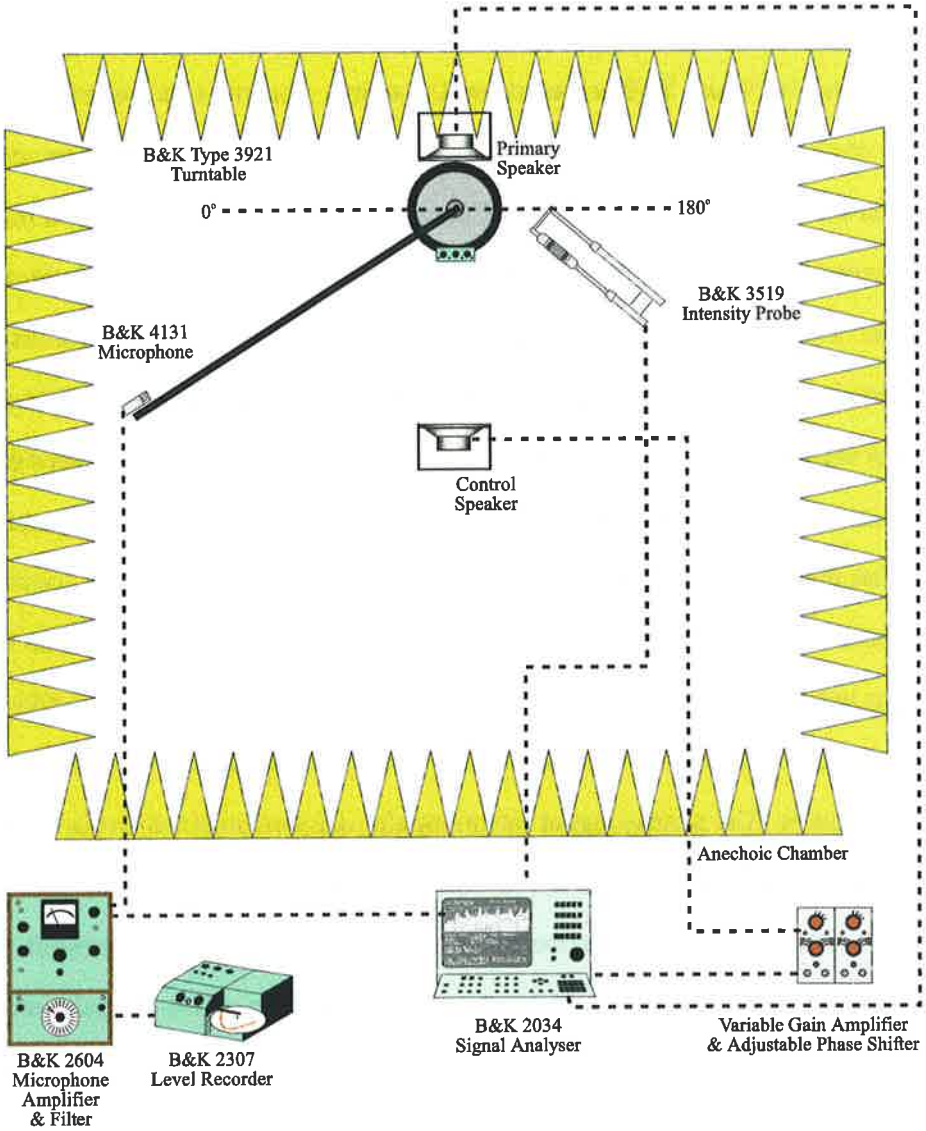


*Figure 3.31: Experimental setup for measuring the far field pressure distribution before and after active control is applied to minimise a squared pressure and active intensity amplitude cost function.*

to a microphone boom which was located just behind the primary source and extended 1.8 metres out. The signal from the B&K Type 4131 condenser microphone was sent to B&K Type 2307 Level Recorder which plotted the results on polar paper. The results were then scanned into a computer using Corel Trace™ and placed on a half circle polar graph. The B&K Type 4131 condenser microphone was not calibrated, since we are only interested in the pressure reduction. Shown in Figure 3.32 is the "control system". For this experiment it was decided for lack of a control system which could handle an active intensity error criterion, that manual control would be used, as was also done by Conover (1956), Pan et al. (1992). It is noted that for later experiments (Chapters 4 - 6) a suitable intensity control system was developed and implemented. The signal generator of the EZ-ANC™ was used to generate a 100Hz signal which was used as a reference signal and as the primary noise source. This 100Hz signal was put through a variable gain amplifier (also on the EZ-ANC™) and a power amplifier and then fed to the primary speaker in the anechoic chamber. The reference signal was passed through a phase shifter and then a variable gain amplifier and then it was fed to the control speaker in the anechoic chamber. A portable B&K Type 2144 Dual Channel Real-Time Frequency Analyser was used to measure the active intensity and pressure amplitude at 100Hz from the intensity probe. A HP Oscilloscope was used to check the actual amplitude reduction of the primary noise source. The control signal was manually adjusted until the levels of the primary noise source had been reduced by between 30 and 40dB. Figure 3.13 shows the location of the error sensors tested in these experiments. Illustrated in Figure 3.33 is the result of far field error sensing with either an acoustic pressure error sensor or an active intensity error sensor. The error sensor was located a distance of $\lambda$ from the primary source (see Figure 3.13). As expected, the outcome when using either a pressure or intensity error signal is similar.

Figure 3.34 shows the result of minimising the pressure and active intensity amplitude at a position closer to the primary and control sources at a distance of $\lambda/5$ from the primary source (see Figure 3.13). As predicted in the simulations, the active intensity result is marginally better than the pressure result in this instance.

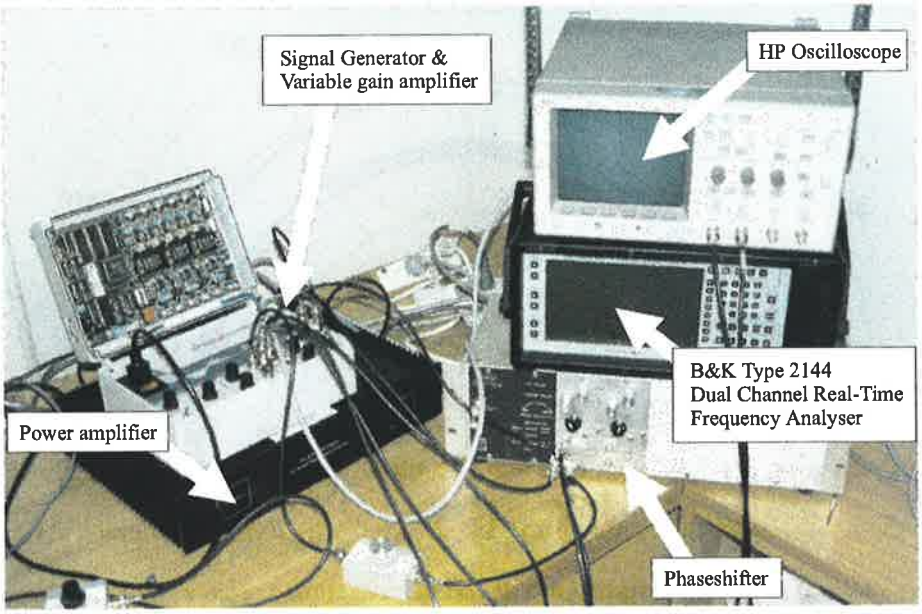


*Figure 3.32: Experimental setup for measuring the far field pressure distribution before and after active control is applied to minimise a squared pressure and active intensity amplitude cost function.*

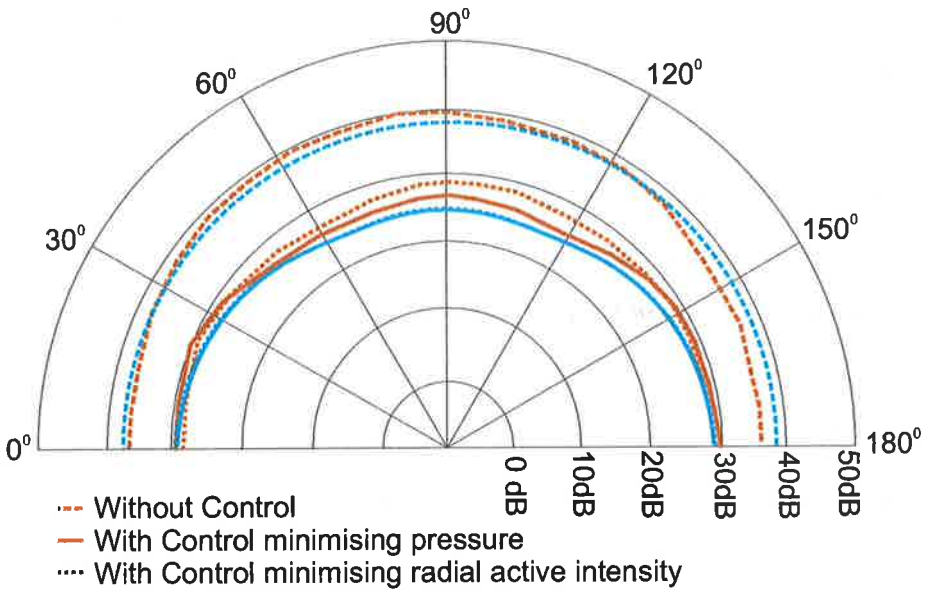


*Figure 3.33: Far field pressure before and after control when employing a single acoustic pressure or radial active intensity error sensor at $\lambda$ from the primary source on the x-axis to control a 100Hz tone from a monopole primary source with a single monopole control source. The red lines indicate the experimental measurements. The blue lines indicate the theoretically predicted results with a 1% error in amplitude and $1^o$ error in phase of the control signal.*

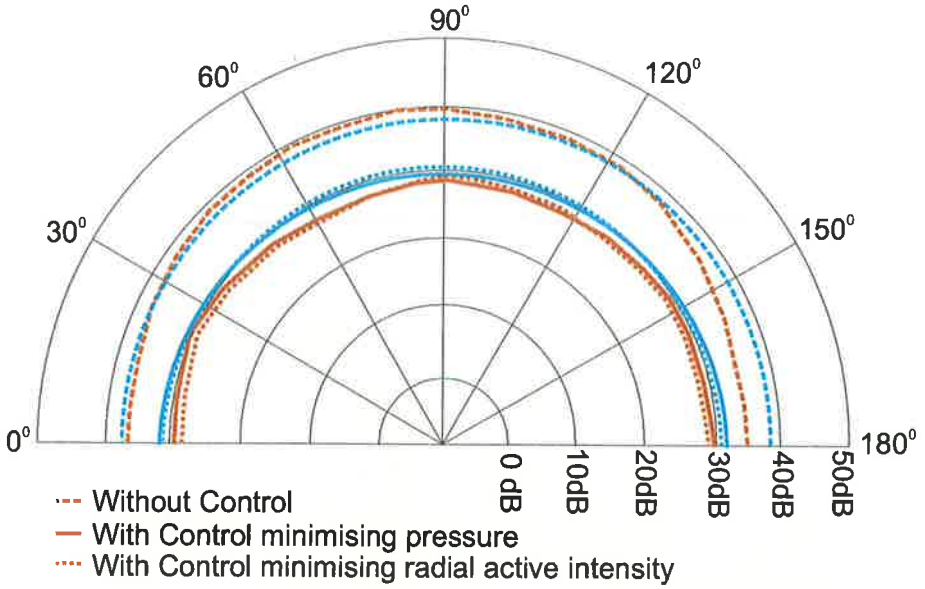


*Figure 3.34: Far field pressure before and after control when employing a single acoustic pressure or radial active intensity error sensor at $\lambda/5$ from the primary source on the x-axis to control a 100Hz tone from a monopole primary source with a single monopole control source. The red lines indicate the experimental measurements. The blue lines indicate the theoretically predicted results with a 1% error in amplitude and $1^o$ error in phase of the control signal.*

Illustrated in Figure 3.35 is the result of sensing the pressure and active intensity amplitude in the near field, between the primary and control sources at a distance of $\lambda/20$ from the primary source (see Figure 3.13). Since active intensity has not minimum at this error sensor location, the active intensity amplitude, instead of the active intensity is a more appropriate error criterion. An active intensity amplitude error criterion is predicted have a locus of infinitely many minima. In the case of the experiment, significant global attenuation was achieved with the pressure error sensor. However when the active intensity amplitude was minimised a net increase in the far field pressure resulted; this arises because an intensity amplitude error criterion can not guarantee a minimum close to the optimal power minimum and hence the performance is potentially much worse.

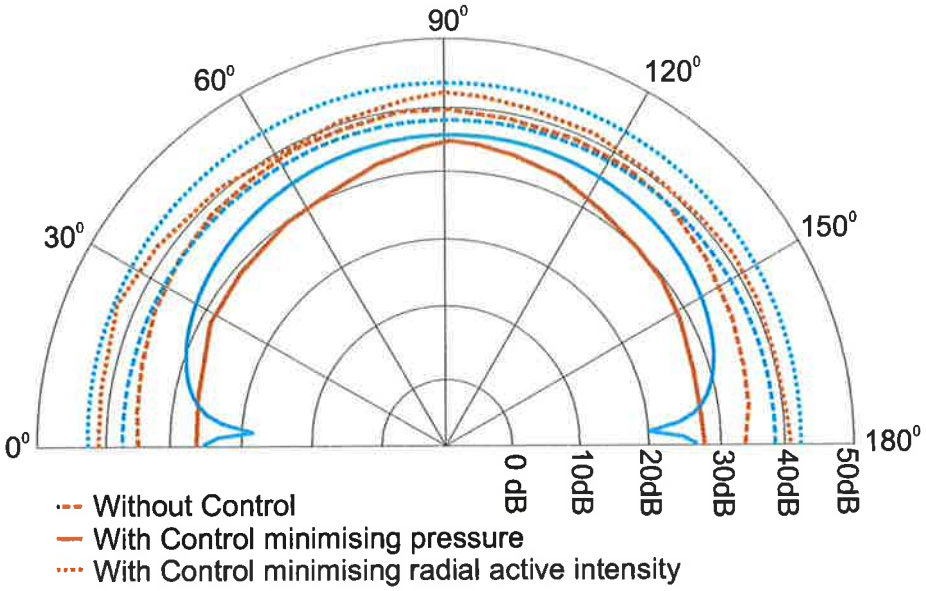


*Figure 3.35: Far field pressure before and after control when employing a single acoustic pressure or radial active intensity error sensor located at $\lambda/20$, halfway between the primary and control sources to control a 100Hz tone from a monopole primary source with a single monopole control source. The red lines indicate the experimental measurements. The blue lines indicate the theoretically predicted results with a 1% error in amplitude and $1^0$ error in phase of the control signal.*

### 3.4.3.3 Active intensity versus control source strength

In order to test the validity of the theoretical prediction of negative active intensity, measurements were made of the active intensity at the midpoint between the primary and control sources at different control source strengths. Figure 3.36 shows the setup used in the experiment. The primary and control speakers were again mounted on stands in an anechoic chamber (dimensions over wedge tips: 4.79m × 3.9m × 3.94m) and separated by a distance of $\lambda/10$ as shown in Figure 3.36. The B&K Type 2134 Sound Intensity Analyser's intensity probe was positioned at the midpoint between the primary and control source and at a distance of $\lambda$ from the primary source along a line passing through the primary and control sources. The primary and control sources were driven by a 100Hz tone. The intensity signal is 1/3 octave band pass filtered in the 100Hz 1/3 octave band.

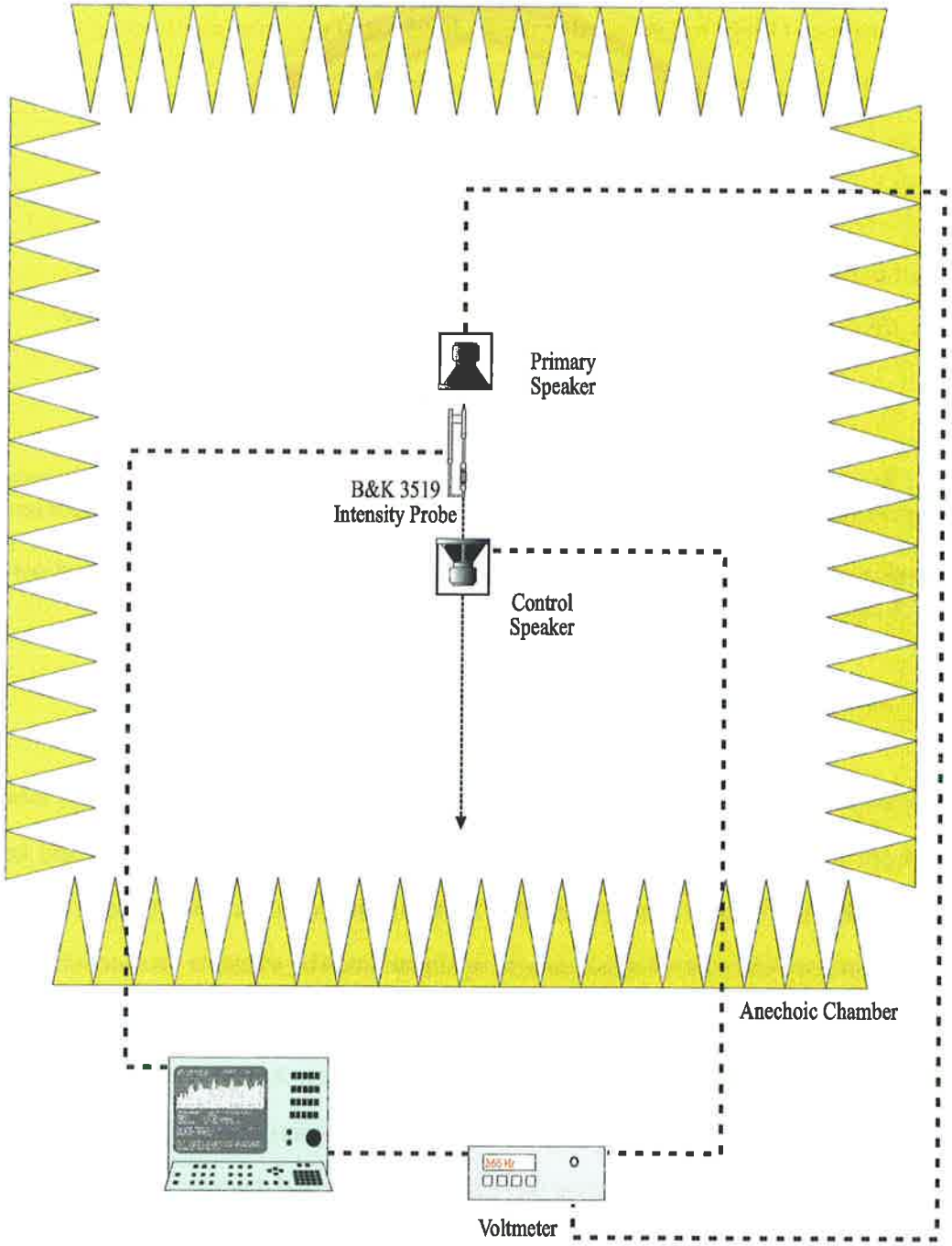


*Figure 3.36: Experimental setup to measure the active intensity located halfway between the primary and control monopole sources at 100Hz at different control source strengths.*

**Relationship of source strength and the speaker input voltage** The only original work that the author could find on modelling real sound sources was by Beranek (1996) and Small (1972b). Beranek (1996) has shown that the far field sound pressure amplitude of an enclosed speaker is directly proportional to the input voltage applied to it .

$$|p| \propto V_{input} \tag{3.48}$$

An exact expression is given by Beranek (1996) for the sound pressure amplitude at distance $r$ at low frequencies by

$$|p| = \frac{f\rho\,|U_c|}{2r} \tag{3.49}$$

where $f$ is the frequency in Hz, $\rho$ is the density of the acoustic medium (air) and $|U_c|$ is the magnitude of the rms volume velocity or the source strength. It is assumed in writing equation (3.49) that $r$ is large with respect to the wavelength of interest.

The magnitude of the rms volume velocity or source strength is given by

$$|U_c| = \frac{V_{input} Bl}{S_D(R_g + R_E)\sqrt{R_A^2 + [\omega M_A - (1/\omega C_A)]^2}} \tag{3.50}$$

where $B$ is the flux density in the air gap in webers per square metre, $l$ is the length of the wire wound on the voice coil in metres, $V_{input}$ is the open circuit voltage of the amplifier driving the speaker, $R_g$ is the generator resistance i.e. the resistance of the power amplifier driving the speaker, $R_E$ is the voice-coil resistance, $S_D$ is the effective area of the speaker cone, $\omega$ is the frequency in radians per second.

$$R_A = \frac{B^2 l^2}{(R_g + R_E)S_D^2} + R_{AS} + R_{AB} + \Re_{AR} \tag{3.51}$$

$$M_A = M_{AD} + M_{A1} + M_{AB} \tag{3.52}$$

$$C_A = \frac{C_{AS} C_{AB}}{C_{AS} + C_{AB}} \tag{3.53}$$

where $R_{AS}$ is the acoustic resistance of the suspensions in mks, $R_{AB}$ is the real part of the impedance of the enclosure presented to the back of the speaker cone, $\Re_{AR}$ is the radiation resistance for a piston in an infinite baffle in mks, $M_{AD}$ is the acoustic mass of the speaker cone and voice-coil in kilograms per metre, $M_{A1} = \frac{0.27\rho}{a}$, where $a$ is the effective radius of the speaker cone, $M_{AB} = \frac{B\rho}{\pi a}$, $C_{AS}$ is the acoustic compliance of the speaker cone suspensions, $C_{AB} = \frac{V_B}{\gamma P_0}$, where $V_B$ is the volume of the enclosure, $\gamma = 1.4$ for air for adiabatic compressions, $P_0$ is the atmospheric pressure in Pascals.

The magnitude of the rms volume velocity or source strength which has been up to now identified by the variable $q$, is directly proportional to the speaker input voltage $V_{input}$. The equations (3.49) and (3.50) from which this relationship was derived, assume that the sound pressure is measured in the far field. The point of interest here is the midpoint between the primary and control source which is at $\lambda/20$ from the primary source, well inside the near field range. At low frequencies the enclosed speaker behaves like a monopole source, and hence has no near field. It is therefore possible to imply a far field relationship between the active intensity $\mathbf{I}$ and the input voltage $V_{input}$. From equation (3.48) the active intensity is directly proportional to the squared input voltage as

$$\mathbf{I} \propto |p|^2 \propto V_{input}^2 \tag{3.54}$$

It is possible to say that the source strength or volume velocity $q$ of an enclosed speaker is directly proportional to the input voltage $V_{input}$. Hence the active intensity is directly proportional to the square of the source strength $q^2$.

#### 3.4.3.4 Results of the relative total active intensity

The intensity probe positioned as described above, was used to measure the active intensity when the primary speaker was driven with a reference voltage $V_p$ at 100Hz and the input voltage to the control speaker $V_c$ was adjusted. The voltmeter in Figure 3.36 was used to

measure the input voltage $V_{input} = V_c$ to the enclosed speakers. The active intensity value and the relative voltage $V_c/V_p$ was recorded. The active intensity values were then converted from dB to a linear scale and the relative voltage $V_c/V_p$ was squared and then plotted in Matlab™.

Figure 3.37 shows total active intensity (from both primary and control sources) relative to the primary active intensity on its own, plotted against the control source strength relative to the primary source strength when the intensity probe is located at the midpoint between primary and control sources. The results show a discrepancy between the theoretically predicted relative total active intensity and that which was measured by experiment described above. Experiment has verified that the active intensity does indeed become negative for certain control source strengths, the difference between theory and experiment can be put down to experimental error. Such as for example the measurement accuracy of the active intensity at a relative control speaker input voltage in dB conversion to a linear scale. The active intensity varied by approximately 10dB across the range of voltages which were measured, sometimes only by 0.2dB between voltage increments.

Figure 3.38 shows total active intensity (from both primary and control sources) relative to the primary active intensity on its own, plotted against the control source strength relative to the primary source strength when the intensity probe is located at a distance of $\lambda$ from the primary source along a line passing through the primary and control sources. Table 3.1 summarises the results. The results show a slight discrepancy between the theoretically predicted relative total active intensity and that which was measured by experiment described previously. Experiment has verified that the active intensity does remain positive definite at this location. The differences between theory and experiment can be put down to experimental error as described before.

| Error Signal | Sensor Location | Comparison | Relevant Figures |
|---|---|---|---|
| Active intensity | $\lambda/20$ | inverted parabola, maximum | 3.37 |
| Active intensity | $\lambda$ | positive definite | 3.38 |

*Table 3.1: Monopole intensity vs source strength results summary table.*

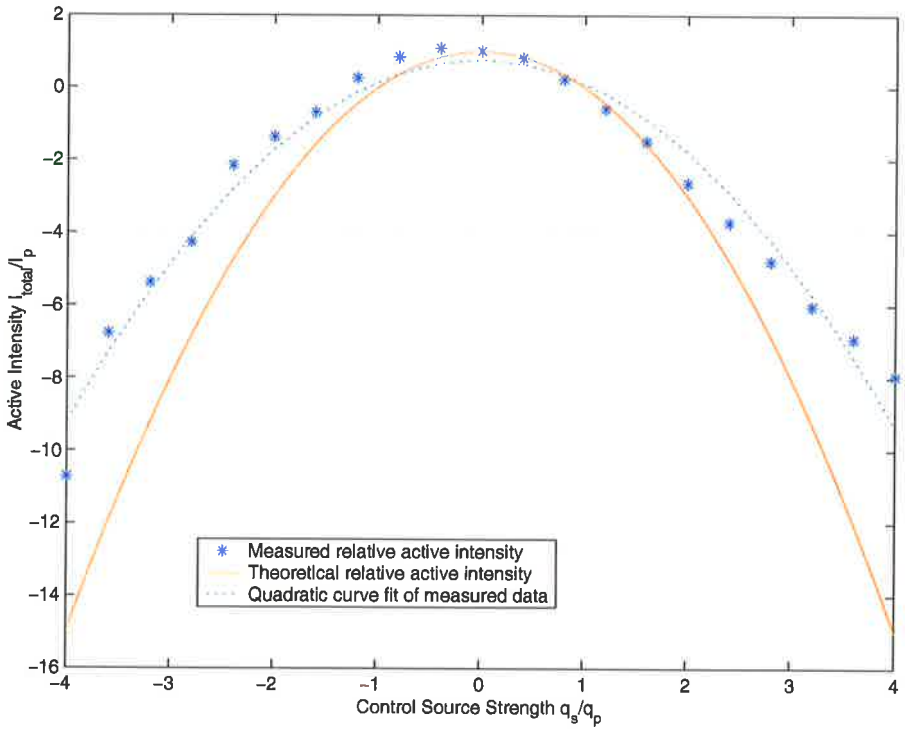


*Figure 3.37: Relative total active intensity plotted against the relative control source strength at the midpoint between the primary and control sources.*

## 3.5 Conclusion

The performance of active control of free field tonal noise from a single monopole primary source via introduction of a single monopole control source using far field error sensing is *not* significantly improved with the use of active intensity error sensors in place of pressure error sensors. A single minimum exists in both the acoustic pressure and active intensity error criteria, at roughly the same control source strength, leading to similar outcomes. Significant differences *do* exist in the pressure and intensity error criteria for sensing locations in the near field. At some near field locations, the global disturbance attenuation that accompanies intensity error sensing is greater than that achieved with pressure error sensing, as previously reported. However, for some sensing locations the active intensity cost function can be made negative and have a maximum value. If intensity amplitude is considered, the cost function is now positive definite, however, it is also no longer quadratic. In this case there may be

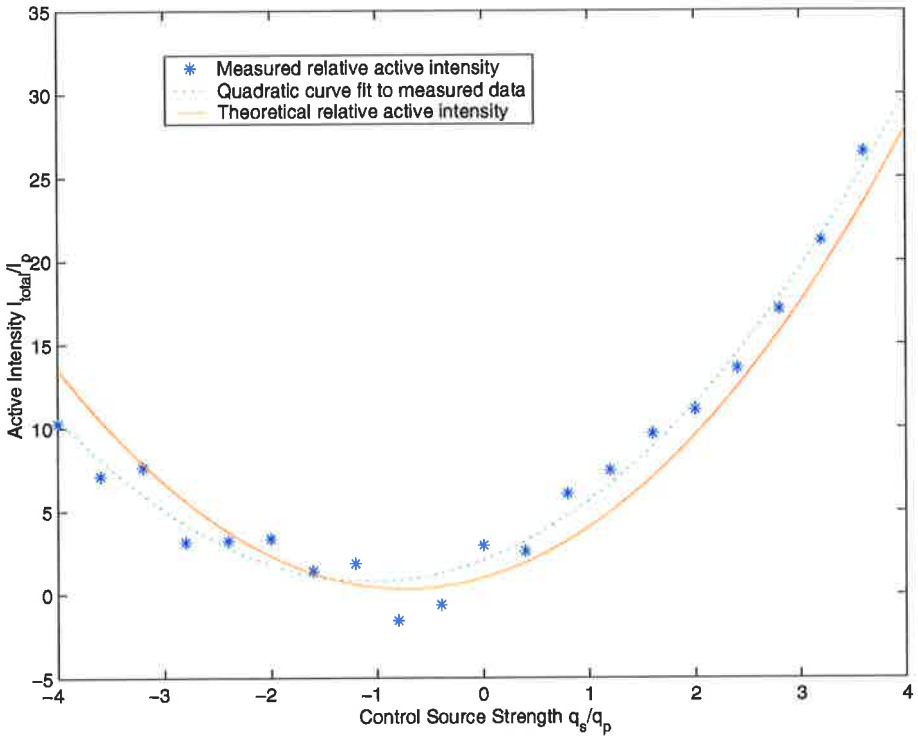


*Figure 3.38: Relative total active intensity plotted against the relative control source strength at a distance of λ from the primary source along a line passing through both primary and control sources.*

infinitely many control source settings that yield a zero intensity result. Furthermore, if one restricts the control source strength to be real, two possible control source settings yield zero intensity. One of these corresponds to a pressure minimum, and one corresponds to a particle velocity minimum. The former of these leads to attenuation of the total radiated acoustic power, while the latter leads to an increase in total power.

The conclusion that must be drawn is that no simple statement can be made about the utility of near field intensity sensing for error signal input in an active control system. In cases where the error sensor location is such that the radial active intensity due to the primary disturbance and control source are both positive, intensity sensing will yield a result (marginally) superior to that achieved with pressure sensing. However, in cases where the error sensor location is such that the radial active intensity due to the primary disturbance is negative or due to the control source is negative, the result can also be much worse.

| Sensor Type | Location | far field Attenuation | Relevant Figures | Comments |
|---|---|---|---|---|
| Pressure | $\lambda/20$ | good | 3.35 | between 9-10dB attenuation |
| Intensity | $\lambda/20$ | very bad (increase) | 3.35 | 6-7dB increase in sound pressure |
| Pressure | $\lambda/5$ | good | 3.34 | between 8-10dB attenuation |
| Intensity | $\lambda/5$ | good | 3.34 | approximately equal to pressure |
| Pressure | $\lambda$ | very good | 3.33 | ~10dB attenuation |
| Intensity | $\lambda$ | very good | 3.33 | slightly worse than pressure |

*Table 3.2: Monopole experimental results summary table.*

# Chapter 4

# Active suppression of a single monopole primary source in an infinite baffle by a single monopole control source

## 4.1 Introduction


*Figure 4.1: Thesis Flow chart.*

Chapter 3 reconsidered the case of active control a monopole source by a single monopole control source as has already been done by (Qiu et al. (1998)). The slightly better performance of active intensity error sensors over that of pressure error sensors just behind the control source, noted by Qiu et al. (1998) has been experimentally confirmed. Furthermore a region described in Figure 3.7, has been found to yield far worse performance by active intensity error sensors. This region is defined by the active intensity cost function possibly being negative and having only a maximum extreme point, instead of the minimum as produced by a positive

definite cost function. Figure 4.1 details the progression of this thesis in examining active intensity error sensing. Chapter 4 considers the case of a monopole source located on an infinite baffle. Chapter 5 considers the case of a simply supported rectangular steel plate. Chapter 6 analyses the practical case of small electrical transformer on a hard floor in an anechoic chamber. Finally Chapter 7 draws conclusions and discusses possible future work.

## 4.2 Theory

### 4.2.1 Introduction

In order to further assess, in simulation, the potential of intensity-based error sensing as part of a feedforward active noise control system implementation in free space, the more realistic problem of controlling acoustic radiation from one monopole source located on an infinite baffle via the introduction of a second monopole source will next be considered. This arrangement is illustrated in Figure 4.2a. This baffled monopole radiation problem is similar to what has been used in fundamental studies of a plane two monopole arrangement in the past, for assessing limits on acoustic power attenuation Nelson and Elliott (1992), the potential of acoustic pressure error sensing Nelson and Elliott (1992), for studies directed at optimising error sensor placement Hansen and Snyder (1997), Qiu et al. (1998), and for studies of acoustic intensity error sensing Qiu et al. (1998). The problem considered here is a more complicated planar radiation problem, which is still easily analysed theoretically in simulations. The previous work on two monopoles in Chapter 3 is extended here to this planar radiation problem.

As outlined in Chapter 3, assessment of the quality of error sensing strategies for the baffled monopole radiation problem requires several steps (restated here):

Step 1: Calculation the acoustic power output of the primary source in the absence of control.

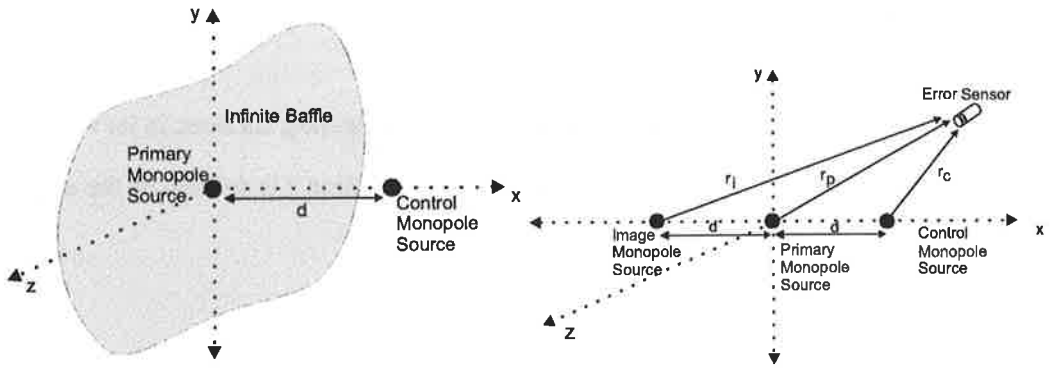


*(a) Single monopole primary source in an infinite baffle and a single monopole control source.*

*(b) Single monopole primary source in an infinite baffle with a single monopole control source and its image source which models the baffle.*

*Figure 4.2: Single monopole primary source in an infinite baffle and a single monopole control source arrangement.*

Step 2: Calculation of the maximum possible acoustic power attenuation for the given control source arrangement.

Step 3: Calculation of the control source volume velocity that will minimise the error criteria of interest (acoustic pressure at a point in space, acoustic intensity at a point in space, etc) for the given error sensing arrangement.

Step 4: Calculation of the total acoustic power output of the primary + control source arrangement using the control source volume velocity from step 3, followed by the acoustic power attenuation through comparison with the original (primary only) acoustic power output.

Step 5: Comparison of the attenuation in step 4 with the maximum possible attenuation for the given control source arrangement calculated in step 2. This will provide some assessment of the efficiency of the error sensing strategy.

### 4.2.2 Minimising the total sound power

Consider first a monopole source with no baffle, or other reflecting surfaces in its vicinity. The sound pressure distribution of such a monopole source at location $\mathbf{r}$ is defined by the expression

$$p(\mathbf{r}) = \frac{j\omega\rho q}{4\pi r} e^{-jkr} = j\omega\rho q G_f(\mathbf{r_q}|\mathbf{r}) \tag{4.1}$$

where $\mathbf{r_q}$ is the location of the source and $G_f$ is the free space Green's function,

$$G_f(\mathbf{r_q}|\mathbf{r}) = \frac{e^{-jkr}}{4\pi r} \tag{4.2}$$

where $q$ is the source strength, $\omega$ is the angular frequency of the source, $\rho$ is the density of the acoustic medium, $k$ is the wave number, $r = |\mathbf{r} - \mathbf{r_q}|$ and $j = \sqrt{-1}$. The radiation transfer function for this source of strength $q$ at location $\mathbf{r}$ is, from equation (4.1),

$$Z_q(\mathbf{r}) = j\omega\rho G_f(\mathbf{r_q}|\mathbf{r}) \tag{4.3}$$

The sound power of a simple monopole source is defined by

$$W = \frac{1}{2}\mathbf{Re}\{qp^*(\mathbf{r})\} \tag{4.4}$$

where **Re** denotes the real part and * denotes the complex conjugate.

Consider now the arrangement shown in Figure 4.2a, the total acoustic power output of the primary monopole source radiating into a half space and control monopole source in front of the baffle at a separation distance $d$ is given by

$$W = \frac{1}{2}\mathbf{Re}\{[p_c(\mathbf{r_c}) + p_p(\mathbf{r_c})]^* q_c + [p_p(\mathbf{r_p}) + p_c(\mathbf{r_p})]^* q_p\} \tag{4.5}$$

where $q_c$ and $q_p$ are the control and primary source strengths respectively and $p_c(\mathbf{r_c})$ and $p_p(\mathbf{r_c})$ are the sound pressures produced at the control source location $\mathbf{r}_c$ by the control and primary sources respectively. Similarly $p_p(\mathbf{r}_p)$ and $p_c(\mathbf{r}_p)$ are the sound pressures produced at the primary source location $\mathbf{r}_p$ by the primary and control sources, respectively.

A source in the presence of a rigid walled baffle of infinite extent can be modelled by replacing the baffle with an image source at $(0,0,-d)$ (Pierce (1989)) as shown in Figure 4.2b, where $d$ is the separation distance between the primary and control sources.

Substituting the radiation transfer functions into equation (4.5) gives

$$W = \frac{1}{2}\mathbf{Re}\{|q_c|^2 Z_c^*(\mathbf{r_c}) + q_c Z_p^*(\mathbf{r_c}) q_p^* + q_p Z_c^*(\mathbf{r}_p) q_c^* + |q_p|^2 Z_p^*(\mathbf{r}_p)^*\} \tag{4.6}$$

where $Z_c(\mathbf{r}) = j\omega\rho G_f(\mathbf{r_c}|\mathbf{r}) + j\omega\rho G_f(\mathbf{r_i}|\mathbf{r})$ and $Z_p(\mathbf{r}) = j\omega\rho G_f(\mathbf{r_p}|\mathbf{r})$

Using the following identity $\mathbf{Re}\{ab^*c^* + a^*bc^*\} = ab^*\mathbf{Re}\{c\} + a^*b\mathbf{Re}\{c\}$, where $a$ and $b$ and $c$ are complex numbers, equation (4.6) can be rewritten as

$$W = \frac{1}{2}[|q_c|^2 \mathbf{Re}\{Z_c(\mathbf{r_c})\} + q_c \mathbf{Re}\{Z_p(\mathbf{r_c})\} q_p^* + q_p \mathbf{Re}\{Z_c(\mathbf{r}_p)\} q_c^* + |q_p|^2 \mathbf{Re}\{Z_p(\mathbf{r}_p)\}] \tag{4.7}$$

By neglecting wind effects the principle of acoustic reciprocity exists and therefore $Z_p(\mathbf{r_c}) = Z_c(\mathbf{r}_p)$, or in other words *the radiation transfer function due to the primary source at the control source is equal to the radiation transfer function due to the control source at the primary source*. The total sound power output can be expressed as a quadratic function of the control source strength Nelson and Elliott (1992)

$$W = A_W |q_c|^2 + q_c^* b_W + b_W^* q_c + c_W \tag{4.8}$$

where $A_W = \frac{1}{2}\mathbf{Re}\{Z_c(\mathbf{r_c})\}$ and $b_W = \frac{1}{2}\mathbf{Re}\{Z_p(\mathbf{r_c})\}q_p^*$ and $c_W = \frac{1}{2}\mathbf{Re}\{Z_p(\mathbf{r}_p)\}|q_p|^2$. $A_W$ represents the "power" of the control source operating on its own in the presence of the infinite baffle, $c_W$ represents the power of the primary source operating on it own in the infinite baffle. If the control source strength $q_c$ is adjusted so that the total sound power is minimised, $b_W$ represents the "control effect" of controlling the total sound power. Hence the expressions for $A_W$, $b_W$ and $c_W$ can now calculated from equations (4.1) and (4.2) giving

$$A_W = \frac{1}{2}\mathbf{Re}\{Z_c(\mathbf{r_c})\} = \frac{1}{2}\mathbf{Re}\{j\omega\rho[G_f(\mathbf{r_c}|\mathbf{r}_c) + G_f(\mathbf{r}_i|\mathbf{r}_c)]\} \tag{4.9}$$

$$= \frac{1}{2}\mathbf{Re}\{j\omega\rho[\frac{e^{-jkr_{cc}}}{4\pi r_{cc}} + \frac{e^{-jkr_{ic}}}{4\pi r_{ic}}]\} \tag{4.10}$$

where $r_{cc} = |\mathbf{r}_c - \mathbf{r}_c| = 0$ and $r_{ic} = |\mathbf{r}_i - \mathbf{r}_c| = 2d$, which leads to

$$A_W = \frac{\omega\rho k}{8\pi}(1 + sinc\,2kd) \tag{4.11}$$

where $sinc(x) = \frac{sin\,x}{x}$

$$b_W = \frac{1}{2}\mathbf{Re}\{Z_p(\mathbf{r_c})\}q_p^* = \frac{1}{2}\mathbf{Re}\{j\omega\rho[G_f(\mathbf{r}_p|\mathbf{r}_c) + G_f(\mathbf{r}_p|\mathbf{r}_i)]\}q_p^* \tag{4.12}$$

$$= \frac{1}{2}\mathbf{Re}\{j\omega\rho[\frac{e^{-jkr_{pc}}}{4\pi r_{pc}} + \frac{e^{-jkr_{pi}}}{4\pi r_{pi}}]\}q_p^* \tag{4.13}$$

where $r_{pc} = |\mathbf{r}_p - \mathbf{r}_c| = d$ and $r_{pi} = |\mathbf{r}_p - \mathbf{r}_i| = d$, which gives

$$b_W = q_p\frac{\omega\rho k}{4\pi}sinc\,kd \tag{4.14}$$

$A_W|q_c|^2$ represents the power from the control source at a distance $d$ from the baffle if it were acting alone. By setting $d = 0$ the expression for the power of the primary source $c_W$ in the baffle acting alone can be calculated giving

$$c_W = \frac{\omega \rho k}{4\pi} |q_p|^2 \tag{4.15}$$

The expression $1 + sinc\,2kd$ is always greater than zero and hence, $A_W$ is guaranteed to be positive definite. Hence the expression for the total sound power output given by equation (4.8) has a unique minimum given by the optimal control source strength

$$q_{c,opt} = -A_W^{-1} b_W = -q_p \frac{2\,sinc\,kd}{(1 + sinc\,2kd)} \tag{4.16}$$

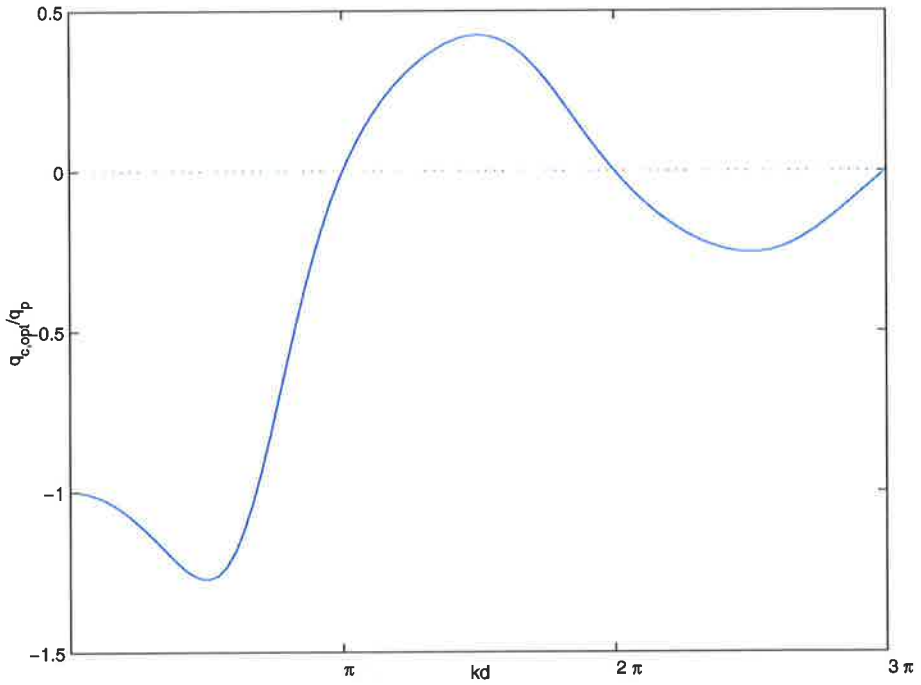


*Figure 4.3: Optimal control source strength $q_{c,opt}$ relative to the primary source strength $q_p$ as a function of the separation distance $d$ at a particular wavenumber $k$.*

Figure 4.3 shows the optimal control source strength as a function of the separation distance $d$ at a particular wavenumber $k$.

Substituting this result into the quadratic expression and normalising in terms of the uncontrolled acoustic power output, the maximum possible acoustic power attenuation is found to be:

$$\frac{W_p}{W_{min}} = \frac{1 + sinc\,2kd}{1 + sinc\,2kd - 2\,sinc^2\,kd} \tag{4.17}$$

where $W_{min}$ is the acoustic power when the optimal control source strength is applied and $W_p$ is the acoustic power of the primary source acting alone. Figure 4.4 shows the acoustic power attenuation as a function of the separation distance $d$ at a particular wavenumber $k$.

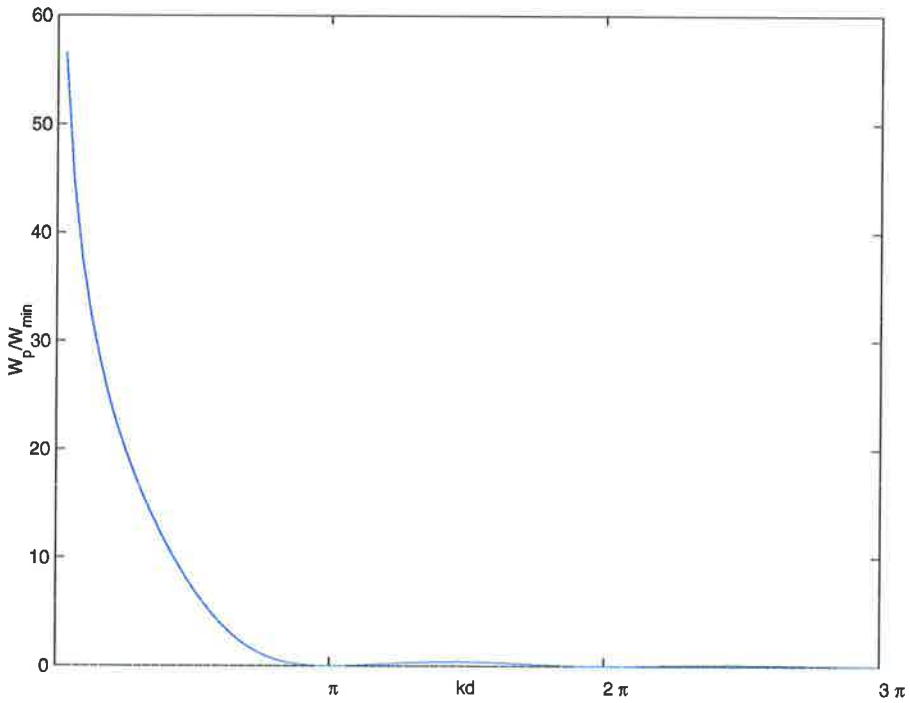


*Figure 4.4: Optimal power attenuation $W_p/W_{min}(dB)$ as a function of the separation distance $d$ at a particular wavenumber $k$.*

Hence if appreciable power attenuation of a monopole primary source is desired then a monopole control source would need to be located within a tenth of a wavelength. At a separation distance of $d = \lambda/10$ the level of power attenuation is approximately 24.2dB. This computed level of power attenuation sets an upper limit on the global control achievable with a single source.

### 4.2.3 Minimising pressure

Considering minimisation of acoustic pressure first, the squared acoustic pressure amplitude at a point in space $\mathbf{r}$ can be expressed as a quadratic

$$|p_{total}(\mathbf{r})|^2 = A_p|q_c|^2 + q_c^* b_p + b_p^* q_c + c_p \tag{4.18}$$

where $A_p = |Z_c(\mathbf{r})|^2$, $b_p = q_p Z_c^*(\mathbf{r}) Z_p(\mathbf{r})$, $c_p = |Z_p(\mathbf{r})|^2$ and

$$\begin{aligned} Z_c(\mathbf{r}) &= j\omega\rho[G_f(\mathbf{r_c}|\mathbf{r}) + G_f(\mathbf{r}_i|\mathbf{r})] && (4.19)\\ &= j\omega\rho[\frac{e^{-jkr_c}}{4\pi r_c} + \frac{e^{-jkr_i}}{4\pi r_i}] && (4.20)\\ Z_p(\mathbf{r}) &= 2j\omega\rho G_f(\mathbf{r}_p|\mathbf{r}) && (4.21)\\ &= 2j\omega\rho\frac{e^{-jkr_p}}{4\pi r_p} && (4.22) \end{aligned}$$

where $r_p$, $r_c$ and $r_i$ are the distances between the error sensor location and the primary, control and image sources, respectively, as shown in Figure 4.2b.

As with radiated acoustic power, since $A_p$ is positive definite, this expression has a unique minimum given by the (pressure) optimal control source strength (see Appendix E):

$$q_{c,p} = -A_p^{-1} b_p \tag{4.23}$$

Substituting this result back into the expression for acoustic power given in equation (4.8), and normalising with respect to the uncontrolled acoustic power output, the sound power attenuation that results from minimising squared acoustic pressure amplitude at a point in space is given by

$$\frac{W_p}{W_{min}} = \frac{c_W}{A_W \left|A_p^{-1} b_p\right|^2 - (A_p^{-1} b_p)^* b_W - b_W^* (A_p^{-1} b_p) + c_W} \tag{4.24}$$

### 4.2.4 Minimising radial active intensity

The total acoustic particle velocity in the direction $\hat{\mathbf{u}}_{total}$ of both sources at an observation point $\mathbf{r}$ in the free field is given by the sum of the particle velocities of the primary and control sources given by

$$\mathbf{u}_{total}(\mathbf{r}) = \mathbf{u}_p(\mathbf{r}) + \mathbf{u}_c(\mathbf{r}) \tag{4.25}$$

which can be rewritten as

$$\mathbf{u}_{total}(\mathbf{r}) = u_{total}\hat{\mathbf{u}}_{total} = u_p\hat{\mathbf{u}}_p + u_c\hat{\mathbf{u}}_c \tag{4.26}$$

where the unit vector $\hat{\mathbf{u}}_p$ is in the radial direction relative to the primary source, $\hat{\mathbf{u}}_c = \hat{\mathbf{u}}_{c,0} + \hat{\mathbf{u}}_i$ is in the direction of the sum of the radial unit vectors $\hat{\mathbf{u}}_{c,0}$ ,$\hat{\mathbf{u}}_i$ with respect to the control source and the image source respectively (see Figure 4.5).

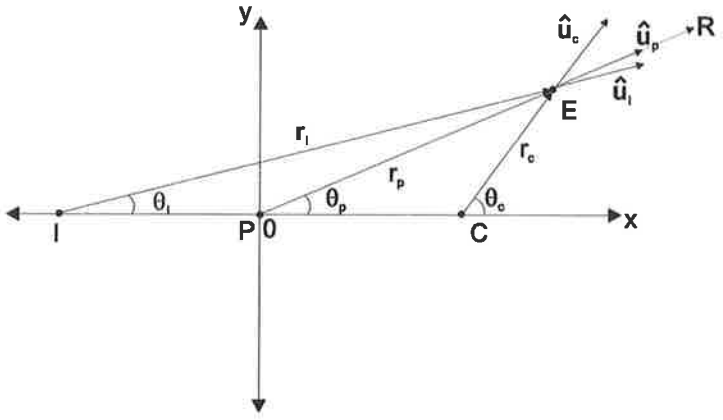


*Figure 4.5: Particle velocity vectors.*

The total active intensity in the direction of $\mathbf{u}_{total}$ is given by

$$\mathbf{I}_{total}(\mathbf{r}) = \frac{1}{2} Re\left\{p^*_{total}(\mathbf{r})\mathbf{u}_{total}(\mathbf{r})\right\} \tag{4.27}$$

where

$$p_{total}(\mathbf{r}) = p_c(\mathbf{r}) + p_p(\mathbf{r}) \tag{4.28}$$

It is desired to minimise the radial (with respect to the primary source, in the same direction as the vector $\mathbf{u}_p$) active intensity. Hence it is the component of $\mathbf{I}_{total}$ in equation (4.27) in the direction of $\mathbf{I}_p$ henceforth labelled $\mathbf{I}_{radial}$ as shown in Appendix A which must be minimised and is given by

$$\mathbf{I}_{radial}(\mathbf{r}) = proj_{\mathbf{I}_{radial}}\mathbf{I}_{total} = (\mathbf{I}_{radial} \bullet \mathbf{I}_{total})\mathbf{I}_{radial} \tag{4.29}$$

The notation $proj_{\mathbf{X}}\mathbf{Y}$ is used to denote the orthogonal projection of vector $\mathbf{Y}$ on vector $\mathbf{X}$. The direction of positive intensity is $\hat{\mathbf{u}}_p$ (see Figure 4.6). Substituting (4.25) and (4.28) gives

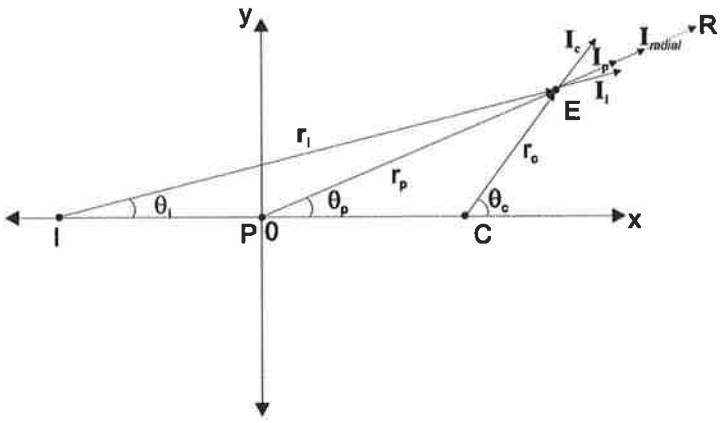


*Figure 4.6: Radial active intensity vector.*

$$\mathbf{I}_{total} = \frac{1}{2} Re\left\{(p^*_p + p^*_c)(\mathbf{u}_p + \mathbf{u}_c)\right\} \tag{4.30}$$

$$= \frac{1}{2} Re\left\{(p^*_p\mathbf{u}_p + p^*_p\mathbf{u}_c + p^*_c\mathbf{u}_p + p^*_c\mathbf{u}_c\right\} \tag{4.31}$$

where $\mathbf{u}_p = \mathbf{H}_p(r_p)q_p$ and $\mathbf{u}_c = \mathbf{H}_c(r_{c,i})q_c$, where $r_p$ and $r_c = r_i$ are defined as before. $\mathbf{H}_p$ and $\mathbf{H}_c$ both describe the acoustic velocity transfer impedances due to the primary and control sources respectively at the observation point $\mathbf{r}$ and are given by

$$\mathbf{H}_p(r_p) = \frac{1}{4\pi}\left(\frac{1}{r_p^2}+\frac{jk}{r_p}\right)e^{-jkr_p}\hat{\mathbf{u}}_p \tag{4.32}$$

$$\mathbf{H}_c(r_{c,i}) = \mathbf{H}_{c,0}(r_c)+\mathbf{H}_i(r_i) \tag{4.33}$$

$$= \frac{1}{4\pi}\left(\frac{1}{r_c^2}+\frac{jk}{r_c}\right)e^{-jkr_c}\hat{\mathbf{u}}_{c,0}+\frac{1}{4\pi}\left(\frac{1}{r_i^2}+\frac{jk}{r_i}\right)e^{-jkr_i}\hat{\mathbf{u}}_i \tag{4.34}$$

The active intensity in the direction $\hat{\mathbf{u}}_{total}$ can be re-expressed in a hermitian quadratic form as

$$\mathbf{I}_{total} = \mathbf{A}_I|q_c|^2 + q_c^*\mathbf{b}_I + \mathbf{b}_I^* q_c + \mathbf{c}_I \tag{4.35}$$

where $\mathbf{A}_I = \frac{1}{2}Re\{Z_c^*\mathbf{H}_c\}$ and $\mathbf{b}_I = \frac{1}{4}q_p(\mathbf{H}_c^* Z_p + \mathbf{H}_p Z_c^*)$ and $\mathbf{c}_I = \frac{1}{2}Re\{Z_p^*\mathbf{H}_p\}|q_p|^2$ where $X^*$ represents the complex conjugate of $X$.

The radial active intensity can be written as

$$\mathbf{I}_{radial}(\mathbf{r}) = proj_{\mathbf{I}_{radial}}\mathbf{I}_{total} \tag{4.36}$$

$$= (\mathbf{I}_{radial} \bullet \mathbf{I}_{total})\mathbf{I}_{radial} \tag{4.37}$$

$$= \mathbf{A}_{I_{radial}}|q_c|^2 + q_c^*\mathbf{b}_{I_{radial}} + \mathbf{b}_{I_{radial}}^* q_c + \mathbf{c}_{I_{radial}} \tag{4.38}$$

where $\mathbf{A}_{I_{radial}}$, $\mathbf{b}_{I_{radial}}$ and $\mathbf{c}_{I_{radial}}$ can be written as

$$\mathbf{A}_{I_{radial}} = \frac{1}{2}Re\left\{Z_c^*(H_{c,0}proj_{\hat{\mathbf{u}}_p}\hat{\mathbf{u}}_{c,0} + H_i proj_{\hat{\mathbf{u}}_p}\hat{\mathbf{u}}_i)\right\} \tag{4.39}$$

$$\mathbf{b}_{I_{radial}} = \frac{1}{4} q_p ((H^*_{c,0} proj_{\widehat{\mathbf{u}_p}} \widehat{\mathbf{u}}_{c,0} + H^*_i proj_{\widehat{\mathbf{u}_p}} \widehat{\mathbf{u}}_i) Z_p + Z^*_c H_p \widehat{\mathbf{u}_p}) \tag{4.40}$$

$$\mathbf{c}_{I_{radial}} = \frac{1}{2} Re\left\{Z^*_p H_p\right\} |q_p|^2 \widehat{\mathbf{u}_p} \tag{4.41}$$

where $H_{rad} = ||\mathbf{H}_{rad}||$, $H_{c,0} = ||\mathbf{H}_{c,0}||$ and $H_i = ||\mathbf{H}_i||$ are the complex vector magnitudes of the corresponding vectors describing the velocity transfer impedances.

Consider equation (4.39) for the active intensity of the control source acting on its own $\mathbf{A}_{I_{radial}}$, if the direction $\widehat{\mathbf{u}_p}$ is defined to be positive then we can write

$$\mathbf{A}_{I_{radial}} = A_{I_{radial}} \widehat{\mathbf{u}_p} \tag{4.42}$$

where

$$A_{I_{radial}} = \frac{1}{2} Re\left\{Z^*_c (H_{c,0} (\widehat{\mathbf{u}}_{c,0} \bullet \widehat{\mathbf{u}_p}) + H_i (\widehat{\mathbf{u}}_i \bullet \widehat{\mathbf{u}_p}))\right\} \tag{4.43}$$

Appendix E shows that provided $A_{I_{radial}}$ is positive, there exists a unique minimum given by the optimal control source strength $q_{c,opt}$. This is not necessarily the case for an active intensity cost function which may be negative at certain locations. The term $proj_{\widehat{\mathbf{u}_p}} \widehat{\mathbf{u}}_{c,0}$ in equation (4.39) which is defined by

$$proj_{\widehat{\mathbf{u}_p}} \widehat{\mathbf{u}}_{c,0} = (\widehat{\mathbf{u}}_{c,0} \bullet \widehat{\mathbf{u}_p}) \widehat{\mathbf{u}_p} \tag{4.44}$$

can at certain error sensor locations be negative, when the dot product $\widehat{\mathbf{u}}_{c,0} \bullet \widehat{\mathbf{u}_p}$ is negative, or the angle between $\widehat{\mathbf{u}_p}$ and $\widehat{\mathbf{u}}_{c,0}$ is obtuse. The term $proj_{\widehat{\mathbf{u}_p}} \widehat{\mathbf{u}}_i$ which is defined by

$$proj_{\widehat{\mathbf{u}_p}} \widehat{\mathbf{u}}_i = (\widehat{\mathbf{u}}_i \bullet \widehat{\mathbf{u}_p}) \widehat{\mathbf{u}_p} \tag{4.45}$$

as can be seen from Figure 4.5 is always positive, as the dot product $\widehat{\mathbf{u}}_i \bullet \widehat{\mathbf{u}_p} > 0$ because the

angle between $\widehat{\mathbf{u}_p}$ and $\widehat{\mathbf{u}}_i$ is always acute.

Expanding equation (4.39) gives

$$\mathbf{A}_{I_{radial}} = \frac{1}{2} Re\left\{Z_c^*\left(H_{c,0}(\widehat{\mathbf{u}}_{c,0} \bullet \widehat{\mathbf{u}_p})\widehat{\mathbf{u}_p} + H_i(\widehat{\mathbf{u}}_i \bullet \widehat{\mathbf{u}_p})\widehat{\mathbf{u}_p}\right)\right\} \tag{4.46}$$

now substituting equation (4.20) where we define the terms $Z_{c,0}(\mathbf{r})$ and $Z_i(\mathbf{r})$ to write $Z_c(\mathbf{r}) = Z_{c,0}(\mathbf{r}) + Z_i(\mathbf{r})$ giving

$$\begin{aligned}
\mathbf{A}_{I_{radial}} &= \frac{1}{2} Re\left\{(Z_{c,0}^* + Z_i^*)\left(H_{c,0}(\widehat{\mathbf{u}}_{c,0} \bullet \widehat{\mathbf{u}_p})\widehat{\mathbf{u}_p} + H_i(\widehat{\mathbf{u}}_i \bullet \widehat{\mathbf{u}_p})\widehat{\mathbf{u}_p}\right)\right\} && (4.47)\\
&= \frac{1}{2} Re\left\{\left(Z_{c,0}^* H_{c,0} + Z_i^* H_{c,0}(\widehat{\mathbf{u}}_{c,0} \bullet \widehat{\mathbf{u}_p})\right)\widehat{\mathbf{u}_p} + \left(Z_{c,0}^* H_i + Z_i^* H_i(\widehat{\mathbf{u}}_i \bullet \widehat{\mathbf{u}_p})\right)\widehat{\mathbf{u}_p}\right\} && (4.48)\\
&= \left(\frac{1}{2} Re\left\{Z_{c,0}^* H_{c,0}\right\} + \frac{1}{2} Re\left\{Z_i^* H_{c,0}\right\}\right)(\widehat{\mathbf{u}}_{c,0} \bullet \widehat{\mathbf{u}_p})\widehat{\mathbf{u}_p} + \ldots \\
&\quad + \left(\frac{1}{2} Re\left\{Z_{c,0}^* H_i\right\} + \frac{1}{2} Re\left\{Z_i^* H_i\right\}\right)(\widehat{\mathbf{u}}_i \bullet \widehat{\mathbf{u}_p})\widehat{\mathbf{u}_p}) && (4.49)
\end{aligned}$$

It can be seen from equation (4.49) that $\mathbf{A}_{I_{radial}}$ comprises terms for the active intensity due to the control source on its own and the image source on its own plus cross terms.

When $\widehat{\mathbf{u}}_{c,0} \bullet \widehat{\mathbf{u}_p} < 0$, $A_{I_{radial}}$ will be negative when the first term in equation (4.49) is less than the second term, or alternatively the following condition is met:

$$\left(\frac{1}{2} Re\left\{Z_{c,0}^* H_{c,0}\right\} + \frac{1}{2} Re\left\{Z_i^* H_{c,0}\right\}\right)(\widehat{\mathbf{u}}_{c,0} \bullet \widehat{\mathbf{u}_p}) < \left(\frac{1}{2} Re\left\{Z_{c,0}^* H_i\right\} + \frac{1}{2} Re\left\{Z_i^* H_i\right\}\right)(\widehat{\mathbf{u}}_i \bullet \widehat{\mathbf{u}_p}) \tag{4.50}$$

If condition (4.50) is met at a particular error sensor location $\mathbf{r}$ when $\widehat{\mathbf{u}}_{c,0} \bullet \widehat{\mathbf{u}_p} < 0$ then $A_{I_{radial}} < 0$ and hence there is only a unique maximum exists as derived in Appendix E.

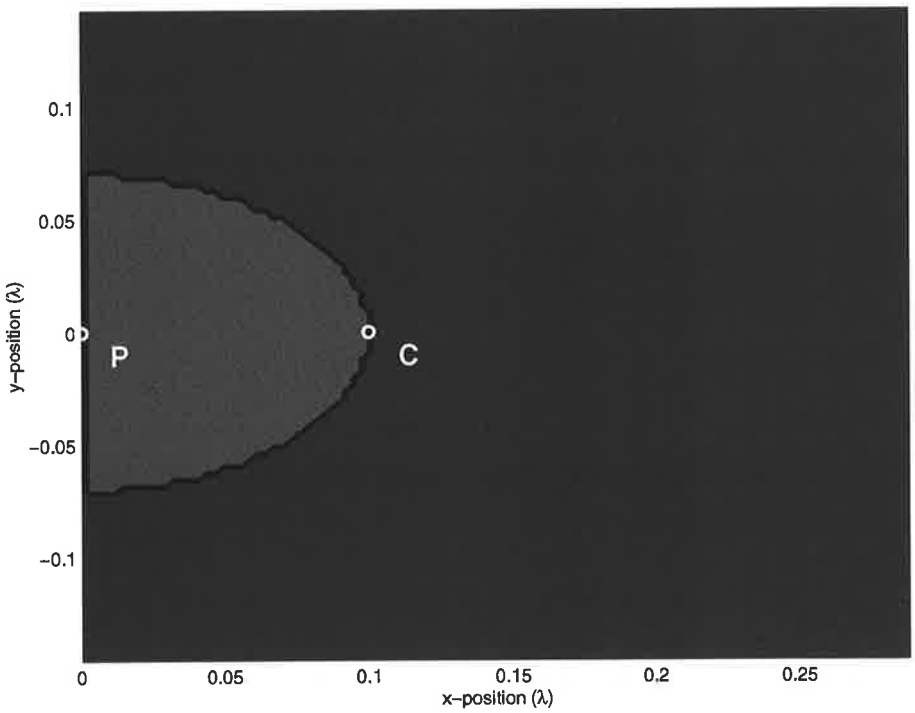


*Figure 4.7: The region (indicated by the colour red) where $A_{I_{radial}} < 0$, and hence the radial active intensity can become negative, leading to an optimal control source strength which maximises the radial active intensity. The blue region indicates the region where $A_{I_{radial}} > 0$ and hence the radial active intensity is positive definite and the optimal control source strength minimises the radial active intensity.*

Condition (4.50) can best be illustrated as shown in Figure 4.7 If $A_{I_{radial}} > 0$ a unique minimum exists or if $A_{I_{radial}} < 0$ then a unique maximum exists and in either case the extreme control source strength is given by

$$q_{c,opt} = -A^{-1}_{I_{radial}} b_{I_{radial}} \tag{4.51}$$

Therefore to optimise the radial active intensity at a particular location **r** from a baffled monopole primary source by a single control monopole source (4.51) is substituted into (4.27).

The amount of sound power attenuation when the active intensity is minimised at the error sensor location is found by substituting (4.51) into (4.8) giving

$$\frac{W_p}{W_{min}} = \frac{c_W}{A_W \left| -\frac{1}{2}A^{-1}_{I_{radial}}(b_{I_{radial}}) \right|^2 - (-\frac{1}{2}A^{-1}_{I_{radial}} b_{I_{radial}})^* b_W - b^*_W(-\frac{1}{2}A^{-1}_{I_{radial}} b_{I_{radial}}) + c_W} \tag{4.52}$$

## 4.3 Comparison of power attenuation when minimising pressure and intensity error criterion

As described several times, the aim of the work presented here is to compare the performance of pressure and intensity error sensing strategies for a simple (but more complicated than simple free field monopoles) free space radiation problem. Referring to Figure 4.2a, the problem to be studied here has a single monopole control source separated from a single monopole primary source embedded in an infinite baffle by one-tenth of a wavelength. Using equation (4.17), the maximum possible acoustic power attenuation for this arrangement is 24.2 dB.

Illustrated in Figures 4.8 and 4.9 is the acoustic power attenuation that would result from minimising the square acoustic pressure amplitude at a point in space. The results in Figures

4.8 and 4.9 are to different scales: Figure 4.8 depicts results for minimising acoustic pressure at points in space for x,y positions over 3 wavelengths, while Figure 4.9 depicts results over a 0.3 wavelength region. Observe that significant attenuation can be achieved at error sensor locations perpendicular to a line joining the sources.

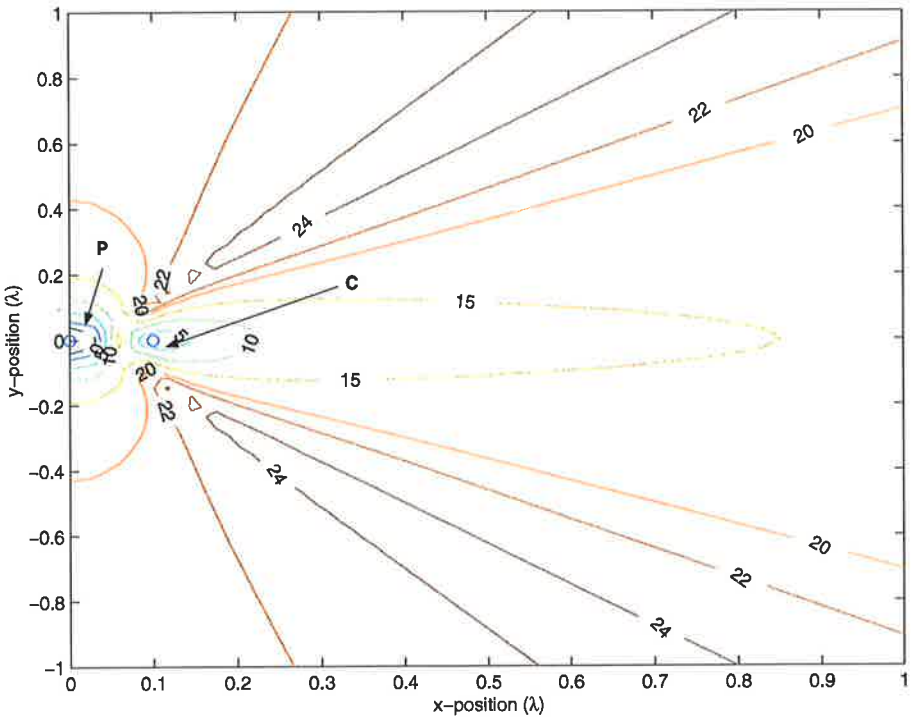


*Figure 4.8: Acoustic power attenuation in dB as a function of pressure error sensor placement, single monopole primary at the origin in an infinite baffle in the z-plane and control sources separated by $\lambda/10$ wavelength in far field view. The circle ◯ on the left is the primary monopole source location, and the circle ◯ on the right is the control monopole source location.*

Illustrated in Figures 4.10 and 4.11 are results for the same geometry, but where acoustic intensity is minimised as opposed to square acoustic pressure amplitude. For these results, the acoustic intensity vector is minimised in the radial direction along a line joining both the primary and control sources. Comparing Figures 4.8 and 4.10, the results obtained when minimising acoustic intensity at locations distant from the sources are very similar to the acoustic pressure results. However, when comparing the results in Figures 4.9 and 4.11, it is evident that the results obtained when minimising the error criteria at locations close to the sources are very different. In fact, the acoustic power attenuation that results from minimising acoustic

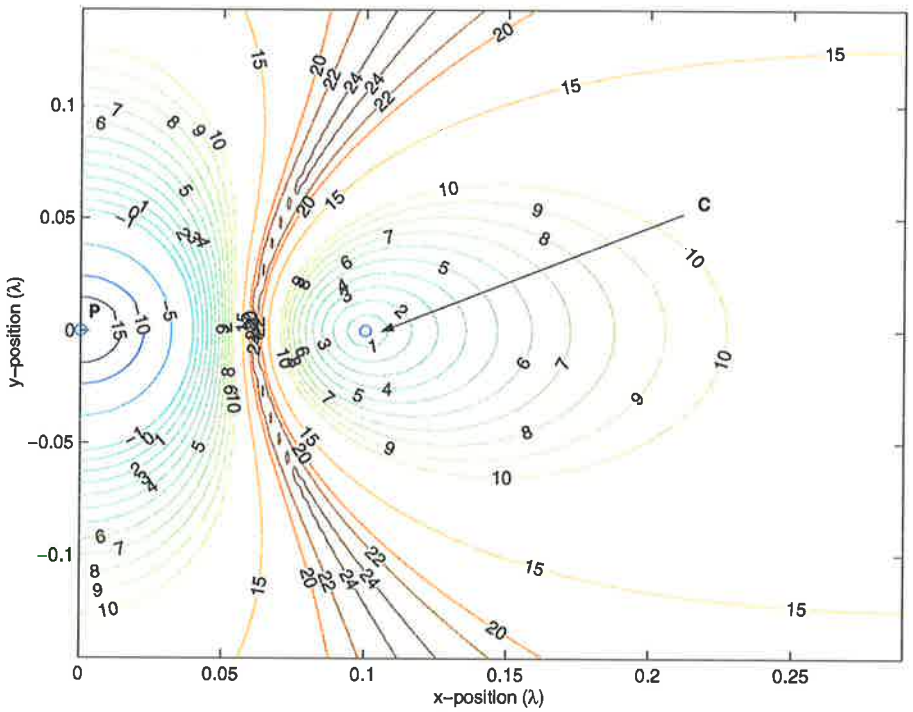


*Figure 4.9: Acoustic power attenuation in dB as a function of pressure error sensor placement, single monopole primary at the origin in an infinite baffle in the z-plane and control sources separated by $\lambda/10$ wavelength in near field view. The circle ◯ on the left is the primary monopole source location, and the circle ◯ on the right is the control monopole source location.*

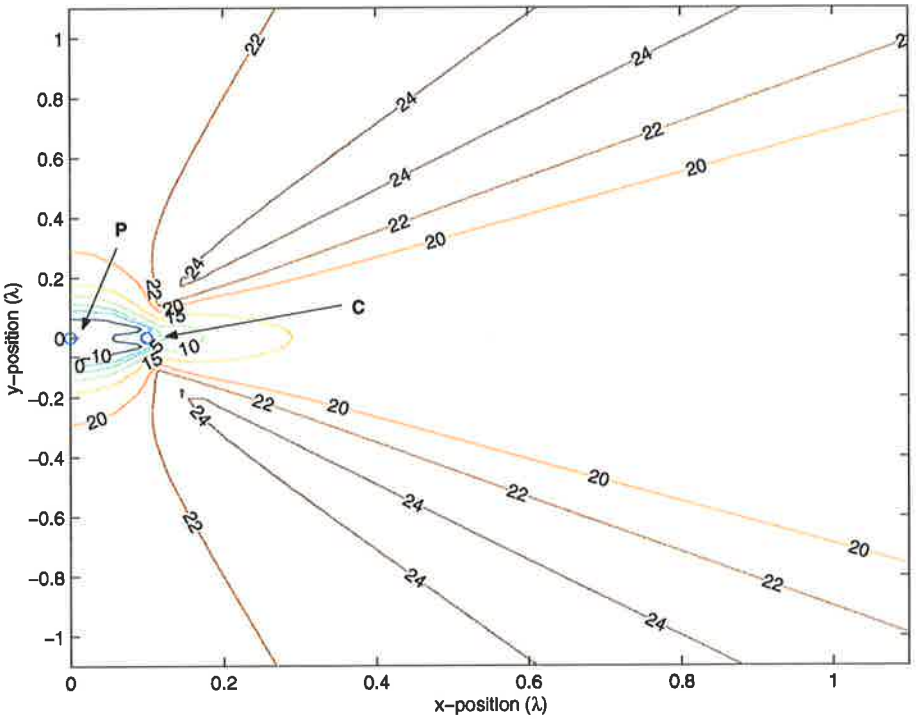


*Figure 4.10: Acoustic power attenuation in dB as a function of radial active intensity error sensor placement (radial with respect to the primary source), single monopole primary at the origin in an infinite baffle in the z-plane and control sources separated by λ/10 wavelength in far field view. The circle ◯ on the left is the primary monopole source location, and the circle ◯ on the right is the control monopole source location.*

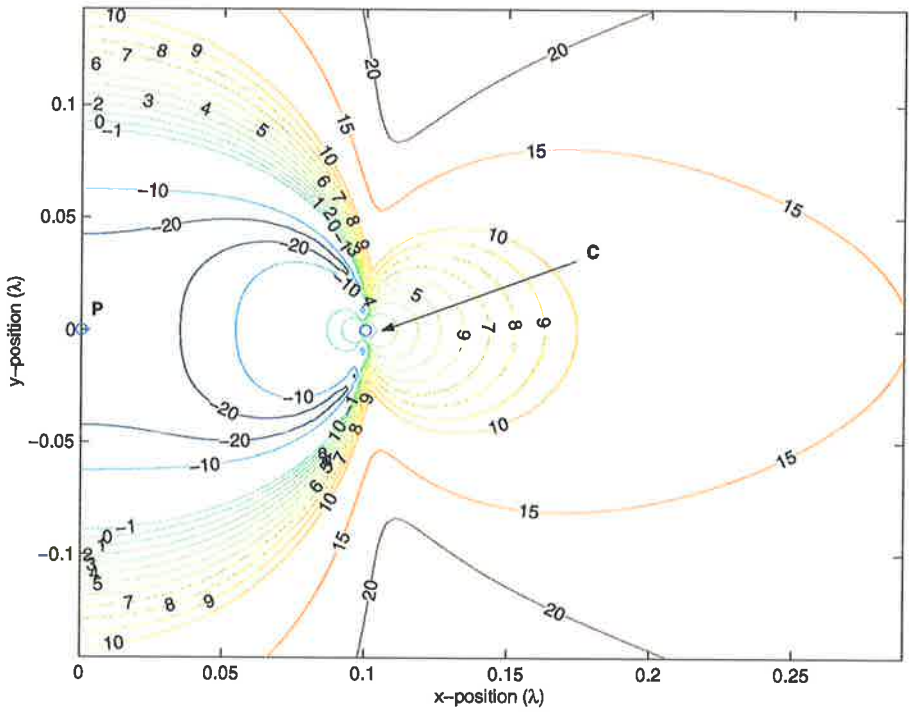


*Figure 4.11: Acoustic power attenuation in dB as a function of radial active intensity error sensor placement (radial with respect to the primary source), single monopole primary at the origin in an infinite baffle in the z-plane and control sources separated by $\lambda/10$ wavelength in near field view. The circle ◯ on the left is the primary monopole source location, and the circle ◯ on the right is the control monopole source location.*

intensity is far worse than when minimising squared acoustic pressure. As with the monopole result, the areas of poor performance are well predicted by the plot $A_{I_{radial}}$ in Figure 4.7.

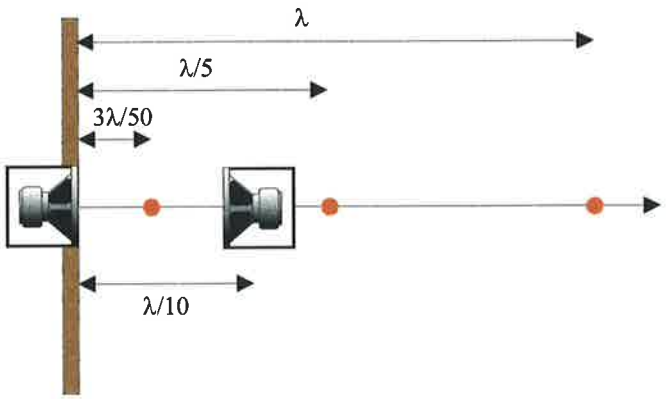


*Figure 4.12: The three sensor locations considered. The red dots indicate the error sensor location.*

Referring back to the five steps outlined at the start of Section 4.2, for an error sensing strategy to be of "high quality", the control source volume velocity that minimises the error criterion of interest, derived in step 3, must be virtually identical to the control source volume velocity that provides maximum acoustic power attenuation, calculated in step 2. Shown in Figures 4.13a and 4.13b are plots of the squared pressure and intensity error criteria evaluated at a location which is λ (shown in Figure 4.12) from the primary source and directly in front, of the control source as a function of complex control source volume velocity. Observe that both the pressure and intensity error surfaces have a single minimum, at approximately the same volume velocity, and that these minima are close to volume velocity that is optimal in terms of acoustic power attenuation.

The result is similar for error sensors located at a position of λ/5 (shown in Figure 4.12) from the primary source, just behind the control source, as evident in the error surface plots shown in Figures 4.14a and 4.14b. In this case the intensity minima is slightly closer to the value that will minimise radiated acoustic power than is the pressure minima. Hence at this location acoustic intensity error sensing would produce a superior result.

The results are very different, however, for an error sensing location of 3λ/50 (shown in Figure 4.12) from the primary source, approximately mid way between the primary and control

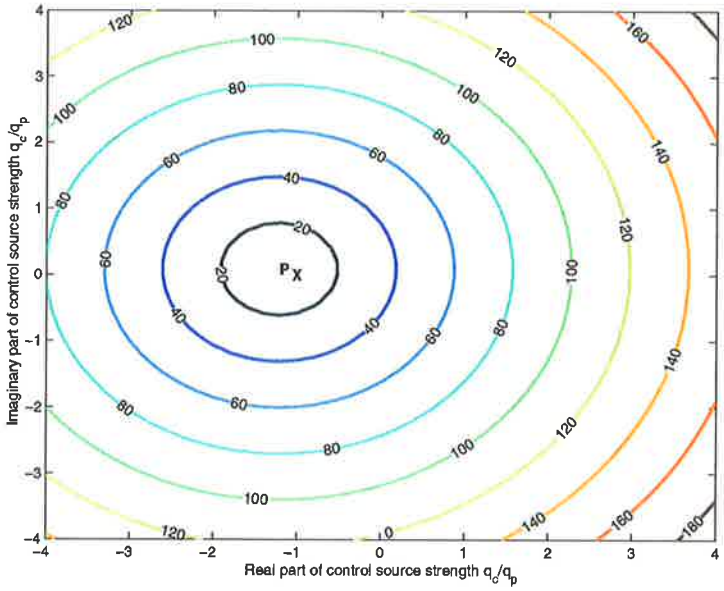


*(a) Pressure amplitude as a function of the real and imaginary parts of the relative control source strength*

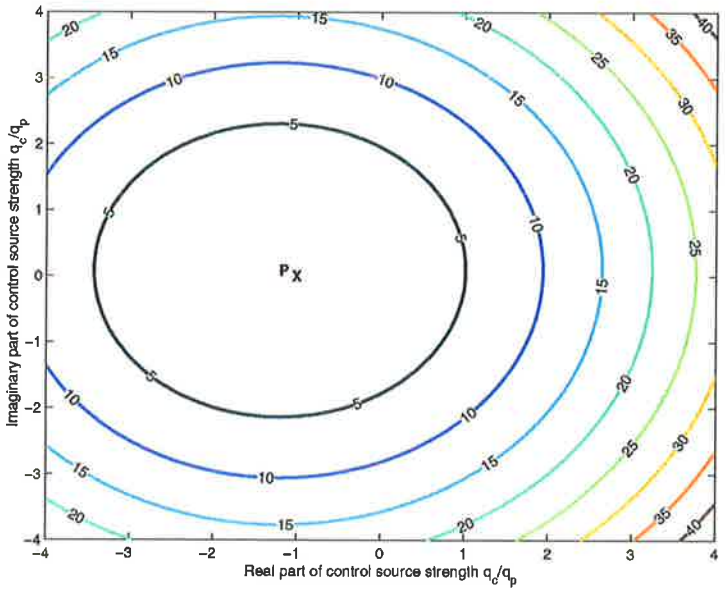


*(b) Radial active intensity as a function of the real and imaginary parts of the relative control source strength*

*Figure 4.13: Pressure amplitude and radial active intensity as a function of the real and imaginary parts of the control source strength $q_c$ relative to a unitary primary source strength, at the sensor location $r_e = (\lambda, 0)$ (the calculations are relative to a unitary primary source strength). **X** indicates the optimal control source strength when minimising acoustic power. **P** indicates the optimal control source strength when minimising squared pressure. **I** indicates the optimal control source strength when minimising radial active intensity.*

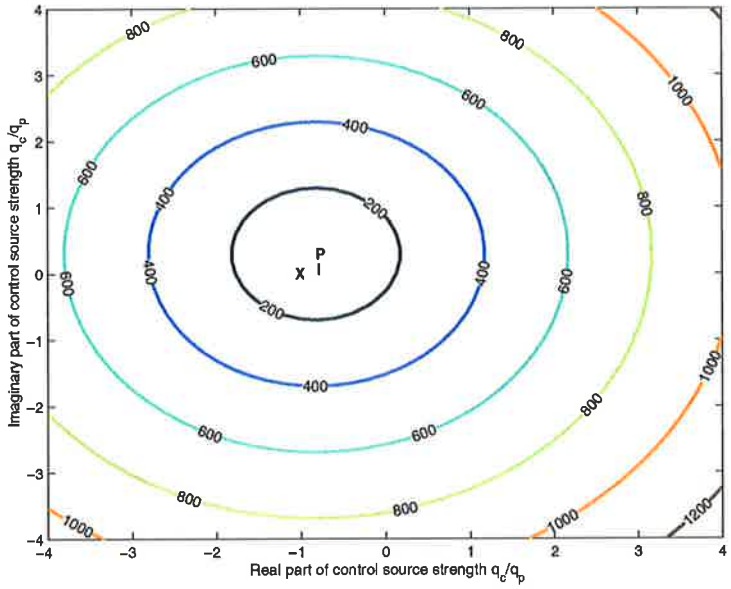


*(a) Pressure amplitude as a function of the real and imaginary parts of the relative control source strength*

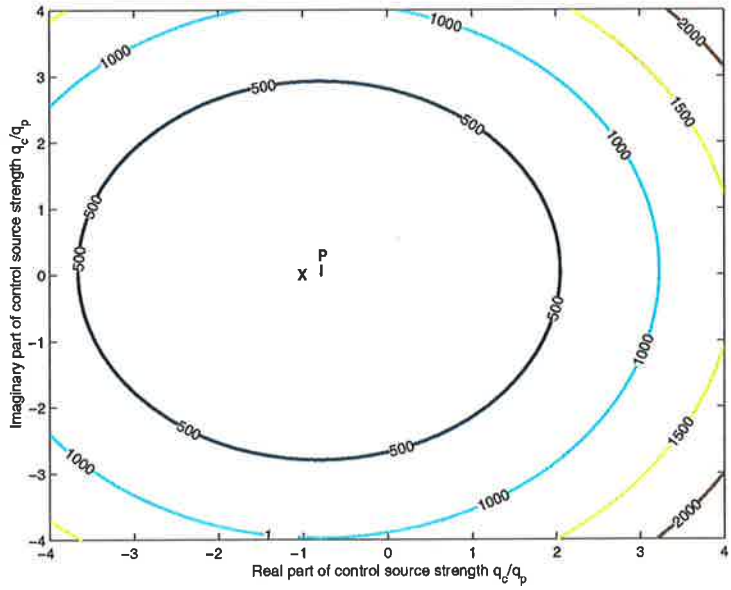


*(b) Radial active intensity as a function of the real and imaginary parts of the relative control source strength*

*Figure 4.14: Pressure amplitude and radial active intensity as a function of the real and imaginary parts of the control source strength $q_c$ relative to a unitary primary source strength, at the sensor location $r_e = (\lambda/5, 0)$ (the calculations are relative to a unitary primary source strength). **X** indicates the optimal control source strength when minimising acoustic power. **P** indicates the optimal control source strength when minimising squared pressure. **I** indicates the optimal control source strength when minimising radial active intensity.*

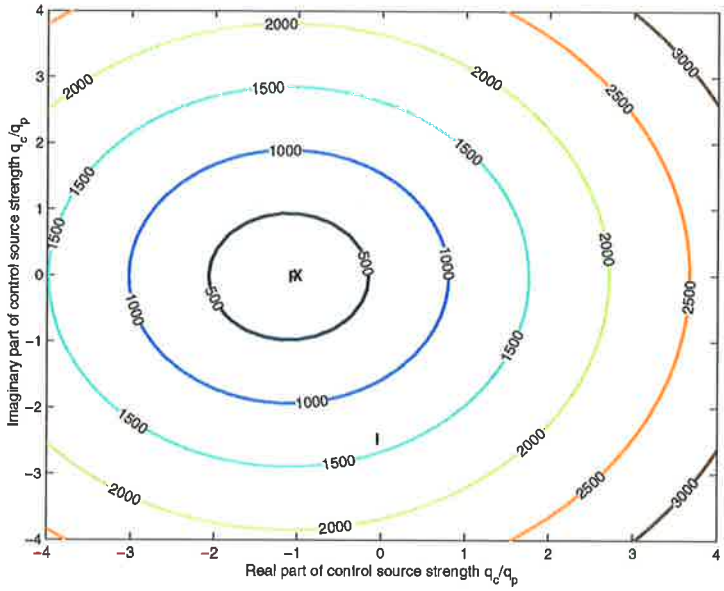


*(a) Pressure amplitude as a function of the real and imaginary parts of the relative control source strength*

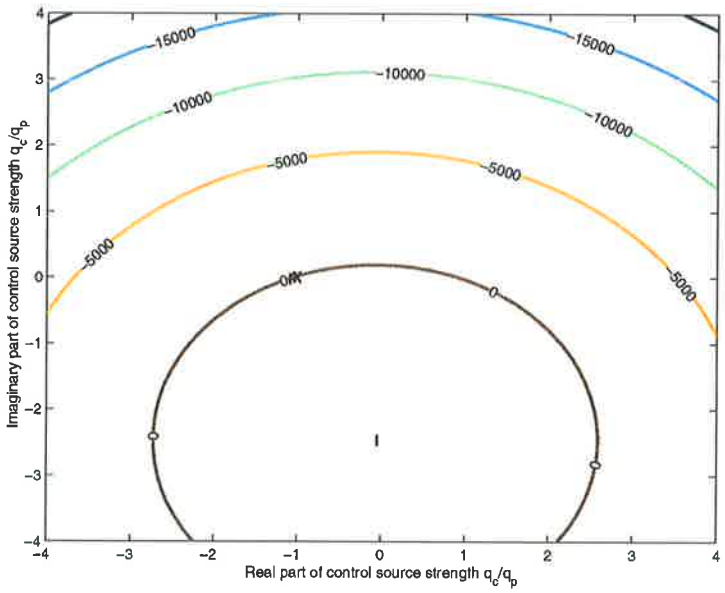


*(b) Radial active intensity as a function of the real and imaginary parts of the relative control source strength*

*Figure 4.15: Pressure amplitude and radial active intensity as a function of the real and imaginary parts of the control source strength $q_c$ relative to a unitary primary source strength, at the sensor location $r_e = (3\lambda/50, 0)$ (the calculations are relative to a unitary primary source strength). **X** indicates the optimal control source strength when minimising acoustic power. **P** indicates the optimal control source strength when minimising squared pressure. **I** indicates the optimal control source strength when minimising radial active intensity.*

sources. Referring to Figure 4.15b, observe that with acoustic active intensity there is no global minimum. In fact, the point of inflexion is a global maximum. If the error criterion is modified to be intensity amplitude, then there are a ring of infinitely many points where the error criterion has a zero value.

To examine this result further, consider the results where the imaginary part of the control source volume velocity is equal to zero. The plot of the intensity error surface as a function of (the real part of) control source volume velocity is illustrated in Figure 4.16a.

Observe that there are two points where intensity amplitude becomes zero: where the control source volume velocity is equal in amplitude and phase to the primary source volume velocity, and where the control source volume velocity is equal in amplitude and opposite in phase to the primary source volume velocity. To explain why there are two locations of zero intensity, the acoustic pressure and particle velocity at the error sensing location are also plotted for this range of control source volume velocities, in Figures 4.16b and 4.16c, respectively. Observe that one of the points of zero intensity corresponds to a point of zero acoustic pressure. The other corresponds to a point of zero acoustic particle velocity. Referring to the plot of sound power attenuation in Figure 4.16d, it is clear that the point corresponding to zero acoustic pressure produces the desired power attenuation, while the point corresponding to zero acoustic particle velocity equates to an increase in total acoustic power output.

It is worthwhile considering these results in terms of active noise control system implementation. First, for the simple baffled monopole example being considered here, there is little difference between the pressure and intensity minimisation results when the sensor is remote from the sources. Second, in some error sensing locations, particularly between the primary and control sources, there is no global minimum in the intensity error surface. Finally, if the error criterion is modified to be intensity amplitude, then there are two points where the error criterion has a zero value: one where acoustic pressure is equal to zero, and one where acoustic particle velocity is equal to zero. The use of a control source volume velocity corresponding to the first of these points yields good sound power attenuation. The use of a control source

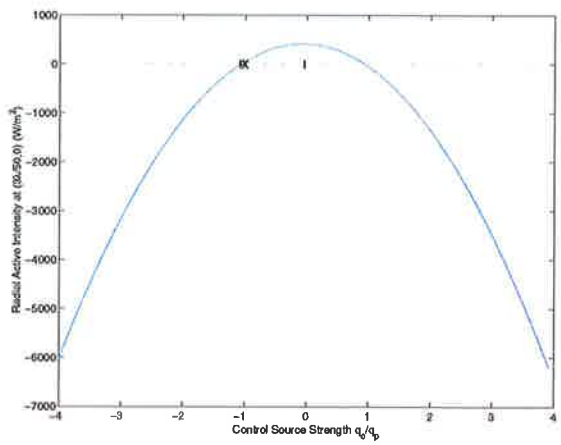


*(a) radial active intensity amplitude as a function of relative control source strength*

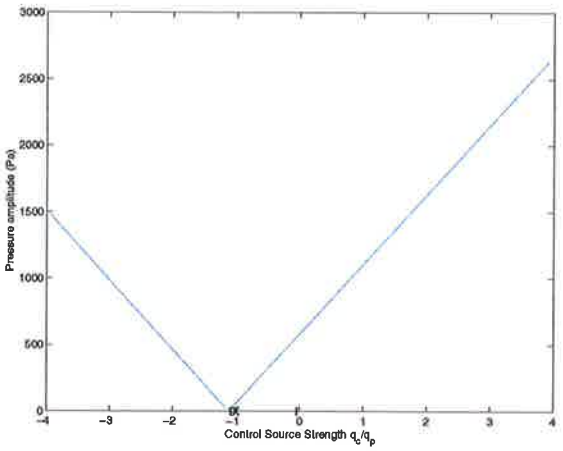


*(b) pressure amplitude as a function of relative control source strength*

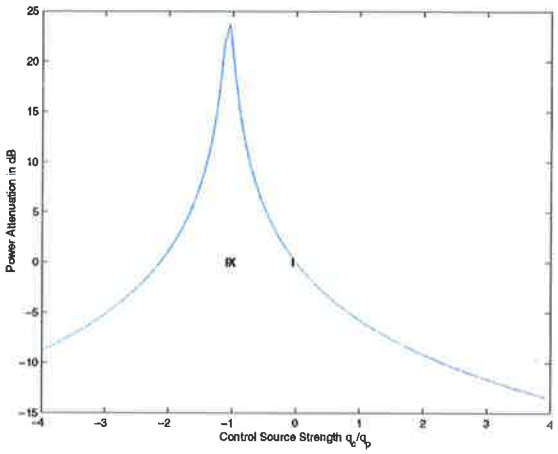


*(c) Sound power attenuation in dB as a function of relative control source strength*

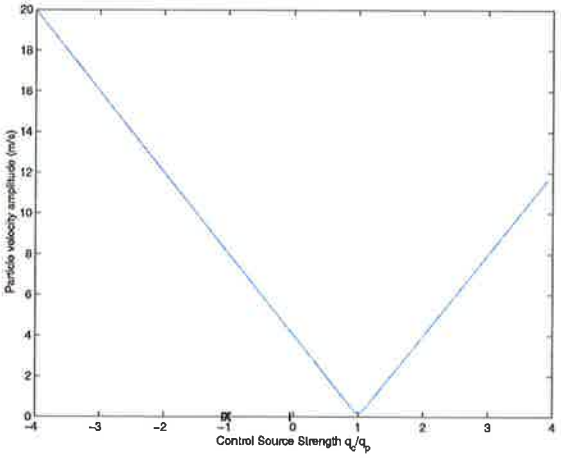


*(d) particle velocity amplitude as a function of relative control source strength*

*Figure 4.16: Radial active intensity amplitude, Sound power attenuation, pressure amplitude and particle velocity amplitude as a function of the control source strength $q_c$ relative to a unitary primary source strength, at sensor location $r_e = (3\lambda/50, 0)$ (the calculations are relative to a unitary primary source strength). **X** indicates the optimal control source strength when minimising acoustic power. **P** indicates the optimal control source strength when minimising squared pressure. **I** indicates the optimal control source strength when minimising radial active intensity.*

volume velocity corresponding to the second of these points results in an increase in sound power output.

To highlight the regions where negative intensity is produced when minimising both pressure and radial active intensity it would be helpful to have contour plots of the pressure field and active intensity field before and after control because this also serves as a global control indicator.

### 4.3.1 Pressure and active intensity fields before and after control minimising the acoustic pressure

Figure 4.17a shows the theoretical pressure distribution before control, with just the primary monopole source in operation in the infinite baffle when minimising the pressure at a distance of one wavelength from the primary source. Figure 4.17b shows the pressure distribution after control. It can be seen that the result of far field pressure sensing is to reduce the pressure field globally. Figure 4.18a shows the radial active intensity distribution in dB (Figure 4.19a on a linear scale) before pressure minimising control, with just the primary monopole source in operation in the infinite baffle when minimising the pressure at a distance of one wavelength from the primary source. Figure 4.18b shows the radial active intensity distribution in dB (Figure 4.19b on a linear scale) after control. It can be seen that the result of far field radial active intensity sensing is to also reduce the pressure field globally.

Figure 4.20a shows the pressure distribution before control, with just the primary monopole source in operation in the infinite baffle when minimising the pressure at a distance of one fifth of a wavelength from the primary source. Figure 4.20b shows the pressure distribution after control. It can be seen that the result of far field pressure sensing is to reduce the pressure field globally. Figure 4.21a shows the radial active intensity distribution in dB (Figure 4.22a on a linear scale) before control, with just the primary monopole source in operation in the infinite baffle when minimising the pressure at a distance of one fifth of a wavelength from the

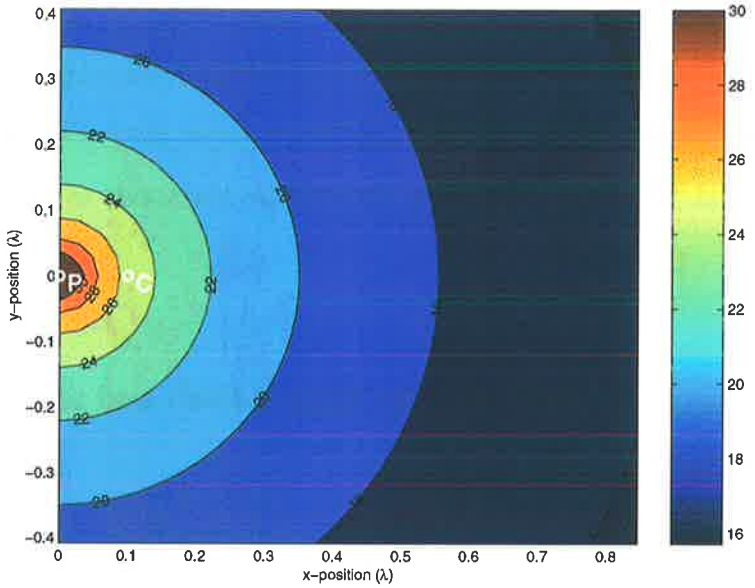


*(a) Pressure distribution before control*

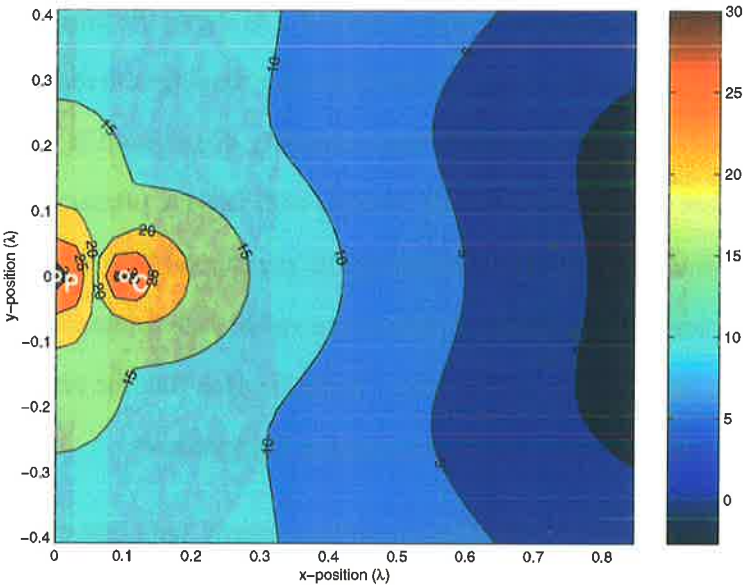


*(b) Pressure distribution after control*

*Figure 4.17: Pressure amplitude distribution in dB before and after control minimising pressure at the pressure sensor location $r_e = (\lambda, 0)$ (the calculations are relative to a unitary primary source strength). The circle ◯ on the left is the primary monopole source location, and the circle ◯ on the right is the control monopole source location.*

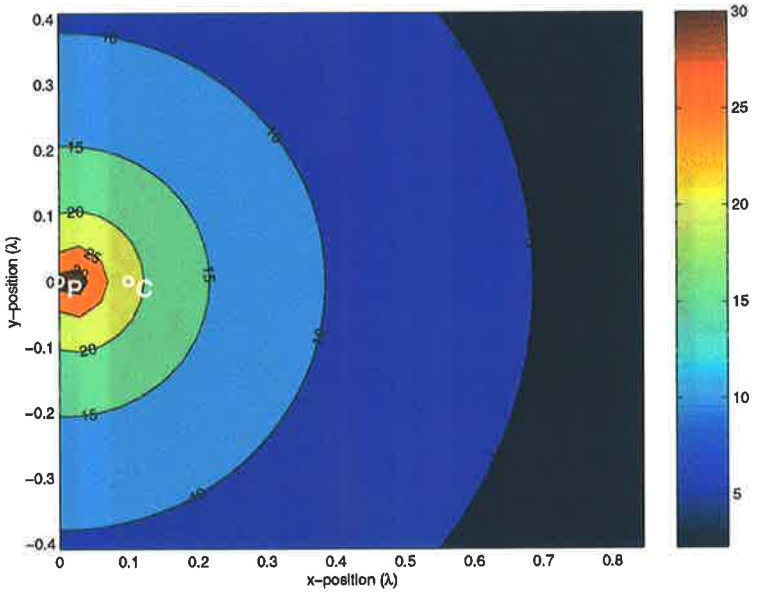


(a) Radial active intensity distribution before control

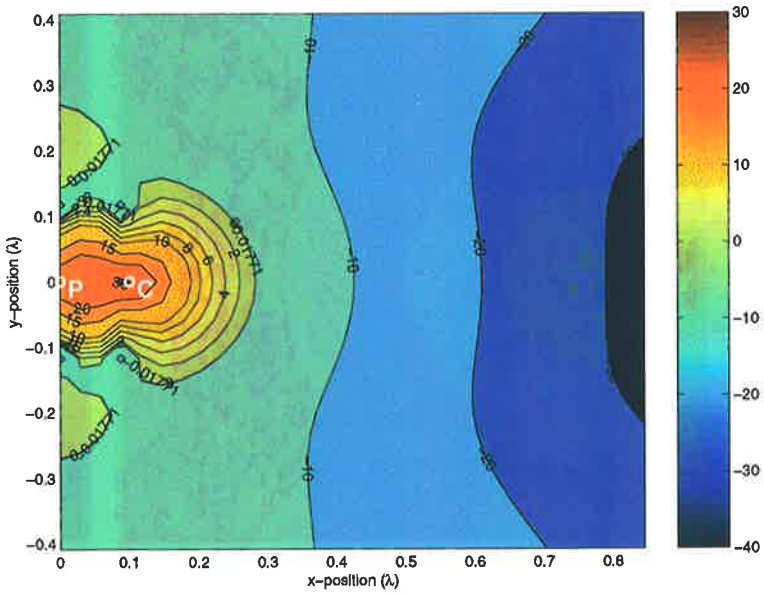


(b) Radial active intensity distribution after control

*Figure 4.18: Radial active intensity distribution in dB before and after control minimising pressure at the pressure sensor location $r_e = (\lambda, 0)$ (the calculations are relative to a unitary primary source strength). The circle ◯ on the left is the primary monopole source location, and the circle ◯ on the right is the control monopole source location.*

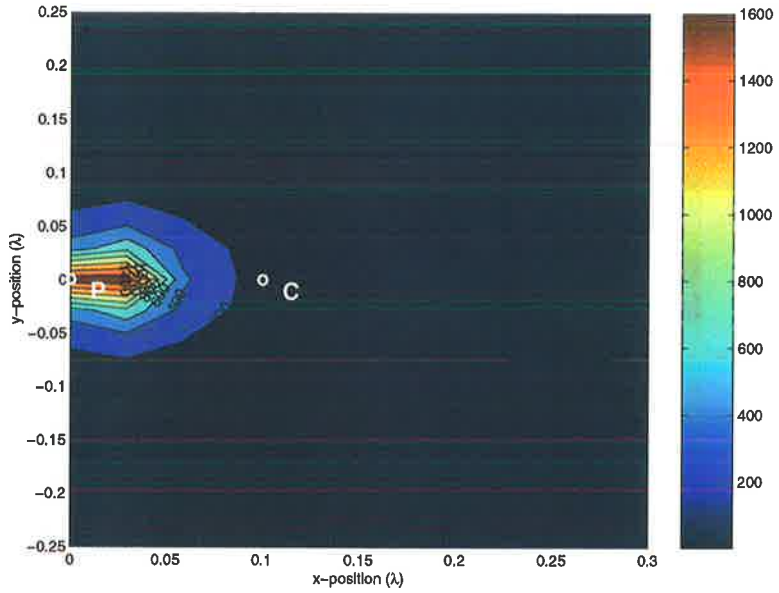


*(a) Radial active intensity distribution before control*

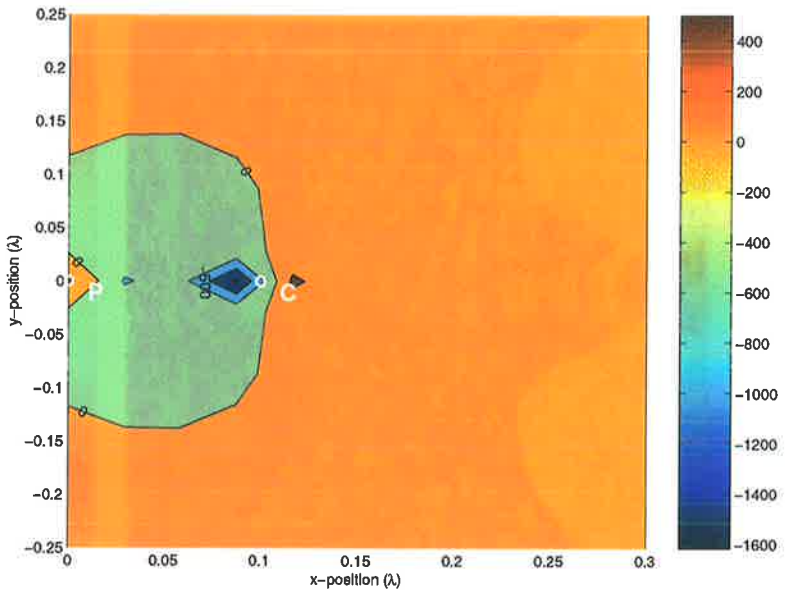


*(b) Radial active intensity distribution after control*

*Figure 4.19: Radial active intensity distribution in $W/m^3$ before and after control minimising pressure at the pressure sensor location $r_e = (\lambda, 0)$ (the calculations are relative to a unitary primary source strength). The circle ◯ on the left is the primary monopole source location, and the circle ◯ on the right is the control monopole source location.*

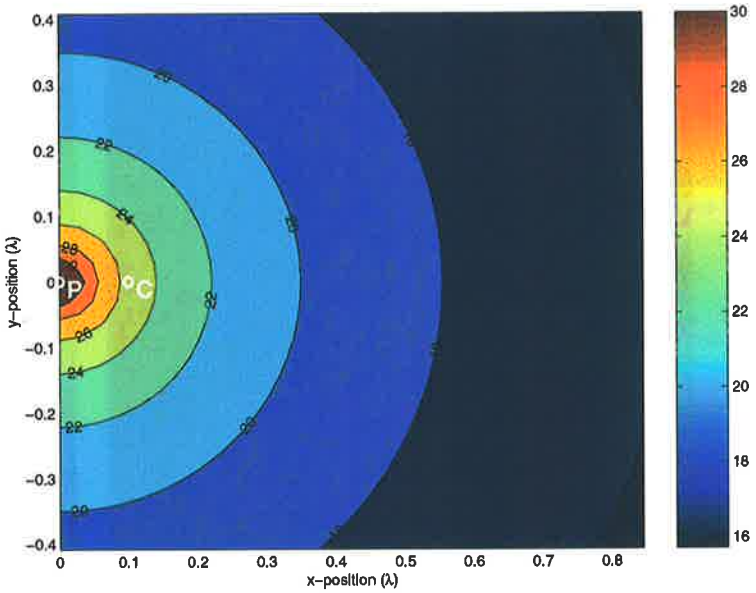


(a) Pressure distribution before control

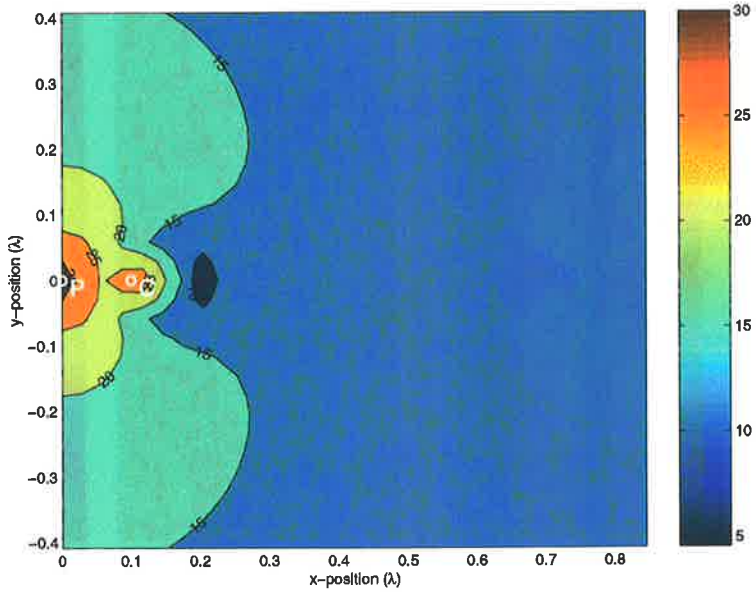


(b) Pressure distribution after control

*Figure 4.20: Pressure amplitude distribution in dB before and after control minimising pressure at the pressure sensor location $r_e = (\lambda/5, 0)$ (the calculations are relative to a unitary primary source strength). The circle ◯ on the left is the primary monopole source location, and the circle ◯ on the right is the control monopole source location.*

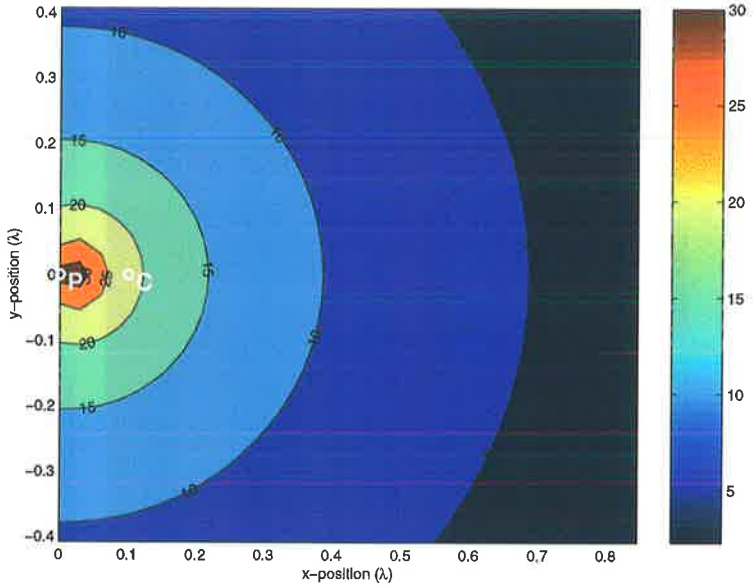


(a) Radial active intensity distribution before control

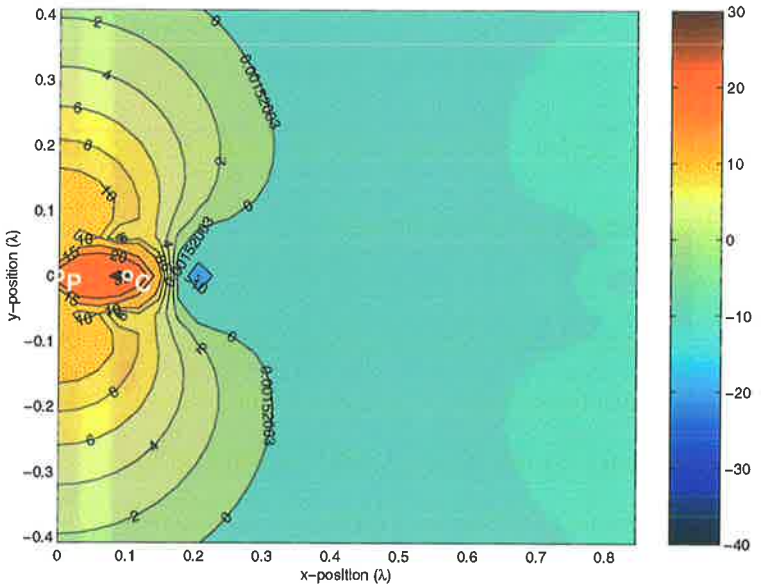


(b) Radial active intensity distribution after control

*Figure 4.21: Radial active intensity distribution in dB before and after control minimising pressure at the pressure sensor location $r_e = (\lambda/5, 0)$ (the calculations are relative to a unitary primary source strength). The circle ◯ on the left is the primary monopole source location, and the circle ◯ on the right is the control monopole source location.*

primary source. Figure 4.21b shows the radial active intensity distribution in dB (Figure 4.22b on a linear scale) after control. It can be seen that the result of far field radial active intensity sensing is to also reduce the pressure field globally.

Figure 4.23a shows the pressure distribution before control, with just the primary monopole source in operation in the infinite baffle when minimising the pressure at a distance of three fiftieths of a wavelength from the primary source. Figure 4.23b shows the pressure distribution after control. It can be seen that the result of far field pressure sensing is to reduce the pressure field globally. Figure 4.24a shows the radial active intensity distribution in dB (Figure 4.25a on a linear scale) before control, with just the primary monopole source in operation in the infinite baffle when minimising the pressure at a distance of three fiftieths of a wavelength from the primary source. Figure 4.24b shows the radial active intensity distribution in dB (Figure 4.25b on a linear scale) after control. It can be seen that the result of far field radial active intensity sensing is to also reduce the pressure field globally.

### 4.3.2 Pressure and active intensity fields before and after control minimising the radial active intensity

Figure 4.26a shows the pressure distribution before control, with just the primary monopole source in operation in the infinite baffle when minimising the pressure at a distance of one wavelength from the primary source. Figure 4.26b shows the pressure distribution after control. It can be seen that the result of far field pressure sensing is to reduce the pressure field globally. Figure 4.27a shows the radial active intensity distribution in dB (Figure 4.28a on a linear scale) before control, with just the primary monopole source in operation in the infinite baffle when minimising the pressure at a distance of one wavelength from the primary source. Figure 4.27b shows the radial active intensity distribution in dB (Figure 4.28b on a linear scale) after control. It can be seen that the result of far field radial active intensity sensing is to also reduce the pressure field globally.

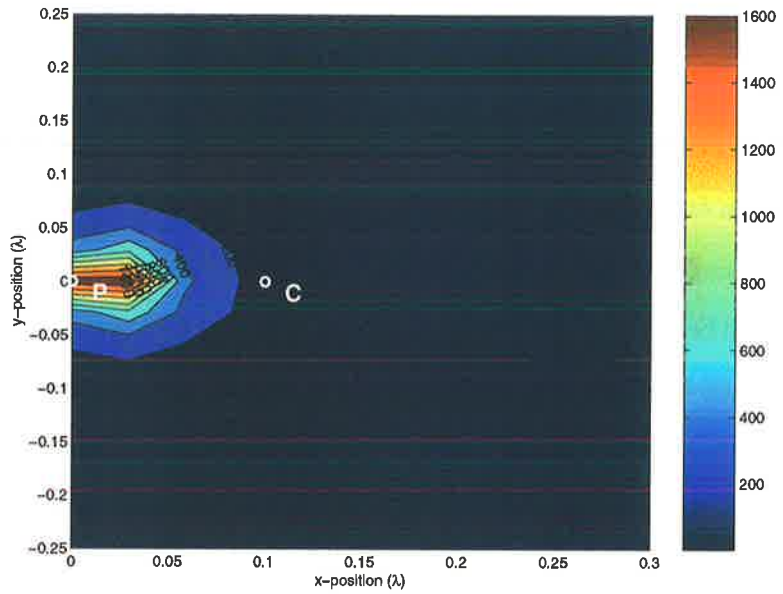


*(a) Radial active intensity distribution before control*

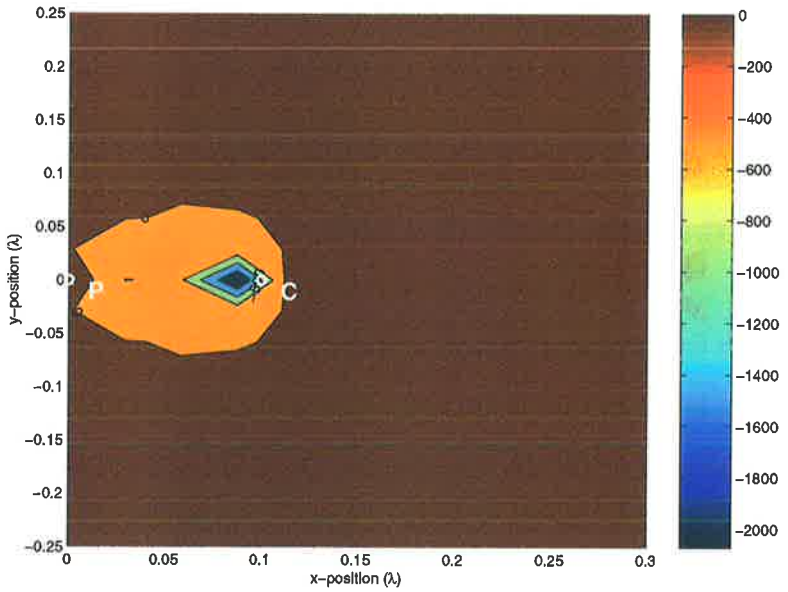


*(b) Radial active intensity distribution after control*

*Figure 4.22: Radial active intensity distribution in $W/m^3$ before and after control minimising pressure at the pressure sensor location $r_e = (\lambda/5, 0)$ (the calculations are relative to a unitary primary source strength). The circle ◯ on the left is the primary monopole source location, and the circle ◯ on the right is the control monopole source location.*

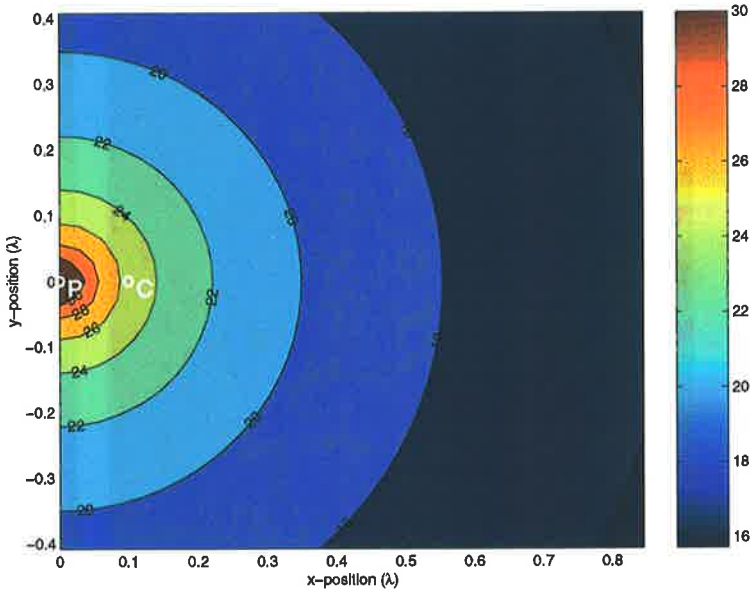


(a) Pressure distribution before control

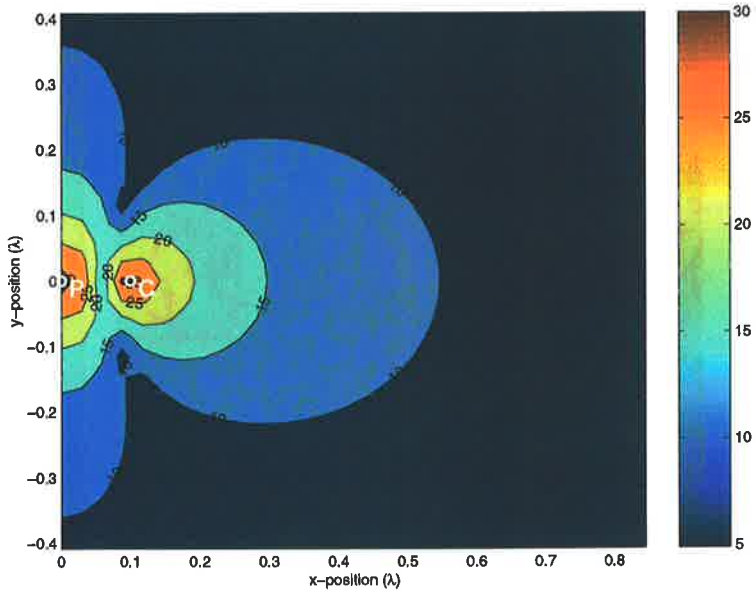


(b) Pressure distribution after control

*Figure 4.23: Pressure amplitude distribution in dB before and after control minimising pressure at the pressure sensor location $r_e = (3\lambda/50, 0)$ (the calculations are relative to a unitary primary source strength). The circle ◯ on the left is the primary monopole source location, and the circle ◯ on the right is the control monopole source location.*

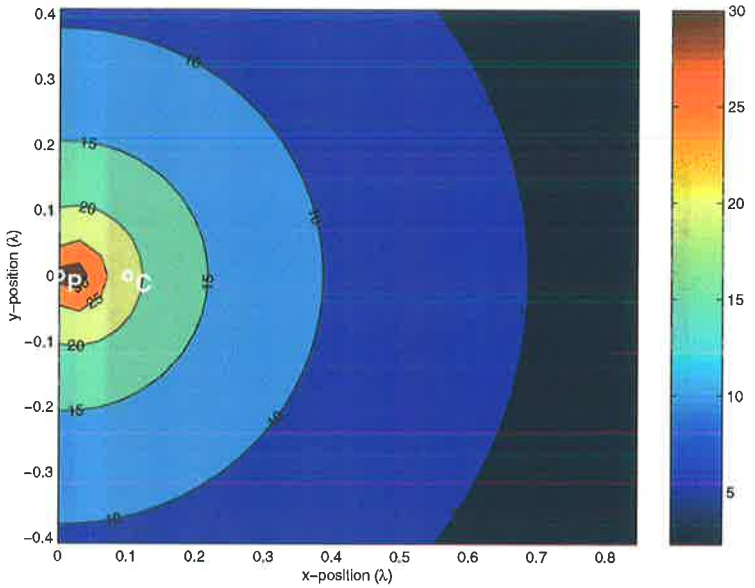


*(a) Radial active intensity distribution before control*

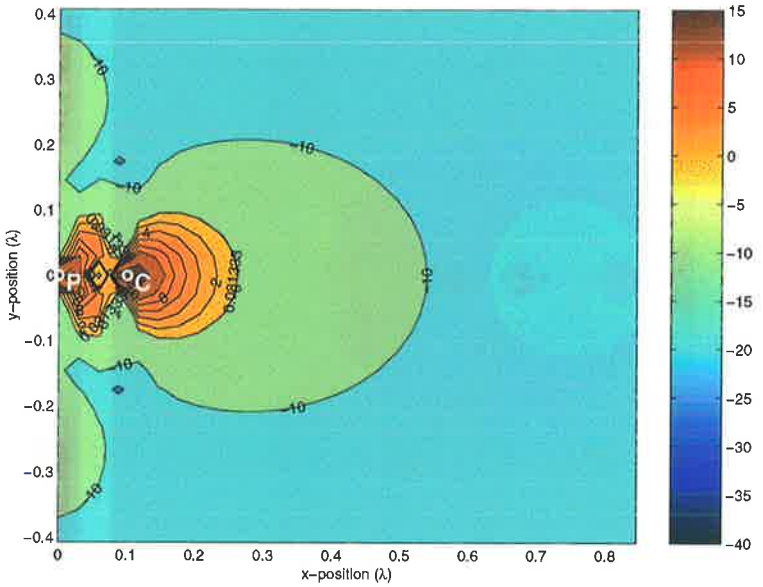


*(b) Radial active intensity distribution after control*

*Figure 4.24: Radial active intensity distribution in dB before and after control minimising pressure at the pressure sensor location $r_e = (3\lambda/50, 0)$ (the calculations are relative to a unitary primary source strength). The circle ◯ on the left is the primary monopole source location, and the circle ◯ on the right is the control monopole source location.*

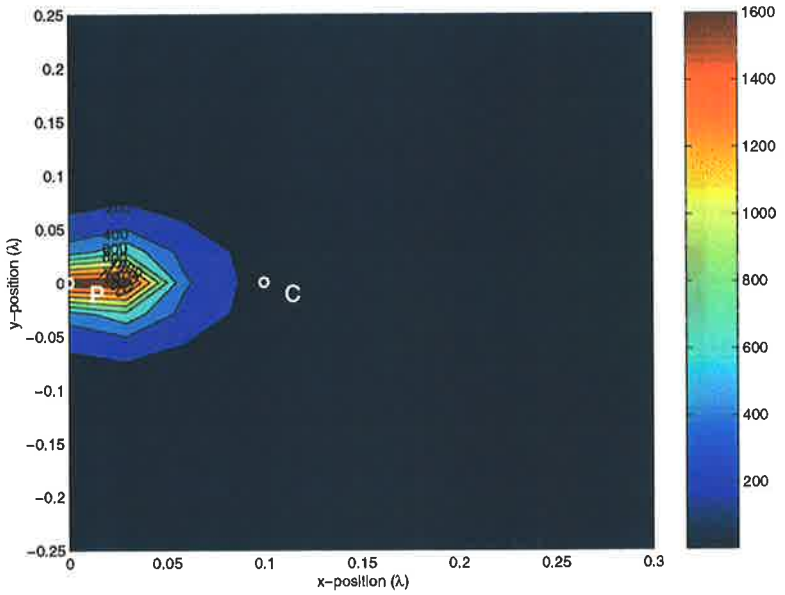


*(a) Radial active intensity distribution before control*

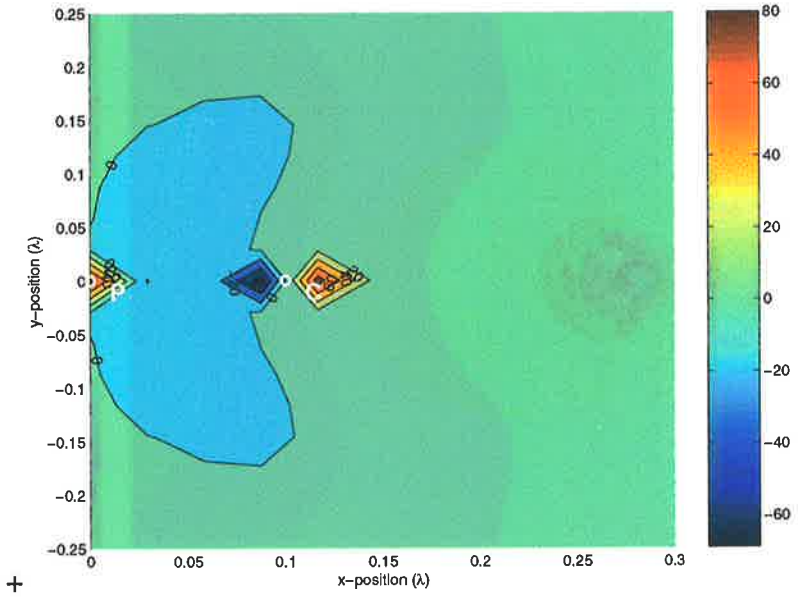


*(b) Radial active intensity distribution after control*

*Figure 4.25: Radial active intensity distribution in $W/m^3$ before and after control minimising pressure at the pressure sensor location $r_e = (3\lambda/50, 0)$ (the calculations are relative to a unitary primary source strength). The circle ◯ on the left is the primary monopole source location, and the circle ◯ on the right is the control monopole source location.*

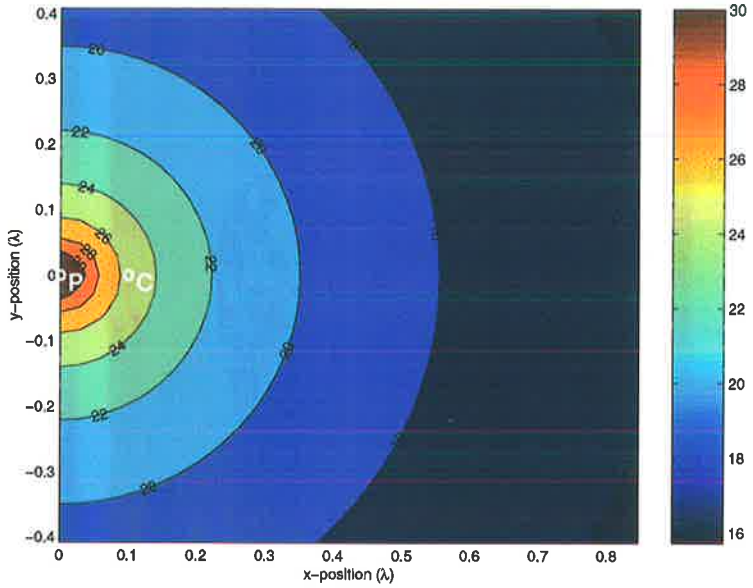


*(a) Pressure distribution before control*

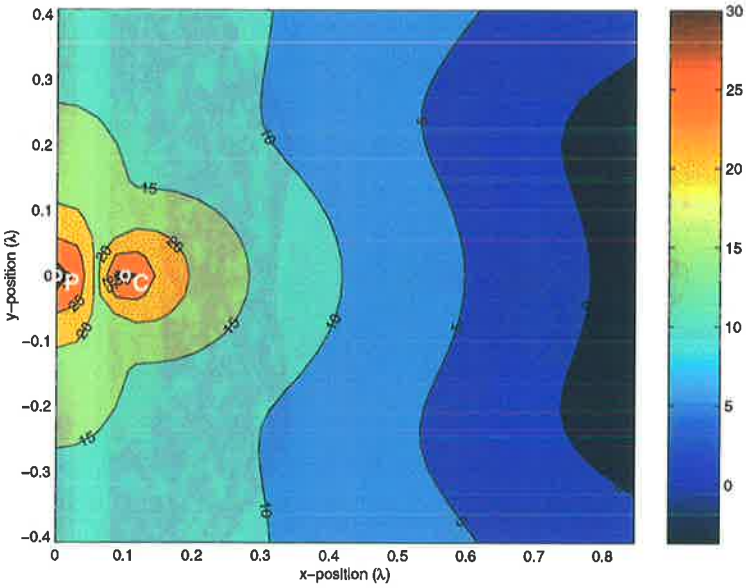


*(b) Pressure distribution after control*

*Figure 4.26: Pressure amplitude distribution in dB before and after control minimising the radial active intensity at the radial active intensity sensor location $r_e = (\lambda, 0)$ (the calculations are relative to a unitary primary source strength). The circle ◯ on the left is the primary monopole source location, and the circle ◯ on the right is the control monopole source location.*

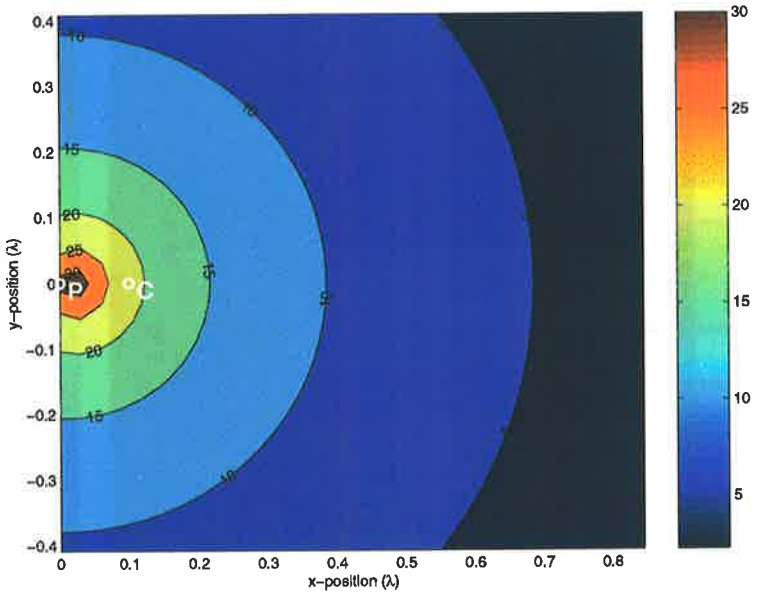


(a) Radial active intensity distribution before control

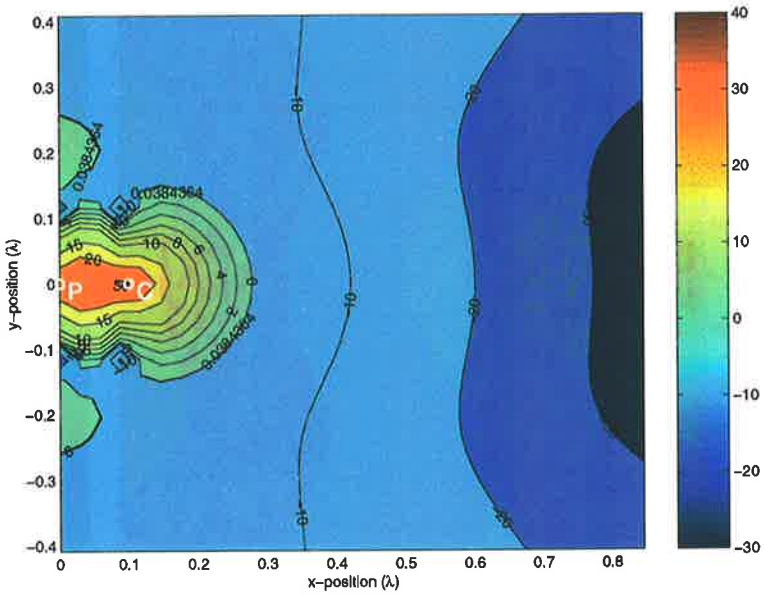


(b) Radial active intensity distribution after control

*Figure 4.27: Radial active intensity distribution in dB before and after control minimising the radial active intensity at the radial active intensity sensor location $r_e = (\lambda, 0)$ (the calculations are relative to a unitary primary source strength). The circle ◯ on the left is the primary monopole source location, and the circle ◯ on the right is the control monopole source location.*

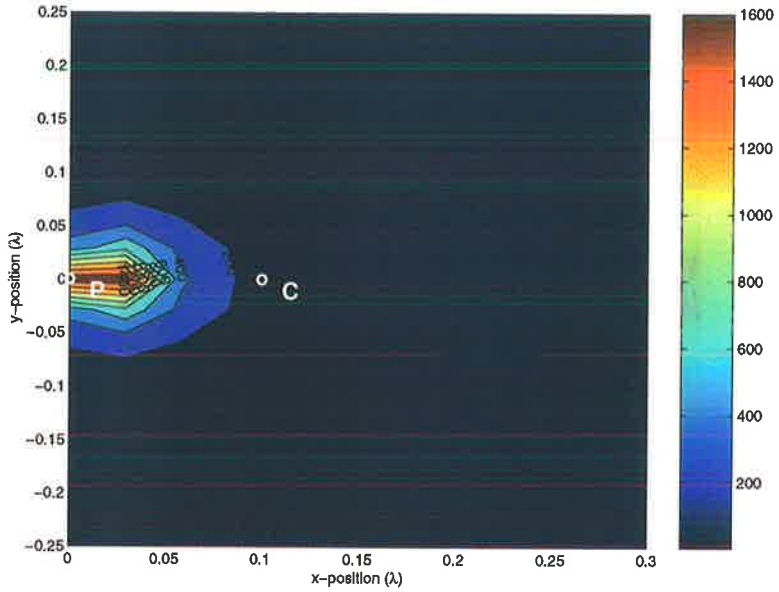


*(a) Radial active intensity distribution before control*

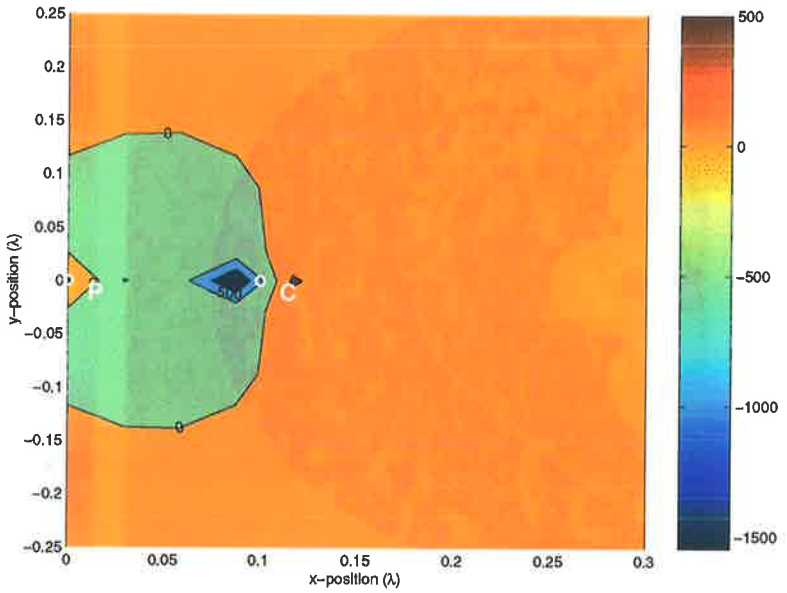


*(b) Radial active intensity distribution after control*

*Figure 4.28: Radial active intensity distribution in $W/m^3$ before and after control minimising the radial active intensity at the radial active intensity sensor location $r_e = (\lambda, 0)$ (the calculations are relative to a unitary primary source strength). The circle ◯ on the left is the primary monopole source location, and the circle ◯ on the right is the control monopole source location.*

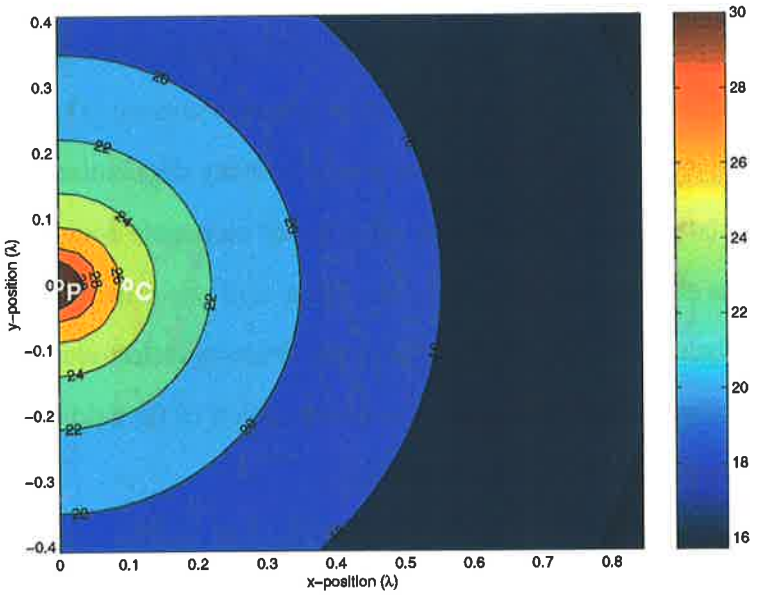


(a) Pressure distribution before control

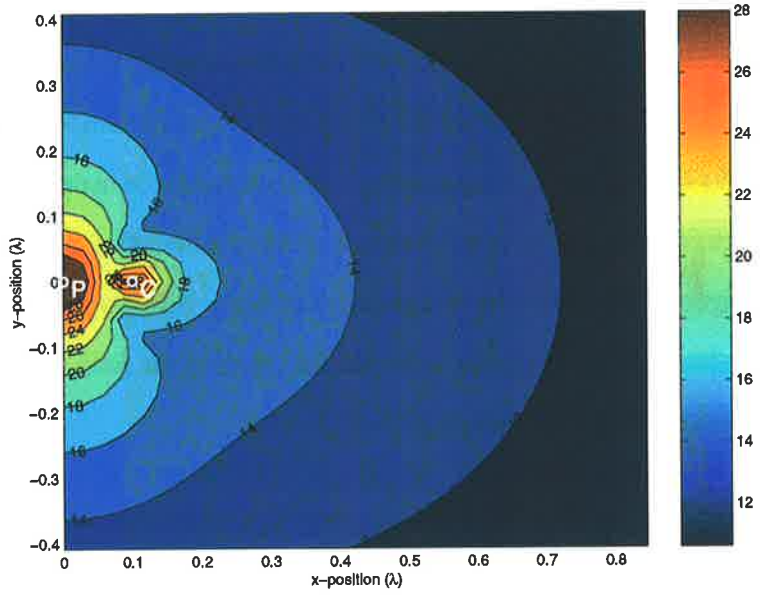


(b) Pressure distribution after control

*Figure 4.29: Pressure amplitude distribution in dB before and after control minimising the radial active intensity at the radial active intensity sensor location $r_e = (\lambda/5, 0)$ (the calculations are relative to a unitary primary source strength). The circle ◯ on the left is the primary monopole source location, and the circle ◯ on the right is the control monopole source location.*

Figure 4.29a shows the pressure distribution before control, with just the primary monopole source in operation in the infinite baffle when minimising the pressure at a distance of one fifth of a wavelength from the primary source. Figure 4.29b shows the pressure distribution after control. It can be seen that the result of far field pressure sensing is to reduce the pressure field globally. Figure 4.30a shows the radial active intensity distribution in dB (Figure 4.31a on a linear scale) before control, with just the primary monopole source in operation in the infinite baffle when minimising the pressure at a distance of one fifth of a wavelength from the primary source. Figure 4.30b shows the radial active intensity distribution in dB (Figure 4.31b on a linear scale) after control. It can be seen that the result of far field radial active intensity sensing is to also reduce the pressure field globally.

Figure 4.32a shows the pressure distribution before control, with just the primary monopole source in operation in the infinite baffle when minimising the pressure at a distance of three fiftieths of a wavelength from the primary source. Figure 4.32b shows the pressure distribution after control. It can be seen that the result of far field pressure sensing is to reduce the pressure field globally. Figure 4.33a shows the radial active intensity distribution in dB (Figure 4.34a on a linear scale) before control, with just the primary monopole source in operation in the infinite baffle when minimising the pressure at a distance of three fiftieths of a wavelength from the primary source. Figure 4.33b shows the radial active intensity distribution in dB (Figure 4.34b on a linear scale) after control. It can be seen that the result of far field radial active intensity sensing is to also reduce the pressure field globally.

Table 4.1 summarises the results. In short, the use of a sound intensity error criterion for the simple monopole radiation case offers little improvement over the acoustic pressure error criterion at best, and can lead to greatly reduced performance in some sensing locations where condition (4.50) is met.

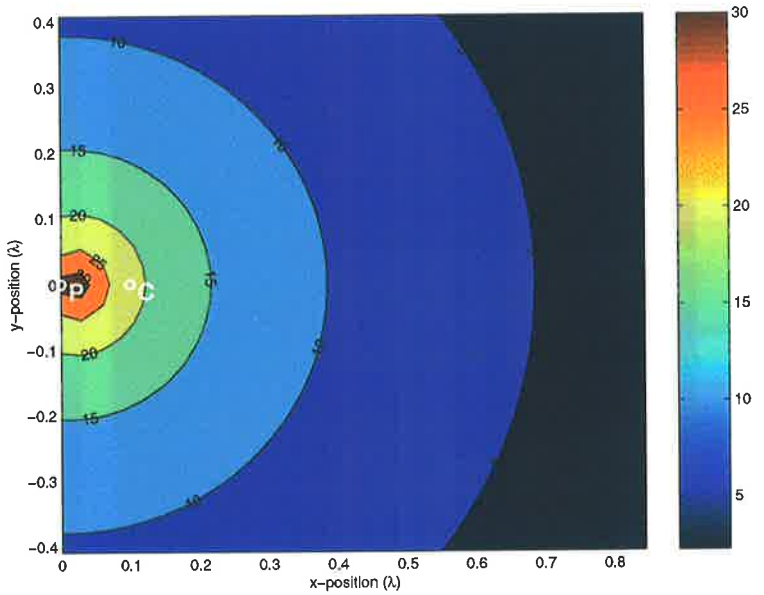


(a) Radial active intensity distribution before control

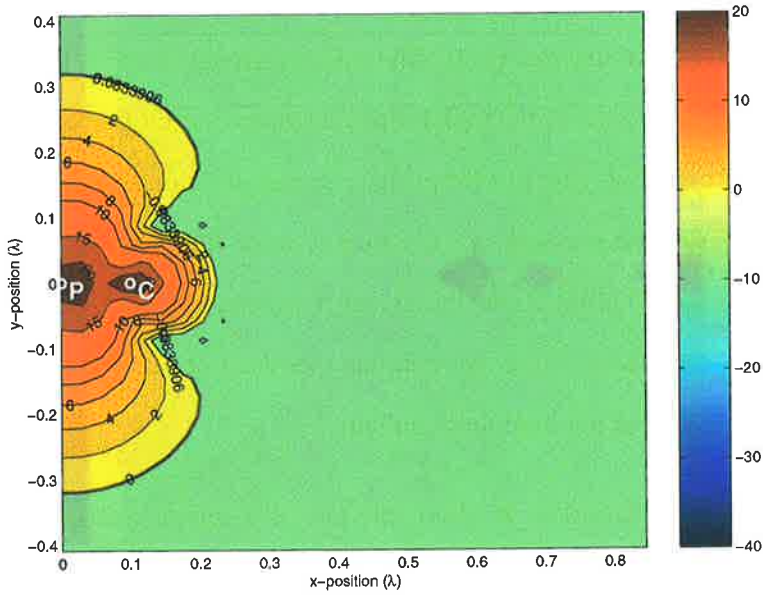


(b) Radial active intensity distribution after control

*Figure 4.30: Radial active intensity distribution in dB before and after control minimising the radial active intensity at the radial active intensity sensor location $r_e = (\lambda/5, 0)$ (the calculations are relative to a unitary primary source strength). The circle ◯ on the left is the primary monopole source location, and the circle ◯ on the right is the control monopole source location.*

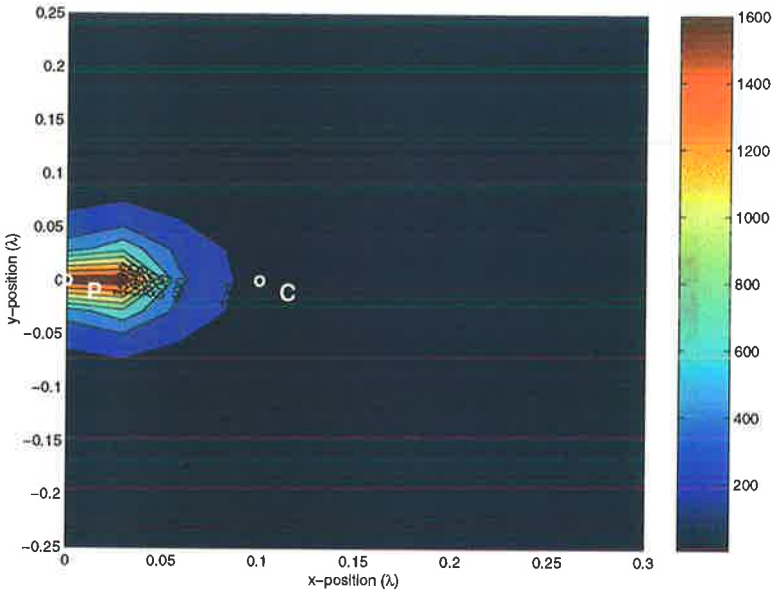


*(a) Radial active intensity distribution before control*

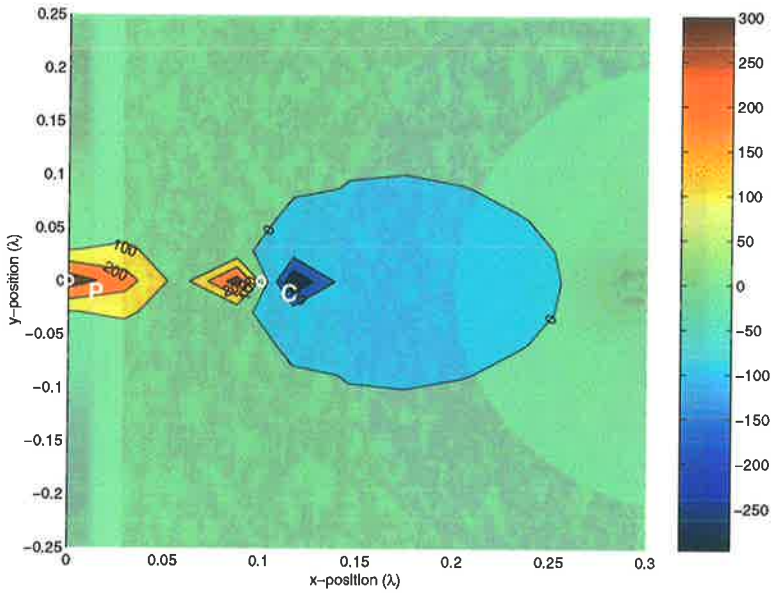


*(b) Radial active intensity distribution after control*

*Figure 4.31: Radial active intensity distribution in $W/m^3$ before and after control minimising the radial active intensity at the radial active intensity sensor location $r_e = (\lambda/5, 0)$ (the calculations are relative to a unitary primary source strength). The circle ◯ on the left is the primary monopole source location, and the circle ◯ on the right is the control monopole source location.*

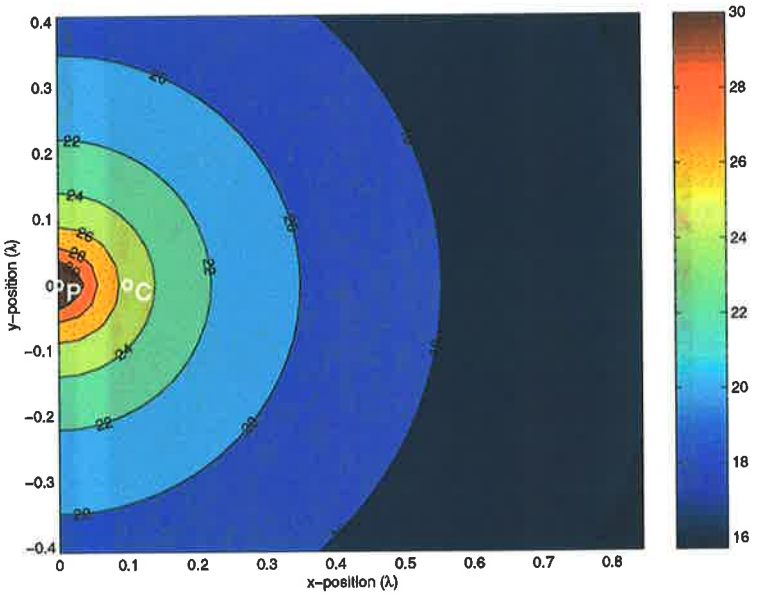


(a) Pressure distribution before control

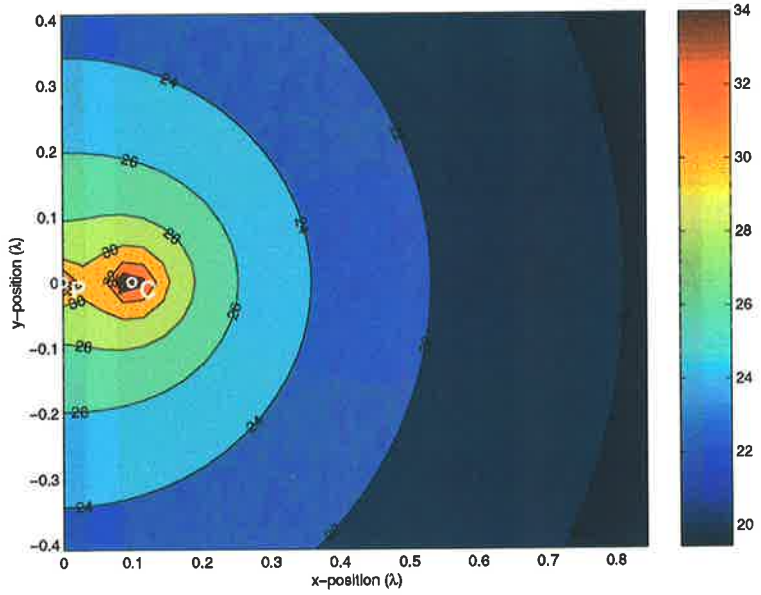


(b) Pressure distribution after control

*Figure 4.32: Pressure amplitude distribution in dB before and after control minimising the radial active intensity at the radial active intensity sensor location* $r_e = (3\lambda/50, 0)$ *(the calculations are relative to a unitary primary source strength). The circle* ◯ *on the left is the primary monopole source location, and the circle* ◯ *on the right is the control monopole source location.*

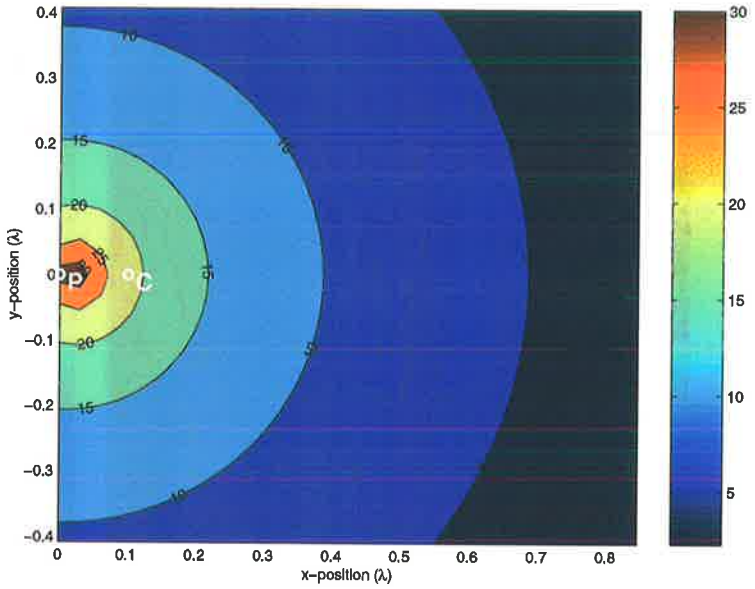


(a) Radial active intensity distribution before control

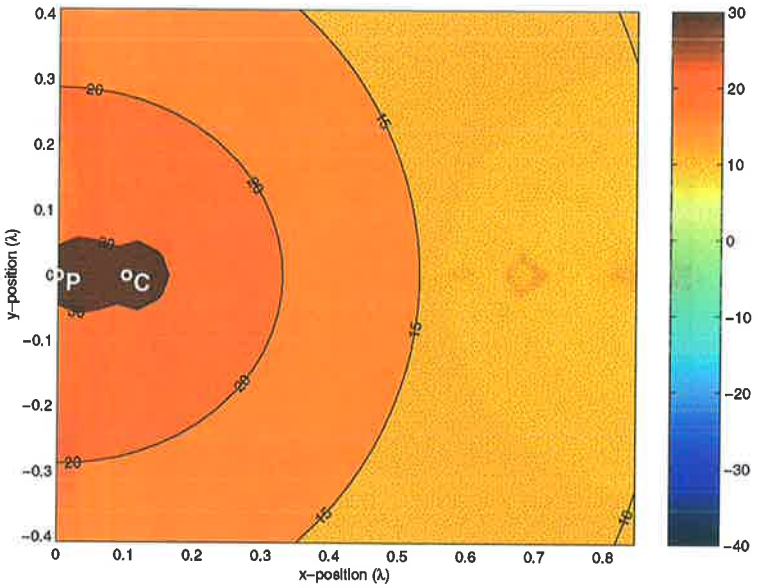


(b) Radial active intensity distribution after control

*Figure 4.33: Radial active intensity distribution in dB before and after control minimising the radial active intensity at the radial active intensity sensor location $r_e = (3\lambda/50, 0)$ (the calculations are relative to a unitary primary source strength). The circle ◯ on the left is the primary monopole source location, and the circle ◯ on the right is the control monopole source location.*

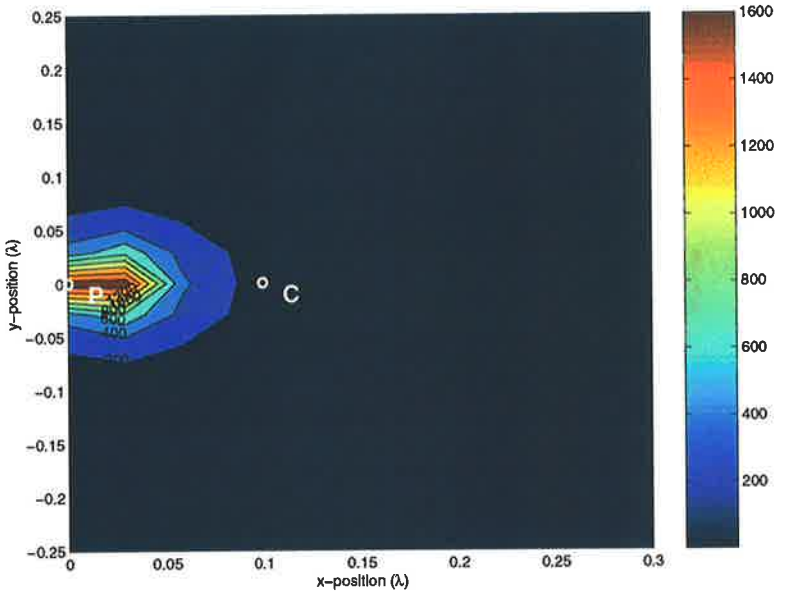


*(a) Radial active intensity distribution before control*

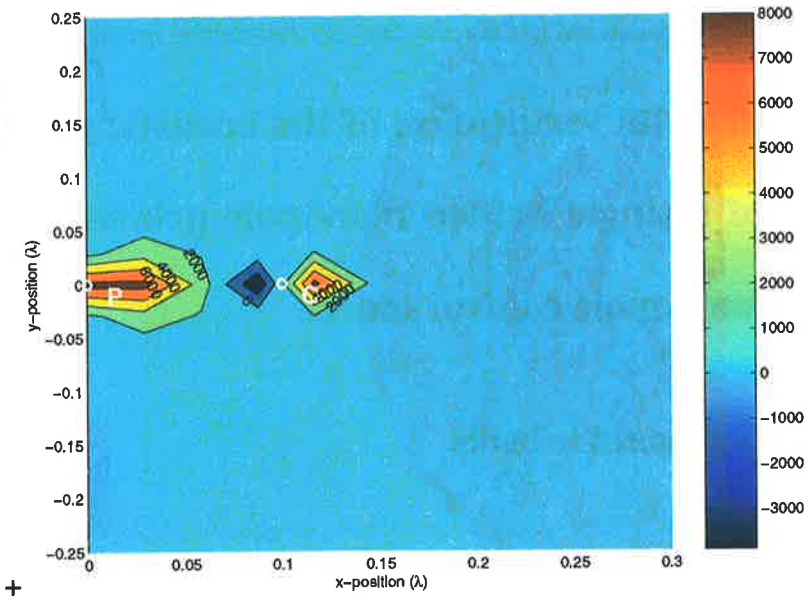


*(b) Radial active intensity distribution after control*

*Figure 4.34: Radial active intensity distribution in $W/m^3$ before and after control minimising the radial active intensity at the radial active intensity sensor location $r_e = (3\lambda/50, 0)$ (the calculations are relative to a unitary primary source strength). The circle ◯ on the left is the primary monopole source location, and the circle ◯ on the right is the control monopole source location.*

| Minimising | Error Sensor Location | Comments far field Pressure | Comments far field Intensity | Relevant Figures |
|---|---|---|---|---|
| Pressure | $(\lambda, 0)$ | $\downarrow$ by ~ 16dB | $\downarrow$ by ~ 40dB, near field negative intensity between primary and control | 4.17, 4.18, 4.19 |
| Intensity | $(\lambda, 0)$ | $\downarrow$ by ~ 20dB | $\downarrow$ by ~ 35dB, near field negative intensity between primary and control | 4.26, 4.27, 4.28 |
| Pressure | $(\lambda/5, 0)$ | $\downarrow$ by ~ 11dB | $\downarrow$ by ~ 15dB, near field negative intensity between primary and control | 4.20, 4.21, 4.22 |
| Intensity | $(\lambda/5, 0)$ | $\downarrow$ by ~ 4dB | $\downarrow$ by ~ 13dB, negative intensity behind control source | 4.29, 4.30, 4.31 |
| Pressure | $(3\lambda/50, 0)$ | $\downarrow$ by ~ 11dB | $\downarrow$ by ~ 15dB, near field negative intensity between primary and control | 4.23, 4.24, 4.25 |
| Intensity | $(3\lambda/50, 0)$ | $\uparrow$ by ~ 4dB | $\uparrow$ by ~ 7dB, near field negative intensity between primary and control | 4.32, 4.33, 4.34 |

*Table 4.1: Pressure and radial active intensity distribution results summary.*

## 4.4 Experimental verification of the acoustic power attenuation of a single baffled monopole primary source and single monopole control source

### 4.4.1 Speaker mounted in baffle

#### 4.4.1.1 Introduction

In order to model in experiment an acoustic monopole in an infinite baffle, a speaker of roughly the same size as was used (see Figure 4.35) for the monopole experiments, but mounted in a large baffle in an anechoic chamber (dimensions over wedge tips: 4.79m $\times$ 3.9m $\times$ 3.94m) with a lower cut-off frequency of 85Hz. It has been previously noted (Beranek (1996)) that at low frequencies a speaker can be approximated as a monopole source. The pressure amplitude

generated by the baffled speaker, used in the experiments, was measured radially away from the speaker, and a directivity measurement was made, to verify that it was a suitable model for an acoustic monopole source in a baffle.

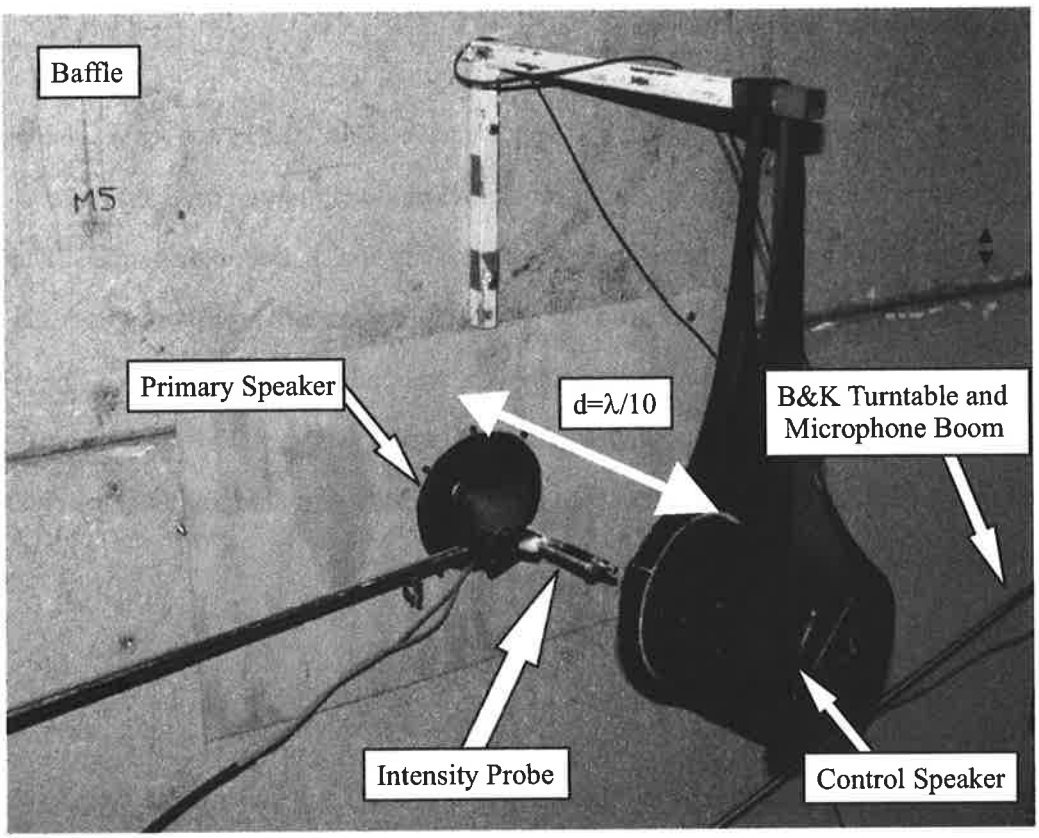


*Figure 4.35: Speaker mounted in baffle (110mm diameter SEAS driver) primary source, control enclosed speaker hung from a support arm by an elastic sling for isolation. Separation distance* $d = \lambda/10$.

#### 4.4.1.2 Baffled speaker specifications

The speaker (see Figure 4.35) used in the experiments consisted of a 110mm SEAS Driver Model number W11CY001. The speaker has a sensitivity of 86dB/mW and a nominal impedance of 8Ω. The maximum input power was 75Wrms. A baffle was constructed from 12mm thick medium density fiber board (MDF). The approximate dimensions of the baffle were 3 metres long by 2.5 metres high. The baffle was g-clamped vertically to a heavy steel table. Due to the weight of the table, it had to be positioned on the support poles of the floor structure in the

anechoic chamber, which meant that the position of the baffle limited the useful measurement space of the anechoic chamber to 75%.

#### 4.4.1.3 Monopole approximation

A speaker radiating into an acoustic half-space can be modelled as a circular piston in an infinite baffle (Beranek (1996)). It was found that when the circumference of the piston is less than half the wavelength, the piston behaves essentially like a monopole source. That is at low frequencies (where $ka < \frac{1}{2}$, $k$ being the wave number and $a$ the speaker radius) a speaker radiating into a half-space can be considered as a monopole source (Beranek (1996)). The speaker used in the following experiments has a radius of $a = 55$mm. Driven at a frequency of 100Hz, $ka = 0.1$. As this is much less than 0.5, the speaker was able to model the behaviour of monopole sources.

#### 4.4.1.4 Radial pressure distribution

The radial pressure distribution of the speaker was measured with the a B&K Type 4131 condenser microphone starting at 50mm from the speaker front face, at radial intervals of 50mm. A 3 metre length of 30 by 30mm Aluminum angle section with holes drilled at 50mm intervals to fit the 1/2" B&K Type 4131 condenser microphones was used to measure the pressure transfer function, between the speaker input and the B&K Type 4131 microphone output. The speaker was driven with random noise and 100 linear averages were applied to measure the pressure transfer functions at each radial location. The experimental setup is shown in Figure 4.36.

The experiment was conducted in an anechoic chamber (dimensions over wedge tips: 4.79m $\times$ 3.9m $\times$ 3.94m). The speaker was driven with random noise and at each 50mm interval location the acoustic signal was measured with the B&K Type 4131 condenser microphone. A Hewlett Packard 35665A Digital Signal Analyser was used to measure the transfer function

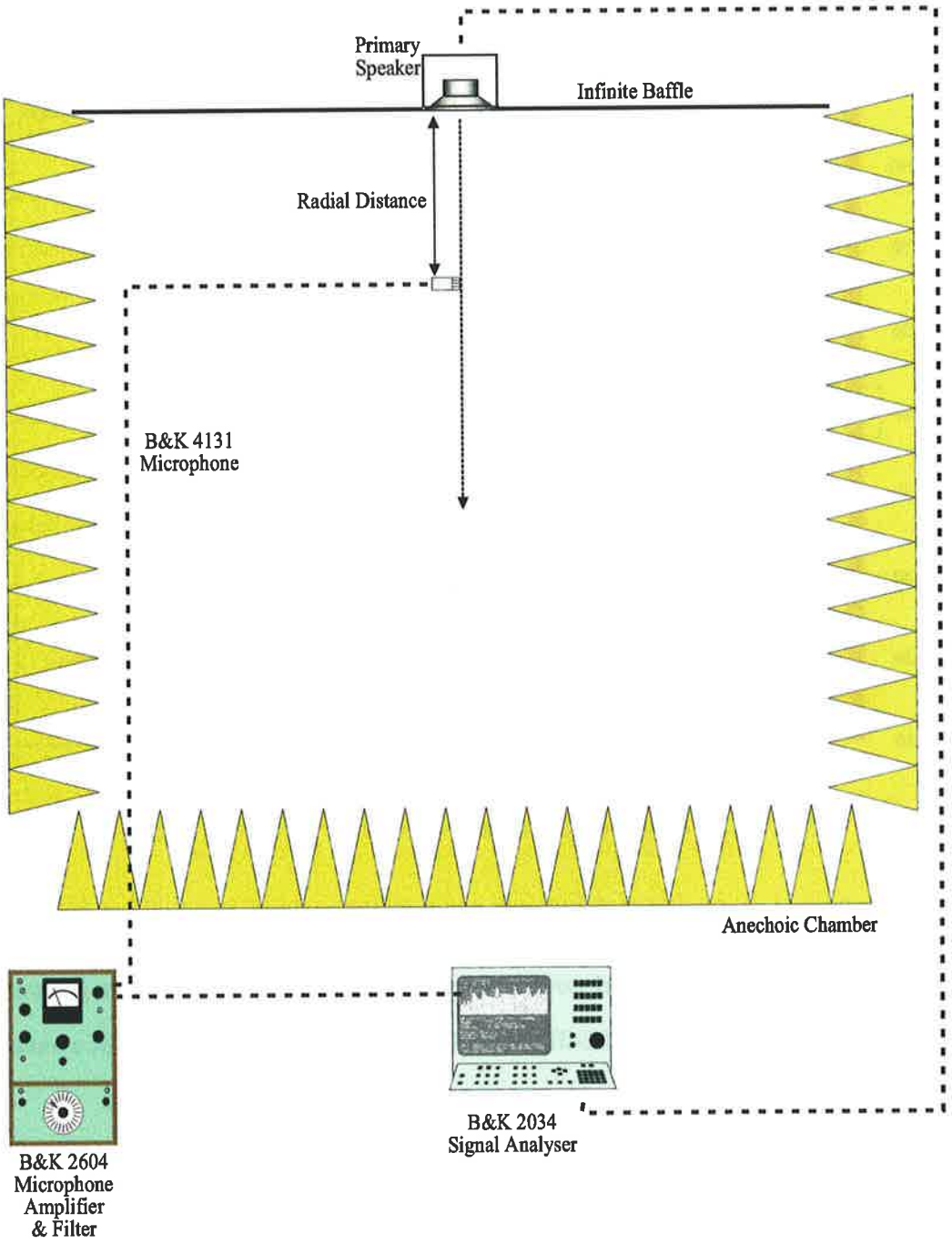


*Figure 4.36: Experimental setup for the measurement of the radial pressure distribution of a speaker in a baffle model of a monopole source in an infinite baffle.*

between the speaker output and the microphone input. 100 linear averages were used in the transfer function measurement. The radial pressure distribution produced is shown in Figure 4.37.

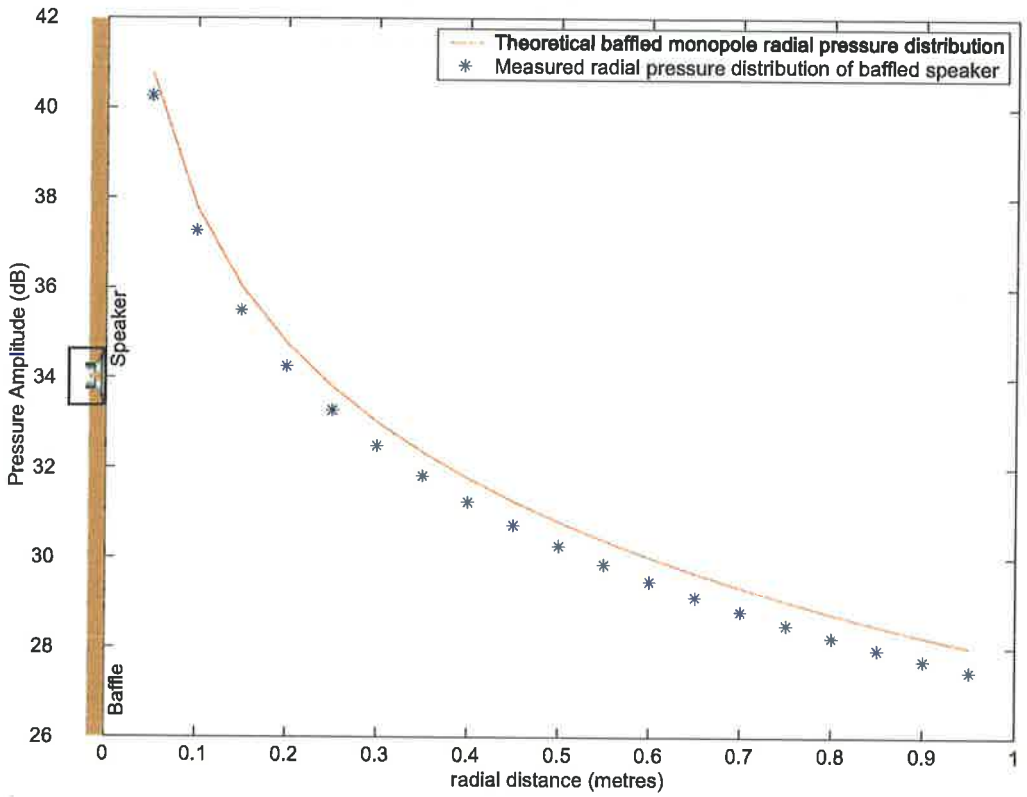


*Figure 4.37: Radial relative pressure distribution of enclosed speaker.*

The B&K Type 4131 condenser microphone was not calibrated and hence Figure 4.37 shows the relative pressure amplitude and not the sound pressure level. At distances greater than 50mm, the enclosed speaker fits the 6dB per doubling of distance characteristic of a monopole source with only a slight deviation which can be attributed to experimental error.

#### 4.4.1.5 Radial active intensity distribution

Based on the transfer function measurements described in Chapter 3, the active intensity along a radial line away from the enclosed speaker was calculated.

Figure 4.38 shows the relative active intensity as a function of radial distance away from the baffled speaker.

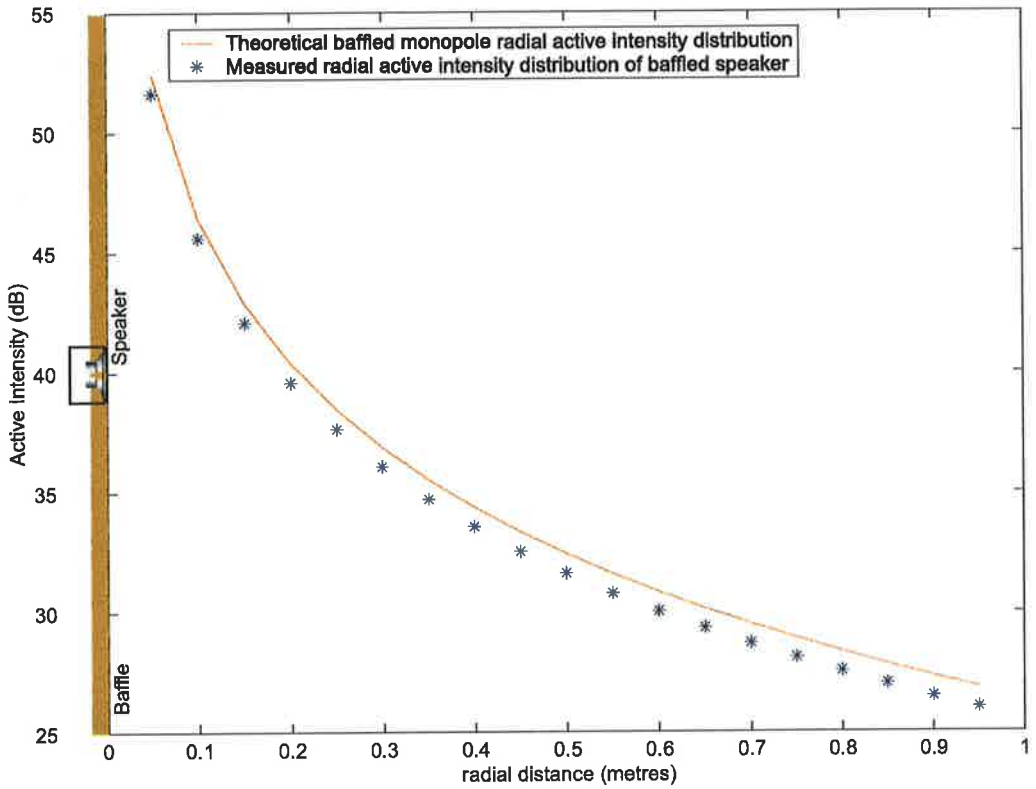


*Figure 4.38: Radial active intensity distribution of the baffled speaker.*

It can be seen in Figure 4.38 that the measured active intensity closely matches the theoretical monopole radial active intensity distribution, as does the measured pressure to the theoretical monopole radial pressure distribution shown in Figure 4.37. There is only a slight variation, the most likely cause of which is experimental error.

#### 4.4.1.6 Baffled speaker directivity pattern

To further test the accuracy of modelling a monopole source by an baffled speaker, an experiment was done to measure the directivity of the baffled speaker. Figure 4.39 shows the setup used. The speaker was mounted in the baffle in the anechoic chamber. At the face of the baffle a B&K Type 3921 Turntable is positioned with a microphone stand and boom (1.8 metres)

attached. A B&K Type 4131 condenser microphone is used to measure the produced sound field. A B&K Type 2034 Signal Analyser is used to generate a tone at 100Hz which is fed to the baffled speaker. The resultant sound field is measure by the B&K Type 4131 condenser microphone which is 1/3 octave band pass filtered in the 100Hz 1/3 octave band. The signal from the filter is fed to a B&K Type 2307 Level Recorder and the signal is plotted on polar plotting paper. The results were scanned into a computer with Corel Trace™. In order to convert the data into a useful electronic format, a number of points were entered into Matlab™ from the traced data. The directivity plot is shown in Figure 4.40. It is noted that the directivity is constant, with only slight deviation in radius by approximately 2dB.

## 4.4.2 Results

### 4.4.2.1 Far field pressure distribution

In order to assess the power attenuation of minimising an active intensity cost function over that which is obtained by minimising the squared pressure the "far field" sound pressure was measured with a microphone attached to a boom and turntable through an arc 180°, before and after control is applied.

Figure 4.41 shows the experimental setup. The primary source used was a speaker embedded in a baffle (as described previously) and a control source which was an enclosed pipe speaker (described previously in Chapter 3). The control source was hung inside a pair of stockings from a cantilever support beam bolted above the primary source to isolate vibrations. The experiment was conducted in an anechoic chamber (dimensions over wedge tips: 4.79m $\times$ 3.9m $\times$ 3.94m with a lower cut-off frequency of 85Hz) and the sources were separated by a distance of $\lambda/10$. A B&K Type 4131 condenser microphone put through a B&K Type 2604 Microphone Amplifier which is 1/3 octave band pass filtered in the 100Hz 1/3 octave band was used to measure the "far field" sound pressure. The B&K Type 4131 condenser microphone was attached to a microphone boom which was located just in in front of the baffled primary

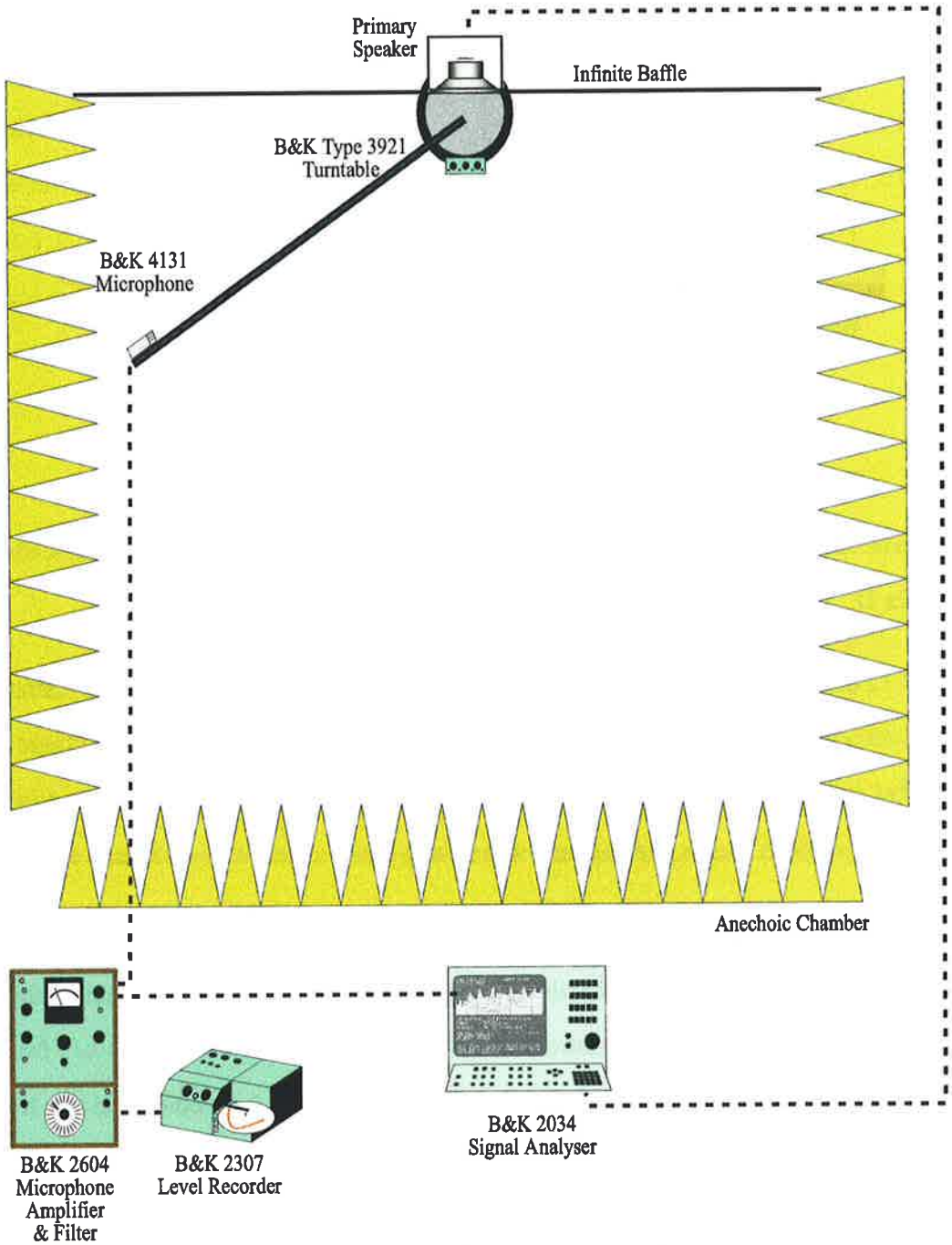


*Figure 4.39: Experimental setup for baffled speaker.*

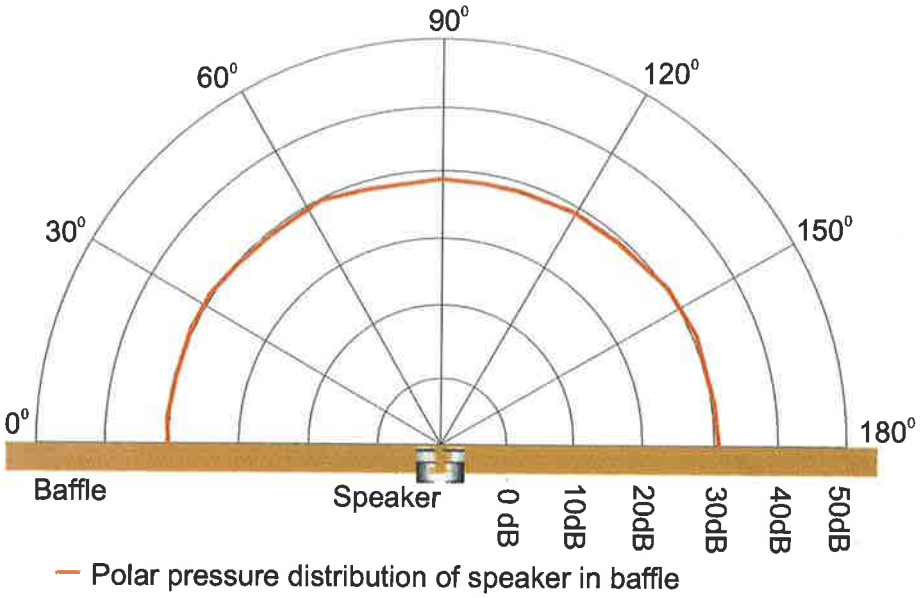


*Figure 4.40: Directivity pattern of baffled speaker.*

source and extended 1.8 metres out (see Figure 4.42). The control system is described in Appendix D.

Figure 4.12 displays the location of the error sensors tested in these experiments. Illustrated in Figure 4.43 is the result of far field error sensing (at $\lambda$ from the primary source, see Figure 4.12) with either an acoustic pressure error sensor or an active intensity error sensor. As expected, based on the previous results, the outcome when using either a pressure or intensity error signal is similar.

Figure 4.44 shows the result of minimising the pressure and active intensity amplitude at a position closer to the primary and control sources. The error sensor is located at $\lambda/5$ from the primary source, just behind the control source, see Figure 4.12. As predicted in the simulations, the active intensity result is marginally better than the pressure result in this instance.

Illustrated in Figure 4.45 is the result of sensing the pressure and active intensity amplitude in the near field, between the primary and control sources at a distance of $3\lambda/50$ from the baffle. Table 4.2 summarises the results. An active intensity cost function (see Appendix D) is predicted to have only a maximum, which leads to an increase in the radiated sound field,

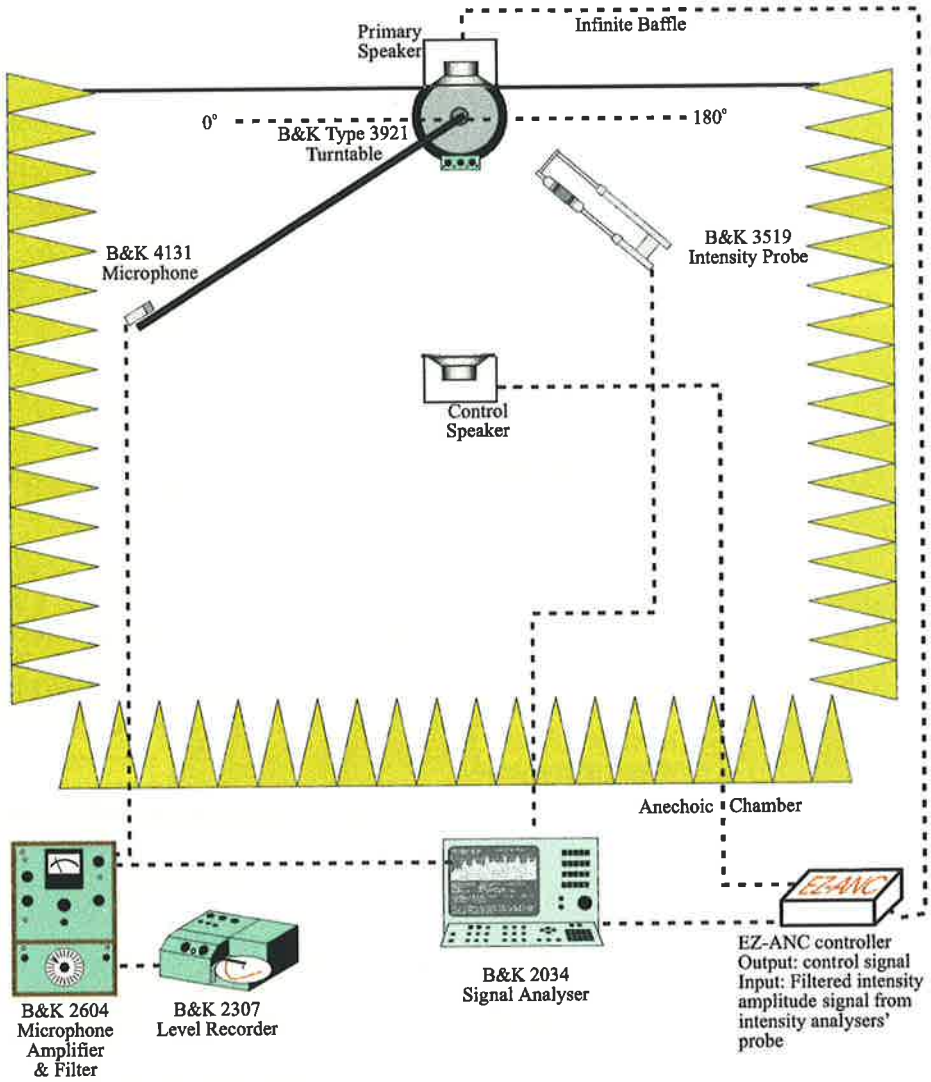


*Figure 4.41: Experimental setup for measuring the far field pressure distribution before and after active control is applied to minimise a squared pressure and active intensity amplitude cost function.*

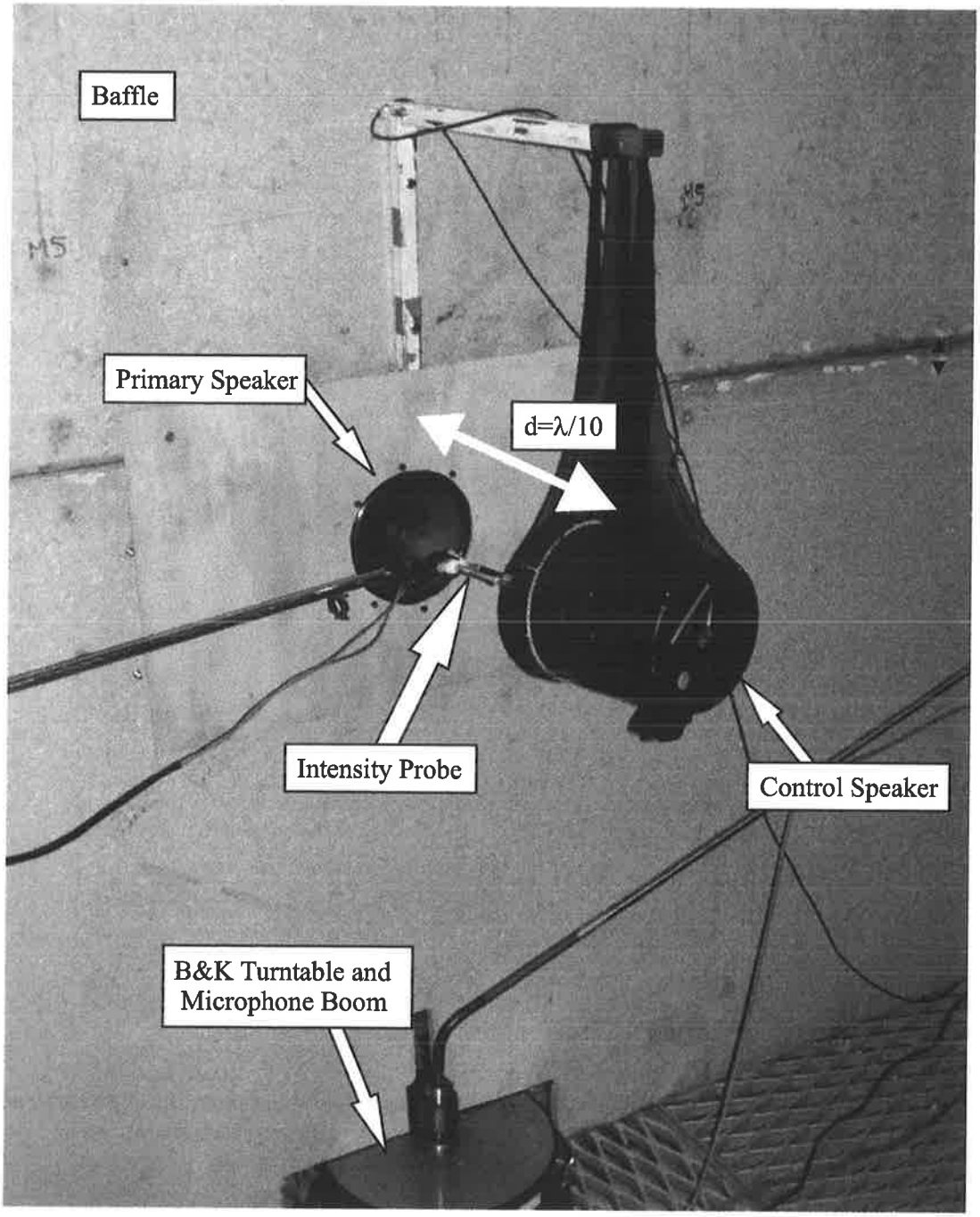


*Figure 4.42: Speaker mounted in baffle (110mm diameter SEAS driver).*

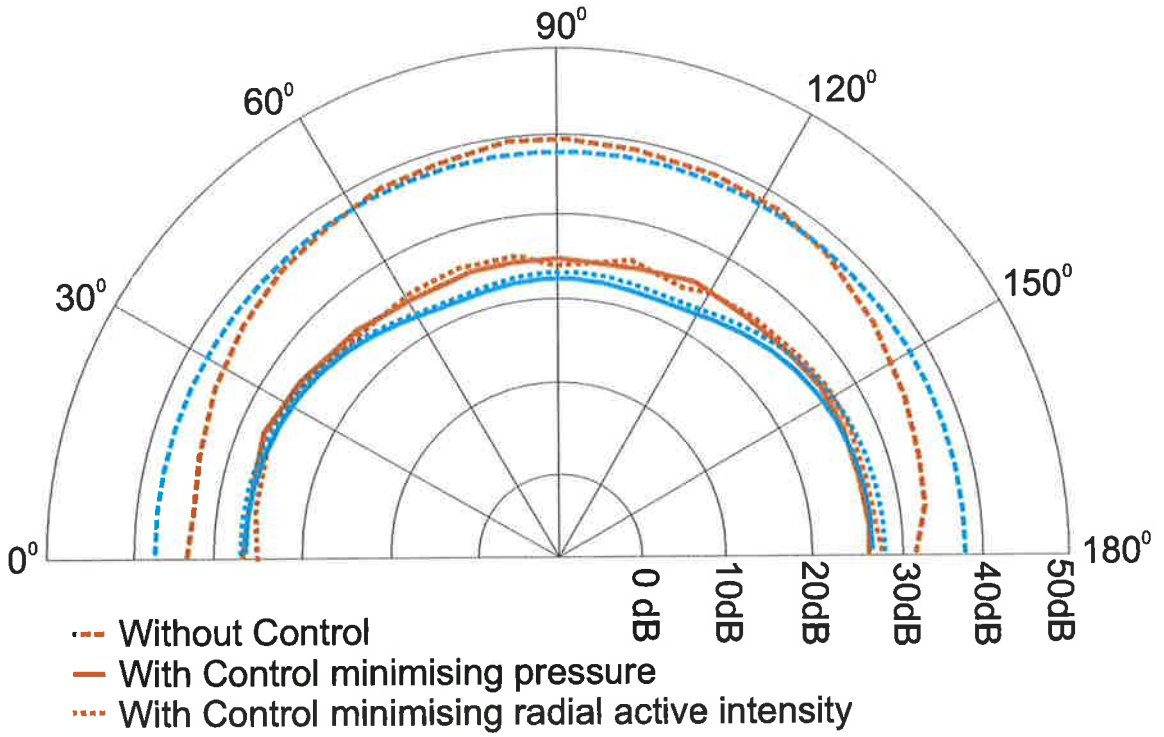


*Figure 4.43: Far field pressure before and after control when employing a single acoustic pressure or radial active intensity error sensor at λ from the primary source on the x-axis to control a 100Hz tone from a monopole primary source with a single monopole control source. The red lines indicate the experimental measurements. The blue lines indicate the theoretically predicted results with a 1% error in amplitude and 1° error in phase of the control signal.*

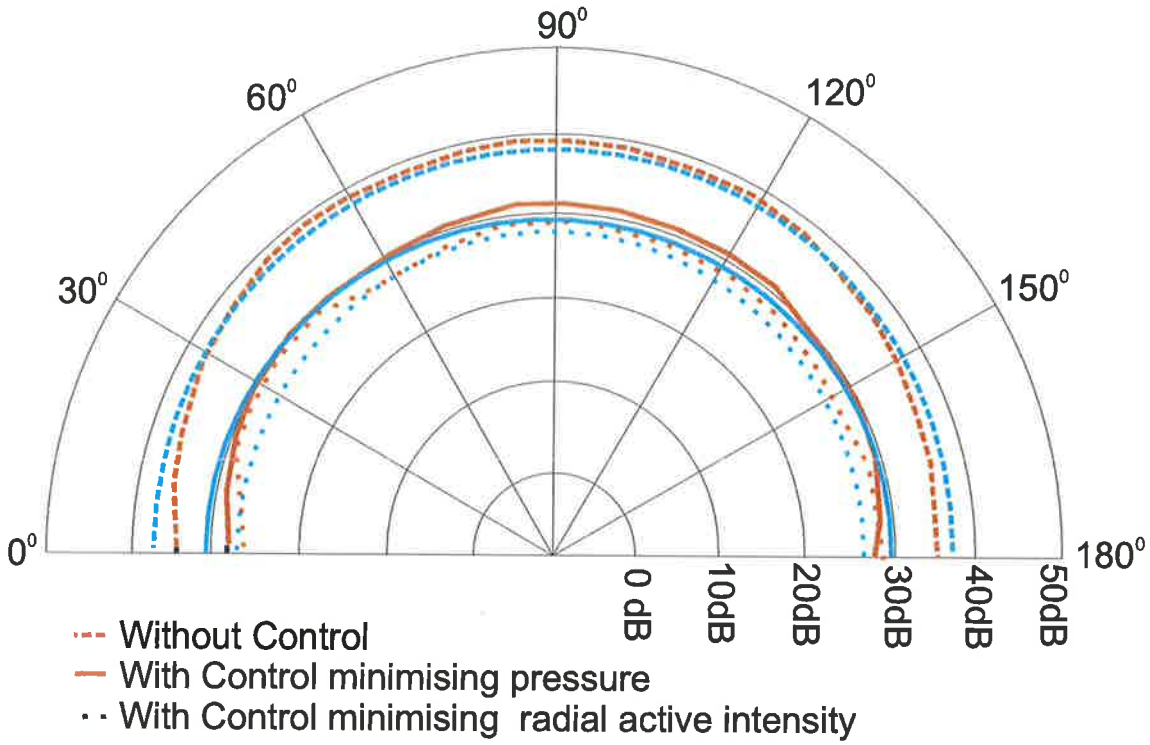


*Figure 4.44: Far field pressure before and after control when employing a single acoustic pressure or radial active intensity error sensor at $\lambda/5$ from the primary source on the x-axis to control a 100Hz tone from a monopole primary source with a single monopole control source. The red lines indicate the experimental measurements. The blue lines indicate the theoretically predicted results with a 1% error in amplitude and $1^o$ error in phase of the control signal.*

when control is applied. Active intensity amplitude is positive definite, but no longer quadratic and from Figure 4.15 is known to have a locus of infinitely many minima. In the case of the experiment, significant global attenuation was achieved with the pressure error sensor. However when the active intensity amplitude was minimised a net increase in the far field pressure resulted. This poor performance is predicted theoretically, as there is no mechanism to force the active intensity amplitude error signal to converge to the pressure or power optimal minimum, it will occur whenever (which is most likely) the active intensity amplitude error signal converges to a minimum other than the pressure or power minimum.

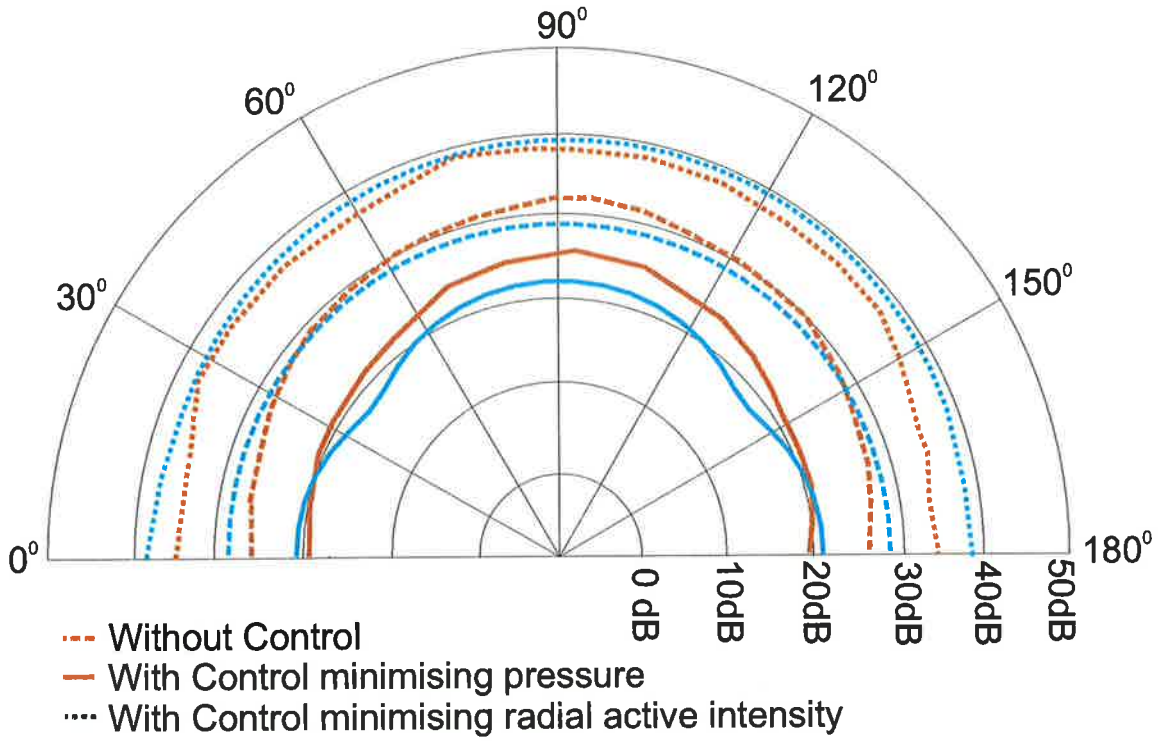


*Figure 4.45: Far field pressure before and after control when employing a single acoustic pressure or radial active intensity error sensor located approximately halfway between the primary and control sources (at radial distance of $3\lambda/50$ from the primary source) to control a 100Hz tone from a monopole primary source with a single monopole control source. The red lines indicate the experimental measurements. The blue lines indicate the theoretically predicted results with a 1% error in amplitude and $1^o$ error in phase of the control signal.*

#### 4.4.2.2 Active intensity versus control source strength

In order to test the validity of the theoretical prediction of negative active intensity, measurements were made of the active intensity at the midpoint between the primary and control sources at different control source strengths. Figure 4.46 shows the setup used in the experiment. The primary speaker was mounted in the baffle (described previously) and the control speaker was again mounted on a stand in an anechoic chamber (dimensions over wedge tips: 4.79m $\times$ 3.9m $\times$ 3.94m) and they were separated by a distance of $\lambda/10$ as shown in Figure 4.46. The B&K Type 2134 Sound Intensity Analyser's intensity probe was positioned at a distance of $3\lambda/50$, $\lambda/5$ and $\lambda$ from the primary source along a line passing through the primary and control sources. The primary and control sources were driven by a 100Hz tone. The intensity signal is 1/3 octave band pass filtered in the 100Hz 1/3 octave band.

#### 4.4.2.3 Results of the relative total active intensity

The intensity probe positioned as described above, was used to measure the active intensity when the primary speaker was driven with a reference voltage $V_p$ at 100Hz and the input voltage to the control speaker $V_c$ was adjusted. The voltmeter in Figure 4.46 was used to measure the input voltage $V_{input} = V_c$ to the enclosed speakers. The active intensity value and the relative voltage $V_c/V_p$ was recorded. The active intensity values were then converted from dB to a linear scale and the relative voltage $V_c/V_p$ was squared and then plotted in Matlab™.

Figure 4.47 shows total active intensity (from both primary and control sources) relative to the primary active intensity on its own, plotted against the control source strength relative to the primary source strength when the intensity probe is located at the approximate midpoint between primary and control sources (at a radial distance of $3\lambda/50$ from the primary source). The results show a deviation between the theoretically predicted relative total active intensity and that which was measured by experiment described above. Experiment has verified that

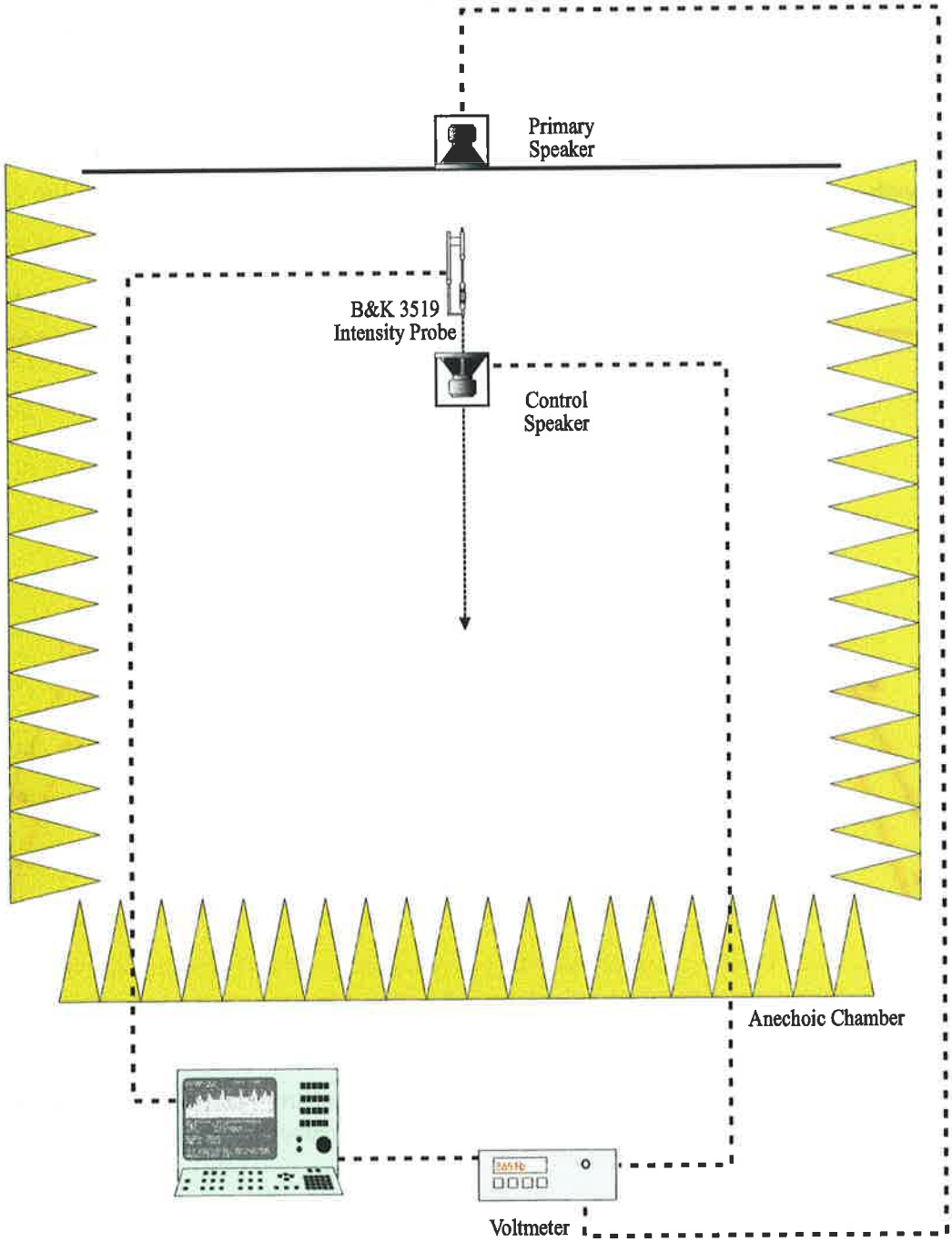


*Figure 4.46: Experimental setup to measure the active intensity located at radial distances of* $3\lambda/50$, $\lambda/5$ *and* $\lambda$ *from the primary source at 100Hz at different control source strengths.*

the active intensity does indeed become negative for certain control source strengths, the difference between theory and experiment can be put down to experimental error. Such as for example the measurement accuracy of the active intensity at a relative control speaker input voltage in dB conversion to a linear scale. The active intensity varied by approximately 10dB across the range of voltages which were measured, sometimes only by 0.2dB between voltage increments.

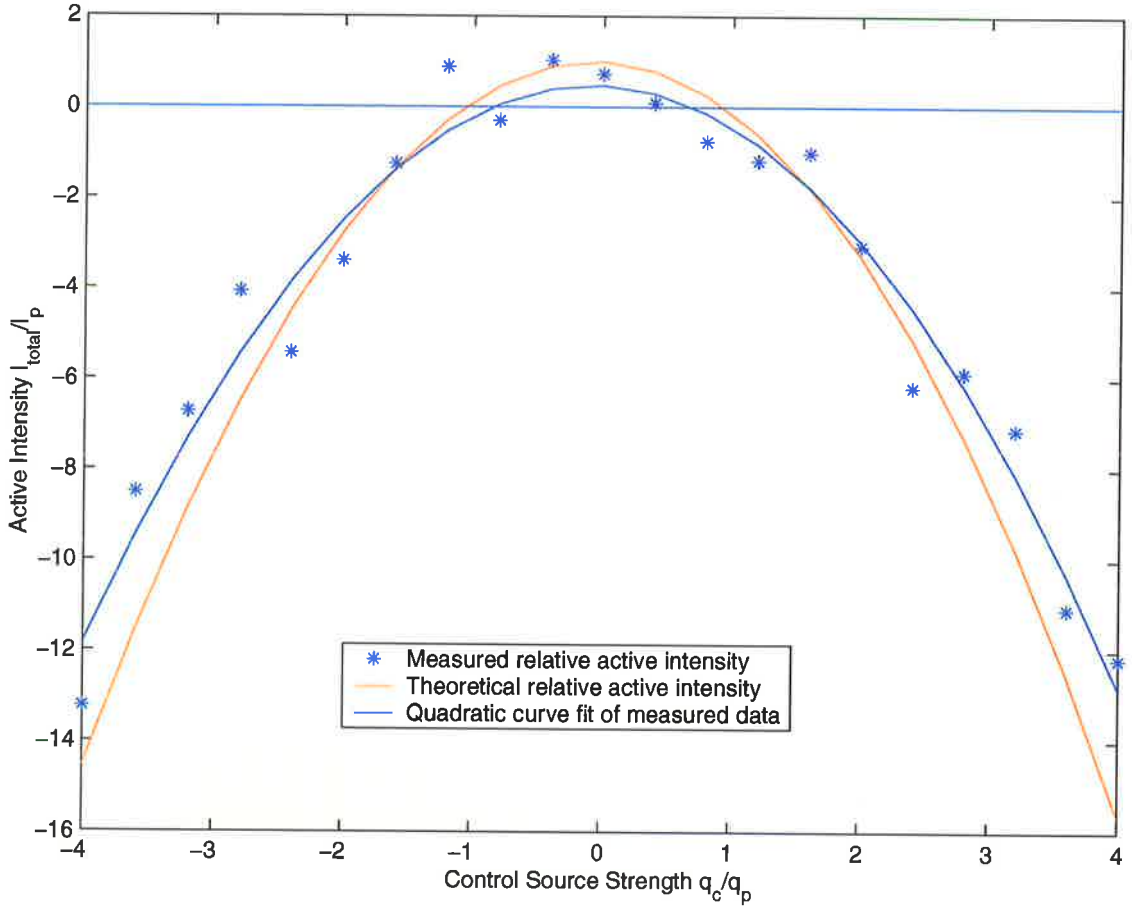


*Figure 4.47: Relative total active intensity plotted against the relative control source strength at the approximately the midpoint between the primary and control sources (at a radial distance of $3\lambda/50$ from the primary source).*

Figure 4.48 shows the total active intensity amplitude relative to the primary active intensity plotted against the control source strength relative to the primary source strength at a radial distance of $3\lambda/50$ from the primary source. From Figure 4.47 it has been shown that the active intensity cost function can be made negative and hence has no minimum value. If an active

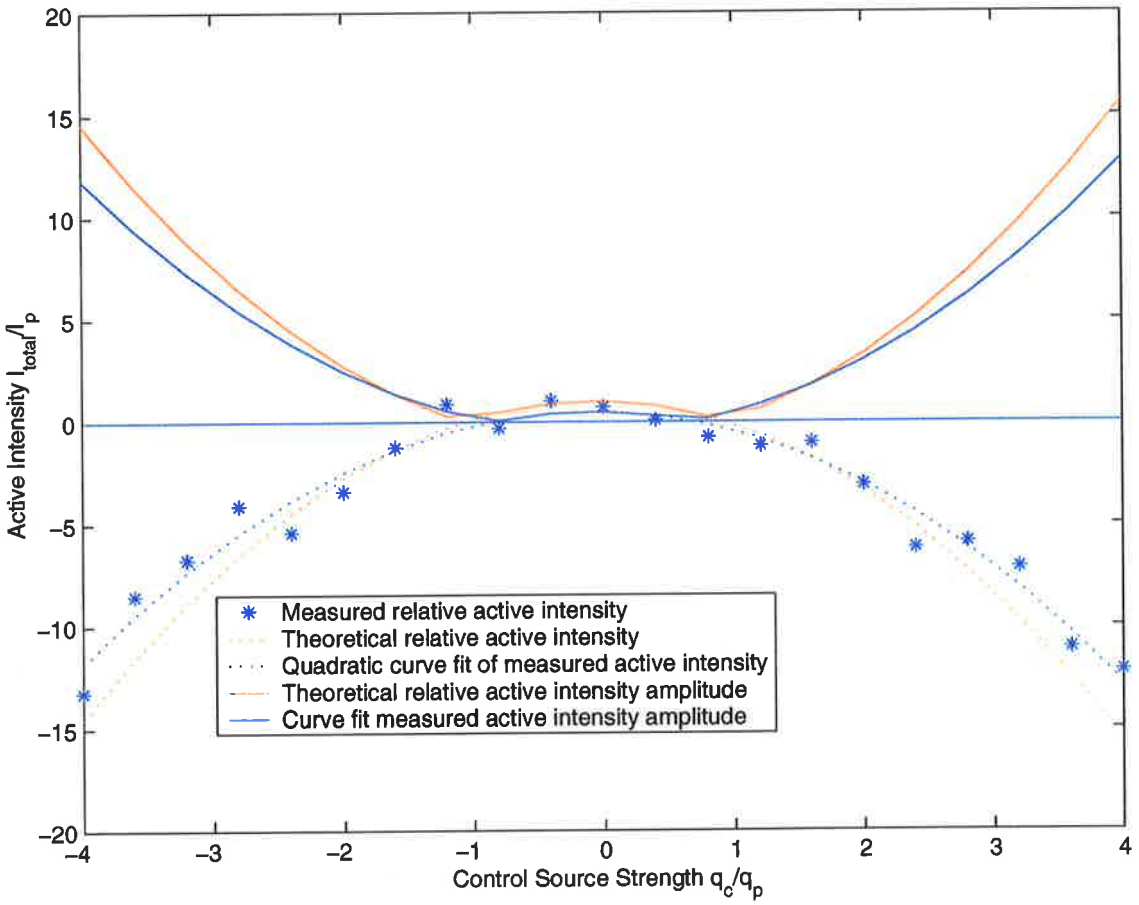


*Figure 4.48: Relative total active intensity amplitude plotted against the relative control source strength at the approximately the midpoint between the primary and control sources (at a radial distance of $3\lambda/50$ from the primary source).*

intensity amplitude cost function is employed, Figure 4.48 shows 2 minima out of infinitely many possible minima (see Figure 4.15).

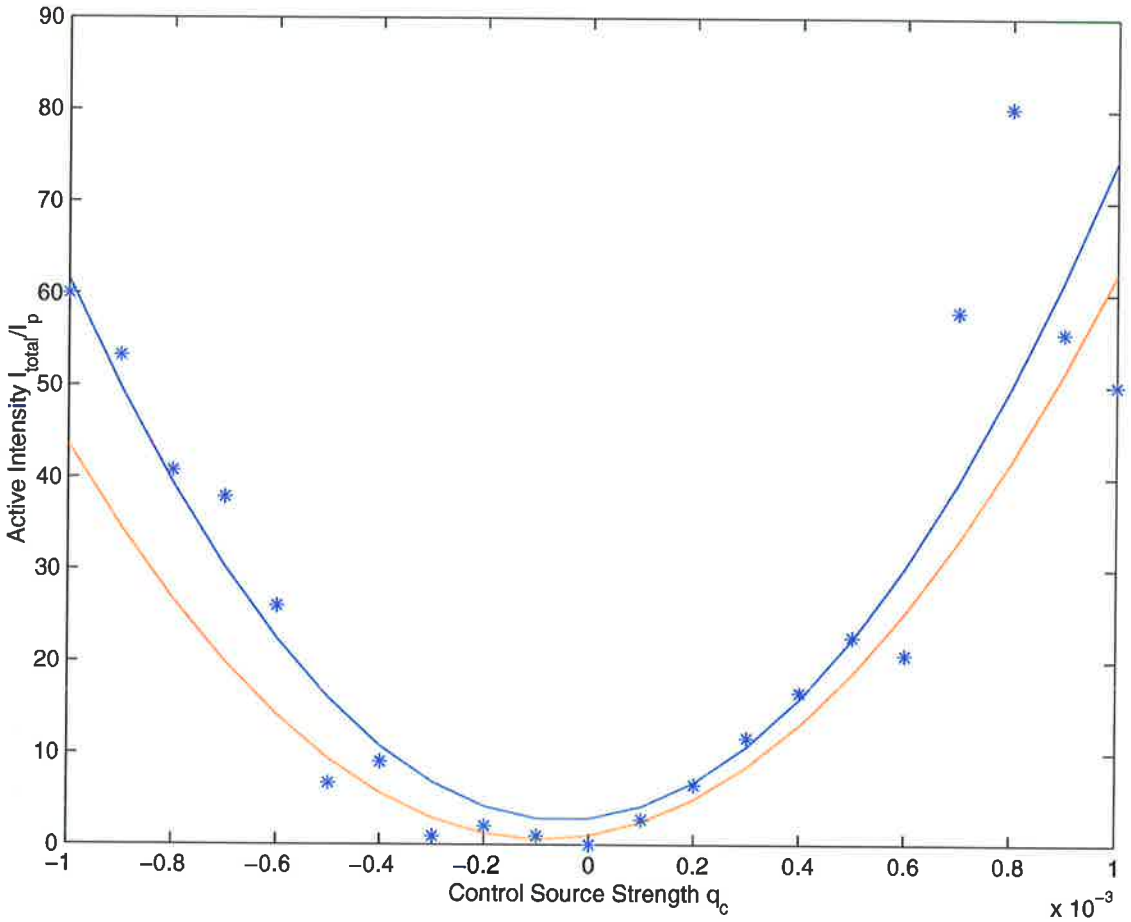


*Figure 4.49: Relative total active intensity plotted against the relative control source strength at a distance of $\lambda/5$ from the primary source along a line passing through both primary and control sources.*

Figure 4.49 and Figure 4.50 show the total active intensity (from both primary and control sources) relative to the primary active intensity on its own, plotted against the control source strength relative to the primary source strength when the intensity probe is located at distances of $\lambda/5$ and $\lambda$ from the primary source along a line passing through the primary and control sources. The results show a slight discrepancy between the theoretically predicted relative total active intensity and that which was measured by experiment described previously. Experiment has verified that the active intensity does remain positive definite at this location. The differences between theory and experiment can be put down to experimental error as described

before.

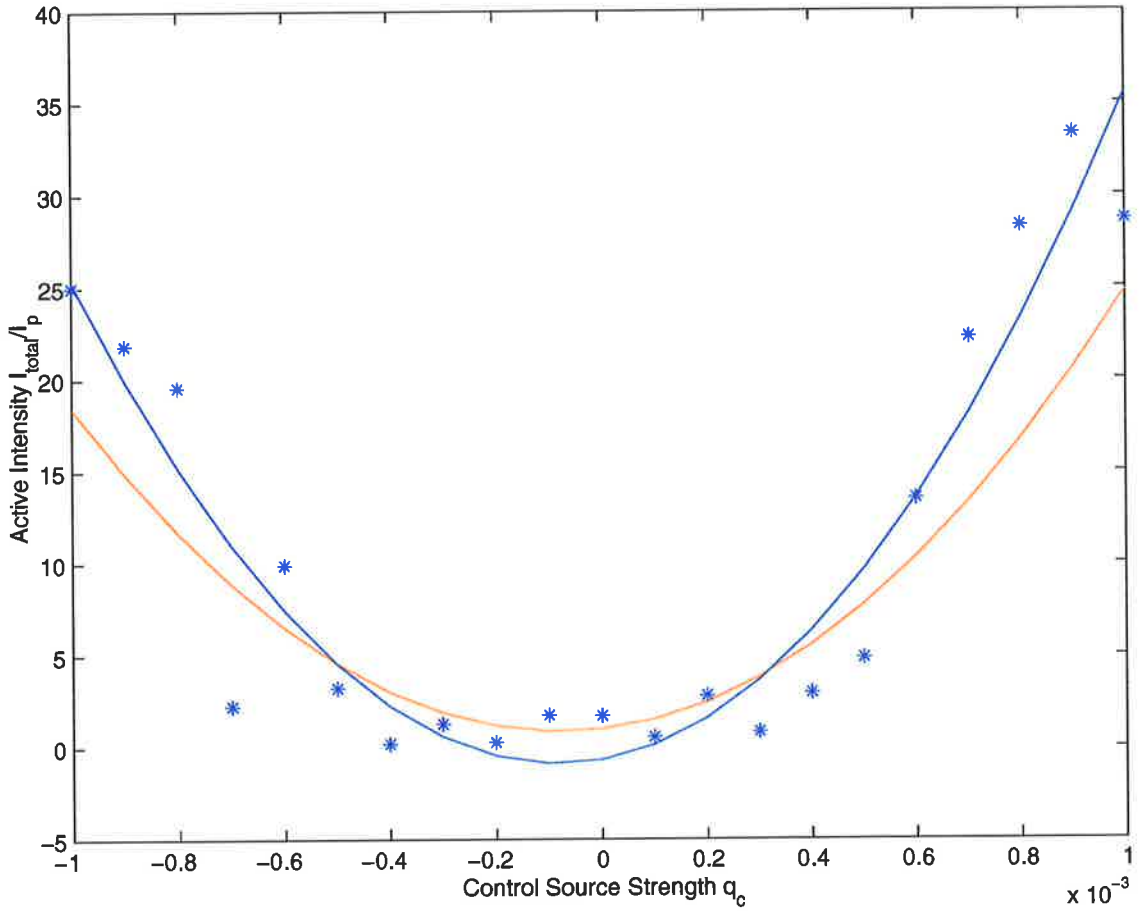


*Figure 4.50: Relative total active intensity plotted against the relative control source strength at a distance of λ from the primary source along a line passing through both primary and control sources.*

## 4.5 Conclusion

The performance of active control of free field tonal noise from a single monopole primary source via introduction of a single monopole control source using far field error sensing is not significantly improved with the use of active intensity error sensors in place of pressure error sensors. A single minimum exists in both the acoustic pressure and active intensity error criteria, at roughly the same control source strength, leading to similar outcomes. Significant differences *do* exist in the pressure and intensity error criteria for sensing locations in the

| Error Signal | Sensor Location | Comparison | Relevant Figures |
|---|---|---|---|
| Active intensity amplitude | $3\lambda/50$ | multiple minima visible | 4.48 |
| Active intensity | $3\lambda/50$ | visible inverted parabola, maximum | 4.47 |
| Active intensity | $\lambda/5$ | positive definite | 4.49 |
| Active intensity | $\lambda$ | positive definite | 4.50 |

*Table 4.2: Baffled monopole active intensity vs source strength results summary table.*

near field. At some near field locations, the global disturbance attenuation that accompanies intensity error sensing is greater than that achieved with pressure error sensing, as previously reported. However, for some sensing locations the active intensity cost function can be made negative and have no minimum value, but in fact a maximum. If at error sensor locations where the active intensity is negative, the cost function that is minimised is switched to active intensity amplitude (guaranteed to be positive definite) there may be multiple control source settings that yield a zero intensity result. At other error sensor locations (where the active intensity is always positive) an active intensity amplitude error criterion is identical to active intensity.

| Sensor Type | Location | far field Attenuation | Relevant Figures | Comments |
|---|---|---|---|---|
| Pressure | $3\lambda/50$ | very good | 4.45 | between 12-16dB attenuation |
| Intensity | $3\lambda/50$ | very bad (increase) | 4.45 | 7-8dB increase in sound pressure |
| Pressure | $\lambda/5$ | good | 4.44 | between 5-8dB attenuation |
| Intensity | $\lambda/5$ | good | 4.44 | between 7-9dB attenuation |
| Pressure | $\lambda$ | very good | 4.43 | ~15dB attenuation |
| Intensity | $\lambda$ | very good | 4.43 | approximately equal to pressure |

*Table 4.3: Baffled monopole experimental results summary table.*

# Chapter 5

# Baffled plate

## 5.1 Introduction


*Figure 5.1: Thesis Flow chart.*

Chapter 4 considered the case of active control a monopole source in an infinite baffle by a single monopole control source. The slightly better performance of active intensity error sensors over that of pressure error sensors just behind the control source, noted by Qiu et al. (1998) for the simple case of monopoles has also been observed experimentally for a baffled monopole (simple planar radiator). Furthermore a region described in Figure 4.7, has been found to yield far worse performance by active intensity error sensors. This region is defined by the active intensity cost function possibly being negative and having only a maximum extreme point, instead of the minimum as produced by a positive definite cost function. Figure 7.1 details the progression of this thesis in examining active intensity error sensing. Chapter 3 reconsidered the case of active control a monopole source by a single monopole control source as has already been done by (Qiu et al. (1998)). Chapter 4 considered the case of a monopole source located on an infinite baffle. Chapter 5 considers the case of a simply supported rectangular

steel plate controlled by a single monopole control source and also a single vibration control source respectively. Chapter 6 analyses the practical case of small electrical transformer on a hard floor in an anechoic chamber. Finally Chapter 7 draws conclusions and discusses possible future work.

Consider a simply supported rectangular steel plate in an infinite baffle as shown in Figure 5.2. This chapter will consider the active control of this plate by a single monopole control source separated by a distance of $\lambda/10$.

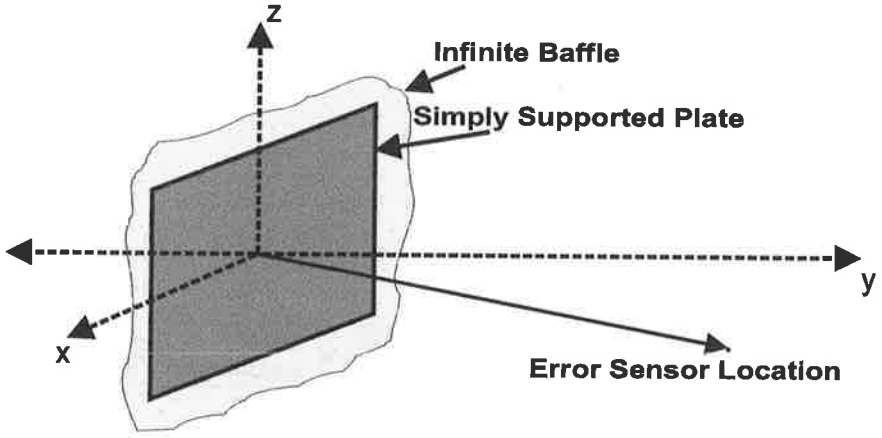


*Figure 5.2: Simply supported rectangular steel plate in an infinite baffle. The origin is in the centre of the plate.*

## 5.2 Inhomogeneous bending-wave equation for thin plates

For harmonic excitations $p(\mathbf{r}_0,t)$ of a thin isotropic plate (as shown in Figure 5.3) in flexure, the bending-wave equation is given by

$$B\nabla^4 w(\mathbf{r},t) - m_s(\mathbf{r})\frac{\partial^2 w(\mathbf{r},t)}{\partial t} = p(\mathbf{r}_0,t) \tag{5.1}$$

where $B = \frac{E(1+j\eta)}{1-\nu^2}\frac{h^3}{12}$ is the bending stiffness, where $E$ is Young's Modulus, $\nu$ is Poisson's Ratio, $(1+j\eta)$ is factored into the bending

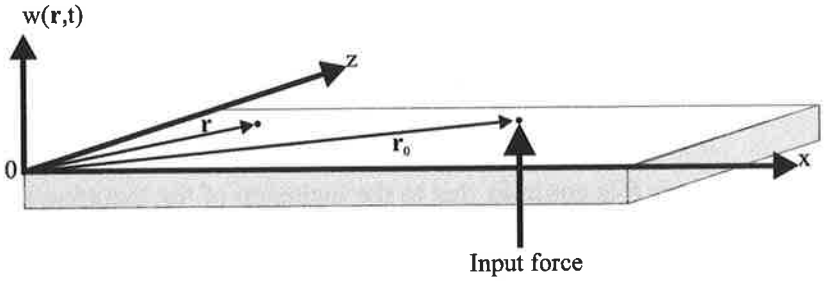


*Figure 5.3: Isotropic plate in flexure under the influence of a harmonic excitation $p(\mathbf{r}_0,t)$ (input force), transverse displacement $w(\mathbf{r},t)$ at location* $\mathbf{r}$.

stiffness to model damping, where $\eta$ is the loss factor and $j=\sqrt{-1}$, $h$ is the thickness of the plate. $m_s(\mathbf{r})$ is the mass per unit area of the surface of the plate, $\psi_n(\mathbf{r})$ is the mode shape function of mode $n$ at location $\mathbf{r}$ on the plate. $w(\mathbf{r},t)$ is the transverse displacement of the plate and $p(\mathbf{r},t)$ is any external force per unit area acting on the plate (Cremer et al. (1973)).

Consider now the homogeneous bending-wave equation for a harmonically excited isotropic thin plate given by

$$\nabla^4 w(\mathbf{r}) - k^4 w(\mathbf{r}) = 0 \tag{5.2}$$

where $k^4 = \frac{\omega^2 m_s}{B}$ where $\omega$ is the excitation frequency in radians per second. It is assumed that the temporal component of the wave equation is given by the harmonic function $e^{j\omega t}$. A solution to (5.2) can be written as

$$w(\mathbf{r})e^{j\omega t} = w_n \psi_n(\mathbf{r})e^{j\omega t} \tag{5.3}$$

where $w_n$ is a complex constant known as the displacement modal amplitude and $\psi_n(\mathbf{r})$ is the displacement mode shape function for the $n$th structural mode. Making the assumption that there is no fluid loading on the plate and substituting (5.3) into (5.2) gives for each structural mode

$$B\nabla^4\psi_n(\mathbf{r}) - \underline{\omega_n^2} m_S \psi_n(\mathbf{r}) = 0 \tag{5.4}$$

Since the bending stiffness $B$ is complex due to the inclusion of the damping model, the resonant frequency $\underline{\omega}_n$ in (5.4) is also complex and can be written as

$$\underline{\omega_n^2} = \omega_n^2(1 + j\eta) \tag{5.5}$$

where the underline indicates a complex resonant frequency.

If the boundary conditions of the plate (see Leissa (1993) for examples of different boundary conditions) are such that no energy can be conducted across the boundaries, then the the mode shape functions $\psi_n$ are orthogonal; that is

$$\int_S m_S(\mathbf{r})\psi_n(\mathbf{r})\psi_m(\mathbf{r})dr = \begin{cases} 0 & if\, m \neq n \\ M_n & if\, m = n \end{cases} \tag{5.6}$$

where $S$ is the surface of the plate and $M_n$ is the modal mass of the $n$th mode. Another way to express this boundary condition is to state that $\psi_n$ must satisfy the condition

$$\frac{\partial \psi_n}{\partial \hat{n}} = 0 \tag{5.7}$$

The mode shape functions can hence be written into a structural Green's function (Morse and Ingard (1968)), which satisfies the same boundary conditions and can be written as

$$G_S(\mathbf{r}, \mathbf{r}_0) = \sum_{n=1}^{\infty} w_n \psi_n(\mathbf{r}) \tag{5.8}$$

where the Green's function is a solution of the following 4th order partial differential equation with a delta function input at $\mathbf{r}_0$, give by

$$\nabla^4 G_S(\mathbf{r},\mathbf{r}_0) - k^4 G_S(\mathbf{r},\mathbf{r}_0) = \delta(\mathbf{r}-\mathbf{r}_0) \tag{5.9}$$

By substituting (5.8) into (5.9), and applying (5.4), (5.9) can be written as

$$\sum_{n=1}^{\infty} w_n m_S(\mathbf{r})\underline{\omega_n^2}\psi_n(\mathbf{r}) - m_S(\mathbf{r})\omega^2 \sum_{n=1}^{\infty} w_n \psi_n(\mathbf{r}) = \delta(\mathbf{r}-\mathbf{r}_0) \tag{5.10}$$

Now multiplying (5.10) by $\psi_m(\mathbf{r})$ and integrating over the surface of the plate and applying (5.6) gives

$$(w_n\underline{\omega_n^2}M_n - w_n\omega^2 M_n) = \psi_n(\mathbf{r}_0) \tag{5.11}$$

thus the displacement modal amplitude is

$$w_n = \frac{\psi_n(\mathbf{r}_0)}{M_n(\underline{\omega_n^2} - \omega^2)} \tag{5.12}$$

Now substituting (5.5) into (5.12) gives the displacement modal amplitude as

$$w_n = \frac{\psi_n(\mathbf{r}_0)}{M_n(\omega_n^2(1+j\eta) - \omega^2)} \tag{5.13}$$

where $\psi_n(\mathbf{r}_0)$ is the mode shape function at the input location $\mathbf{r}_0$.

Hence the structural Green's function is given by

$$G_S(\mathbf{r},\mathbf{r}_0) = \sum_{n=1}^{\infty} \frac{\psi_n(\mathbf{r}_0)\psi_n(\mathbf{r})}{M_n(\omega_n^2(1+j\eta) - \omega^2)} \tag{5.14}$$

The transverse displacement of a plate excited by a harmonic force distribution $p(\mathbf{r}_0,t)$ as specified in (5.1) can be written as

$$w(\mathbf{r}) = \int_S G_S(\mathbf{r},\mathbf{r}_0)p(\mathbf{r}_0,t)d\mathbf{r}_0 \tag{5.15}$$

where a harmonic excitation of the form $e^{j\omega t}$ is assumed.

## 5.3 Modal analysis of a simply supported rectangular plate

### 5.3.1 Modal analysis of a simply supported thin rectangular steel plate

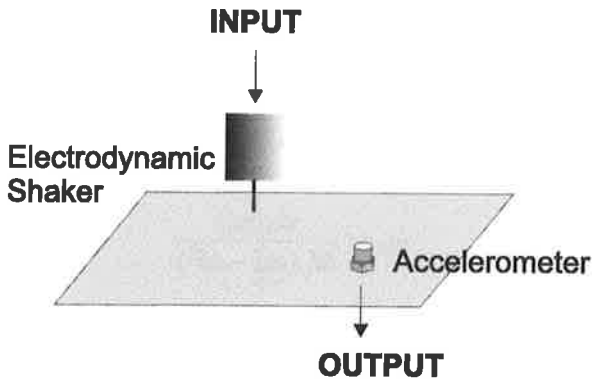


*Figure 5.4: A rectangular simply supported steel plate.*

Consider a simply supported thin rectangular steel plate shown in Figure 5.4. The physical parameters for the theoretical and experimental work are specified below:

| | |
|---|---|
| $L_x$ | 380mm (width of the plate) |
| $L_z$ | 300mm (height of the plate) |
| $h$ | 2mm (thickness of the plate) |
| $E$ | 209GPa (Youngs Modulus for steel) |

$\rho_s$ $7800kg/m^3$ (Density of steel)

$\nu$ 0.3 (Poissons Ratio)

$\eta$ 0.1 (Loss factor)

### 5.3.2 Validation of theoretical model

What follows is a comparison of theoretical and measured values for key quantities.

The resonant frequency $f_n$ in Hz of the $n$th mode is specified by the following equation (Leissa (1993)):

$$f_n = \frac{\omega_n}{2\pi} = \frac{1}{2\pi}\sqrt{\frac{D}{\rho_s h}}\left\{\left(\frac{m\pi x}{L_x}\right)^2 + \left(\frac{n\pi z}{L_z}\right)^2\right\} \tag{5.16}$$

where $D = \frac{Eh^3}{12(1-\nu^2)}$ and $m$ and $n$ are positive integers, referred to as the modal indices.

For the modal indices $m$ in the x direction and $n$ in the z direction, the resonant frequencies can be calculated and ordered from lowest to highest as follows.

| Ordered Modes (m,n) | Theoretical frequencies (Hz) | Measured resonant frequencies (Hz) |
|---|---|---|
| 1,1 | 88.8 | 88 |
| 2,1 | 191 | 188 |
| 1,2 | 252.8 | 246 |
| 2,2 | 355 | 336 |
| 3,1 | 361.4 | 352 |
| 3,2 | 525.4 | 512 |
| 1,3 | 526.2 | unresolved |
| 4,1 | 600 | unresolved |
| 2,3 | 628.4 | unresolved |
| 4,2 | 764 | unresolved |

*Table 5.1: Theoretical and measured resonant frequencies of the simply supported rectangular steel plate. The theoretical resonant frequencies were calculated with a loss factor of 0.1.*

A measurement of the frequency response function and coherence function of the plate (shown in Figure 5.4) where the plate has been excited by white noise input at $(0.3L_x, 0.4L_z)$, with an

accelerometer located at $(0.4L_x, 0.3L_z)$ is shown in Figure 5.6. Figure 5.5 shows a photo of

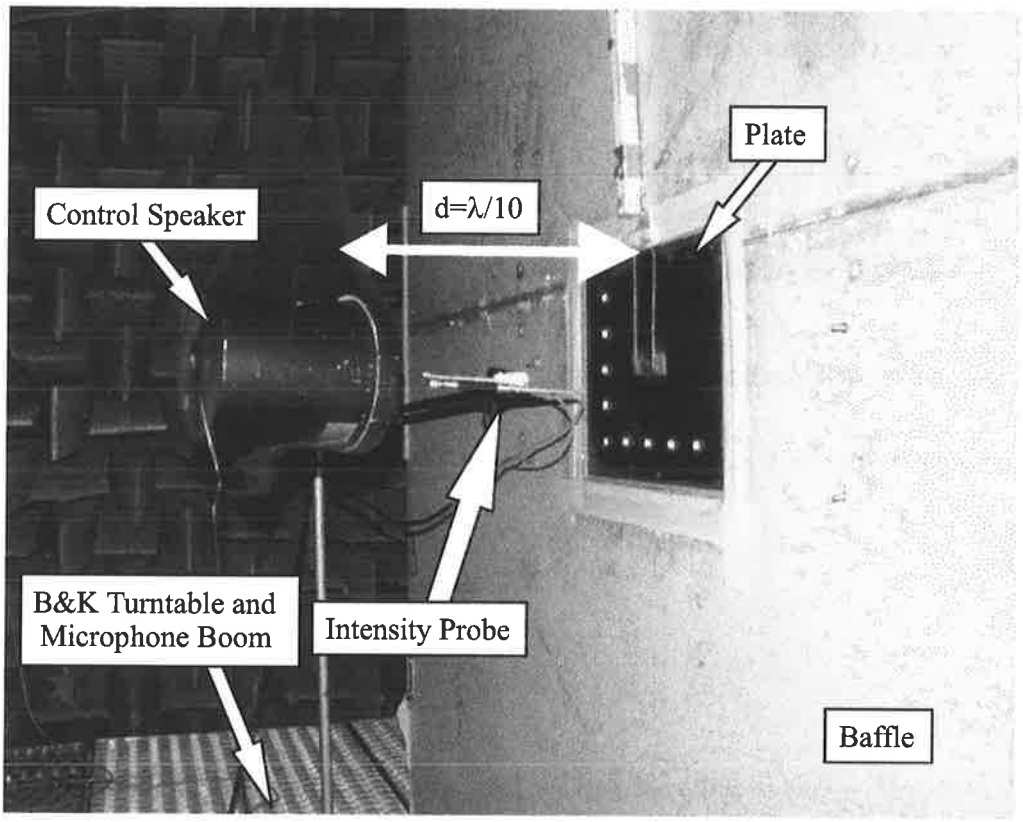


*Figure 5.5: Steel rectangular plate used in the experiments mounted in a wooden baffle.*

the plate setup. The resonant peaks are marked with their respective resonant frequency and modal indices.

Good agreement is obtained between the theoretically predicted resonance and the measured resonance frequencies. The simply supported boundary conditions were implemented by thin shim spring steel strips, one end of which was bolted to a rigid steel frame and the other was glued with a sealant to the edges of the plate. This experimental setup for the plate is identical to that used by Pan et al. (1992), without the noncontacting electromagnetic exciter. The agreement with the theoretical model serves to validate the simply supported boundary condition on the experimental apparatus.

The damping or loss factor of each mode can also be measured. The theoretical model assumes a constant loss factor of each mode of $\eta = 0.1$. To determine whether this is accurate, for

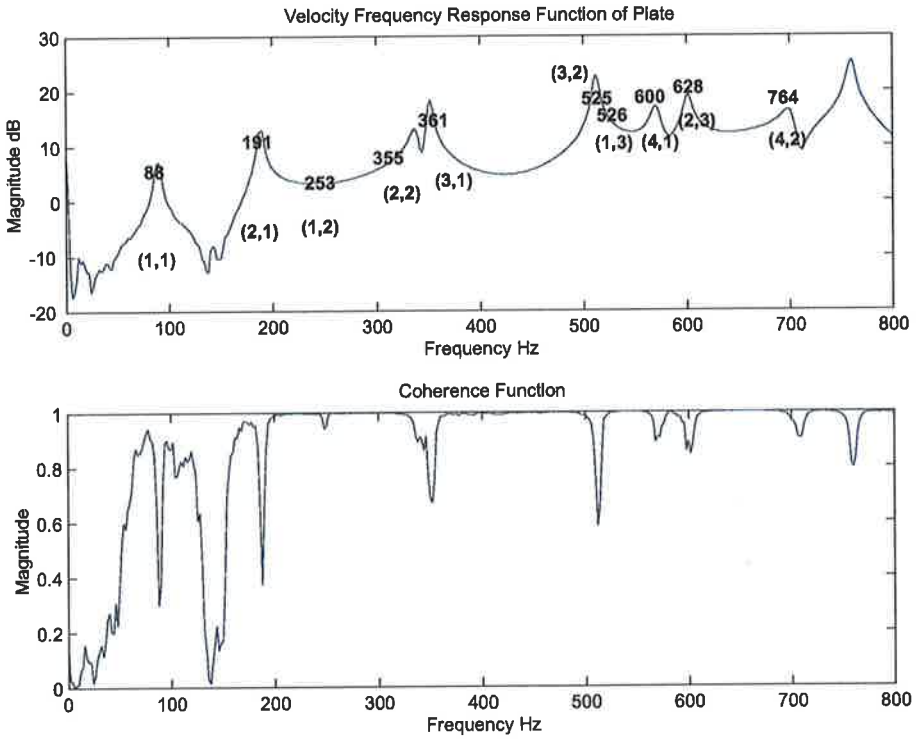


*Figure 5.6: Measured velocity frequency response and coherence function of the plate. The first 6 peaks are identified as structural modes over the range 0 to 550Hz. Structural resonances at higher frequencies were not possible to be resolve experimentally.*

each of the first six modes measured above, the loss factor will be measured. The half-value bandwidth method of estimating the damping in a mode will be used as described by Cremer et al. (1973). This is physically done by zooming in around each resonant peak on the signal analyser and estimating the half-value or 3dB down from the peak-value and determining the bandwidth and dividing this by the resonant frequency as given by

$$\eta = 2\zeta = \frac{\Delta f_n}{f_n} \tag{5.17}$$

where $\zeta$ is the damping ratio and $\Delta f_n$ is the 3dB or half-value bandwidth.

| Mode (m,n) | Loss factor $\eta$ |
|---|---|
| 1,1 | 0.086 |
| 2,1 | 0.12 |
| 1,2 | 0.1 |
| 2,2 | 0.09 |
| 3,1 | 0.11 |
| 3,2 | 0.085 |
| Average: | 0.0985 |

*Table 5.2: The measured loss factor of the plate. The loss factor does not vary appreciably for the modes identified experimentally and the average loss factor is approximately $\eta_{av} \approx 0.1$ with a standard deviation $\sigma = 0.014$.*

Referring to Table 5.2, an average loss factor of approximately $\eta = 0.1$ is measured in the first six modes of the plate and the standard deviation is approximately 0.014. It is therefore a reasonable approximation to model all modes with a loss factor of 0.1.

The mode shape functions of the plate are shown in Figure 5.7.

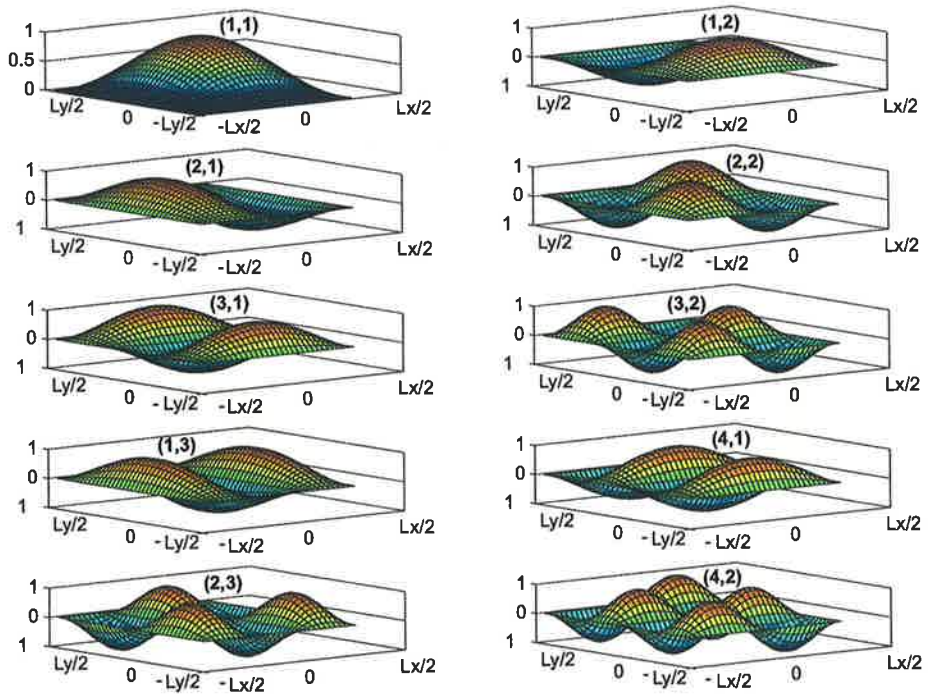


*Figure 5.7: The mode shape function of the first 10 structural modes is plotted. The position of nodal lines in the mode shape functions is coupled to the efficiency of vibration sources located along those lines.*

## 5.4 Baffled plate radiation using an acoustic control source

### 5.4.1 Theory

#### 5.4.1.1 Introduction

In this section, the potential of intensity-based error sensing as part of a feedforward active noise control system implementation in free space, will be tested against the more realistic problem of controlling acoustic radiation from a baffled rectangular panel via the introduction of a monopole control source. This arrangement is illustrated in Figure 5.8a. Pan et al. (1992) have considered this problem for single far field pressure error sensors, with both acoustic and vibration control sources demonstrating significant far field attenuation. The use of multiple active intensity error sensors in the active control of individual plate modes was considered in simulation only by Berry et al. (1999). The plane of error sensor locations used was restricted

to behind (towards the far field) the plane of control sources. The problem considered here involves a more complicated multi-modal plate model akin to (Pan et al. (1992)) and looks at the efficiency of single active intensity error sensors as compared to pressure error sensors in a broader range of locations.

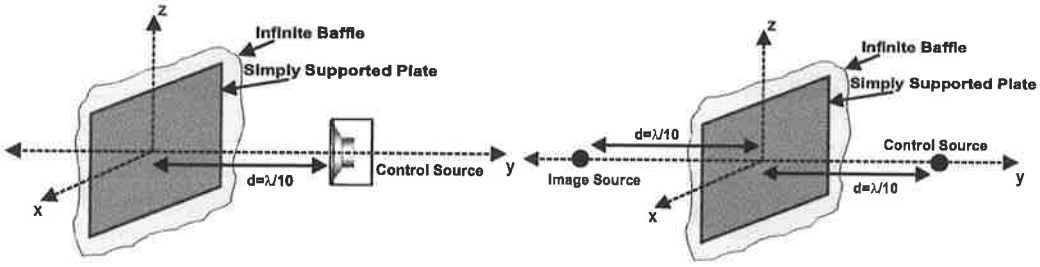


*(a) Rectangular steel plate primary source in an infinite baffle and a single monopole control source.*

*(b) Rectangular steel plate primary source in an infinite baffle with a single monopole control source and its image source which models the baffle.*

*Figure 5.8: Steel rectangular plate primary source in an infinite baffle and a single monopole control source arrangement.*

As outlined in the previous two chapters, assessment of the quality of error sensing strategies for the baffled plate radiation problem requires several steps:

Step 1: Calculation the acoustic power output of the primary monopole source in the absence of control.

Step 2: Calculation of the maximum possible acoustic power attenuation for the given control source arrangement.

Step 3: Calculation of the control source volume velocity that will minimise the error criteria of interest (acoustic pressure at a point in space, acoustic intensity at a point in space, etc) for the given error sensing arrangement.

Step 4: Calculation of the total acoustic power output of the primary + control source arrangement using the control source volume velocity from step 3, followed by the

acoustic power attenuation through comparison with the original (primary only) acoustic power output.

Step 5: Comparison of the attenuation in step 4 with the maximum possible attenuation for the given control source arrangement calculated in step 2. This will provide some assessment of the efficiency of the error sensing strategy.

### 5.4.2 Minimising the total sound power

Consider first a simply supported rectangular plate primary source and monopole control source whose source strength and hence amplitude and phase can be adjusted. Figure 5.8a represents the arrangement of the baffled plate and monopole sources. Calculating the maximum achievable sound power attenuation possible with a rectangular plate primary source in an infinite baffle of surface velocity $v_p$ controlled by a single monopole control source of source strength $q_c$ involves the modelling of an infinite baffle with an image source (as shown in Figure 5.8b) to the control source to take account of the reflection of the sound field by the presence of the baffle. The image source strength $q_i$ should equal that of the control source $q_c$. Again it is assumed that there is no fluid loading on the sources.

Consider now a simply supported rectangular steel plate with the physical properties described in Section 5.3.1. The plate is harmonically excited with a unitary point force excitation at the centre of the plate as given by:

$x_{in} = 0$ mm (x-location of point excitation force)

$z_{in} = 0$ mm (z-location of point excitation force)

The coordinate system used to describe the sound radiated from the plate is shown in Figure 5.9.

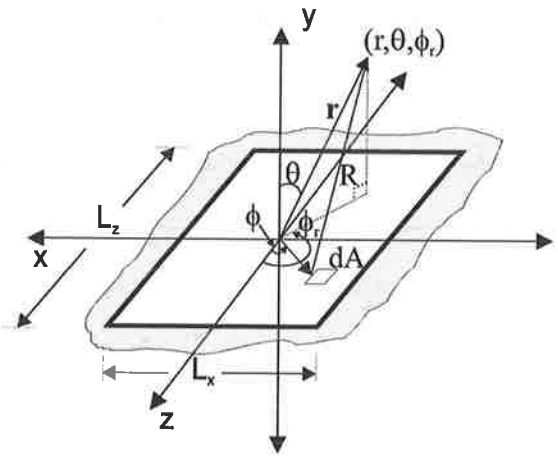


*Figure 5.9: Coordinate system for simply supported rectangular plate.*

Hansen and Snyder (1997) gives the acoustic pressure at some observation point $\mathbf{r} = (r_{e_x}, r_{e_y}, r_{e_z}) = (r, \theta, \phi_r)$ in space due to the harmonic excitation of the plate is given by the Rayleigh integral (Rayleigh (1887)) by

$$p(\mathbf{r}) = \frac{j\omega\rho}{2\pi} \sum_{i=1}^{N} v_i \int_A \frac{e^{-jkR}}{R} \psi_i(\mathbf{x}) dA \tag{5.18}$$

which integrates over the surface area $A$ of the plate and sums all of the structural modes $N$. $v_i$ is the complex velocity amplitude of the $i$th structural mode, $\psi_i(\mathbf{x})$ is the mode shape of the ith structural mode at location $\mathbf{x} = (x, z)$ on the plate $dA = dxdz$ and $R$ is the distance between the point $\mathbf{r}$ and the location $\mathbf{x}$ on the plate,

$$R = |\mathbf{r} - \mathbf{x}| = \sqrt{(r_{e_x} - x)^2 + r_{e_y}^2 + (r_{e_z} - z)^2} \tag{5.19}$$

It should be noted that the Rayleigh integral expression for the radiated acoustic pressure cannot be solved analytically.

When modelling low frequency plate radiation it is not possible nor is it necessary to include infinitely many structural modes in the analysis. For the following analysis the number of modes considered is $N = 100$ . If only a finite number of modes are used the Rayleigh integral

expression can be rewritten in matrix form (Pan et al. (1992) and Hansen and Snyder (1997)) as

$$p(r) = Z_{rad}^T v_p \tag{5.20}$$

where $Z_{rad}$ is the $(N \times 1)$ vector whose ith element is given by

$$Z_{rad,i}(\mathbf{r}) = \frac{j\omega\rho}{2\pi} \int_A \frac{e^{-jkR}}{R} \psi_i(\mathbf{x}) dA \tag{5.21}$$

and $v_p$ is the $(N \times 1)$ vector whose ith element is given by

$$v_{p,i} = \frac{j\omega\psi_i(\mathbf{x}_{in})}{M_i Z_i} \tag{5.22}$$

where $M_i = \frac{\rho_s h A}{4}$ and $Z_i = \omega_i^2 + 2\zeta\omega\omega_i - \omega^2$ , $\omega_i$ is the ith resonant frequency, $\omega$ is the excitation frequency and $\zeta$ is the damping factor. $A$ is the area of the plate.

Nelson and Elliott (1986) gives the acoustic pressure of the monopole control source in the presence of the infinite baffle as

$$p_c(\mathbf{r}) = Z_{mono}(r_c) q_c \tag{5.23}$$

where $Z_{mono}(r_c) = \frac{j\omega\rho}{4\pi} \frac{e^{-jkr_c}}{r_c} + \frac{j\omega\rho}{4\pi} \frac{e^{-jkr_i}}{r_i}$ ,$r_c = |\mathbf{r} - \mathbf{r}_c|$ and $r_i = |\mathbf{r} - \mathbf{r}_i|$

The acoustic power radiated by the plate and monopole combination in the far field is given by (Pan et al. (1992) and Hansen and Snyder (1997)) as

$$W = A_{W_f} |q_c|^2 + q_c^* b_{W_f} + b_{W_f}^* q_c + c_{W_f} \tag{5.24}$$

where

$$A_{W_f} = \int_0^{2\pi} \int_0^{\pi/2} \frac{|Z_{mono}|^2}{2\rho c} r^2 sin\theta d\theta d\phi_r \tag{5.25}$$

$$b_{W_f} = \int_0^{2\pi} \int_0^{\pi/2} \frac{Z^*_{mono} Z^T_{rad} v_p}{2\rho c} r^2 sin\theta d\theta d\phi_r \tag{5.26}$$

$$c_{W_f} = \int_0^{2\pi} \int_0^{\pi/2} \frac{v_p^H Z^H_{rad} Z_{rad} v_p}{2\rho c} r^2 sin\theta d\theta d\phi_r \tag{5.27}$$

where the spherical to rectangular coordinate transformation given by

$$r_{e_x} = r cos\phi_r sin\theta \tag{5.28}$$

$$r_{e_z} = r sin\phi_r sin\theta \tag{5.29}$$

$$r_{e_y} = r cos\theta \tag{5.30}$$

where to be in the far field the radial distance $r >> \lambda$. The integral expression $A_{W_f}$ has an analytic solution given by equation (4.11) in Chapter 4. Where as the integral expressions for $b_{W_f}$ and $c_{W_f}$ are functions of $Z_{rad}$ which has no analytic solution and must be numerically integrated. Hence numerical integration must be performed to calculate the acoustic power radiated by the plate and monopole combination.

If $A_{W_f} > 0$ , equation (5.24) has a unique minimum (see Appendix E for a derivation) given by the optimal control source strength $q_{c,opt}$ (shown in Figures 5.10a and b) where

$$q_{c,opt} = -A^{-1}_{W_f} b_{W_f} \tag{5.31}$$

Since $A_{W_f}$ represents the power output from the monopole control source acting on its own, it is guaranteed to be positive and hence a unique minimum $q_{c,opt}$ is guaranteed.

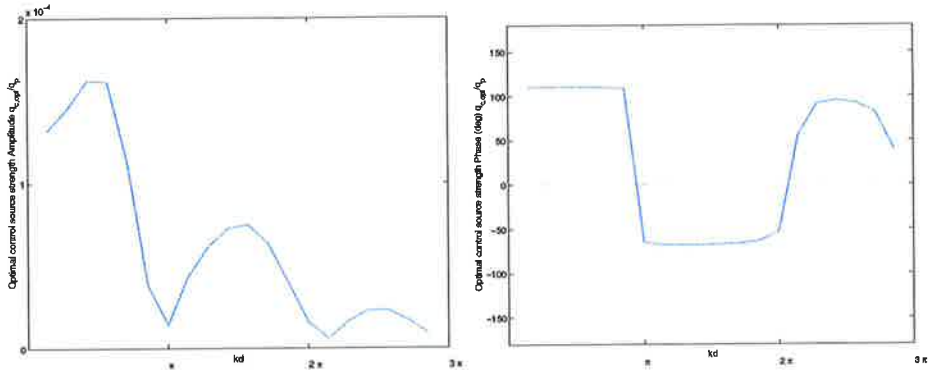

*Figure 5.10: The amplitude and phase of the control source strength which minimises the total sound power versus the separation distance d (N=100).*

Substituting (5.31) into (5.24) gives the minimum power as

$$W_{min} = W_p - b^*_{W_f} A^{-1}_{W_f} b_{W_f} \tag{5.32}$$

where $W_p = c_{W_f}$ is the power due only to the primary source.

Therefore the amount of sound power attenuation achievable by employing a single monopole control source to control the sound field of an infinitely baffled simply supported rectangular plate primary source is given by the ratio of sound power before and after control by

$$\frac{W_p}{W_{min}} = \frac{W_p}{W_p - b^*_{W_f} A^{-1}_{W_f} b_{W_f}} \tag{5.33}$$

The general shape of the power attenuation curve for the plate problem, shown in Figure 5.11, is similar to the monopole radiation curve in Figure 3.4 and baffled monopole radiation curve in Figure 4.4. Hence at a separation distance of $d = \lambda/10$ the maximum achievable power attenuation is approximately 29.4dB. At $d = \lambda/2$ the maximum achievable power attenuation falls to zero. It therefore becomes necessary to make the separation distance very small in order

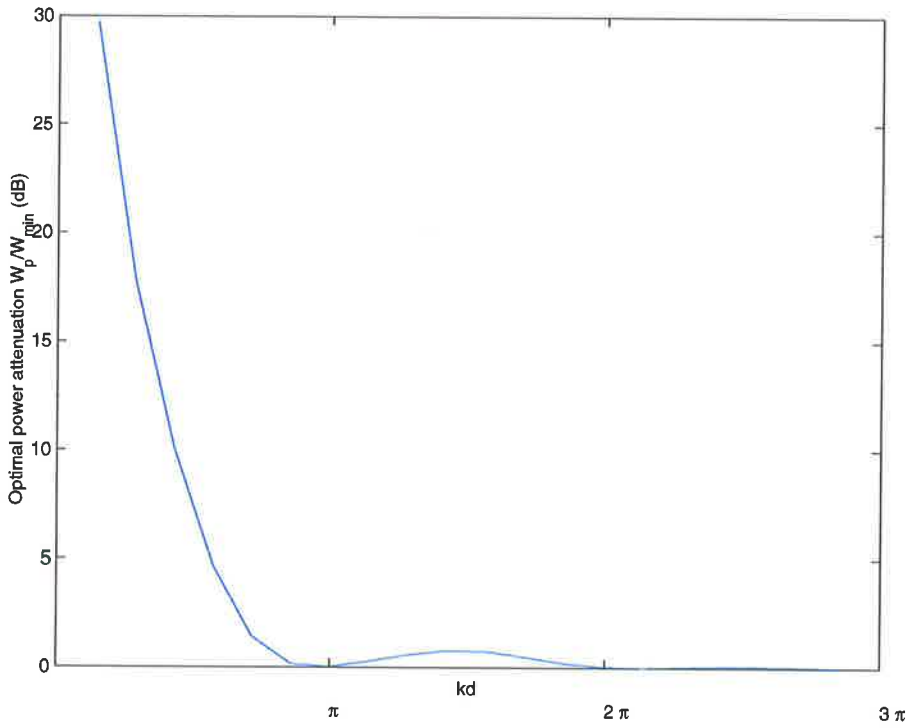


*Figure 5.11: The optimal sound power attenuation (dB) versus the separation distance d (N=100).*

to achieve any appreciable sound power reduction. The sound power before and after control when minimising the sound power plotted as a function of frequency, is shown in Figure 5.12. The maximum power attenuation possible for the problem being considered here, plotted as a function of frequency, is shown in Figure 5.13. Observe that there is good attenuation up to approximately 600Hz. The aim now is to develop an error sensing system that will help practically realise this potential.

### 5.4.3 Minimising squared sound pressure at a point

Consider first the problem of minimising sound pressure at a point in space (practically a microphone location).

The total acoustic pressure of both sources at an observation point **r** in the free field is given by

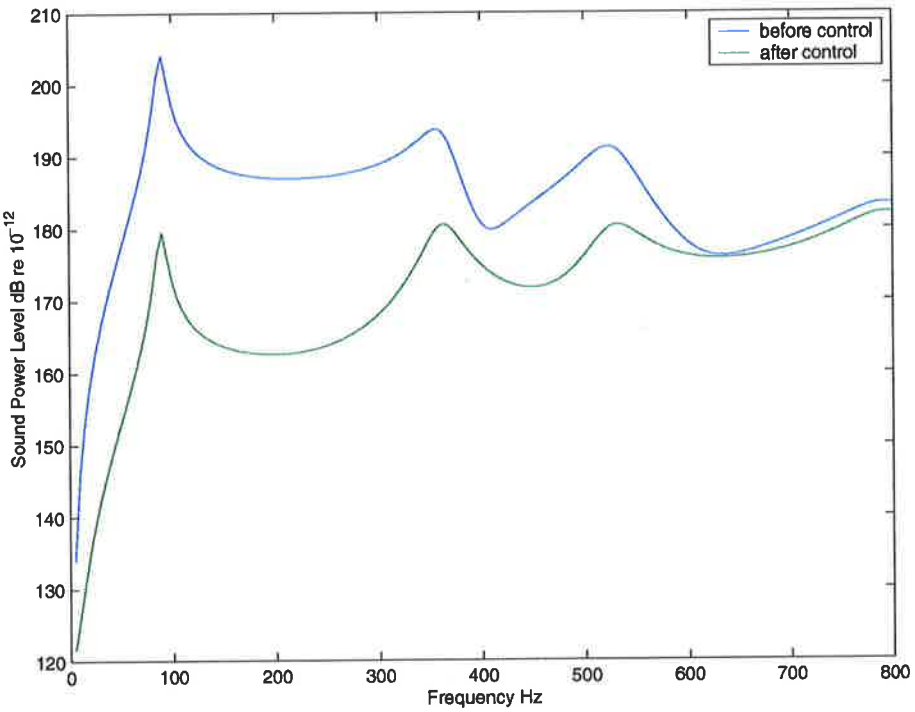


*Figure 5.12: Relative sound power level (dB) before and after control when minimising the sound power with a unitary force applied to the plate centre and a single monopole control source positioned at a separation distance d. (N=100).*

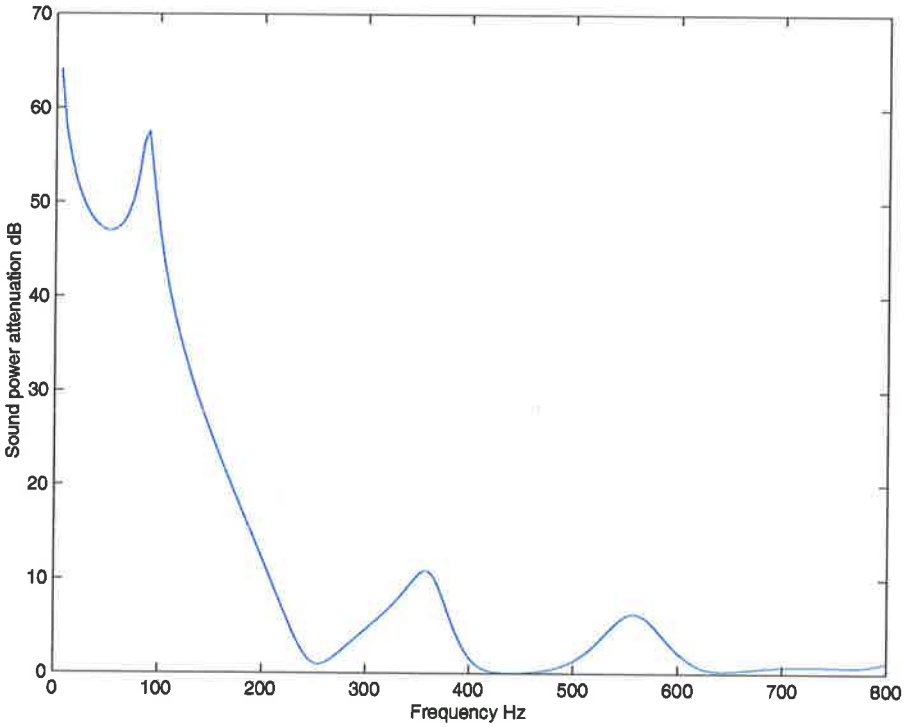


*Figure 5.13: Sound power attenuation (dB) when minimising the sound power with a unitary force applied to the plate centre and a single monopole control source positioned at a separation distance $d$. (N=100).*

$$p_{total}(\mathbf{r}) = p_p(\mathbf{r}) + p_c(\mathbf{r}) \tag{5.34}$$

where $p_p(\mathbf{r})$ is the pressure due to the primary source and $p_c(\mathbf{r})$ is the pressure due to the control source at the observation point $\mathbf{r}$ . If we multiply the total acoustic pressure by its complex conjugate we get an expression for the squared sound pressure amplitude as

$$\begin{aligned} |p_{total}(\mathbf{r})|^2 &= p^*_{total}(\mathbf{r}) p_{total}(\mathbf{r}) && (5.35)\\ &= (p_p(\mathbf{r}) + p_c(\mathbf{r}))^* (p_p(\mathbf{r}) + p_c(\mathbf{r})) && (5.36)\\ &= p^*_p p_p + p^*_c p_p + p^*_p p_c + p^*_c p_c && (5.37) \end{aligned}$$

where the dependence on $\mathbf{r}$ is assumed and hence for brevity, dropped from the equations. $p_p(\mathbf{r}) = Z^T_{rad}(r_p) v_p$ and $p_c(\mathbf{r}) = Z_{mono}(r_{c,i}) q_c$, $r_p = |\mathbf{r} - \mathbf{r}_p|$ is the distance from the primary source to the observation point (error sensor location) and similarly $r_c = |\mathbf{r} - \mathbf{r}_c|$ is the distance from the control source to the observation point as described above. $Z_{rad}$ and $Z_{mono}$ both describe the acoustic transfer impedances due to the primary and control sources respectively at the observation point and are given by

$$Z_{rad}(r_p) = \begin{bmatrix} \frac{j\omega\rho}{2\pi} \int_A \frac{e^{-jkR}}{R} \psi_1(\mathbf{x}) dA \\ \vdots \\ \frac{j\omega\rho}{2\pi} \int_A \frac{e^{-jkR}}{R} \psi_N(\mathbf{x}) dA \end{bmatrix} \tag{5.38}$$

$$v_p = \begin{bmatrix} \frac{j\omega\psi_1(\mathbf{x}_{in})}{M_1 Z_1} \\ \vdots \\ \frac{j\omega\psi_N(\mathbf{x}_{in})}{M_N Z_N} \end{bmatrix} \tag{5.39}$$

$$Z_{mono}(r_{c,i}) = \frac{j\omega\rho}{4\pi} \frac{e^{-jkr_c}}{r_c} + \frac{j\omega\rho}{4\pi} \frac{e^{-jkr_i}}{r_i} \tag{5.40}$$

The squared pressure amplitude can be re-expressed in a hermitian quadratic form (Hansen and Snyder (1997)) as

$$|p_{total}|^2 = A_p |q_c|^2 + q_c^* b_p + b_p^* q_c + c_p \tag{5.41}$$

where

$A_p = Z_{mono}^* Z_{mono}$ and $b_p = Z_{mono}^* Z_{rad}^T v_p$ and $c_p = Z_{rad}^H v_p^* Z_{rad}^T v_p$

again since $A_p$ is always greater than zero, there exists a unique minimum (see Appendix E) given by the optimal control source strength $q_{c,opt}$ where

$$q_{c,opt} = -A_p^{-1} b_p \tag{5.42}$$

Therefore to minimise the squared pressure amplitude at a particular location from a single primary monopole source by a single control monopole source (5.42) is substituted into (5.41).

The amount of sound power attenuation when the squared pressure amplitude is minimised at the error sensor location is found by substituting (5.42) into (5.24), giving

$$\frac{W_p}{W_{min}} = \frac{c_{W_f}}{A_{W_f} \left| -A_p^{-1} b_p \right|^2 - (-A_p^{-1} b_p)^* b_{W_f} - b_{W_f}^* (-A_p^{-1} b_p) + c_W} \tag{5.43}$$

### 5.4.4 Minimising radial active intensity

Consider now minimising radial active intensity at a point in space. The total acoustic particle velocity in the direction $\hat{\mathbf{u}}_{total}$ of both sources at an observation point $\mathbf{r}$ in the free field is given by the sum of the particle velocities of the primary and control sources, given by

$$\mathbf{u}_{total}(\mathbf{r}) = \mathbf{u}_p(\mathbf{r}) + \mathbf{u}_c(\mathbf{r}) \tag{5.44}$$

which can be rewritten as

$$\mathbf{u}_{total}(\mathbf{r}) = u_{total}\hat{\mathbf{u}}_{total} = u_p\hat{\mathbf{u}}_p + u_c\hat{\mathbf{u}}_c \tag{5.45}$$

where the unit vector $\hat{\mathbf{u}}_p$ is in the radial direction relative to the primary source, $\hat{\mathbf{u}}_c = \hat{\mathbf{u}}_{c,0} + \hat{\mathbf{u}}_i$ is in the direction of the sum of the radial unit vectors $\hat{\mathbf{u}}_{c,0}$ ,$\hat{\mathbf{u}}_i$ with respect to the control source and the image source respectively.

The total active intensity in the direction of $\mathbf{u}_{total}$ is given by

$$\mathbf{I}_{total}(\mathbf{r}) = \frac{1}{2}Re\{p^*_{total}(\mathbf{r})\mathbf{u}_{total}(\mathbf{r})\} \tag{5.46}$$

It is desired to minimise the radial (with respect to the primary source, in the same direction as the vector $\mathbf{u}_p$) active intensity. Hence it is the component of $\mathbf{I}_{total}$ in equation (5.46) in the direction of $\mathbf{I}_p$ henceforth labelled $\mathbf{I}_{radial}$ as shown in Appendix A which must be minimised and is given by

$$\mathbf{I}_{radial}(\mathbf{r}) = proj_{\mathbf{I}_{radial}}\mathbf{I}_{total} = (\mathbf{I}_{radial} \bullet \mathbf{I}_{total})\mathbf{I}_{radial} \tag{5.47}$$

The notation $proj_{\mathbf{X}}\mathbf{Y}$ is used to denote the orthogonal projection of vector $\mathbf{Y}$ on vector $\mathbf{X}$. The direction of positive intensity is $\hat{\mathbf{u}}_p$. Substituting (5.45) and (5.34) gives

$$\mathbf{I}_{total} = \frac{1}{2}Re\{(p^*_p + p^*_c)(\mathbf{u}_p + \mathbf{u}_c)\} \tag{5.48}$$

$$= \frac{1}{2}Re\{(p^*_p\mathbf{u}_p + p^*_p\mathbf{u}_c + p^*_c\mathbf{u}_p + p^*_c\mathbf{u}_c\} \tag{5.49}$$

where $\mathbf{u}_p = \mathbf{H}_{rad}^T(r_p)v_p$ and $\mathbf{u}_c = \mathbf{H}_{mono}(r_{c,i})q_c$, where $r_p$ and $r_c$ are defined as before. $\mathbf{H}_{rad}$ and $\mathbf{H}_{mono}$ both describe the acoustic velocity transfer impedances due to the primary and control sources respectively at the observation point $\mathbf{r}$ and are given by

$$\mathbf{H}_{rad}(r_p) = -\frac{1}{j\rho\omega}\nabla Z_{rad}(r_p)\hat{\mathbf{u}}_p \tag{5.50}$$

$$\mathbf{H}_{mono}(r_{c,i}) = \frac{1}{4\pi}\left(\frac{1}{r_c^2}+\frac{jk}{r_c}\right)e^{-jkr_c}\hat{\mathbf{u}}_{c,0} + \frac{1}{4\pi}\left(\frac{1}{r_i^2}+\frac{jk}{r_i}\right)e^{-jkr_i}\hat{\mathbf{u}}_i \tag{5.51}$$

The active intensity in the direction $\hat{\mathbf{u}}_{total}$ can be re-expressed in a hermitian quadratic form as

$$\mathbf{I}_{total} = \mathbf{A}_I|q_c|^2 + q_c^*\mathbf{b}_I + \mathbf{b}_I^* q_c + \mathbf{c}_I \tag{5.52}$$

where $\mathbf{A}_I = \frac{1}{2}Re\{Z_{mono}^*\mathbf{H}_{mono}\}$ and $\mathbf{b}_I = \frac{1}{4}(\mathbf{H}_{mono}^* Z_{rad}^T v_p + \mathbf{H}_{rad}^T v_p Z_{mono}^*)$ and $\mathbf{c}_I = \frac{1}{2}Re\left\{Z_{rad}^H v_p^* \mathbf{H}_{rad}^T v_p\right\}$ where $X^H$ represents the hermitian (conjugate transpose) of $X$.

The radial active intensity can be written as

$$\mathbf{I}_{radial}(\mathbf{r}) = proj_{\mathbf{I}_{radial}}\mathbf{I}_{total} = (\mathbf{I}_{radial}\bullet\mathbf{I}_{total})\mathbf{I}_{radial} = \mathbf{A}_{I_{radial}}|q_c|^2 + q_c^*\mathbf{b}_{I_{radial}} + \mathbf{b}_{I_{radial}}^* q_c + \mathbf{c}_{I_{radial}} \tag{5.53}$$

where $\mathbf{A}_{I_{radial}}$, $\mathbf{b}_{I_{radial}}$ and $\mathbf{c}_{I_{radial}}$ can be written as

$$\mathbf{A}_{I_{radial}} = \frac{1}{2}Re\left\{Z_{mono}^*(H_{c,0}proj_{\hat{\mathbf{u}}_p}\hat{\mathbf{u}}_{c,0} + H_i proj_{\hat{\mathbf{u}}_p}\hat{\mathbf{u}}_i)\right\} \tag{5.54}$$

$$\mathbf{b}_{I_{radial}} = \frac{1}{4}((H_{c,0}^* proj_{\hat{\mathbf{u}}_p}\hat{\mathbf{u}}_{c,0} + H_i^* proj_{\hat{\mathbf{u}}_p}\hat{\mathbf{u}}_i)Z_{rad}^T v_p + Z_{mono}^* H_{rad}^T v_p\hat{\mathbf{u}}_p) \tag{5.55}$$

$$\mathbf{c}_{I_{radial}} = \frac{1}{2}Re\left\{Z_{rad}^H H_{rad}^T\right\}|v_p|^2\hat{\mathbf{u}}_p \tag{5.56}$$

where $H_{rad} = \|\mathbf{H}_{rad}\|$, $H_{c,0} = \|\mathbf{H}_{c,0}\|$ and $H_i = \|\mathbf{H}_i\|$ are the complex vector magnitudes of the corresponding vectors describing the velocity transfer impedances. Which expands to

$$\mathbf{A}_{I_{radial}} = \frac{1}{2} Re\left\{Z^*_{mono}(H_{c,0}(\hat{\mathbf{u}}_{c,0} \bullet \hat{\mathbf{u}}_p)\hat{\mathbf{u}}_p + H_i(\hat{\mathbf{u}}_i \bullet \hat{\mathbf{u}}_p)\hat{\mathbf{u}}_p)\right\} \tag{5.57}$$

$$\mathbf{b}_{I_{radial}} = \frac{1}{4}((H^*_{c,0}(\hat{\mathbf{u}}_{c,0} \bullet \hat{\mathbf{u}}_p)\hat{\mathbf{u}}_p + H^*_i(\hat{\mathbf{u}}_i \bullet \hat{\mathbf{u}}_p)\hat{\mathbf{u}}_p)Z^T_{rad}v_p + Z^*_{mono}H^T_{rad}v_p\hat{\mathbf{u}}_p) \tag{5.58}$$

$$\mathbf{c}_{I_{radial}} = \frac{1}{2} Re\left\{Z^H_{rad}H^T_{rad}\right\}|v_p|^2\hat{\mathbf{u}}_p \tag{5.59}$$

As equations (5.57), (5.58) and (5.59) are all in the direction $\hat{\mathbf{u}}_p$, the vector notation can be removed, giving

$$A_{I_{radial}} = \frac{1}{2} Re\left\{Z^*_{mono}(H_{c,0}(\hat{\mathbf{u}}_{c,0} \bullet \hat{\mathbf{u}}_p) + H_i(\hat{\mathbf{u}}_i \bullet \hat{\mathbf{u}}_p))\right\} \tag{5.60}$$

$$b_{I_{radial}} = \frac{1}{4}((H^*_{c,0}(\hat{\mathbf{u}}_{c,0} \bullet \hat{\mathbf{u}}_p) + H^*_i(\hat{\mathbf{u}}_i \bullet \hat{\mathbf{u}}_p))Z^T_{rad}v_p + Z^*_{mono}H^T_{rad}v_p) \tag{5.61}$$

$$c_{I_{radial}} = \frac{1}{2} Re\left\{Z^H_{rad}H^T_{rad}\right\}|v_p|^2 \tag{5.62}$$

Consider equation (5.54) for the active intensity of the control source acting on its own $\mathbf{A}_{I_{radial}}$. Appendix E shows that provided $A_{I_{radial}}$ is positive, there exists a unique minimum given by the optimal control source strength $q_{c,opt}$. This is not necessarily the case for an active intensity cost function which may be negative at certain locations.

The term $proj_{\hat{\mathbf{u}}_p}\hat{\mathbf{u}}_{c,0}$ which is defined by

$$proj_{\hat{\mathbf{u}}_p}\hat{\mathbf{u}}_{c,0} = (\hat{\mathbf{u}}_{c,0} \bullet \hat{\mathbf{u}}_p)\hat{\mathbf{u}}_p \tag{5.63}$$

can at certain error sensor locations be negative, when the dot product $\hat{\mathbf{u}}_{c,0} \bullet \hat{\mathbf{u}}_p$ is negative, or the angle between $\hat{\mathbf{u}}_p$ and $\hat{\mathbf{u}}_{c,0}$ is obtuse. The term $proj_{\hat{\mathbf{u}}_p}\hat{\mathbf{u}}_i$ which is defined by

$$proj_{\widehat{\mathbf{u}_p}}\widehat{\mathbf{u}}_i = (\widehat{\mathbf{u}}_i \bullet \widehat{\mathbf{u}_p})\widehat{\mathbf{u}_p} \tag{5.64}$$

as can be seen from Figure 5.8b is always positive, as the dot product $\widehat{\mathbf{u}}_i \bullet \widehat{\mathbf{u}_p} > 0$ because the angle between $\widehat{\mathbf{u}_p}$ and $\widehat{\mathbf{u}}_i$ is always acute.

Expanding equation (5.54) gives

$$\mathbf{A}_{I_{radial}} = \frac{1}{2}Re\left\{Z^*_{mono}(H_{c,0}(\widehat{\mathbf{u}}_{c,0} \bullet \widehat{\mathbf{u}_p})\widehat{\mathbf{u}_p} + H_i(\widehat{\mathbf{u}}_i \bullet \widehat{\mathbf{u}_p})\widehat{\mathbf{u}_p})\right\}$$

now substituting equation (5.40) where we define the terms $Z_{c,0}(\mathbf{r})$ and $Z_i(\mathbf{r})$ to write $Z_{mono}(\mathbf{r}) = Z_{c,0}(\mathbf{r}) + Z_i(\mathbf{r})$ giving

$$\begin{aligned}
\mathbf{A}_{I_{radial}} &= \frac{1}{2}Re\left\{(Z^*_{c,0} + Z^*_i)(H_{c,0}(\widehat{\mathbf{u}}_{c,0} \bullet \widehat{\mathbf{u}_p})\widehat{\mathbf{u}_p} + H_i(\widehat{\mathbf{u}}_i \bullet \widehat{\mathbf{u}_p})\widehat{\mathbf{u}_p})\right\} && (5.65)\\
&= \frac{1}{2}Re\left\{\left(Z^*_{c,0}H_{c,0} + Z^*_i H_{c,0}(\widehat{\mathbf{u}}_{c,0} \bullet \widehat{\mathbf{u}_p})\right)\widehat{\mathbf{u}_p} + \left(Z^*_{c,0}H_i + Z^*_i H_i(\widehat{\mathbf{u}}_i \bullet \widehat{\mathbf{u}_p})\right)\widehat{\mathbf{u}_p})\right\} && (5.66)\\
&= \left(\frac{1}{2}Re\left\{Z^*_{c,0}H_{c,0}\right\} + \frac{1}{2}Re\left\{Z^*_i H_{c,0}\right\}\right)(\widehat{\mathbf{u}}_{c,0} \bullet \widehat{\mathbf{u}_p})\widehat{\mathbf{u}_p}\ldots && (5.67)\\
&\quad + \left(\frac{1}{2}Re\left\{Z^*_{c,0}H_i\right\} + \frac{1}{2}Re\left\{Z^*_i H_i\right\}\right)(\widehat{\mathbf{u}}_i \bullet \widehat{\mathbf{u}_p})\widehat{\mathbf{u}_p})
\end{aligned}$$

It can be seen from equation (5.67) that $\mathbf{A}_{I_{radial}}$ comprises terms for the active intensity due to the control source on its own and the image source on its own plus cross terms.

When $\widehat{\mathbf{u}}_{c,0} \bullet \widehat{\mathbf{u}_p} < 0$, $A_{I_{radial}}$ will be negative when the first term in equation (5.67) is less than the second term, or alternatively the following condition is met:

$$\left(\frac{1}{2}Re\left\{Z^*_{c,0}H_{c,0}\right\} + \frac{1}{2}Re\left\{Z^*_i H_{c,0}\right\}\right)(\widehat{\mathbf{u}}_{c,0} \bullet \widehat{\mathbf{u}_p}) < \left(\frac{1}{2}Re\left\{Z^*_{c,0}H_i\right\} + \frac{1}{2}Re\left\{Z^*_i H_i\right\}\right)(\widehat{\mathbf{u}}_i \bullet \widehat{\mathbf{u}_p}) \tag{5.68}$$

If condition (5.68) is met at a particular error sensor location $\mathbf{r}$ when $\widehat{\mathbf{u}}_{c,0} \bullet \widehat{\mathbf{u}_p} < 0$ then $\mathbf{A}_{I_{radial}} < 0$ and hence there is only a unique maximum exists as derived in Appendix E.

Condition (5.68) can best be illustrated as shown in Figure 5.14

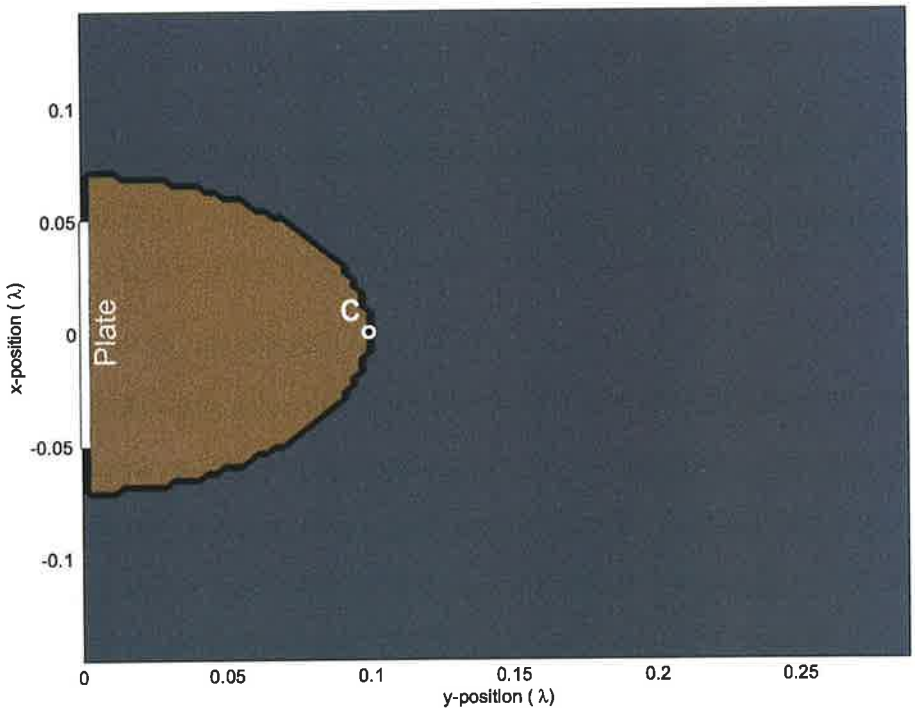


*Figure 5.14: The region (indicated by the colour red) where $A_{I_{radial}} < 0$, and hence the radial active intensity can become negative, leading to an optimal control source strength which maximises the radial active intensity. The blue region indicates the region where $A_{I_{radial}} > 0$ and hence the radial active intensity is positive definite and the optimal control source strength minimises the radial active intensity.*

If $A_{I_{radial}} > 0$ a unique minimum exists or if $A_{I_{radial}} < 0$ then a unique maximum exists and in either case the extreme control source strength is given by

$$q_{c,opt} = -A_{I_{radial}}^{-1} b_{I_{radial}} \tag{5.69}$$

Therefore to optimise the radial active intensity at a particular location $\mathbf{r}$ from a rectangular steel plate primary source by a single control monopole source (5.69) is substituted into (5.52).

The amount of sound power attenuation when the active intensity is minimised at the error sensor location is found by substituting (5.69) into (5.24) giving

$$\frac{W_p}{W_{min}} = \frac{c_{W_f}}{A_{W_f}\left|-\frac{1}{2}A^{-1}_{I_{radial}}(b_{I_{radial}})\right|^2 - (-\frac{1}{2}A^{-1}_{I_{radial}}(b_{I_{radial}}))^* b_{W_f} - b^*_{W_f}(-\frac{1}{2}A^{-1}_{I_{radial}}(b_{I_{radial}})) + c_{W_f}} \quad (5.70)$$

### 5.4.5 Comparison of power attenuation when minimising pressure and intensity error criterion

As described, the aim of the work presented here is to compare the performance of pressure and intensity error sensing strategies for a relatively simple structural radiation problem. Referring to Figure 5.8a, the problem to be studied here has a single monopole control source, separated from a previously described rectangular steel plate primary source, by one-tenth of a wavelength. Using equation (5.33), the maximum possible acoustic power attenuation for this arrangement is 29.4 dB. The plate size is close to $8\lambda/100$, and the plate is driven at its centre. The dominant mode is the (1,1) and hence the plate is behaving like a monopole source.

Illustrated in Figures 5.15 and 5.16 is the acoustic power attenuation that would result from minimising the square acoustic pressure amplitude at a point in space. The results in Figures 5.15 and 5.16 are to different scales: Figure 5.15 depicts results for minimising acoustic pressure at points in space for x,y positions over 7 wavelengths, while Figure 5.16 depicts results over a 1 wavelength region. Observe that significant attenuation can be achieved at locations perpendicular to a line joining the sources. The maximum power attenuation shown in the resolution provided by Figures 5.15 and 5.16 is 24dB, however as the resolution is increased the maximum power attenuation should approach 29.4dB.

Illustrated in Figures 5.17 and 5.18 are results for the same geometry, but where radial active intensity is optimised as opposed to square acoustic pressure amplitude. Comparing Figures 5.15 and 5.17, the results obtained when optimising radial active intensity at locations distant

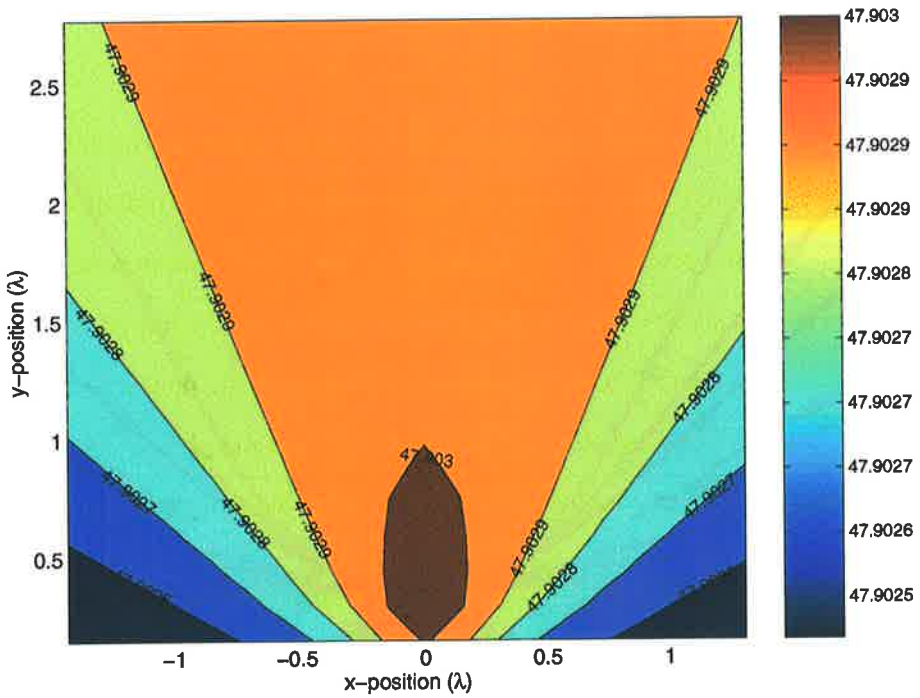


*Figure 5.15: Acoustic power attenuation in dB as a function of pressure error sensor placement, rectangular steel plate primary at the origin in an infinite baffle in the xz-plane and control sources separated by $\lambda/10$ wavelength in far field view. The $\times$ marks the edge of the plate. The circle $\bigcirc$ is the control monopole source location. (N=100).*

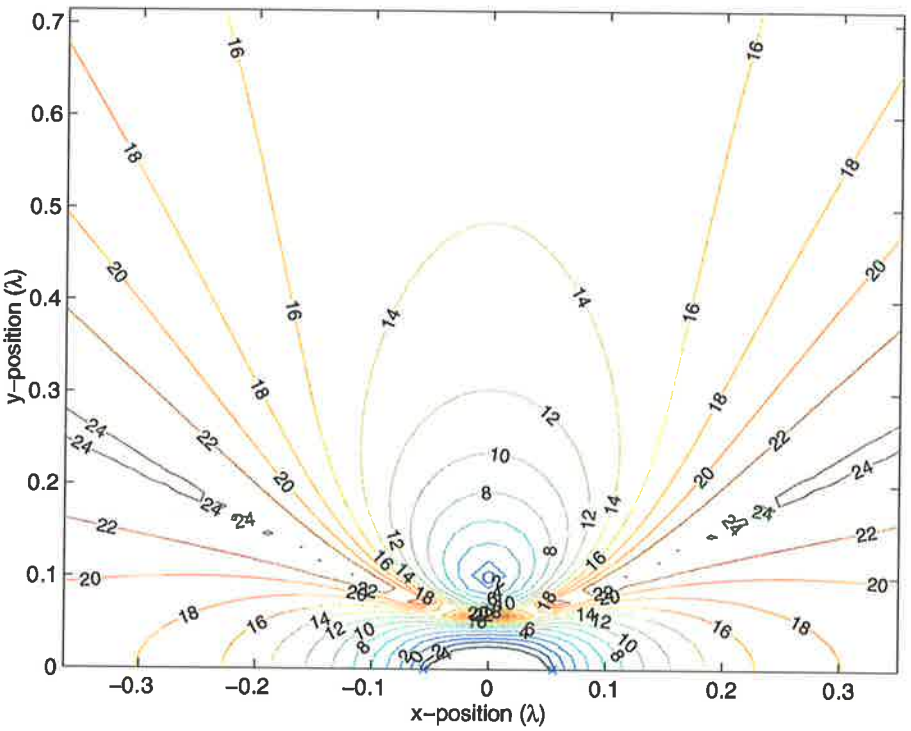


*Figure 5.16: Acoustic power attenuation in dB as a function of pressure error sensor placement, rectangular steel plate primary at the origin in an infinite baffle in the xz-plane and control sources separated by $\lambda/10$ wavelength in near field view. The $\times$ marks the edge of the plate. The circle $\bigcirc$ is the control monopole source location. (N=100).*

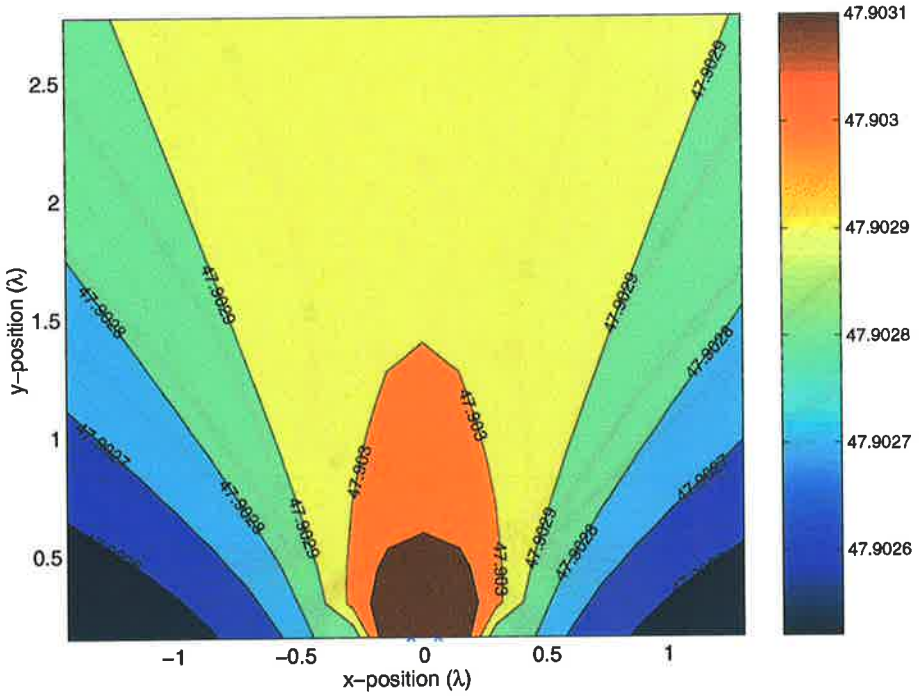


*Figure 5.17: Acoustic power attenuation in dB as a function of radial active intensity error sensor placement (radial with respect to the primary source), rectangular steel plate primary at the origin in an infinite baffle in the xz-plane and control sources separated by $\lambda/10$ wavelength in far field view. The $\times$ marks the edge of the plate. The circle $\bigcirc$ is the control monopole source location. (N=100).*

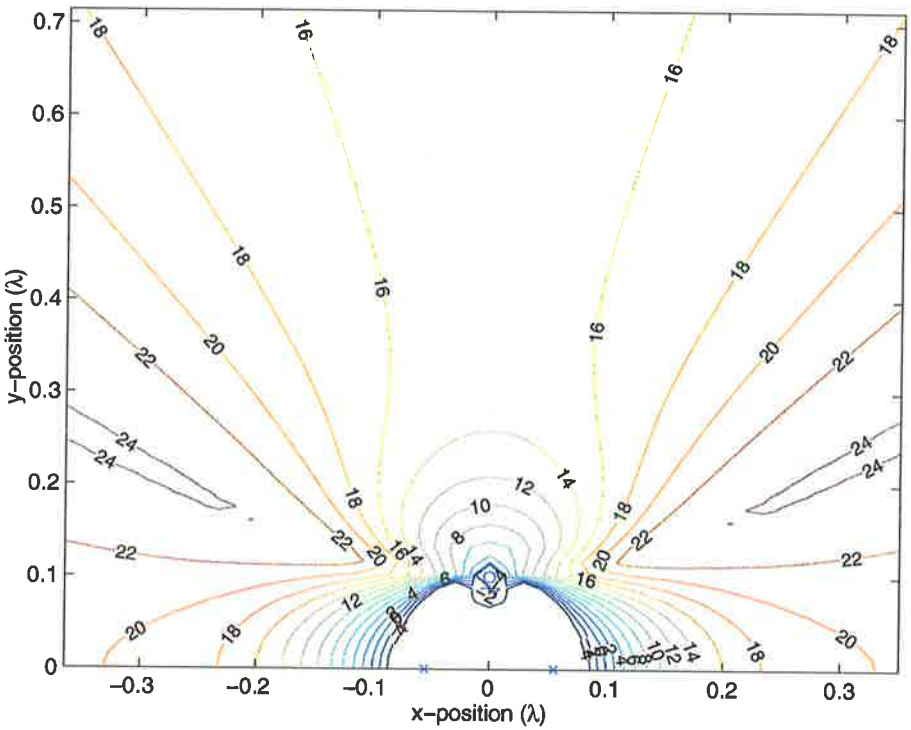


*Figure 5.18: Acoustic power attenuation in dB as a function of radial active intensity error sensor placement (radial with respect to the primary source), rectangular steel plate primary at the origin in an infinite baffle in the xz-plane and control sources separated by $\lambda/10$ wavelength in near field view. The $\times$ marks the edge of the plate. The circle $\bigcirc$ is the control monopole source location. (N=100).*

from the sources are very similar to the acoustic pressure results. However, when comparing the results in Figures 5.16 and 5.18, it is evident that the results obtained when optimising the error criteria at locations close to the sources are very different. In fact, the acoustic power attenuation that results from optimising acoustic intensity is far worse than when optimising squared acoustic pressure. The areas of poor attenuation correspond to areas where $A_{I_{radial}} < 0$, shown in Figure 5.14.

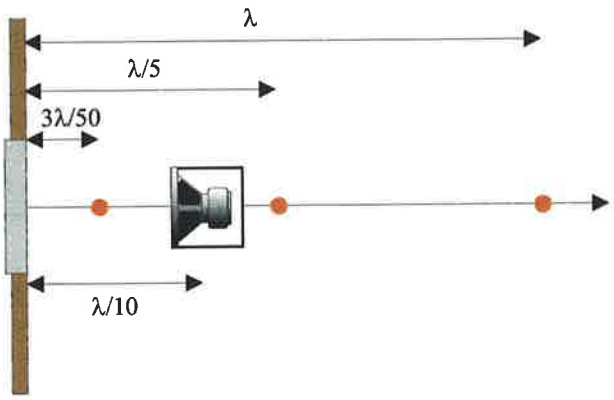


*Figure 5.19: The three sensor locations considered. The red dots indicate the error sensor locations.*

As discussed previously in this thesis, for an error sensing strategy to be of "high quality", the control source volume velocity that minimises the error criterion of interest, derived in step 3, must be virtually identical to the control source volume velocity that provides maximum acoustic power attenuation, calculated in step 2. Shown in Figures 5.20a and 5.20b are plots of the squared pressure and intensity error criteria evaluated at a location which is λ (shown in Figure 5.19) from the primary source and directly in front as a function of complex control source volume velocity. Observe that both the pressure and intensity error surfaces have a single minimum, at approximately the same volume velocity, and that these minima are close to volume velocity that is optimal in terms of acoustic power attenuation.

The result is similar for error sensors located at a position of λ/5 (shown in Figure 5.19) from the primary source, just behind the control source, as evident in the error surface plots shown in Figures 5.21a and 5.21b. In this case the intensity minima is slightly closer to the value

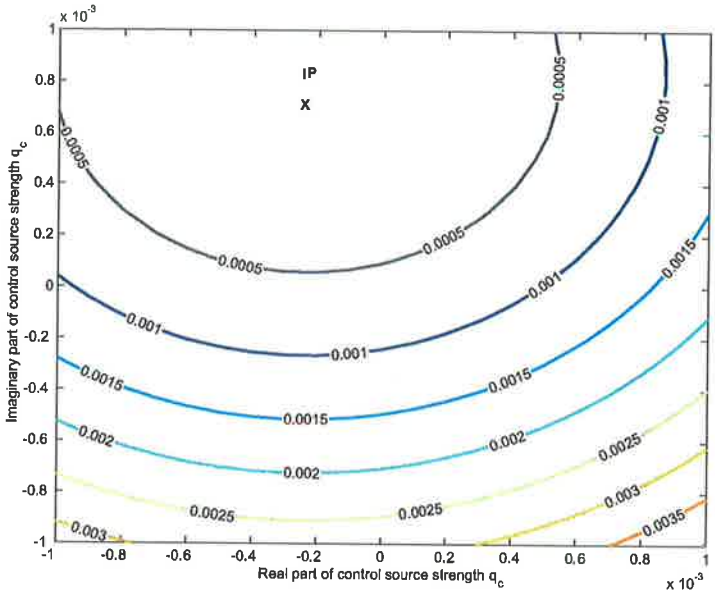


*(a) Pressure amplitude as a function of the real and imaginary parts of the relative control source strength*

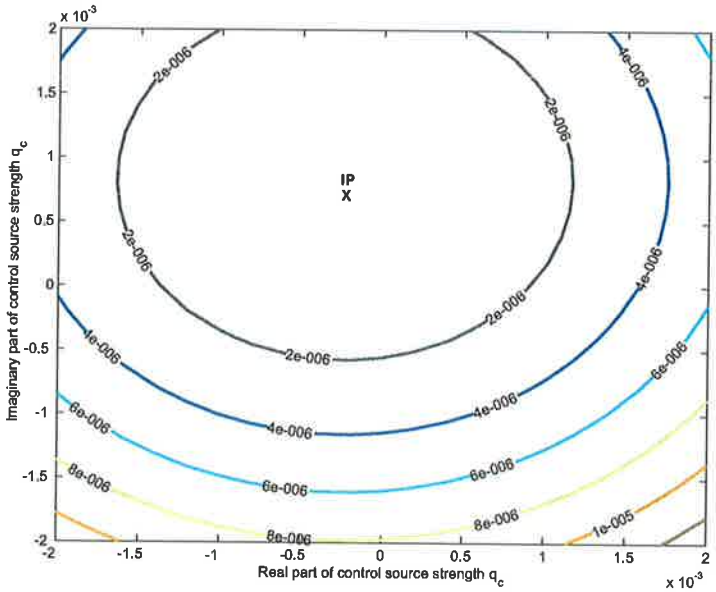


*(b) Radial active intensity as a function of the real and imaginary parts of the relative control source strength*

*Figure 5.20: Squared pressure amplitude and radial active intensity as a function of the real and imaginary parts of the control source strength $q_c$ relative to a unitary primary source strength, at the sensor location $r_e = (\lambda, 0)$. (the calculations are relative to a unitary primary source strength). **X** indicates the optimal control source strength when minimising acoustic power. **P** indicates the optimal control source strength when minimising squared pressure. **I** indicates the optimal control source strength when minimising radial active intensity.*

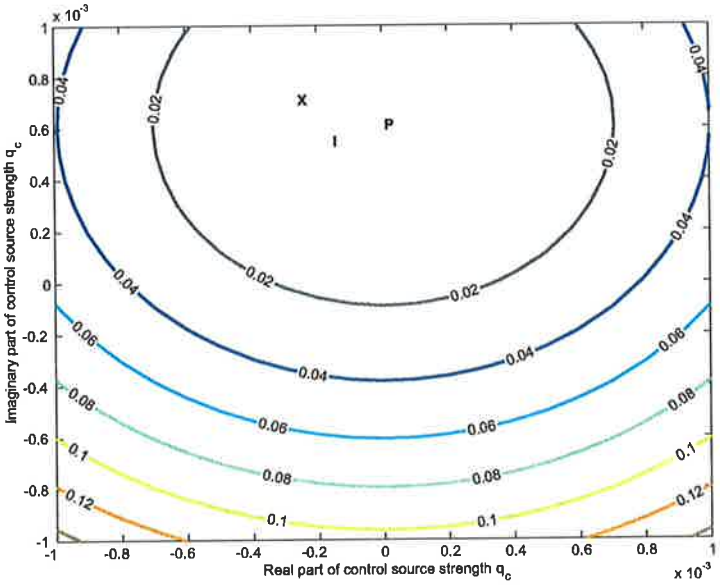


*(a) Pressure amplitude as a function of the real and imaginary parts of the relative control source strength*

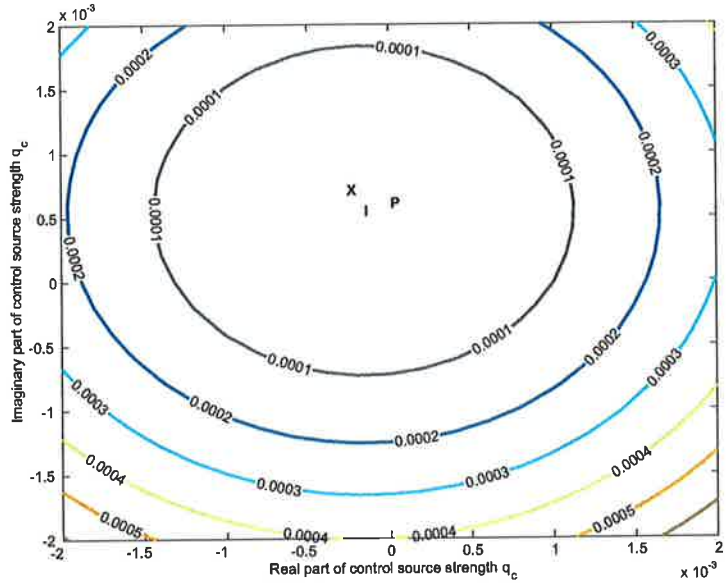


*(b) Radial active intensity as a function of the real and imaginary parts of the relative control source strength*

*Figure 5.21: Squared pressure amplitude and radial active intensity as a function of the real and imaginary parts of the control source strength $q_c$ relative to a unitary primary source strength, at the sensor location $r_e = (\lambda/5, 0)$. (the calculations are relative to a unitary primary source strength). **X** indicates the optimal control source strength when minimising acoustic power. **P** indicates the optimal control source strength when minimising squared pressure. **I** indicates the optimal control source strength when minimising radial active intensity.*

that will minimise radiated acoustic power than is the pressure minima. Hence at this location acoustic intensity error sensing would produce a superior result.

The results are very different, however, for an error sensing location of $3\lambda/50$ (shown in Figure 5.19) from the primary source, approximately mid way between the primary and control sources. Referring to Figure 5.22b, observe that with acoustic active intensity there is no global minimum. In fact, the point of inflexion is a global maximum. The pressure minima is very close to the value that will minimise radiated acoustic power where as the intensity maxima is much further away. If the active intensity only has a global maximum at this sensor location then only poor acoustic power attenuation can be expected. If the error criterion is modified to be intensity amplitude, then there is a locus of points where the error criterion has a zero value. Hence there would be infinitely many possible minima for an intensity amplitude error signal to converge to.

### 5.4.6 Experimental verification of the acoustic power attenuation of a rectangular steel plate primary source in an infinite baffle and single monopole control source

In order to experimentally verify the previous findings a test rig of a simply supported rectangular steel plate in an infinite baffle, a rectangular steel plate of dimensions (380mm $\times$ 300mm $\times$ 2mm) mounted in a heavy steel frame similar to that used by Pan et al. (1992), and set into a baffle. The vibration properties of the plate were checked using modal analysis in Section 5.3 and it was found to accurately model the simply supported boundary conditions. The steel plate was clamped to a heavy steel table to which a large baffle was mounted by bolting it with brackets to the table. The experiments were conducted in an anechoic chamber (dimensions over wedge tips: 4.79m $\times$ 3.9m $\times$ 3.94m) which has a lower cutoff frequency of 85Hz. The same enclosed speaker was used as the control source as was used in Chapters 3 and 4.

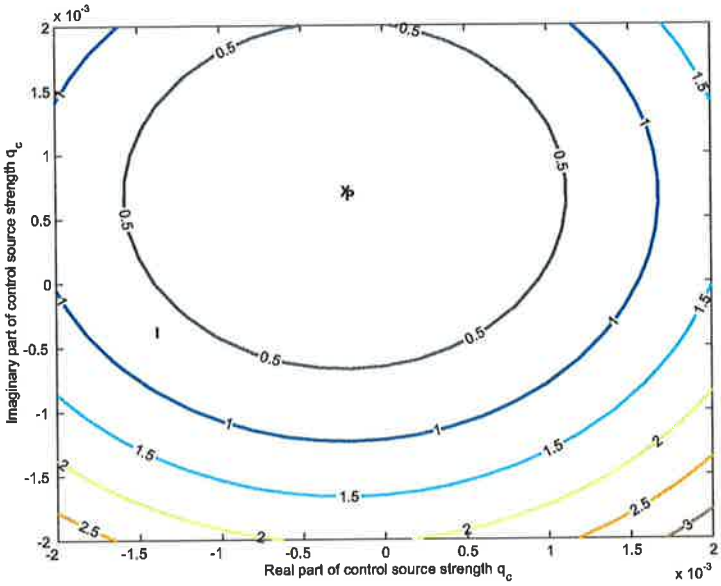


*(a) Pressure amplitude as a function of the real and imaginary parts of the relative control source strength*

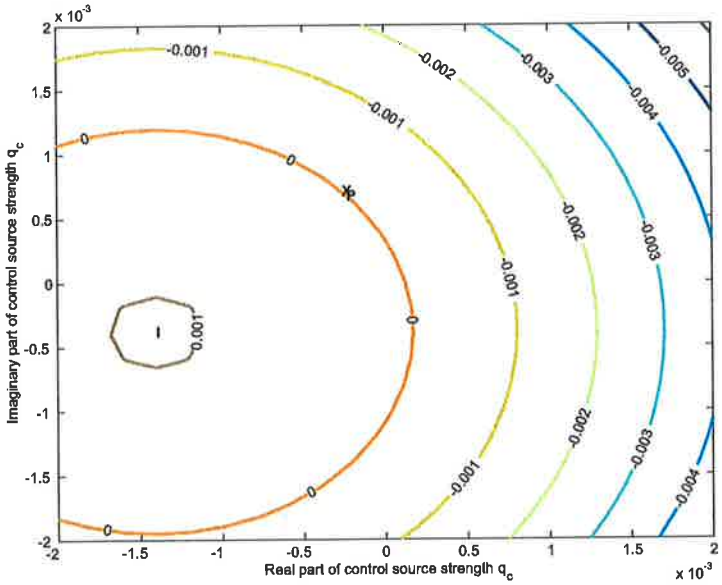


*(b) Radial active intensity as a function of the real and imaginary parts of the relative control source strength*

*Figure 5.22: Squared pressure amplitude and radial active intensity as a function of the real and imaginary parts of the control source strength $q_c$ relative to a unitary primary source strength, at the sensor location $r_e = (3\lambda/50, 0)$. (the calculations are relative to a unitary primary source strength). **P** indicates the optimal control source strength when minimising squared pressure. **I** indicates the optimal control source strength when minimising radial active intensity.*

#### 5.4.6.1 Radial pressure distribution

The radial pressure distribution of the plate was measured with the a B&K Type 4131 condenser microphone starting at 50mm from the plate front face, at radial intervals of 50mm. A 3 metre length of 30 by 30mm Aluminum angle section with holes drilled at 50mm intervals to fit the 1/2" B&K Type 4131 condenser microphones was used to measure the pressure transfer function, between the plate electrodynamic shaker input and the B&K Type 4131 microphone output. The plate was driven with random noise and 100 linear averages were applied to measure the pressure transfer functions at each radial location. The experimental setup is shown in Figure 5.23.

The measured radial relative pressure distribution at 100Hz is shown in Figure 5.24. The measured and theoretical radial relative pressure distributions are also plotted from the baffled monopole case (in Chapter 4) for comparison. The B&K Type 4131 condenser microphone was not calibrated and hence Figure 5.24 shows the relative pressure amplitude and not the sound pressure level. At distances greater than 50mm, the enclosed speaker fits the 6dB per doubling of distance characteristic of a monopole source with only a slight deviation which can be attributed to experimental error, as described in Chapter 4. Observe that there is good agreement between theoretical and experimental values.

#### 5.4.6.2 Radial active intensity distribution

Based on the transfer function measurements described in the previous section, the active intensity along a radial line away from the plate was calculated as in Chapters 3 and 4.

Figure 5.25 shows the active intensity at 100Hz as a function of radial distance away from the baffled speaker. It can be seen in Figure 5.25 that the measured active intensity closely matches the theoretical monopole radial active intensity distribution, as does the measured pressure to the theoretical monopole radial pressure distribution shown in Figure 5.24. There is only a slight variation, which may cause some experimental error.

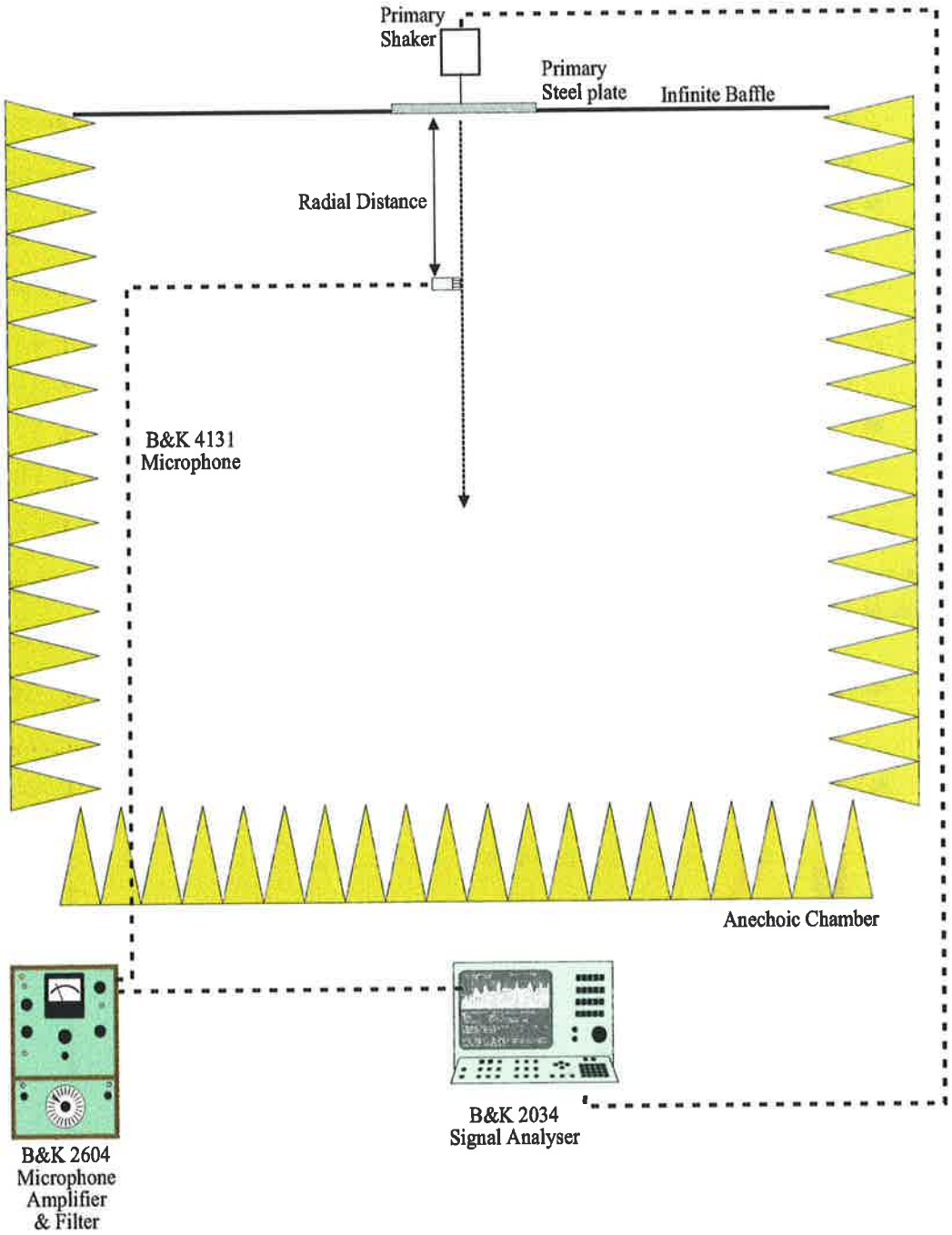


*Figure 5.23: Experimental setup for the measurement of the radial pressure distribution of a speaker in a baffle model of a monopole source in an infinite baffle.*

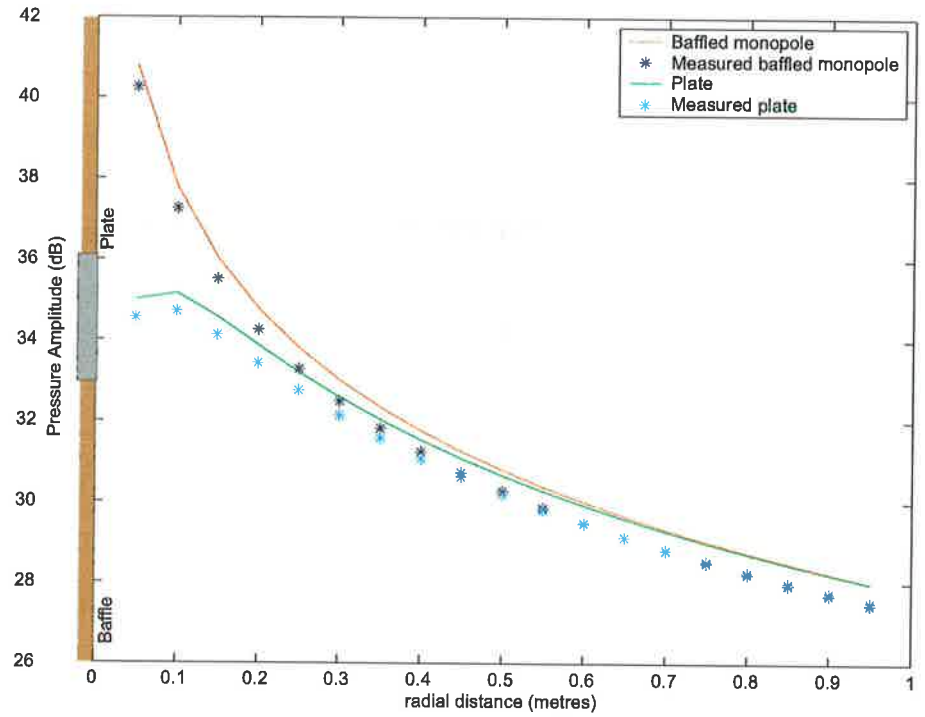


*Figure 5.24: Radial relative pressure distribution the rectangular steel plate in a baffle as compared to a monopole in a baffle from Chapter 4.*

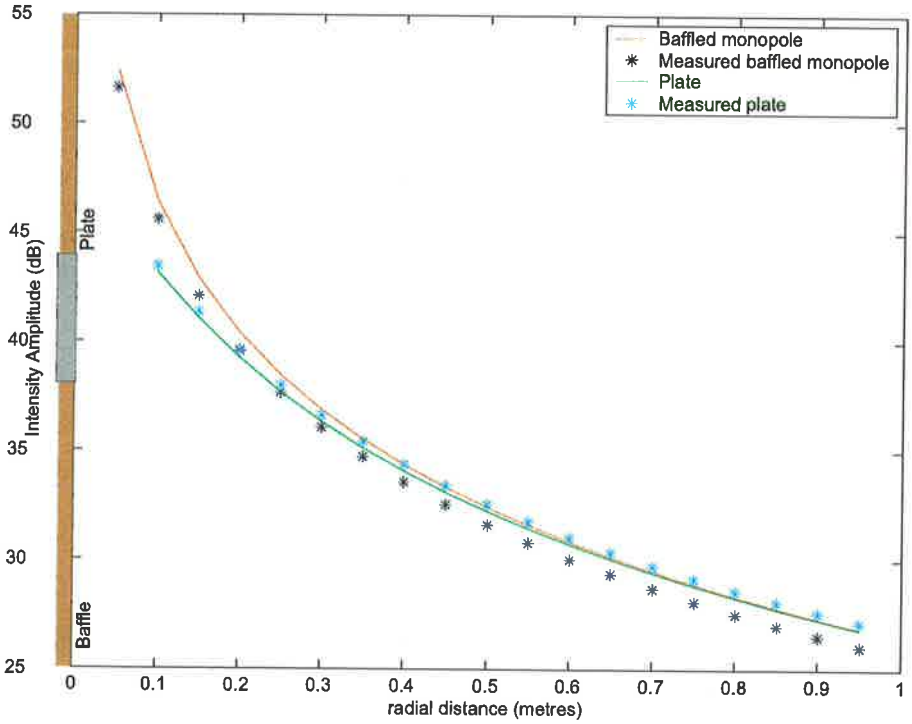


*Figure 5.25: Radial relative active intensity distribution on the rectangular steel plate in a baffle as compared to a monopole in a baffle from Chapter 4.*

## 5.4.7 Results

### 5.4.7.1 Far field pressure distribution

In order to assess the power attenuation of minimising an active intensity cost function compared to that which is obtained by minimising the squared pressure, the "far field" sound pressure was measured with a microphone attached to a boom and turntable through an arc 180°, before and after control is applied. Figure 5.26 shows the experimental setup. The primary source used was a rectangular panel embedded in a baffle (as described previously) and a control source which was an enclosed pipe speaker (described previously in Chapter 3). The control source was hung inside a pair of stockings from a cantilever support beam bolted above the primary source. The experiment was conducted in an anechoic chamber (dimensions over wedge tips: 4.79m × 3.9m × 3.94m) with a lower cut off frequency of 85Hz, and the sources were separated by a distance of $\lambda/10$. A B&K Type 4131 condenser microphone put through a B&K Type 2604 Microphone Amplifier which is 1/3 octave band pass filtered in the 100Hz 1/3 octave band was used to measure the "far field" sound pressure. The B&K Type 4131 condenser microphone was attached to a microphone boom which was located just in front of the baffled primary source and extended 1.8 metres out (see Figure 5.5). The control system is described in Appendix D. The signal from the B&K Type 4131 condenser microphone was sent to B&K Type 2307 Level Recorder which plotted the results on polar paper. The results were then scanned into a computer using Corel Trace™ and placed on a half circle polar graph. The B&K Type 4131 condenser microphone was not calibrated, as interest centres on pressure reduction. A HP Oscilloscope was used to check the actual amplitude reduction of the primary noise source. The control signal reduced the primary signal by between 30 and 40dB.

Figure 5.45 displays the location of the error sensors tested in these experiments. Illustrated in Figure 5.27 is the result of far field error sensing with either an acoustic pressure error sensor or an active intensity amplitude error sensor at $\lambda$ from the plate (see Figure 5.45). As expected, the outcome when using either a pressure or intensity error signal is similar.

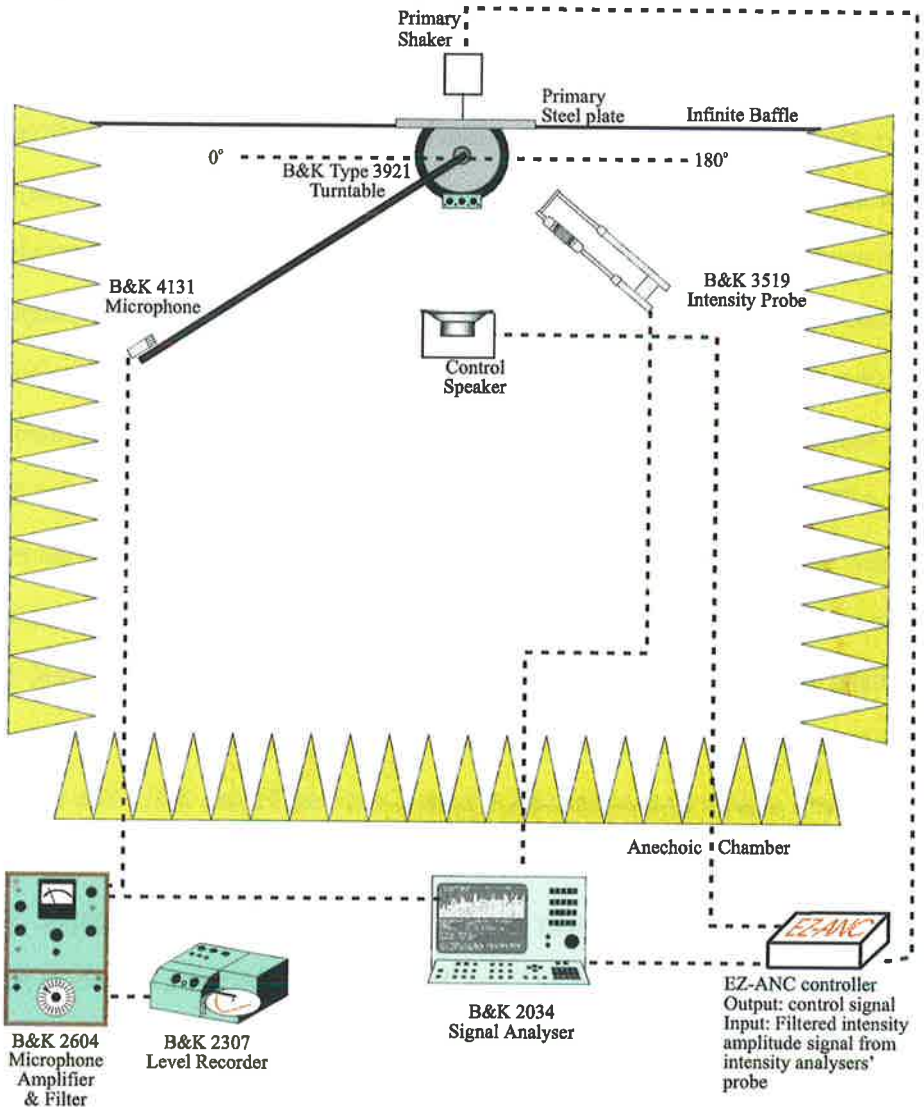


*Figure 5.26: Experimental setup for measuring the far field pressure distribution before and after active control is applied to minimise a squared pressure and active intensity amplitude cost function.*

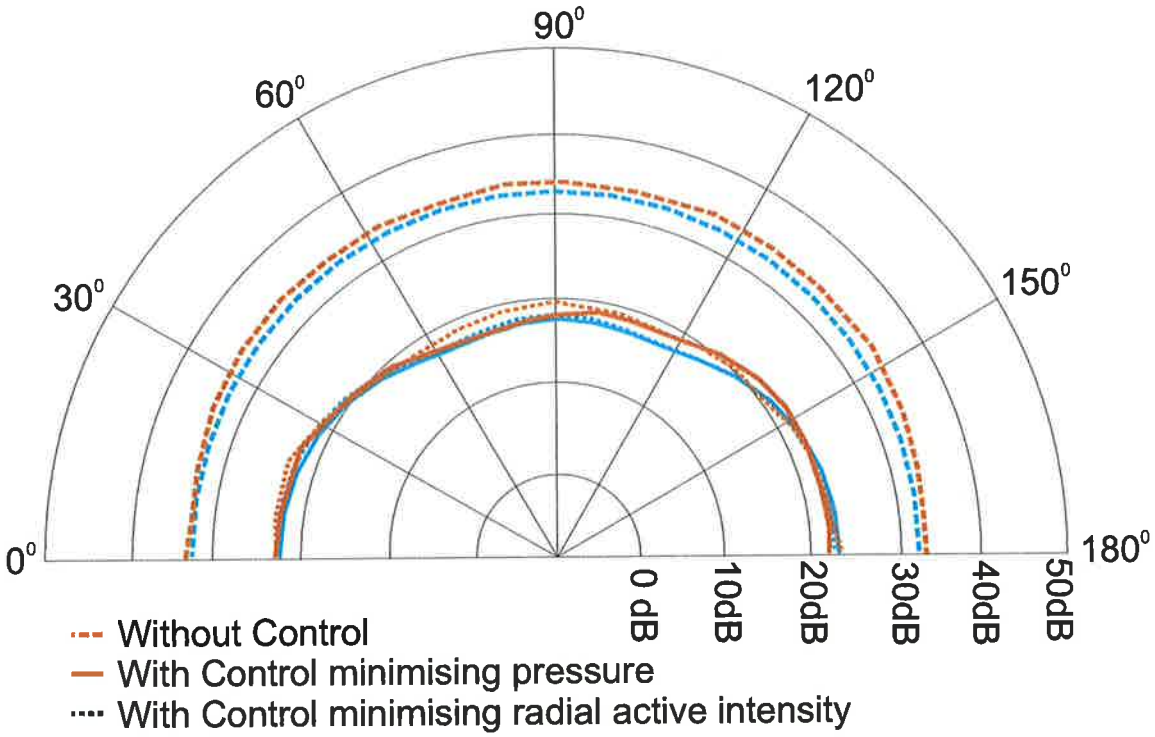


*Figure 5.27: Far field pressure before and after control when employing a single acoustic pressure or radial active intensity amplitude error sensor at λ from the primary source on the x-axis to control a 100Hz tone from a simply supported rectangular plate primary source with a single monopole control source. The red lines indicate the experimental measurements. The blue lines indicate the theoretically predicted results with a 1% error in amplitude and a 1°error in phase of the control signal.*

Figure 5.28 shows the result of minimising the pressure and active intensity amplitude at a position closer to the primary and control sources at $\lambda/5$ from the plate (see Figure 5.45). As predicted in the simulations, the active intensity result is marginally better than the pressure result in this instance.

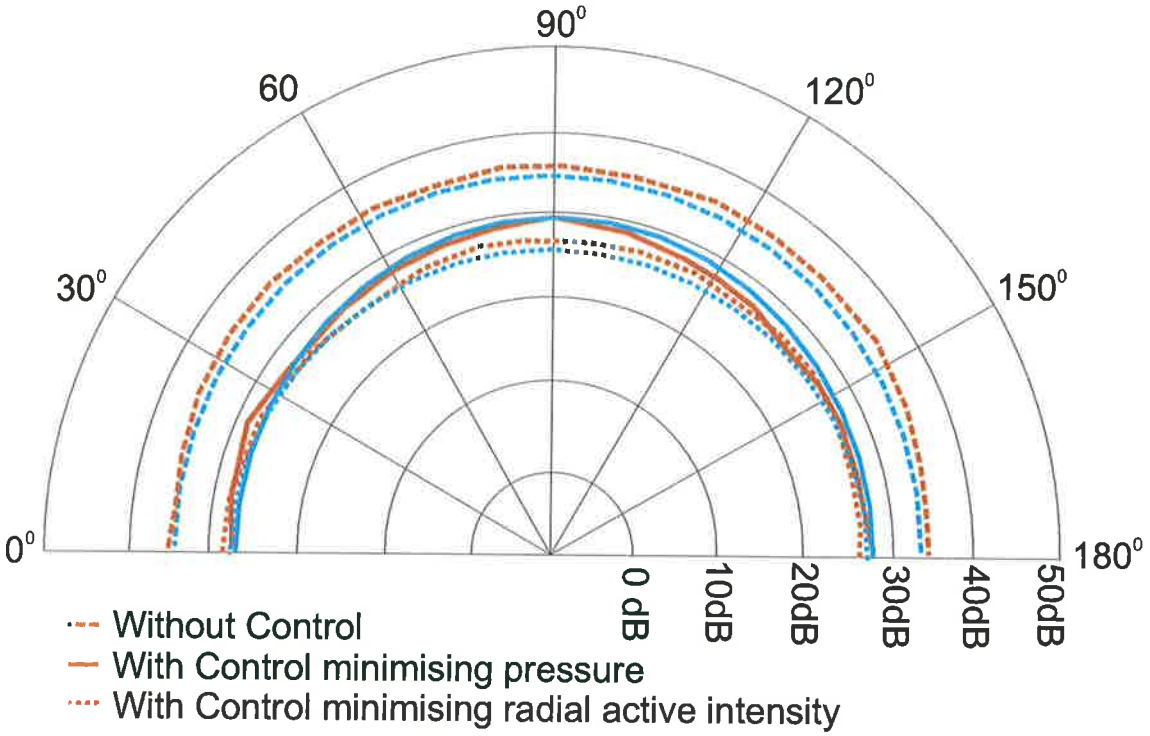


*Figure 5.28: Far field pressure before and after control when employing a single acoustic pressure or radial active intensity amplitude error sensor at $\lambda/5$ from the primary source on the x-axis to control a 100Hz tone from a simply supported rectangular plate primary source with a single monopole control source. The red lines indicate the experimental measurements. The blue lines indicate the theoretically predicted results with a 1% error in amplitude and a 1°error in phase of the control signal.*

Illustrated in Figure 5.29 is the result of error sensing the pressure and active intensity amplitude in the near field, between the primary and control sources at $3\lambda/50$ from the plate (see Figure 5.45). It can be seen that between 15 and 20dB of attenuation is achieved with a pressure error sensor, whereas an active intensity amplitude error sensor achieves an increase in the sound levels by approximately 5dB.

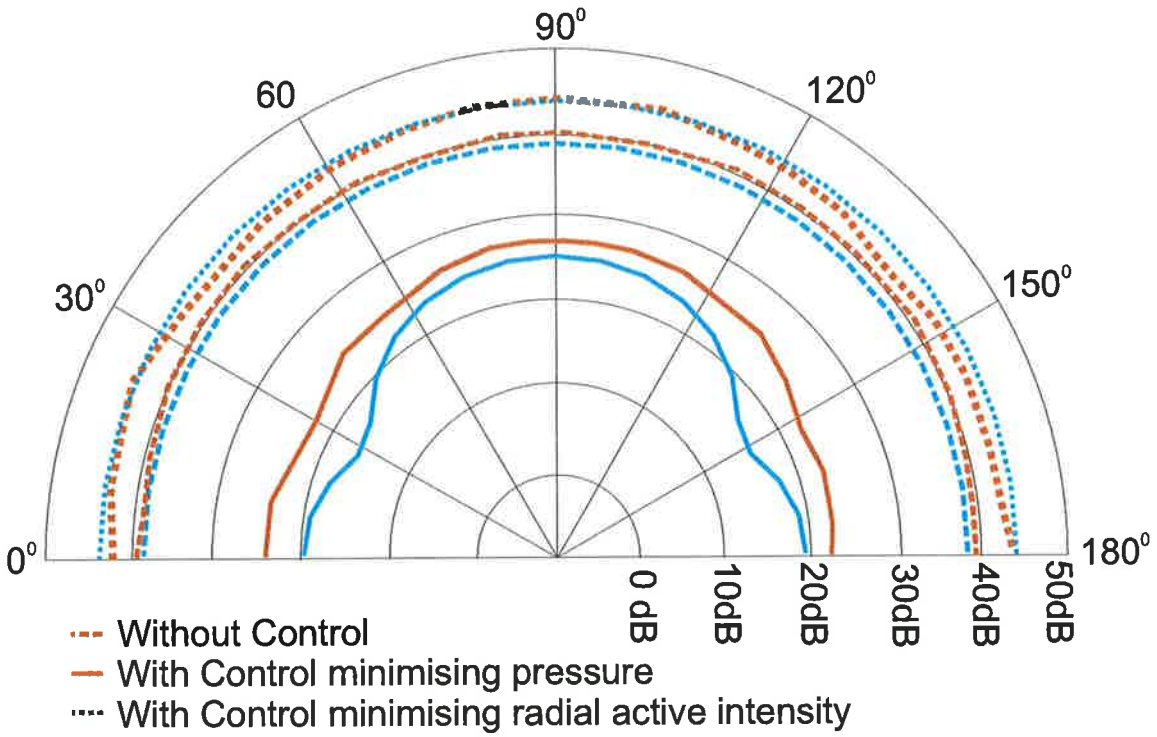


*Figure 5.29: Far field pressure before and after control when employing a single acoustic pressure or radial active intensity amplitude error sensor located approximately halfway between the primary and control sources (at radial distance of $3\lambda/50$ from the primary source) to control a 100Hz tone from a simply supported rectangular plate primary source with a single monopole control source. The red lines indicate the experimental measurements. The blue lines indicate the theoretically predicted results with a 1% error in amplitude and a 1°error in phase of the control signal.*

#### 5.4.7.2 Active intensity versus control source strength

In order to test the theoretical prediction of multiple minima when minimising active intensity amplitude, measurements were made of the active intensity at the midpoint between the primary and control sources at different control source strengths. Figure 5.30 shows the setup used in the experiment. The primary and control speakers were again mounted on stands in an anechoic chamber (dimensions over wedge tips: 4.79m $\times$ 3.9m $\times$ 3.94m) and separated by a distance of $\lambda/10$ as shown in Figure 5.30. The B&K Type 2134 Sound Intensity Analyser's intensity probe was positioned at a distance of $3\lambda/50$, $\lambda/5$ and $\lambda$ from the primary source along a line passing through the primary and control sources. The primary and control sources were driven by a 100Hz tone. The intensity signal is 1/3 octave band pass filtered in the 100Hz 1/3 octave band.

#### 5.4.7.3 Results of the relative total active intensity

The intensity probe positioned as described above, was used to measure the active intensity when the plate was driven with a reference voltage $V_p$ at 100Hz and the input voltage to the control speaker $V_c$ was adjusted. The voltmeter in Figure 5.30 was used to measure the input voltage $V_{input} = V_c$ to the enclosed speakers. The active intensity value and the relative voltage $V_c/V_p$ was recorded. The active intensity values were then converted from dB to a linear scale and the relative voltage $V_c/V_p$ was squared and then plotted in Matlab™.

Figure 5.31 shows total active intensity (from both primary and control sources) relative to the primary active intensity on its own, plotted against the control source strength relative to the primary source strength when the intensity probe is located at the approximate midpoint between primary and control sources (at a radial distance of $3\lambda/50$ from the primary source). The results show a deviation between the theoretically predicted relative total active intensity and that which was measured by experiment described above. Observe that in the experiments the

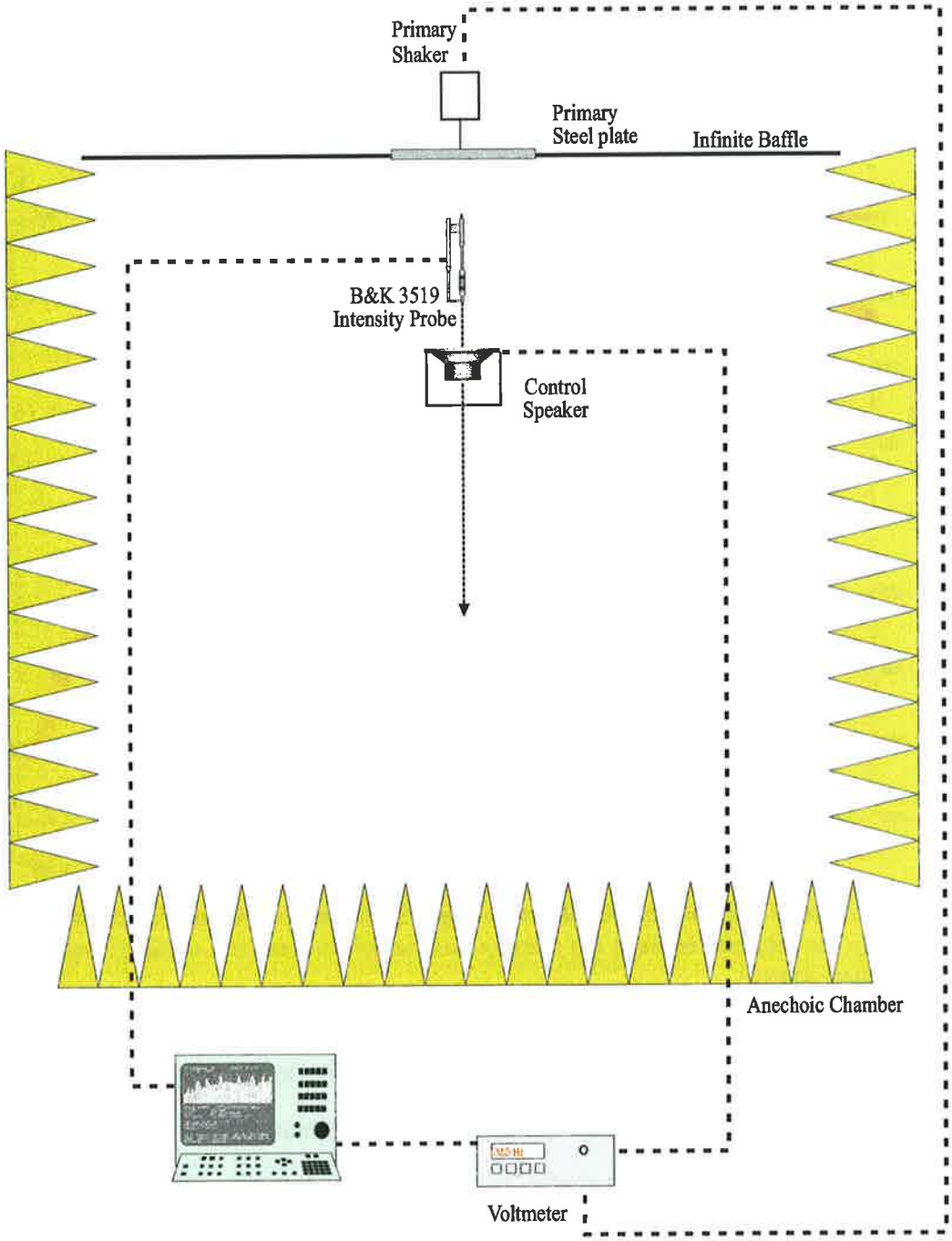


*Figure 5.30: Experimental setup to measure the active intensity located at radial distances of 3λ/50, λ/5 and λ from the primary source at 100Hz at different control source strengths.*

active intensity does indeed become negative for certain control source strengths, the difference between theory and experiment can be put down to experimental error. It is worth noting that the active intensity varied by approximately 10dB across the range of voltages which were measured, sometimes only by 0.2dB between voltage increments.

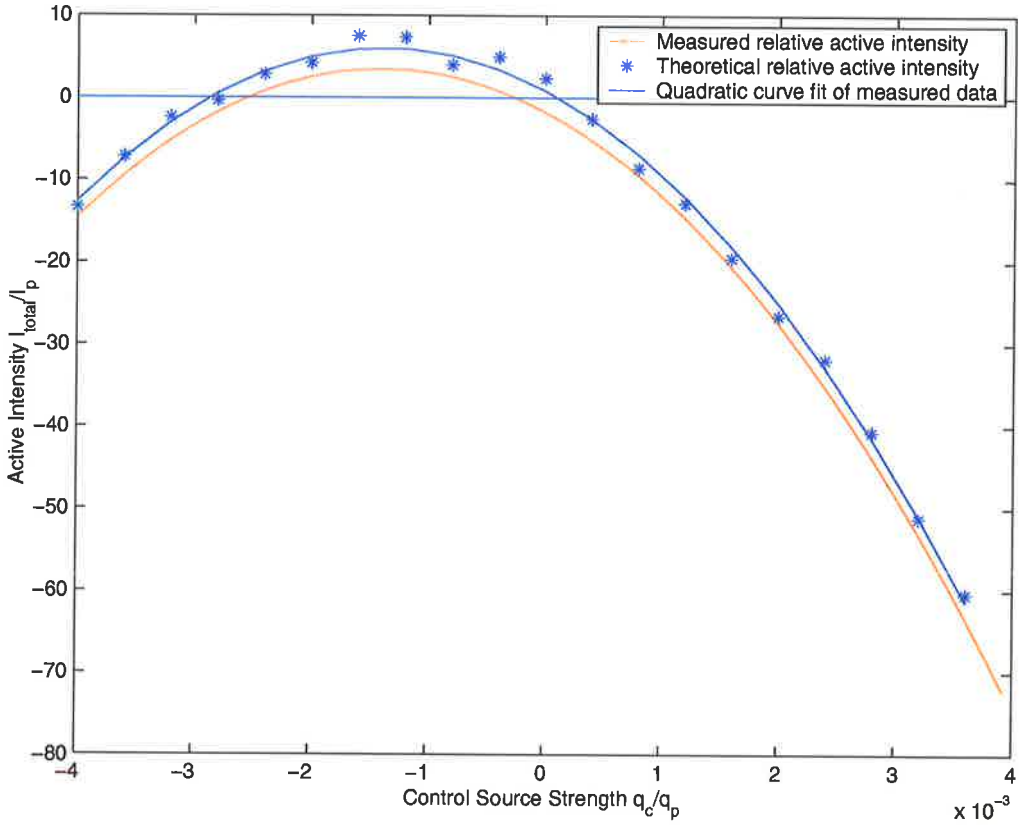


*Figure 5.31: Relative total active intensity plotted against the relative control source strength at the approximately the midpoint between the primary and control sources (at a radial distance of $3\lambda/50$ from the primary source).*

Figure 5.32 shows the total active intensity amplitude relative to the primary active intensity plotted against the control source strength relative to the primary source strength at a radial distance of $3\lambda/50$ from the primary source. From Figure 5.31 it has been shown that the active intensity cost function can be made negative and hence has no minimum value. If an active intensity amplitude cost function is employed, Figure 5.32 shows 2 minima out of infinitely many possible minima (see Figure 5.22).

Figure 5.33 and Figure 5.34 show the total active intensity (from both primary and control

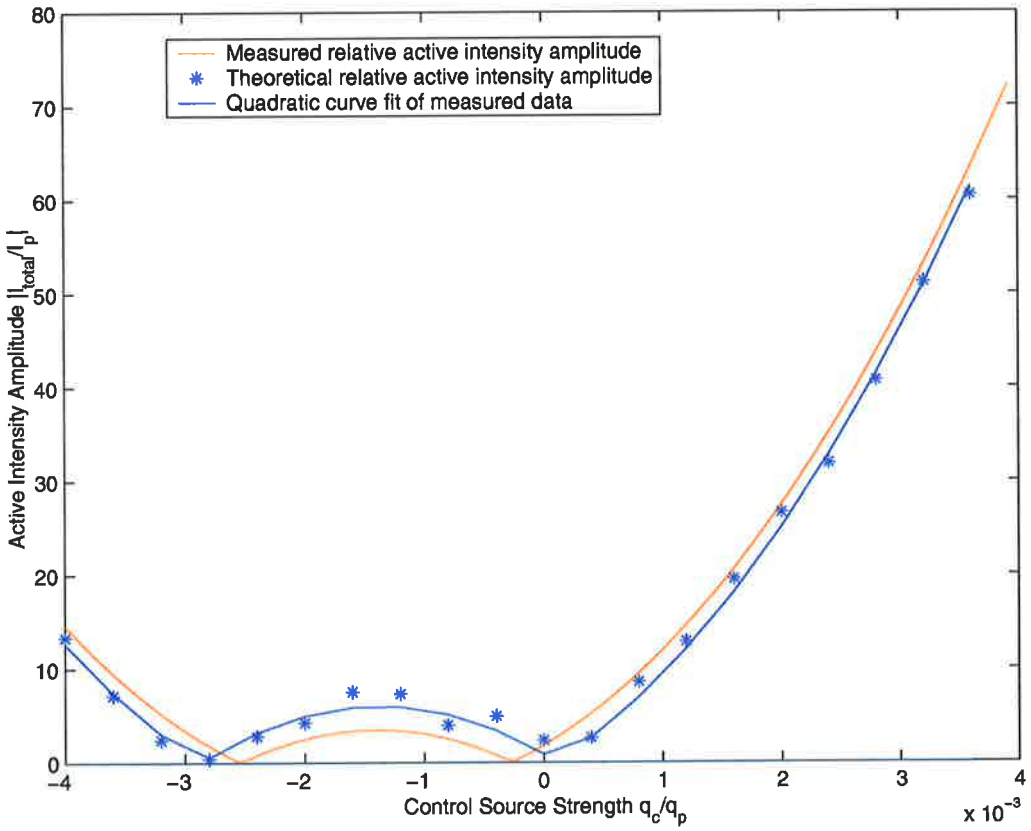


*Figure 5.32: Relative total active intensity amplitude plotted against the relative control source strength at the approximately the midpoint between the primary and control sources (at a radial distance of $3\lambda/50$ from the primary source).*

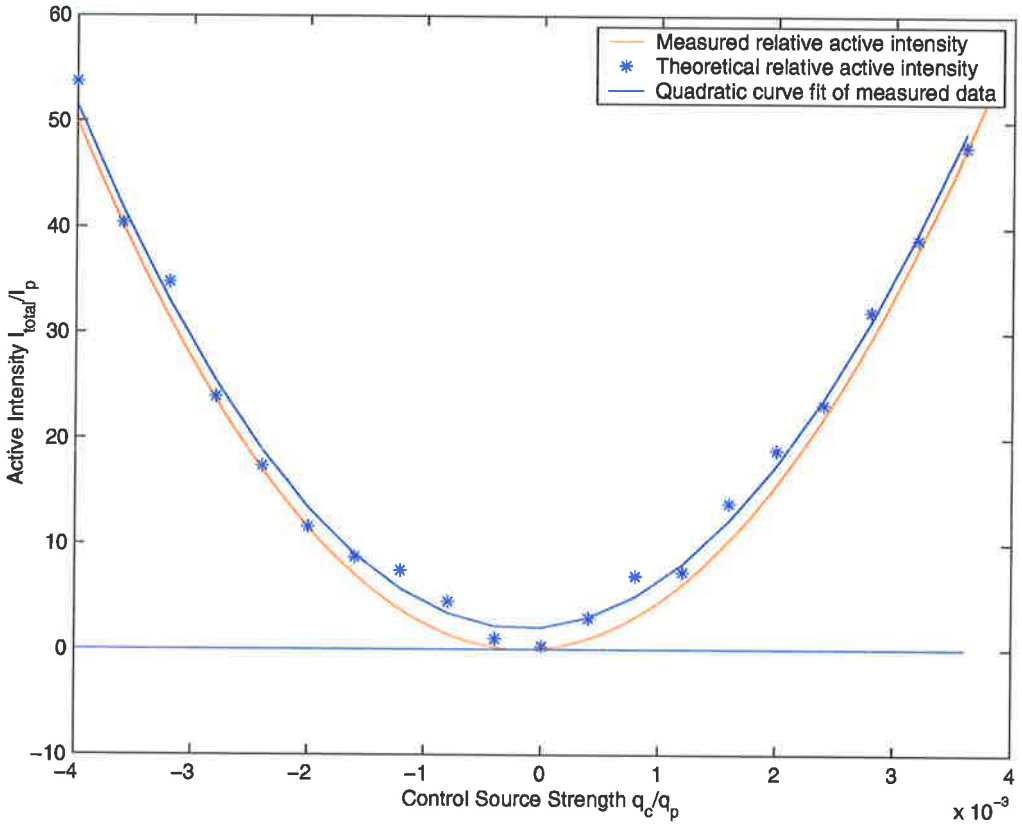


*Figure 5.33: Relative total active intensity plotted against the relative control source strength at a distance of $\lambda/5$ from the primary source along a line passing through both primary and control sources.*

sources) relative to the primary active intensity on its own, plotted against the control source strength relative to the primary source strength when the intensity probe is located at distances of $\lambda/5$ and $\lambda$ from the primary source along a line passing through the primary and control sources. The results show a slight discrepancy between the theoretically predicted relative total active intensity and that which was measured by experiment described previously. The experiment confirms that active intensity does remain positive definite at this location. The differences between theory and experiment can be put down to experimental error as described before.

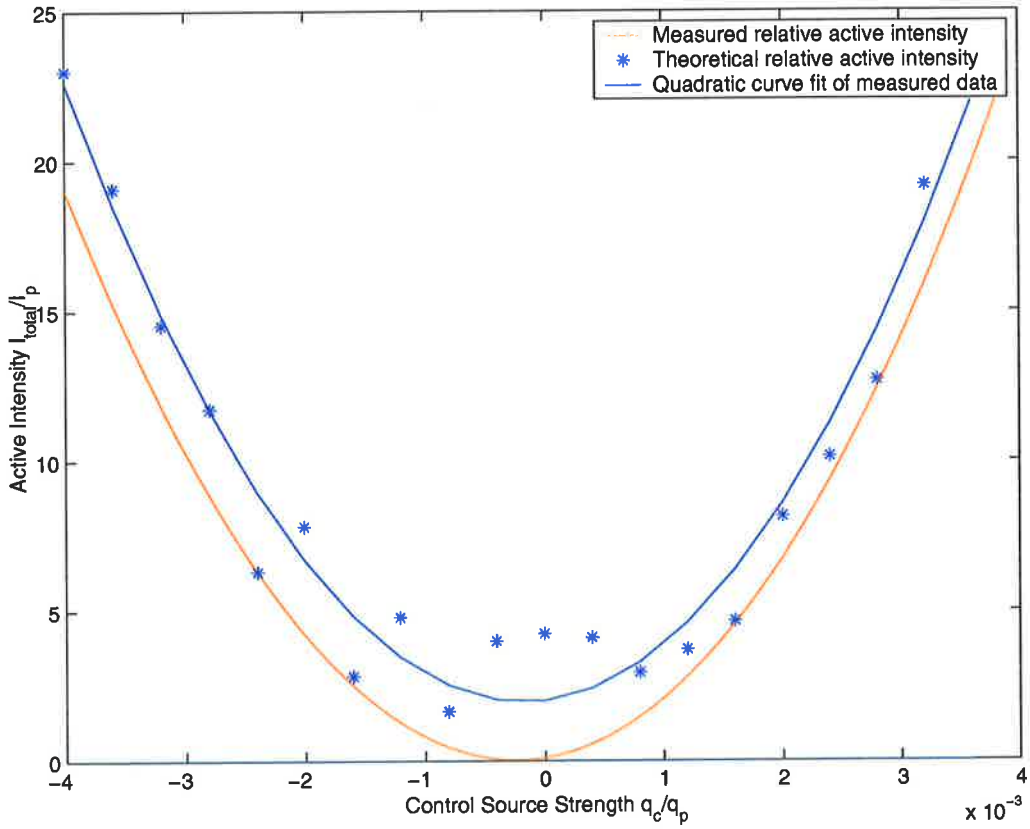


*Figure 5.34: Relative total active intensity plotted against the relative control source strength at a distance of $\lambda$ from the primary source along a line passing through both primary and control sources.*

| Error Signal | Sensor Location | Comparison | Relevant Figures |
|---|---|---|---|
| Active intensity amplitude | $3\lambda/50$ | multiple minima visible | 5.32 |
| Active intensity | $3\lambda/50$ | visible inverted parabola, maximum | 5.31 |
| Active intensity | $\lambda/5$ | positive definite | 5.33 |
| Active intensity | $\lambda$ | positive definite | 5.34 |

*Table 5.3: Plate intensity vs source strength results summary table.*

### 5.4.8 Conclusion

The performance of active control of free field tonal sound radiation from a simply supported rectangular plate in an infinite baffle, via introduction of a single monopole control source using far field error sensing is not significantly improved with the use of active intensity error sensors in place of pressure error sensors. A single minimum exists in both the acoustic pressure and active intensity error criteria, at roughly the same control source strength, leading to similar outcomes. Significant differences *do* exist in the pressure and intensity error criteria for sensing locations in the near field. At some near field locations, the global disturbance attenuation that accompanies intensity error sensing is greater than that achieved with pressure error sensing, as previously reported for monopole radiation and confirmed here for a structural radiation problem. However, for some sensing locations the active intensity cost function can be made negative and have only a maximum value. If active intensity amplitude (identical to active intensity cost function when active intensity is positive definite) is considered there may be multiple control source settings that yield a zero intensity result. One of these minima leads to attenuation of the total radiated acoustic power, while most others lead to an increase in total power.

## 5.5 Baffled plate radiation using a vibration control source

### 5.5.1 Theory

#### 5.5.1.1 Introduction

As described in Chapter 2, a great deal of work has been directed towards the use of vibration control inputs to provide active attenuation of the radiated acoustic field (termed active structural acoustic control (ASAC)). The aim of this section is to repeat the baffled panel work

| Sensor Type | Location | far field Attenuation | Relevant Figures | Comments |
|---|---|---|---|---|
| Pressure | $3\lambda/50$ | very good | 5.29 | between 15-20dB attenuation |
| Intensity | $3\lambda/50$ | very bad (increase) | 5.29 | ~5dB increase in sound pressure |
| Pressure | $\lambda/5$ | good | 5.28 | between 5-8dB attenuation |
| Intensity | $\lambda/5$ | good | 5.28 | between 7-9dB attenuation |
| Pressure | $\lambda$ | very good | 5.27 | ~12-14dB attenuation |
| Intensity | $\lambda$ | very good | 5.27 | approximately equal to pressure |

*Table 5.4: Plate acoustic control results summary table.*

using vibration control sources, again focusing on the differences between pressure and active intensity error sensing.

The arrangement is illustrated in Figure 5.35a.

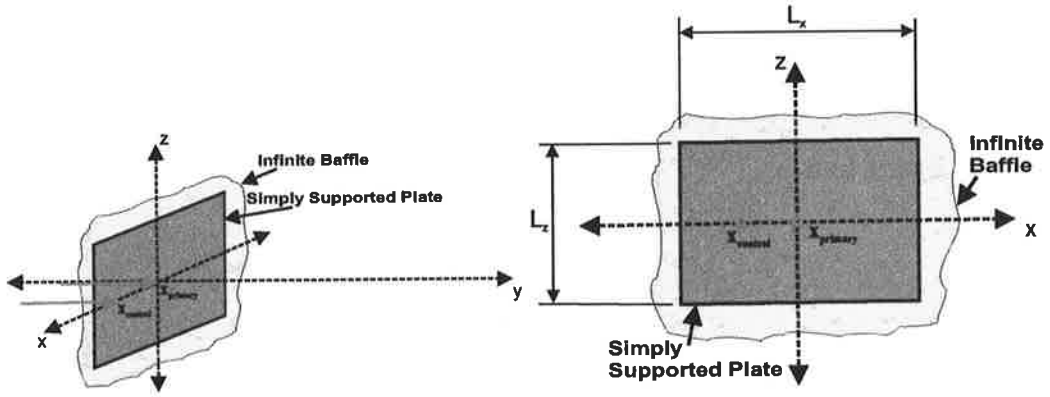


*(a) Rectangular steel plate primary source in an infinite baffle and a single vibration control source.*

*(b) Rectangular steel plate primary source in an infinite baffle with a single vibration control source front view.*

*Figure 5.35: Steel rectangular plate primary source in an infinite baffle and a single vibration control source arrangement.* $\mathbf{x}_{primary} = (0,0)$ *and* $\mathbf{x}_{control} = (-70,0)$ *in millimetres.*

## 5.5.2 Minimising the total sound power

Consider a simply supported rectangular plate primary source excited by a point force excitation at location $\mathbf{x}_{primary} = (x_p, z_p) = (0,0)$ (in mm) and controlled by a point force vibration input at location $\mathbf{x}_{control} = (x_c, z_c) = (-70,0)$ (in mm), whose source strength $f_c$ and hence amplitude and phase can be adjusted. Figure 5.35a represents the arrangement of the baffled plate and vibration sources. Calculating the maximum achievable sound power attenuation possible with a rectangular plate primary source in an infinite baffle of surface velocity $v_p$ controlled by a single vibration control source of source strength $f_c$ involves the modelling of the plate by the Rayleigh's integral to obtain the pressure field and superimposing the Rayleigh integral due to the control source assuming that there is no fluid loading on the plate.

Consider now a simply supported rectangular steel plate with the physical properties described in Section 5.3.2. The plate is excited at 100Hz (near first resonance) with a unitary point force excitation at the centre of the plate given by $\mathbf{x}_{primary} = (0,0)$ (in mm). The coordinate system used to describe the sound radiated from the plate is shown in Figure 5.9.

Referring back to Section 5.4.1, if $N = 100$ modes are again used, then the Rayleigh integral expression, describing the primary source acoustic pressure at a point $\mathbf{r}$ in space, can be rewritten in matrix form as

$$p(\mathbf{r}) = Z_{rad}^T v_p \tag{5.71}$$

where $Z_{rad}$ is the $(N \times 1)$ vector whose ith element is given by

$$Z_{rad,i}(\mathbf{r}) = \frac{j\omega\rho}{2\pi} \int_A \frac{e^{-jkR}}{R} \psi_i(\mathbf{x}) dA \tag{5.72}$$

and $v_p$ is the $(N \times 1)$ vector whose ith element is given by

$$v_{p,i} = \frac{j\omega\psi_i(\mathbf{x}_{primary})}{M_i Z_i} \tag{5.73}$$

where $M_i = \frac{\rho_s h A}{4}$ and $Z_i = \omega_i^2 + 2\zeta\omega\omega_i - \omega^2$ , $\omega_i$ is the ith resonant frequency, $\omega$ is the excitation frequency and $\zeta$ is the damping factor. $A$ is the area of the plate.

Similarly the acoustic pressure at some observation point $\mathbf{r} = (r, \theta, \phi_r)$ in space due to the control force excitation of the plate is given by equation (5.71) as

$$p(r) = Z_{rad}^T v_c f_c \tag{5.74}$$

where $Z_{rad}$ is the $(N \times 1)$ vector whose ith element is given by equation (5.72), $f_c$ is the complex control force and $v_c$ is the $(N \times 1)$ vector whose ith element is given by

$$v_{c,i} = \frac{j\omega\psi_i(\mathbf{x}_{control})}{M_i Z_i} \tag{5.75}$$

The total radiated acoustic power radiated by the plate and monopole combination is given by (Hansen and Snyder (1997)), which is calculated in the far field by

$$W = A_{W_f} |f_c|^2 + f_c^* b_{W_f} + b_{W_f}^* f_c + c_{W_f} \tag{5.76}$$

where

$$A_{W_f} = \int_0^{2\pi} \int_0^{\pi/2} \frac{v_c^H Z_{rad}^H Z_{rad} v_c}{2\rho c} r^2 sin\theta d\theta d\phi_r \tag{5.77}$$

$$b_{W_f} = \int_0^{2\pi} \int_0^{\pi/2} \frac{v_c^H Z_{rad}^H Z_{rad}^T v_p}{2\rho c} r^2 sin\theta d\theta d\phi_r \tag{5.78}$$

$$c_{W_f} = \int_0^{2\pi} \int_0^{\pi/2} \frac{v_p^H Z_{rad}^H Z_{rad} v_p}{2\rho c} r^2 sin\theta d\theta d\phi_r \tag{5.79}$$

where to be in the far field the radial distance $r >> \lambda$. $A_{W_f}$, $b_{W_f}$ and $c_{W_f}$ are functions of $Z_{rad}$ which has no analytic solution and must be numerically integrated. Hence numerical integration must be performed to calculate the acoustic power radiated by the plate and monopole combination.

If $A_{W_f} > 0$ , equation (5.76) has a unique minimum (see Appendix E for a derivation) given by the optimal control source strength $f_{c,opt}$ where

$$f_{c,opt} = -A_{W_f}^{-1} b_{W_f} \tag{5.80}$$

Since $A_{W_f}$ represents the power output from the vibration control source with a unitary control force, acting on its own, it is guaranteed to be positive and hence a unique minimum $f_{c,opt}$ is guaranteed.

Substituting (5.80) into (5.76) gives the minimum power at vibration control source location $\mathbf{x}_{control}$ as

$$W_{min}(\mathbf{x}_{control}) = W_p - b^*_{W_f} A^{-1}_{W_f} b_{W_f} \tag{5.81}$$

where $W_p = c_{W_f}$ is the power due only to the primary source.

Therefore the amount of sound power attenuation achievable by employing a single vibration control source at location $\mathbf{x}_{control}$ to control the sound field of a simply supported rectangular plate in an infinite baffle primary source is given by the ratio of sound power before and after control by

$$\frac{W_p}{W_{min}(\mathbf{x}_{control})} = \frac{W_p}{W_p - b^*_{W_f} A^{-1}_{W_f} b_{W_f}} \tag{5.82}$$

Snyder et al. (1991a), has mapped the optimal vibration control source location on a rectangular plate in an infinite baffle, in terms of power attenuation. For a (3,1) mode, the sound power attenuation achieved by locating a vibration control source anywhere on the plate was plotted. The sound power attenuation was also calculated at control source locations across the surface of the plate as shown in Figure 5.36. Hence at a control source location $\mathbf{x}_{control} = (-70, 0)$ when the primary source location is at $\mathbf{x}_{primary} = (0, 0)$ in millimetres, the maximum achievable power attenuation is approximately 48dB.

The relative sound power level before and after control, when actively controlling the sound power radiated from a simply supported rectangular plate (excited at $\mathbf{x}_{primary} = (0, 0)$ in millimetres) with a single vibration control source located at $\mathbf{x}_{control} = (-70, 0)$ millimetres plot-

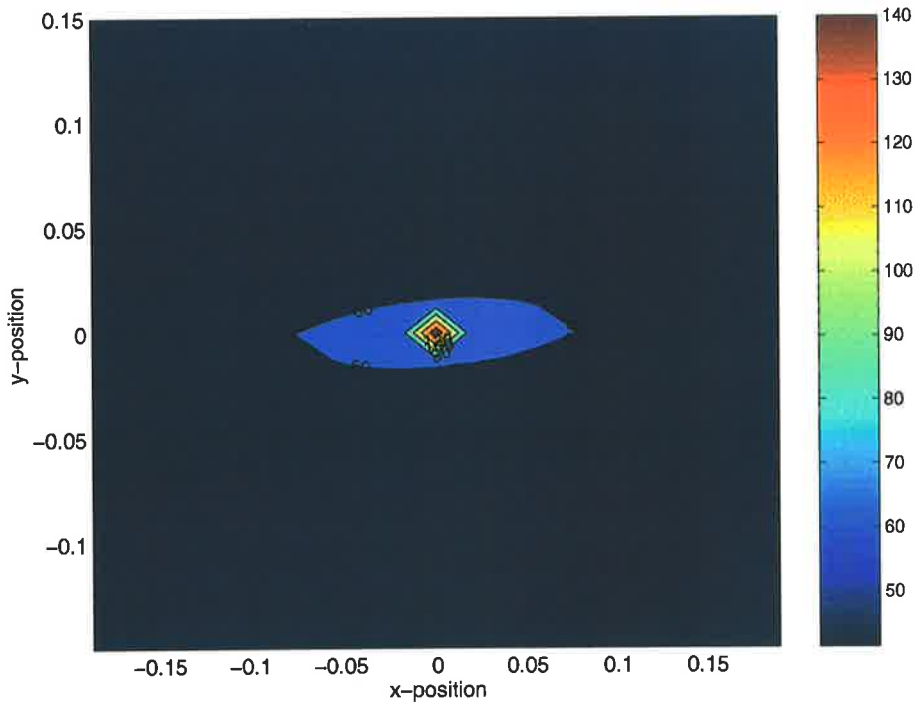


*Figure 5.36: Sound Power attenuation (dB) versus the vibration control source location* $\mathbf{x}_{control}$ *for a primary source location of* $\mathbf{x}_{primary} = (0,0)$ *in millimetres with 100 structural modes included in the model. (N=100).*

ted against frequency is shown in Figure 5.37. Figure 5.38 shows the sound power attenuation plotted against frequency. Observe that large attenuation is predicted below 200Hz, however, above this frequency little sound power attenuation is to be expected.

### 5.5.3 Minimising squared sound pressure

The total acoustic pressure of both sources at an observation point $\mathbf{r}$ in the free field is given by

$$p_{total}(\mathbf{r}) = p_p(\mathbf{r}) + p_c(\mathbf{r}) \tag{5.83}$$

where $p_p(\mathbf{r})$ is the pressure due to the primary source and $p_c(\mathbf{r})$ is the pressure due to the control source at the observation point $\mathbf{r}$ . If we multiply the total acoustic pressure by its

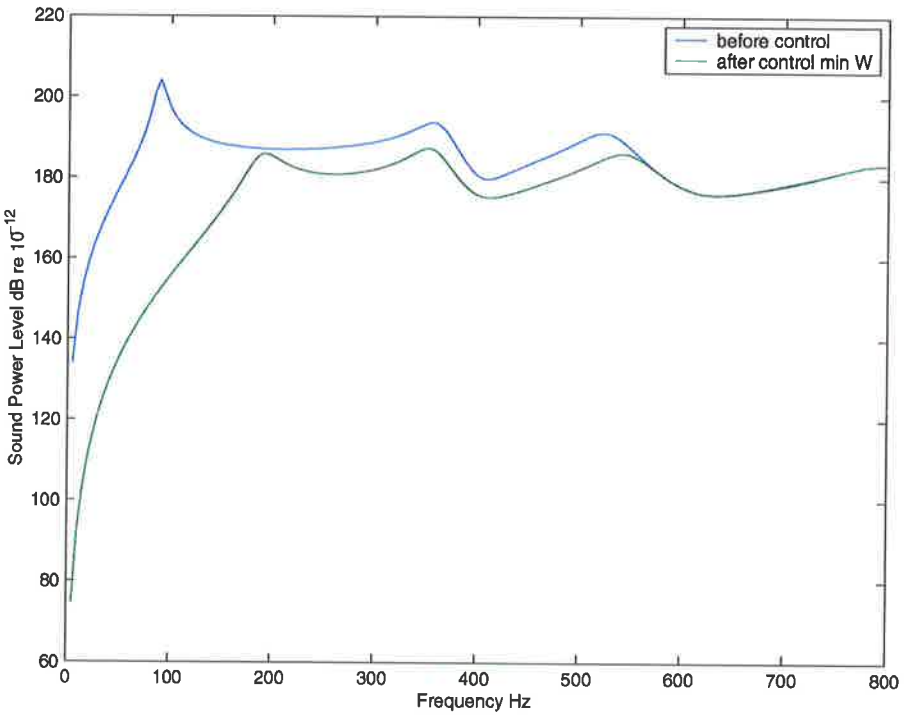


*Figure 5.37: Relative Sound Power Level (dB) before and after control when minimising the sound power with a unitary force applied to the plate centre and a vibration control source is located at* $\mathbf{x}_{control} = (-70, 0)$*mm. (N=100).*

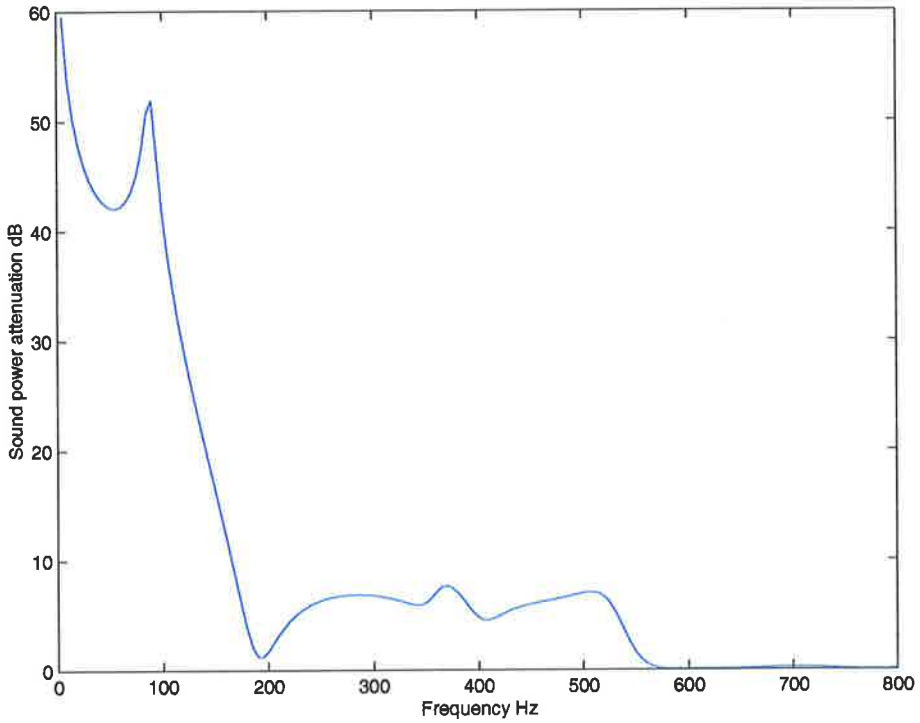


*Figure 5.38: Sound power attenuation (dB) before and after control when minimising the sound power with a unitary force applied to the plate centre and a vibration control source is located at* $\mathbf{x}_{control} = (-70, 0)$*mm. (N=100).*

complex conjugate we get an expression for the squared sound pressure amplitude as

$$|p_{total}(\mathbf{r})|^2 = p^*_{total}(\mathbf{r})p_{total}(\mathbf{r}) \quad (5.84)$$

$$= (p_p(\mathbf{r}) + p_c(\mathbf{r}))^* (p_p(\mathbf{r}) + p_c(\mathbf{r})) \quad (5.85)$$

$$= p^*_p p_p + p^*_c p_p + p^*_p p_c + p^*_c p_c \quad (5.86)$$

where the dependence on $\mathbf{r}$ is assumed and hence for brevity, dropped from the equations. $p_p(\mathbf{r}) = Z^T_{rad}(r_p)v_p$ and $p_c(\mathbf{r}) = Z^T_{rad}(r_c)v_c f_c$, $r_p = |\mathbf{r} - \mathbf{r}_p|$ is the distance from the primary source to the observation point(error sensor location) and similarly $r_c = |\mathbf{r} - \mathbf{r}_c|$ is the distance from the control source to the observation point as described above. Since the primary source and the control source are one and the same, $r_c = r_p$. $Z_{rad}$ describes the acoustic transfer impedance due to the primary and control sources respectively at the observation point and are (Hansen and Snyder (1997)) given by

$$Z_{rad}(r_p) = \begin{bmatrix} \frac{j\omega\rho}{2\pi}\int_A \frac{e^{-jkR}}{R}\psi_1(\mathbf{x})dA \\ \vdots \\ \frac{j\omega\rho}{2\pi}\int_A \frac{e^{-jkR}}{R}\psi_N(\mathbf{x})dA \end{bmatrix} \quad (5.87)$$

$$v_p = \begin{bmatrix} \frac{j\omega\psi_1(\mathbf{x}_{primary})}{M_1 Z_1} \\ \vdots \\ \frac{j\omega\psi_N(\mathbf{x}_{primary})}{M_N Z_N} \end{bmatrix} \quad (5.88)$$

$$v_c = \begin{bmatrix} \frac{j\omega\psi_1(\mathbf{x}_{control})}{M_1 Z_1} \\ \vdots \\ \frac{j\omega\psi_N(\mathbf{x}_{control})}{M_N Z_N} \end{bmatrix} \quad (5.89)$$

The squared pressure amplitude can be re-expressed in a hermitian quadratic form (Hansen

and Snyder (1997)) as

$$|p_{total}|^2 = A_p |f_c|^2 + f_c^* b_p + b_p^* f_c + c_p \tag{5.90}$$

where

$A_p = v_c^* Z_{rad}^H Z_{rad}^T v_c$ and $b_p = v_c^* Z_{rad}^H Z_{rad}^T v_p$ and $c_p = v_p^* Z_{rad}^H Z_{rad}^T v_p$

again since $A_p$ is always greater than zero, there exists a unique minimum (see Appendix E) given by the optimal control source strength $f_{c,opt}$ where

$$f_{c,opt} = -A_p^{-1} b_p \tag{5.91}$$

Therefore to minimise the squared pressure amplitude at a particular location from a single primary monopole source by a single control monopole source (5.91) is substituted into (5.90).

The amount of sound power attenuation when the squared pressure amplitude is minimised at the error sensor location is found by substituting (5.91) into (5.76) giving

$$\frac{W_p}{W_{min}} = \frac{c_{W_f}}{A_{W_f} \left| -A_p^{-1} b_p \right|^2 - (-A_p^{-1} b_p)^* b_{W_f} - b_{W_f}^* (-A_p^{-1} b_p) + c_{W_f}} \tag{5.92}$$

Since the control source is located on the primary source and control is achieved by altering the structural vibrations of the plate, the sound power attenuation achieved is independent of the error sensor location. The relative sound power level before and after control, when actively controlling the sound power radiated from a simply supported rectangular plate (excited at $\mathbf{x}_{primary} = (0,0)$ in millimetres) with a single vibration control source located at $\mathbf{x}_{control} = (-70,0)$ millimetres plotted against frequency is shown in Figure 5.39. Figure 5.40 shows the sound power attenuation plotted against frequency. Observe that large attenuation

is predicted below 200Hz as shown in Figure 5.38, however above this frequency little sound power attenuation is to be expected.

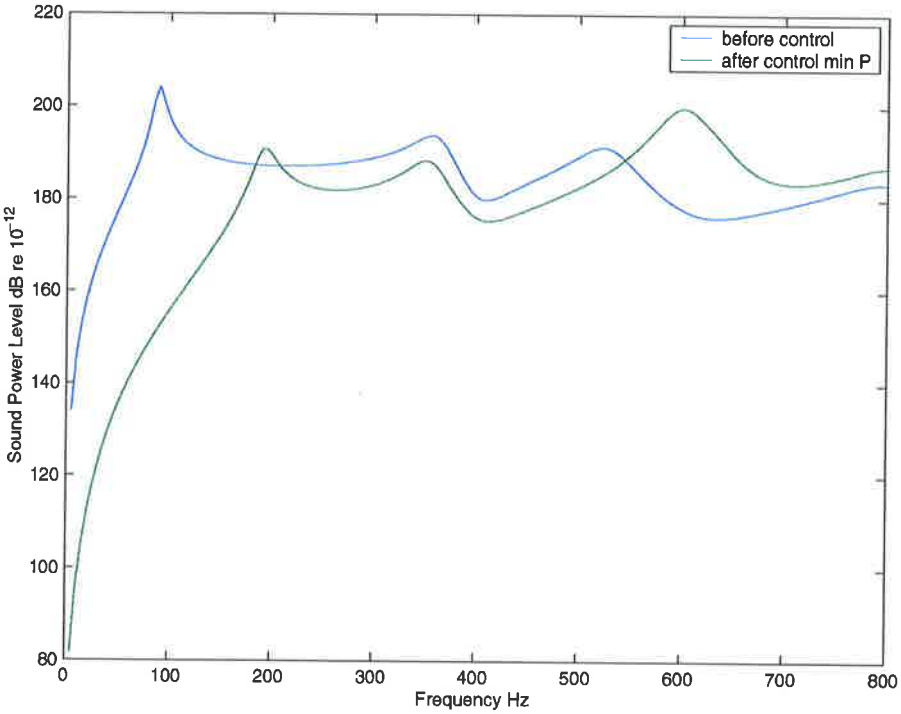


*Figure 5.39: Relative sound power level (dB) before and after control when minimising the squared sound pressure with a unitary force applied to the plate centre and a vibration control source is located at* $\mathbf{x}_{control} = (-70,0)$*mm. (N=100).*

### 5.5.4 Minimising radial active intensity

The total acoustic particle velocity in the direction $\hat{\mathbf{u}}_{total}$ of both sources at an observation point $\mathbf{r}$ in the free field is given by the sum of the particle velocities of the primary and control sources given by

$$\mathbf{u}_{total}(\mathbf{r}) = \mathbf{u}_p(\mathbf{r}) + \mathbf{u}_c(\mathbf{r}) \tag{5.93}$$

which can be rewritten as

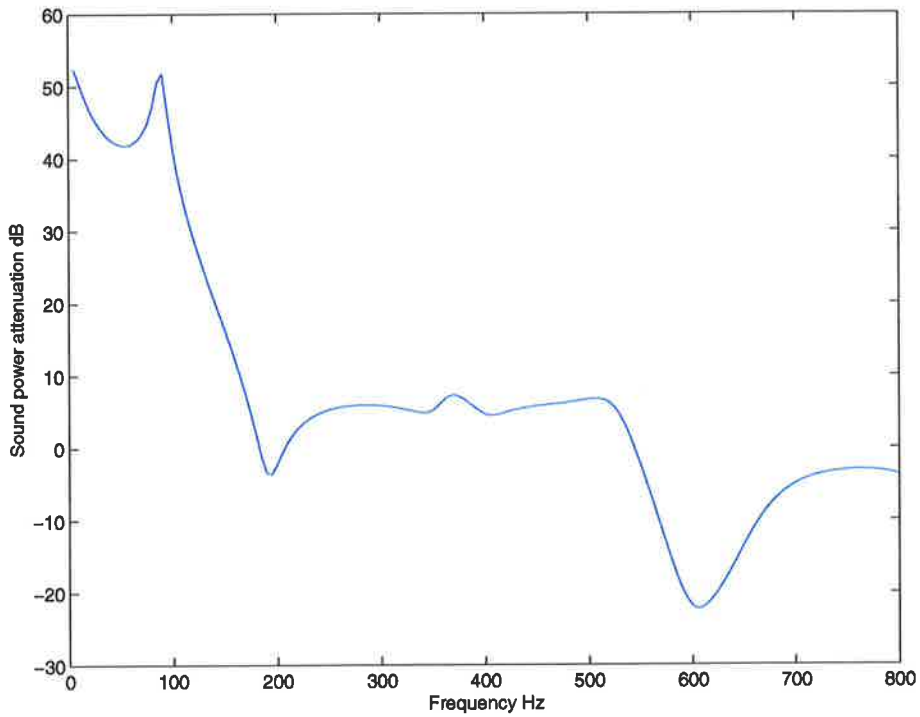


*Figure 5.40: Sound power attenuation (dB) when minimising the squared sound pressure with a unitary force applied to the plate centre and a vibration control source is located at* $\mathbf{x}_{control} = (-70, 0)$*mm. (N=100).*

$$\mathbf{u}_{total}(\mathbf{r}) = u_{total}\hat{\mathbf{u}}_{total} = u_p\hat{\mathbf{u}}_p + u_c\hat{\mathbf{u}}_c \tag{5.94}$$

where the unit vector $\hat{\mathbf{u}}_p$ is in the radial direction relative to the primary source, $\hat{\mathbf{u}}_c$ is in the radial direction relative to the control source. Since the primary and control sources are one and the same, the direction of the particle velocity at an error sensor location $\mathbf{r}$, $\hat{\mathbf{u}}_c = \hat{\mathbf{u}}_p$, simplifying the theoretical development, giving

$$\mathbf{u}_{total}(\mathbf{r}) = u_{total}\hat{\mathbf{u}}_{total} = (u_p + u_c)\hat{\mathbf{u}}_p \tag{5.95}$$

The total active intensity in the direction of $\mathbf{u}_{total}$ is given by

$$\mathbf{I}_{total}(\mathbf{r}) = \frac{1}{2}Re\{p^*_{total}(\mathbf{r})\mathbf{u}_{total}(\mathbf{r})\} \tag{5.96}$$

It is desired to minimise the radial (with respect to the primary source, in the same direction as the vector $\mathbf{u}_p$) active intensity labelled $\mathbf{I}_{radial}$ is identical to $\mathbf{I}_{total}$.

$$\mathbf{I}_{radial}(\mathbf{r}) = proj_{\mathbf{I}_{radial}}\mathbf{I}_{total} = (\mathbf{I}_{radial} \bullet \mathbf{I}_{total})\mathbf{I}_{radial} = \mathbf{I}_{total} \tag{5.97}$$

The notation $proj_{\mathbf{X}}\mathbf{Y}$ is used to denote the orthogonal projection of vector $\mathbf{Y}$ on vector $\mathbf{X}$. The direction of positive intensity is $\hat{\mathbf{u}}_p$. Substituting (5.93) and (5.83) gives

$$\mathbf{I}_{total} = \frac{1}{2}Re\{(p^*_p + p^*_c)(\mathbf{u}_p + \mathbf{u}_c)\} \tag{5.98}$$

$$= \frac{1}{2}Re\{(p^*_p\mathbf{u}_p + p^*_p\mathbf{u}_c + p^*_c\mathbf{u}_p + p^*_c\mathbf{u}_c\} \tag{5.99}$$

where $\mathbf{u}_p = \mathbf{H}_{rad}^T(r_p)v_p$ and $\mathbf{u}_c = \mathbf{H}_{rad}^T(r_p)f_c$, where $r_p$ is defined as before. $\mathbf{H}_{rad}$ describes the acoustic velocity transfer impedance due to the primary and control source respectively at the observation point $\mathbf{r}$ and are given by

$$\mathbf{H}_{rad}(r_p) = -\frac{1}{j\rho\omega}\nabla Z_{rad}(r_p)\hat{\mathbf{u}}_p \tag{5.100}$$

The active intensity in the direction $\hat{\mathbf{u}}_{total}$ can be re-expressed in a hermitian quadratic form as

$$\mathbf{I}_{total} = \mathbf{A}_I |f_c|^2 + f_c^* \mathbf{b}_I + \mathbf{b}_I^* f_c + \mathbf{c}_I \tag{5.101}$$

where $\mathbf{A}_I = \frac{1}{2}Re\left\{v_c^* Z_{rad}^H \mathbf{H}_{rad}^T v_c\right\}$ and $\mathbf{b}_I = \frac{1}{2}Re\left\{v_c \mathbf{H}_{rad}^* Z_{rad}^T v_p\right\}$ and $\mathbf{c}_I = \frac{1}{2}Re\left\{v_p^* Z_{rad}^H \mathbf{H}_{rad}^T v_p\right\}$ where $X^H$ represents the hermitian (conjugate transpose) of $X$.

The radial active intensity can be written as

$$\mathbf{I}_{radial}(\mathbf{r}) = \mathbf{A}_{I_{radial}} |f_c|^2 + f_c^* \mathbf{b}_{I_{radial}} + \mathbf{b}_{I_{radial}}^* f_c + \mathbf{c}_{I_{radial}} \tag{5.102}$$

where $\mathbf{A}_{I_{radial}}$, $\mathbf{b}_{I_{radial}}$ and $\mathbf{c}_{I_{radial}}$ can be written as

$$\mathbf{A}_{I_{radial}} = \frac{1}{2}Re\left\{Z_{rad}^H H_{rad}^T\right\} |v_c|^2 \widehat{\mathbf{u}_p} \tag{5.103}$$

$$\mathbf{b}_{I_{radial}} = \frac{1}{2}Re\left\{v_c H_{rad}^* Z_{rad}^T v_p\right\} \widehat{\mathbf{u}_p} \tag{5.104}$$

$$\mathbf{c}_{I_{radial}} = \frac{1}{2}Re\left\{Z_{rad}^H H_{rad}^T\right\} |v_p|^2 \widehat{\mathbf{u}_p} \tag{5.105}$$

where $H_{rad} = ||\mathbf{H}_{rad}||$ is the complex vector magnitude of the vector describing the velocity transfer impedance. Since $\mathbf{A}_{I_{radial}}$, $\mathbf{b}_{I_{radial}}$ and $\mathbf{c}_{I_{radial}}$ are all in the direction $\widehat{\mathbf{u}_p}$, the vector notation can be discarded, giving

$$A_{I_{radial}} = \frac{1}{2} Re\left\{Z^H_{rad} H^T_{rad}\right\} |v_c|^2 \quad (5.106)$$

$$b_{I_{radial}} = \frac{1}{2} Re\left\{v_c H^*_{rad} Z^T_{rad} v_p\right\} \quad (5.107)$$

$$c_{I_{radial}} = \frac{1}{2} Re\left\{Z^H_{rad} H^T_{rad}\right\} |v_p|^2 \quad (5.108)$$

Appendix E shows that if $A_{I_{radial}} > 0$ a unique minimum exists and the optimal control source strength is given by

$$f_{c,opt} = -A^{-1}_{I_{radial}} b_{I_{radial}} \quad (5.109)$$

Therefore to optimise the radial active intensity at a particular location $\mathbf{r}$ from a rectangular steel plate primary source by a single vibration control source (5.109) is substituted into (5.101).

The amount of sound power attenuation when the active intensity is minimised at the error sensor location is found by substituting (5.109) into (5.76) giving

$$\frac{W_p}{W_{min}} = \frac{c_{W_f}}{A_{W_f}\left|-\frac{1}{2}A^{-1}_{I_{radial}} b_{I_{radial}}\right|^2 - (-\frac{1}{2}A^{-1}_{I_{radial}} b_{I_{radial}})^* b_{W_f} - b^*_{W_f}(-\frac{1}{2}A^{-1}_{I_{radial}} b_{I_{radial}}) + c_{W_f}} \quad (5.110)$$

The relative sound power level before and after control, when actively controlling the sound power radiated from a simply supported rectangular plate (excited at $\mathbf{x}_{primary} = (0,0)$ in millimetres) with a single vibration control source located at $\mathbf{x}_{control} = (-70,0)$ millimetres plotted against frequency is shown in Figure 5.41. Figure 5.42 shows the sound power attenuation plotted against frequency. Observe that large attenuation is predicted below 200Hz as shown in Figure 5.38, however above this frequency little sound power attenuation is to be expected. Is should also be noted from Figure 5.42 that at frequencies above 200Hz active intensity er-

ror sensing is predicted to produce slightly better sound power attenuation than pressure error sensors.

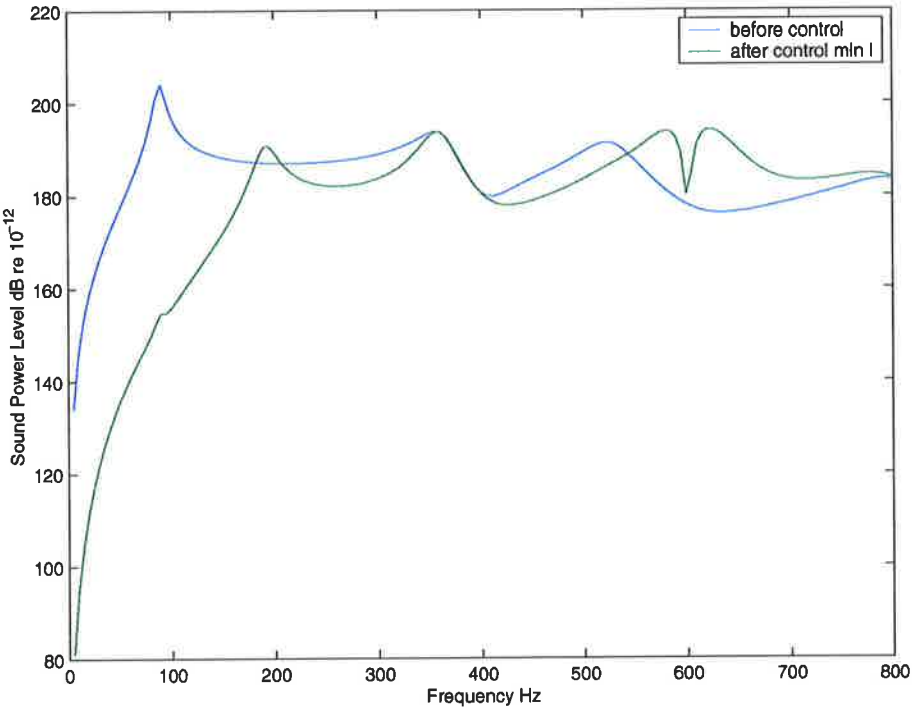


*Figure 5.41: Relative sound power level (dB) before and after control when minimising the radial active intensity with a unitary force applied to the plate centre and a vibration control source is located at* $\mathbf{x}_{control} = (-70, 0)mm$. *(N=100).*

## 5.5.5 Results

### 5.5.5.1 Far field pressure distribution

In order to assess the power attenuation of minimising an active intensity cost function over that which is obtained by minimising the squared pressure the "far field" sound pressure was measured with a microphone attached to a boom and turntable through an arc 180°, before and after control is applied. Figure 5.43 shows the experimental setup. The primary source used was the simply supported rectangular steel plate embedded in a baffle (as described previously) and excited at the plate centre by a point force electrodynamic shaker and a vibration control

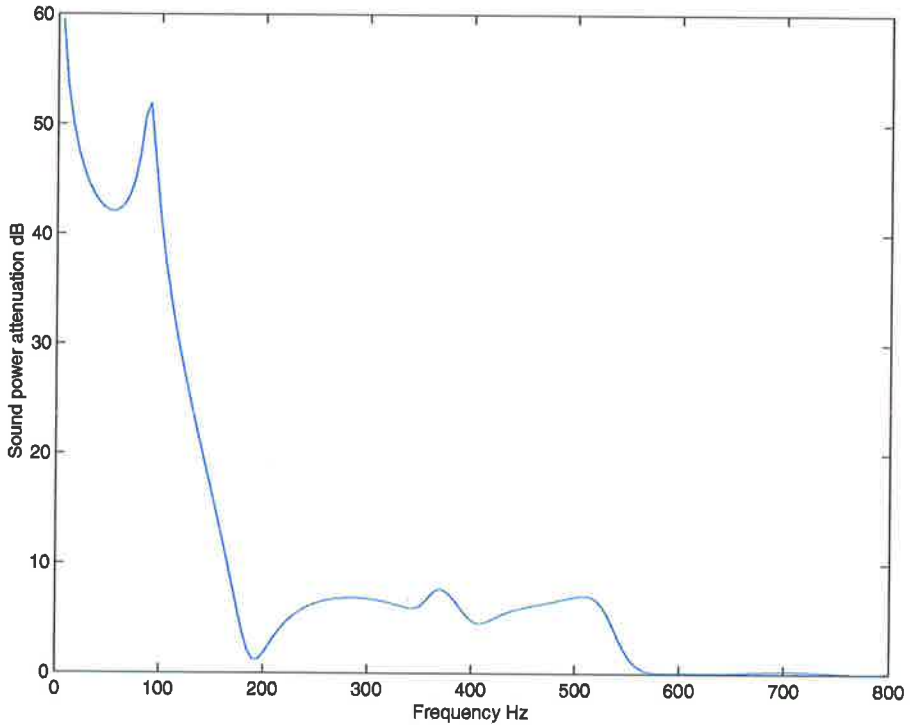


*Figure 5.42: Sound power attenuation (dB) when minimising the radial active intensity with a unitary force applied to the plate centre and a vibration control source is located at* $\mathbf{x}_{control} = (-70, 0)$*mm. (N=100).*

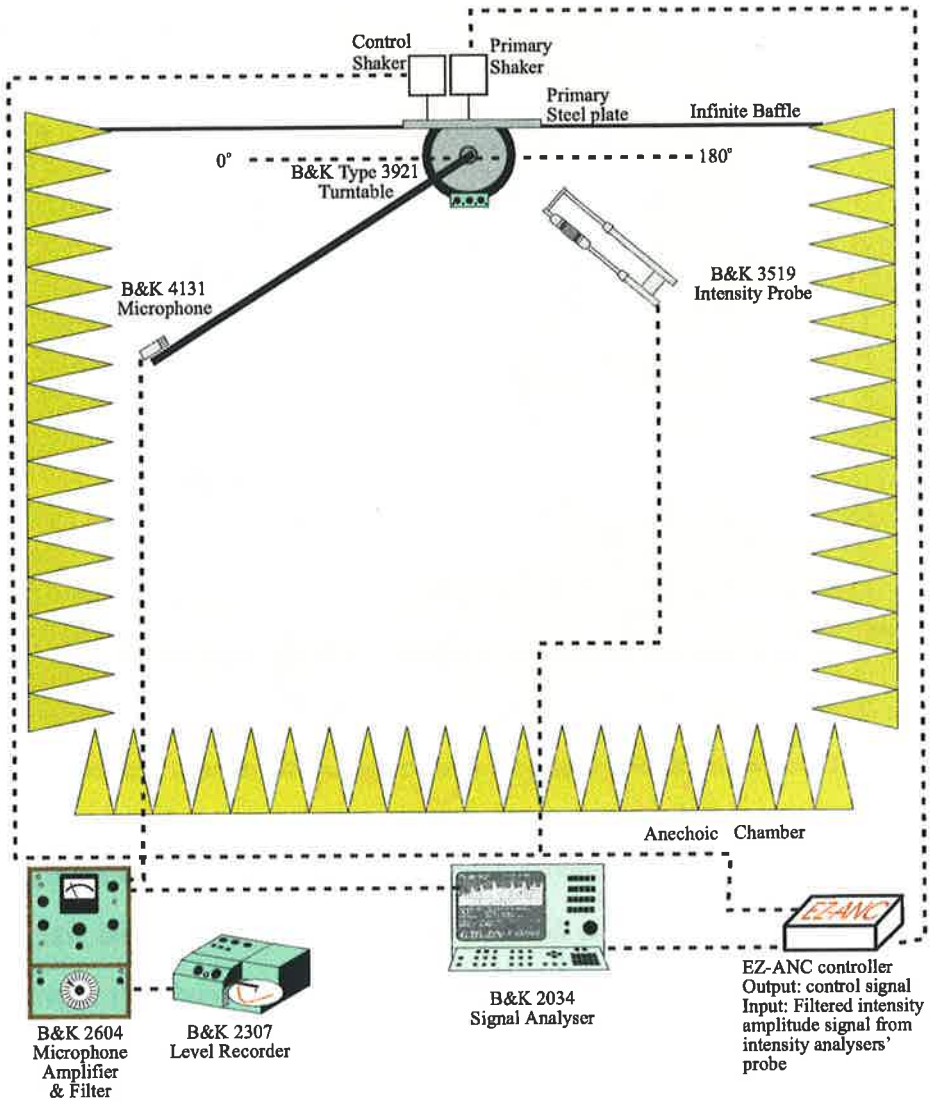


*Figure 5.43: Experimental setup for measuring the far field pressure distribution before and after active control is applied to minimise a squared pressure and active intensity amplitude cost function.*

source (point force electrodynamic shaker) located at $\mathbf{x}_{control} = (-70, 0)$mm shown in Figure 5.44.

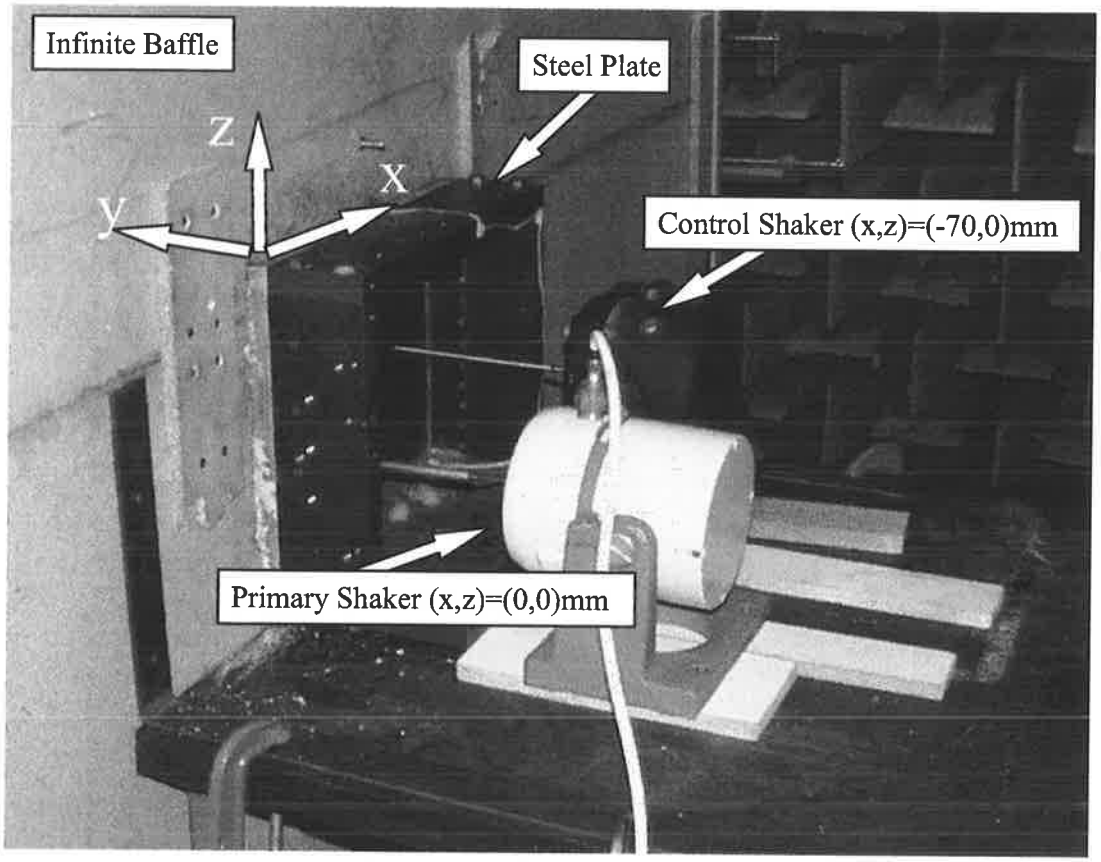


*Figure 5.44: Location of the electrodynamic shakers used as the primary and control sources.*

A B&K Type 4131 condenser microphone connected to a B&K Type 2604 Microphone Amplifier which is 1/3 octave band pass filtered in the 100Hz 1/3 octave band was again used to measure the "far field" sound pressure. The B&K Type 4131 condenser microphone was attached to a microphone boom which was located just in front of the baffled primary source and extended 1.8 metres out (see Figure 5.5). The control system employed is identical to that used for the baffled monopole experiments in Chapter 4 and baffled plate and monopole source in Section 5.4.7.

Figure 5.45 displays the location of the error sensors tested in these experiments. Illustrated in Figure 5.46 is the result of far field error sensing with either an acoustic pressure error sensor or an active intensity error sensor. As expected, the outcome when using either a pressure or

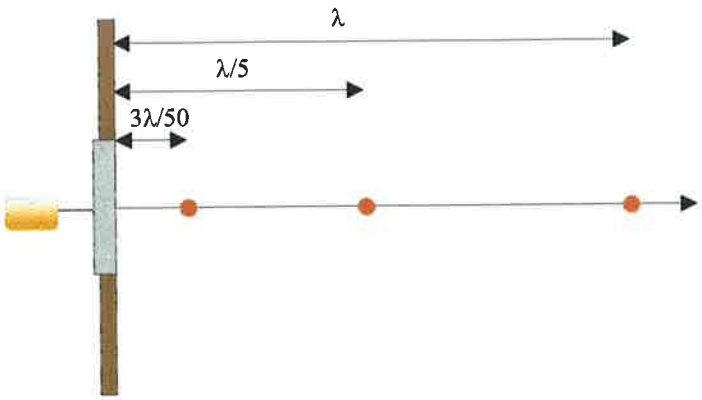


*Figure 5.45: The three sensor locations considered. The red dots indicate the error sensor locations.*

intensity error signal is similar. The level of attenuation achieved was approximately 21dB. Observe that when a 1% error in amplitude and $1^o$ error in phase of the control signal is included, the theoretical attenuation predicted is approximately 32dB. With the accuracy of the control system (see Figure 2.6) it was not possible to achieve more than approximately 20dB of attenuation.

The normalised modal amplitudes before and after control are shown in Figure 5.47 for the first 10 structural modes. The mechanism of control is clearly modal control (Snyder et al. (1991a)) as opposed to modal rearrangement. The dominant mode is the (1,1) and this has been attenuated by more than 15dB. It is of interest to note that the particular cost function employed appears to be irrelevant to the resulting modal amplitudes after control.

Figure 5.48 shows the result of minimising the pressure and active intensity amplitude at a position closer to the primary and source. As expected, the outcome when using either a pressure or intensity error signal is similar. The level of attenuation achieved was approximately 21dB. Observe that when a 1% error in amplitude and $1^o$ error in phase of the control signal is included, the theoretical attenuation predicted is approximately 32dB. With the accuracy of the control system (see Figure 2.6) it was not possible to achieve more than approximately 20dB of attenuation.

The normalised modal amplitudes before and after control are shown in Figure 5.49 for the

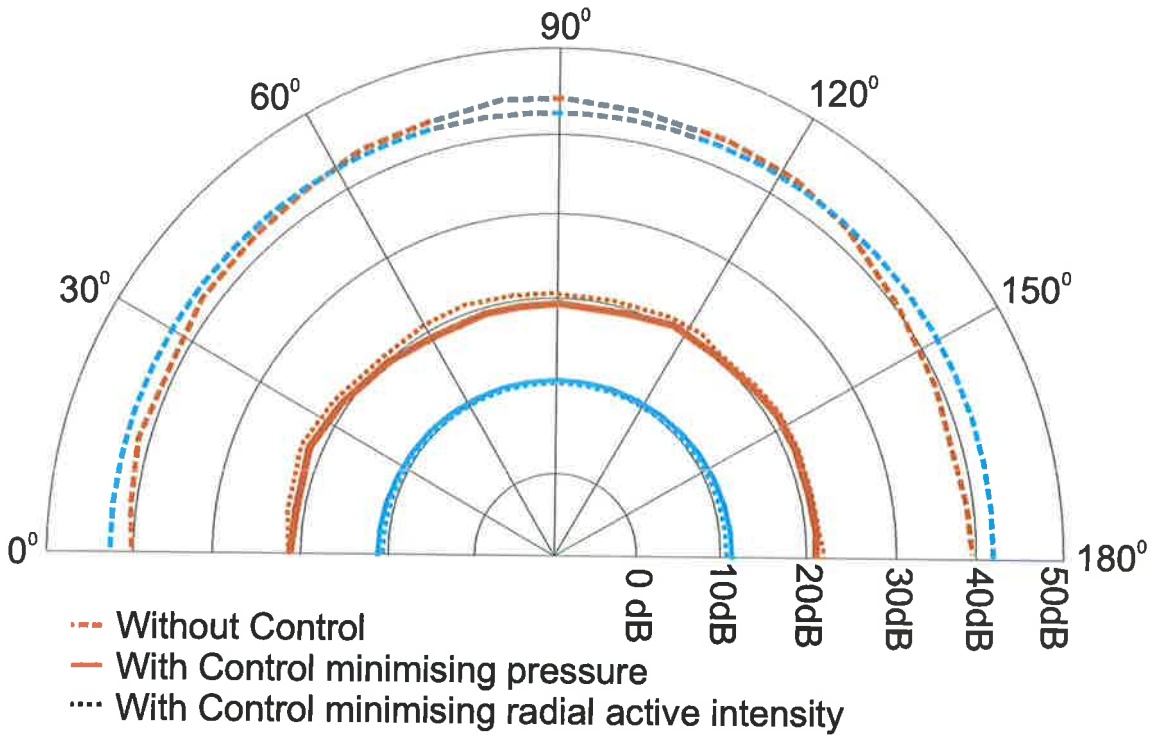


*Figure 5.46: Far field pressure before and after control when employing a single acoustic pressure or radial active intensity error sensor at $\lambda$ from the primary source on the y-axis to control a 100Hz tone from a simply supported rectangular plate primary source with a single vibration control source at location $\mathbf{x}_{control} = (-70, 0)mm$. The red lines indicate the experimental measurements. The blue lines indicate the theoretically predicted results with a 1% error in amplitude and 1° error in phase of the control signal.*

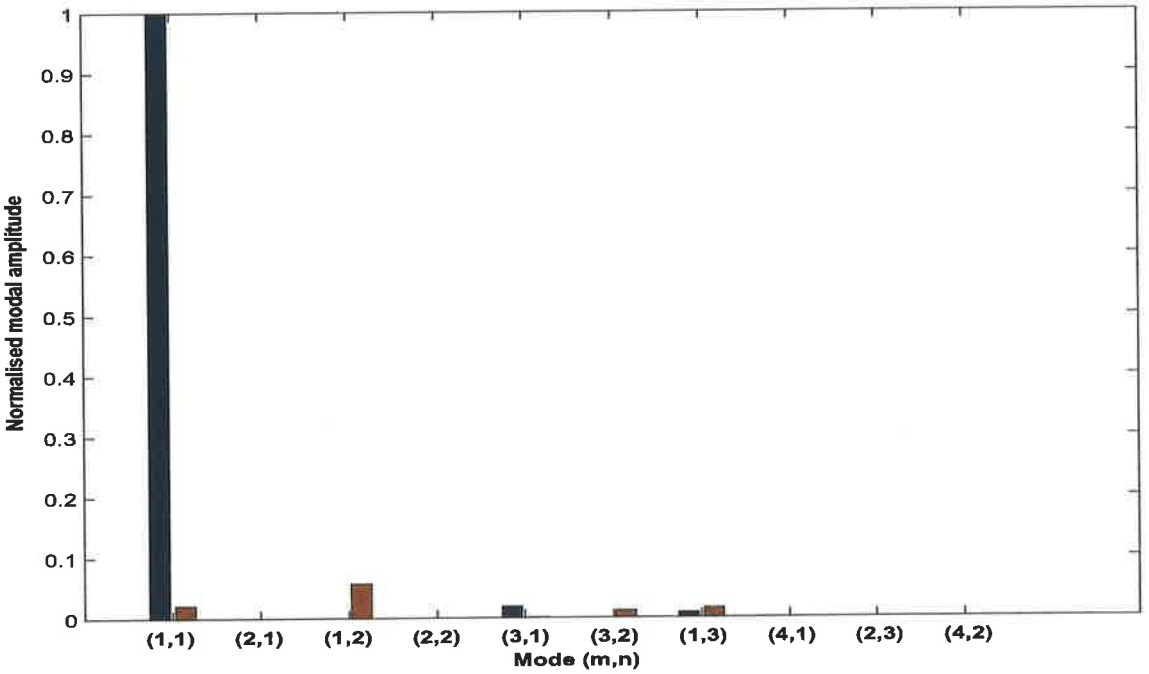


*(a) Minimising the squared pressure*

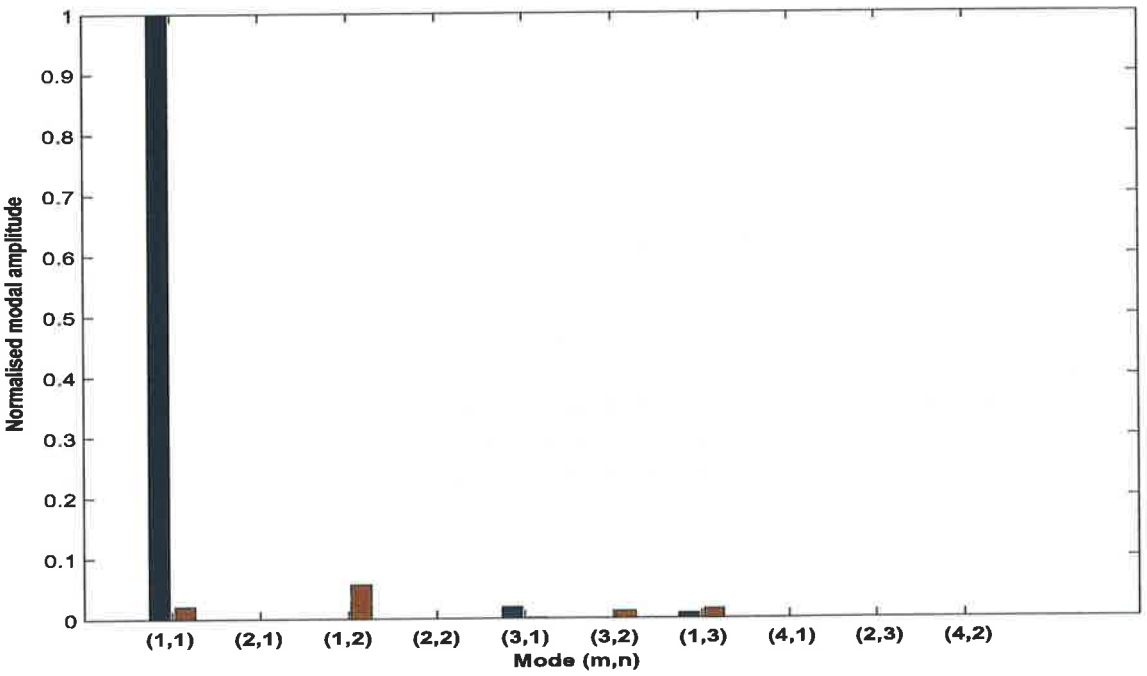


*(b) Minimising radial active intensity*

*Figure 5.47: Normalised modal amplitude when employing a single acoustic pressure or radial active intensity error sensor at $\lambda$ from the primary source on the y-axis to control a 100Hz tone from a simply supported rectangular plate primary source with a single vibration control source at location $\mathbf{x}_{control} = (-70, 0)$mm. The blue indicates before control and the red indicates after control where the computations included a 1% error in amplitude and $1^{o}$ error in phase of the control signal.*

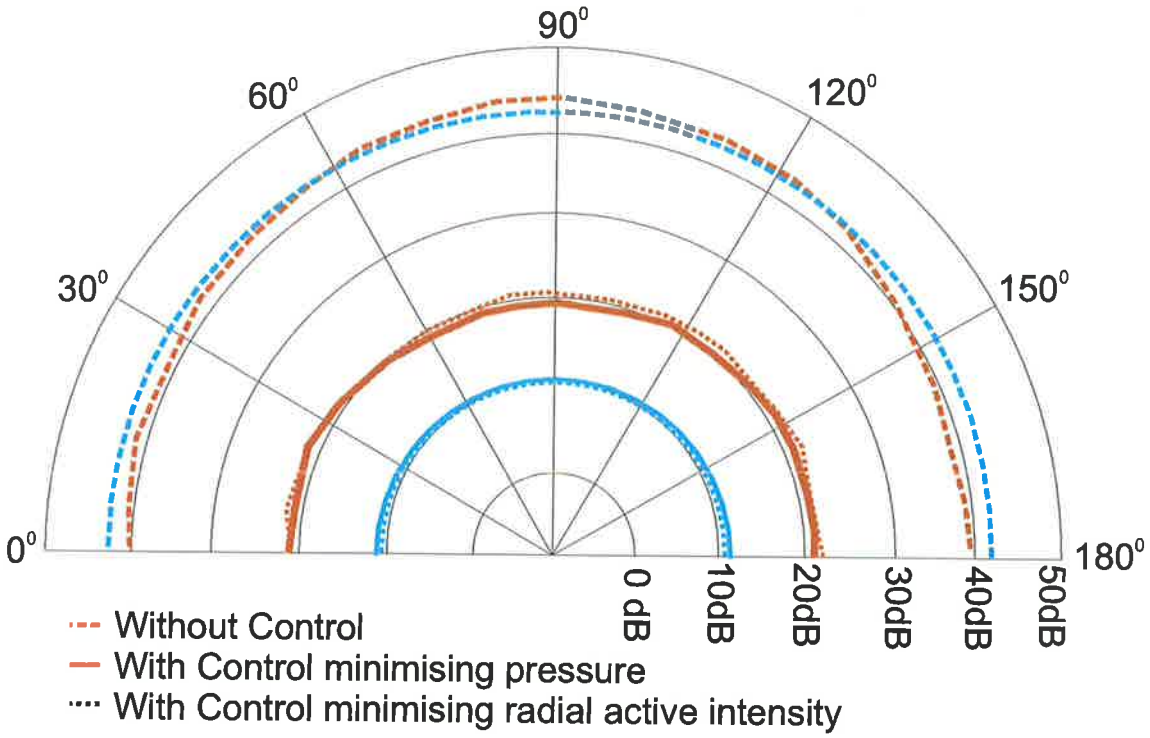


*Figure 5.48: Far field pressure before and after control when employing a single acoustic pressure or radial active intensity error sensor at $\lambda/5$ from the primary source on the y-axis to control a 100Hz tone from a simply supported rectangular plate primary source with a single vibration control source at location $\mathbf{x}_{control} = (-70, 0)mm$. The red lines indicate the experimental measurements. The blue lines indicate the theoretically predicted results with a 1% error in amplitude and 1° error in phase of the control signal.*

first 10 structural modes. The mechanism of control is clearly modal control (Snyder et al. (1991a)) as opposed to modal rearrangement. The dominant mode is the (1,1) and this has been attenuated by more than 15dB.

Illustrated in Figure 5.50 is the result of sensing the pressure and active intensity amplitude in the near field. Again, as expected, the outcome when using either a pressure or intensity error signal is similar. The level of attenuation achieved was approximately 21dB. Observe that when a 1% error in amplitude and $1^o$ error in phase of the control signal is included, the theoretical attenuation predicted is approximately 32dB. With the accuracy of the control system (see Figure 2.6) it was not possible to achieve more than approximately 20dB of attenuation.

The normalised modal amplitudes before and after control are shown in Figure 5.49 for the first 10 structural modes. The mechanism of control is clearly modal control (Snyder et al. (1991a)) as opposed to modal rearrangement. The dominant mode is the (1,1) and this has been attenuated by more than 15dB. It is also interesting to note that the error sensor location does not appear to influence the modal amplitudes after control.

### 5.5.6 Conclusion

The performance of active control of free field tonal sound radiation from a simply supported rectangular plate in an infinite baffle, via introduction of a point vibration control source using near or far field error sensing does not appear to be improved with the use of active intensity error sensors in place of pressure error sensors (see Table 5.5). The control mechanism is clearly modal control in the case considered (see Table 5.6), with the (1,1) mode being attenuated by more than 15dB. As opposed to active acoustic control of tonal plate radiation, there is no near field poor performance of active intensity sensors when employing vibration control sources. Therefore it would appear that active intensity error sensors must not be located between the plate and control source (in the region shown in Figure 5.14).

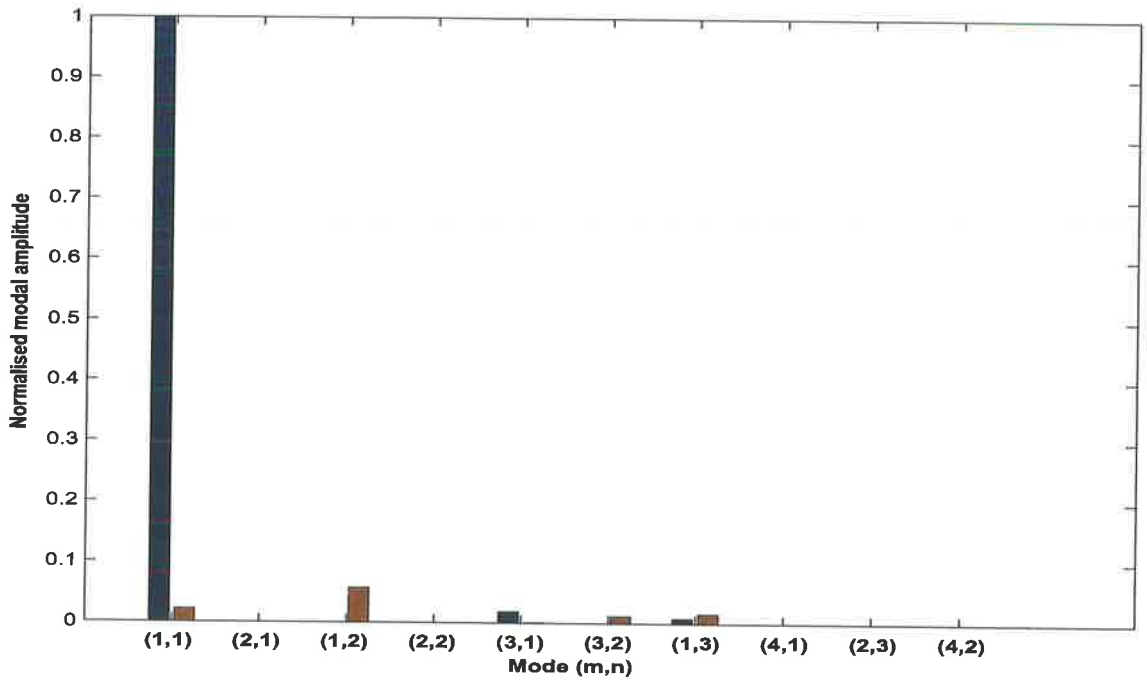


*(a) Minimising the squared pressure*

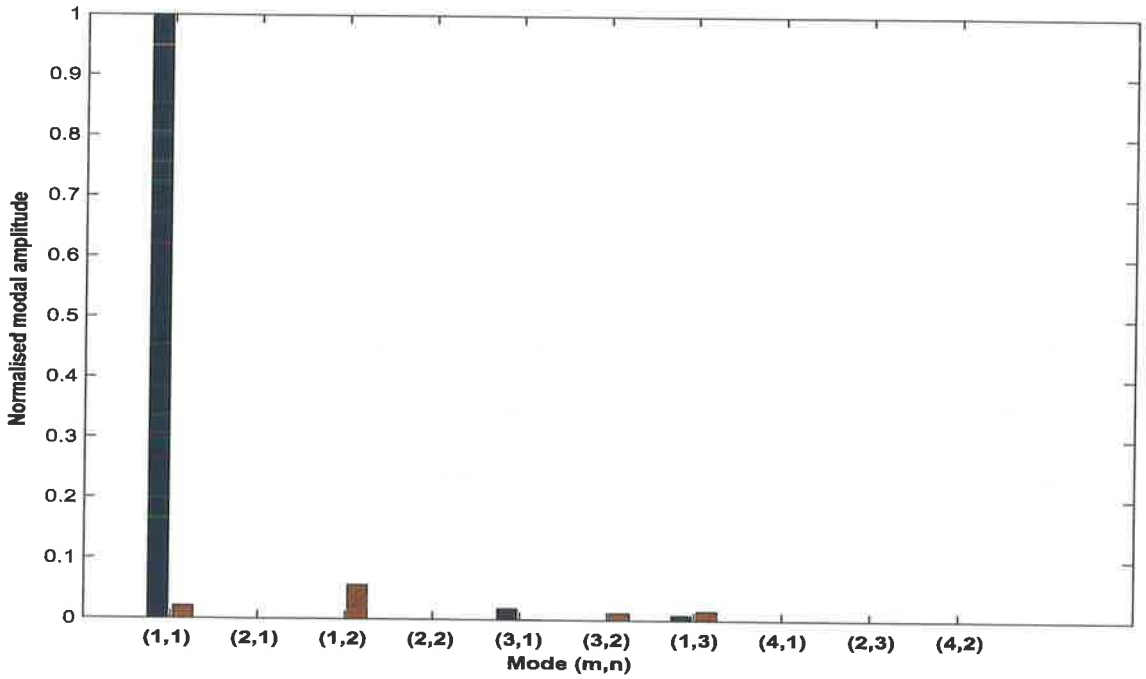


*(b) Minimising radial active intensity*

*Figure 5.49: Normalised modal amplitude when employing a single acoustic pressure or radial active intensity error sensor at $\lambda/5$ from the primary source on the y-axis to control a 100Hz tone from a simply supported rectangular plate primary source with a single vibration control source at location $\mathbf{x}_{control} = (-70, 0)$mm. The blue indicates before control and the red indicates after control where the computations included a 1% error in amplitude and $1^{o}$ error in phase of the control signal.*

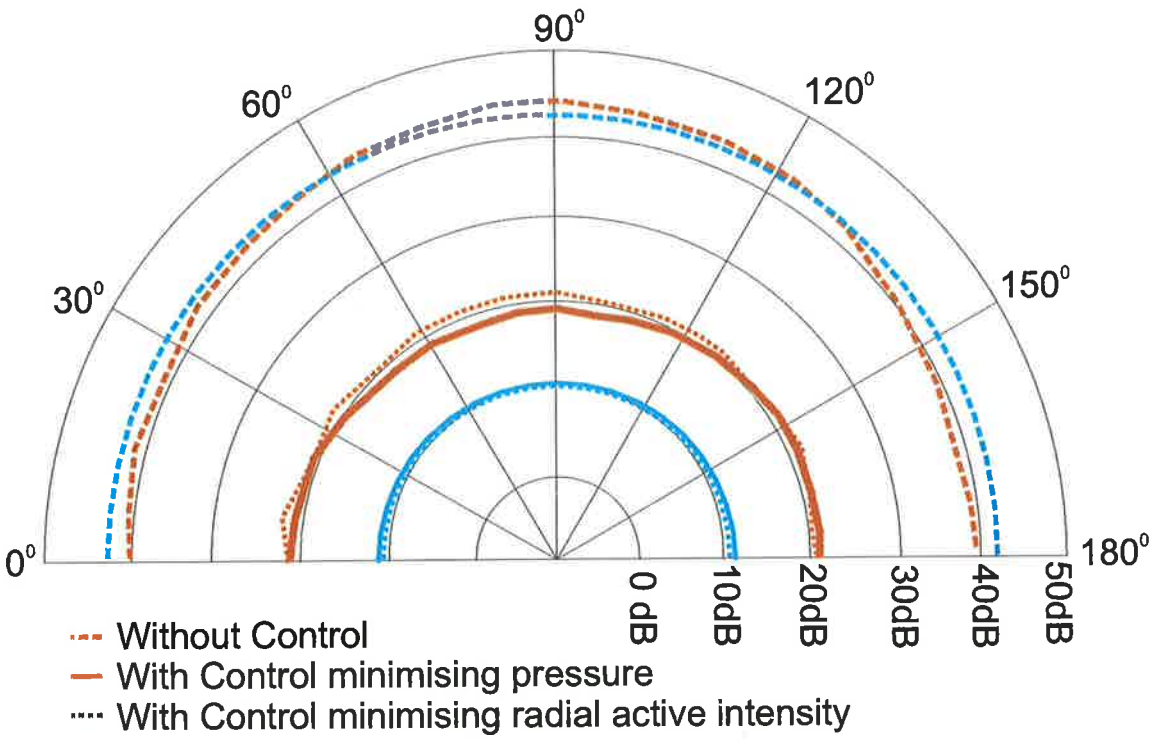


*Figure 5.50: Far field pressure before and after control when employing a single acoustic pressure or radial active intensity error sensor located $3\lambda/50$ from the primary source on the y-axis to control a 100Hz tone from a simply supported rectangular plate primary source with a single vibration control source at location $\mathbf{x}_{control} = (-70,0)$mm. The red lines indicate the experimental measurements. The blue lines indicate the theoretically predicted results with a 1% error in amplitude and 1° error in phase of the control signal.*

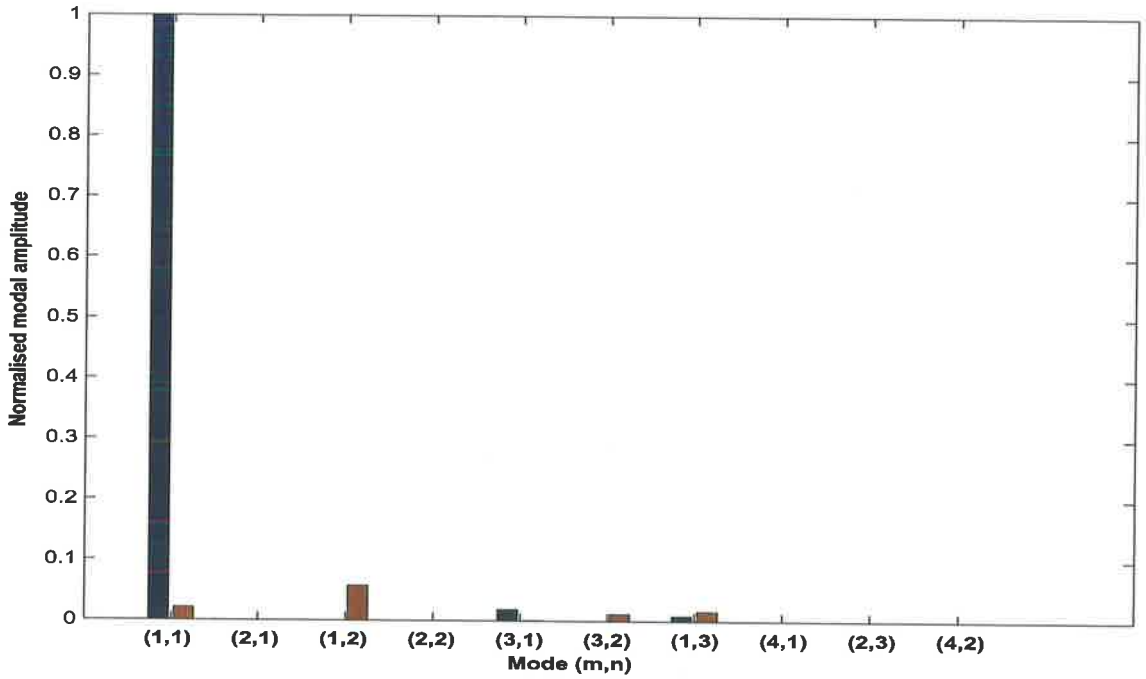


*(a) Minimising the squared pressure*

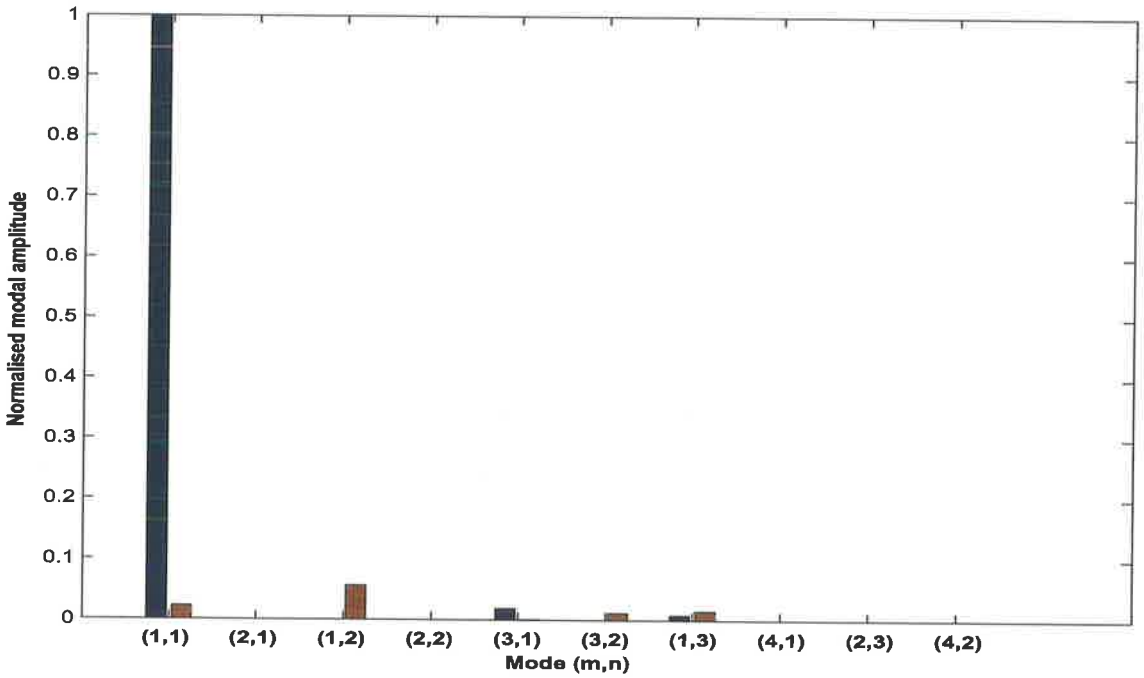


*(b) Minimising radial active intensity*

*Figure 5.51: Normalised modal amplitude when employing a single acoustic pressure or radial active intensity error sensor at $3\lambda/50$ from the primary source on the y-axis to control a 100Hz tone from a simply supported rectangular plate primary source with a single vibration control source at location $\mathbf{x}_{control} = (-70,0)$mm. The blue indicates before control and the red indicates after control where the computations included a 1% error in amplitude and $1^{o}$ error in phase of the control signal.*

| Sensor Type | Location | far field Attenuation | Relevant Figures | Comments |
|---|---|---|---|---|
| Pressure | $3\lambda/50$ | very good | 5.50 | ~21dB attenuation, less than theory predicted |
| Intensity | $3\lambda/50$ | very good | 5.50 | ~21dB attenuation, less than theory predicted |
| Pressure | $\lambda/5$ | very good | 5.48 | ~21dB attenuation, less than theory predicted |
| Intensity | $\lambda/5$ | very good | 5.48 | ~21dB attenuation, less than theory predicted |
| Pressure | $\lambda$ | very good | 5.46 | ~21dB attenuation, less than theory predicted |
| Intensity | $\lambda$ | very good | 5.46 | ~21dB attenuation, less than theory predicted |

*Table 5.5: Plate vibration control results summary table.*

| Sensor Type | Location | Modal amplitude attenuation | Relevant Figures | Comments |
|---|---|---|---|---|
| Pressure | $3\lambda/50$ | (1,1) $\downarrow$ by 15dB | 5.51 | identical to intensity |
| Intensity | $3\lambda/50$ | (1,1) $\downarrow$ by 15dB | 5.51 | identical to pressure |
| Pressure | $\lambda/5$ | (1,1) $\downarrow$ by 15dB | 5.49 | identical to intensity |
| Intensity | $\lambda/5$ | (1,1) $\downarrow$ by 15dB | 5.49 | identical to pressure |
| Pressure | $\lambda$ | (1,1) $\downarrow$ by 15dB | 5.47 | identical to intensity |
| Intensity | $\lambda$ | (1,1) $\downarrow$ by 15dB | 5.47 | identical to pressure |

*Table 5.6: Plate modal amplitude results summary table.*

# Chapter 6

# Small transformer

## 6.1 Introduction


*Figure 6.1: Thesis Flow chart*

Chapter 5 considered the case of a simply supported rectangular steel plate controlled by a single monopole control source and single point vibration control source. Chapter 4 considered the case of active control a monopole source in an infinite baffle by a single monopole control source. Chapter 3 reconsidered the case of active control a monopole source by a single monopole control source as has already been done by (Qiu et al. (1998)). Chapter 6 analyses the practical case of small electrical transformer on a hard floor in an anechoic chamber. The previously investigated systems and in particular the baffled monopole and baffled plate cases, are to a good approximation planar radiation models of the sound radiation of one side of a transformer tank. However, as noted early in this thesis, there is a breadth of laboratory and fundamental results, but relatively few practical studies. It is important to test that the previous fundamental results in Chapters 3 - 5 translate onto a practical example.

This chapter will apply the active intensity error sensing technique to three sensor locations of the most interest and test the techniques efficiency. Finally Chapter 7 draws conclusions and discusses possible future work.

## 6.2 Transformer noise

One of the most common practical targets for the active control of free field sound has been electrical transformer noise (Conover (1956), Hesselmann (1978), Ross (1978), Angevine (1981), Brungardt et al. (1997), ADTP (1997), Qiu et al. (1998) and Li (2000)). The annoyance and the need for transformer noise attenuation was possibly first recognised in the 50's by Lambert (1951) and 60's by Schultz and Ringlee (1960) and later by Gordon (1979) and Schuller (1982). Transformer noise is tonal, with a fundamental frequency equal to twice the line frequency (50Hz line frequency equals 100Hz fundamental in Europe/Australia, 60Hz line frequency equals 120Hz fundamental in the USA), plus harmonics. An in-service 275kV transformer located in a remote location (Cherry Gardens) in the Adelaide hills, shown in Figure 6.2, demonstrates the characteristic noise problems, described above. The noise spectrum of the Cherry Gardens transformer is shown in Figure 6.3. As described, the noise is dominated by tonal components. The fundamental frequency is 100Hz and the harmonics of 200Hz and 300Hz are also large contributors.

The spatial characteristics of transformer noise have been investigated by a number of authors, Reiplinger (1978), Reiplinger et al. (1978), Usry et al. (1980) Foster and Reiplinger (1981), Schuller (1982), Champoux et al. (1988), Gosselin et al. (1992), Laroche et al. (1992), Sakuta et al. (1992), Savard (1992), Angevine (1994), Teplitzky (1995) , Hu (1995), Ming et al. (1999). In general, the sound field is spatially very complicated as demonstrated in Figure 6.4.

The internal construction of the transformer contains an iron core and windings. The cause of the tonal noise is periodic magnetostrictive forces within the core. The vibration in the

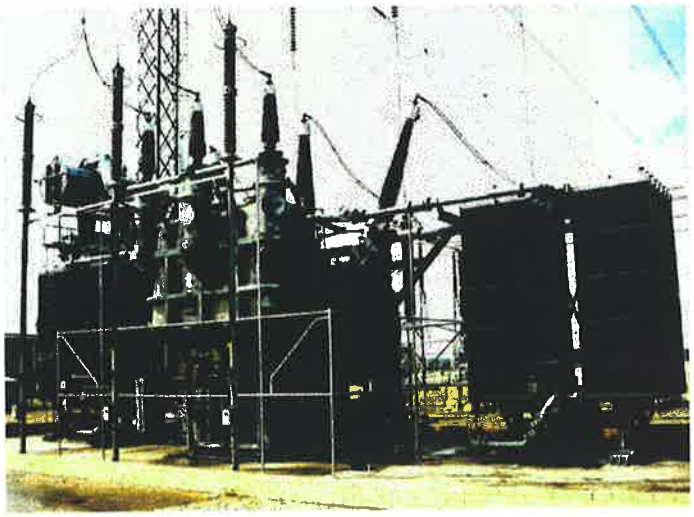

*Figure 6.2: An example of a large-scale transformer rated at 275kV, located in the remote suburb of Cherry Gardens in the Adelaide Hills, approximately 20 kilometres from the centre of Adelaide, South Australia.*

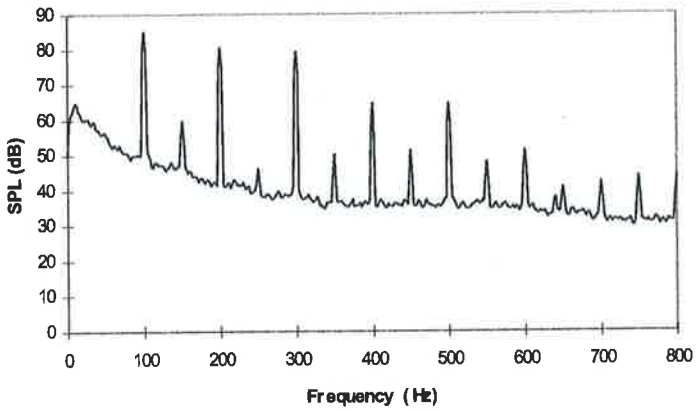


*Figure 6.3: Sound pressure level spectrum of the 275kV transformer at Cherry Gardens. After (Hansen et al. (1997)).*

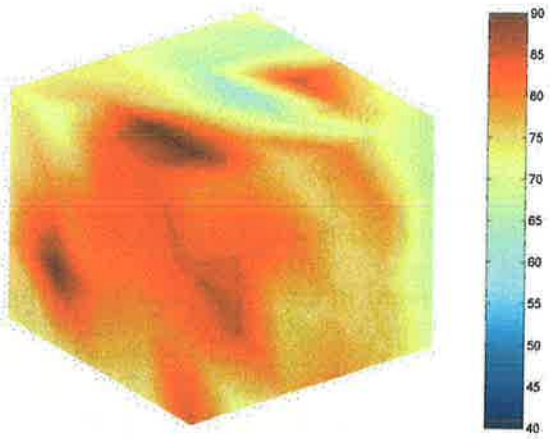


*Figure 6.4: Sound pressure level (dB) measured at 100Hz at a distance of 1 metre from the 275kV transformer at Cherry Gardens. After (Li (2000)).*

core is transmitted through the transformer cooling fluid and through the transformer tank casing, where it radiates sound predominantly at the fundamental and its harmonics. The spatial distribution of the sound field is therefore complicated by the structural design of the transformer.

The transformer noise problem is predominantly a free field problem. However, in some European countries, utility transformers are enclosed in a custom building as described by Berge et al. (1987, 1988). In such cases passive noise control techniques can be more easily applied, because the barrier is already present. They still need to include ventilation openings in the enclosure walls, as described by Berge et al. (1987, 1988), which in their research was the location of control sources. In North America and Australia most utility transformers are not enclosed. They are installed in substations, and most problems arise from residential development around or near the substation (Hansen et al. (1997)). Since the design life of a large transformer can be of the order of 50 years, in situ noise control is most common. Active noise control appears well suited as an add-on fix. Control sources, error sensors and control electronics can be easily located around the primary disturbance, and a solution to low frequency noise control can be potentially achieved.

Intensive experimental work on active transformer noise control began in the 1970s. Work by Hesselmann (1976) and Hesselmann (1978) tested a transformer in an anechoic chamber. Hesselmann performed active tonal noise control using 2 control sources positioned to form a longitudinal quadrupole (which is a poor radiator at low frequencies) with the transformer tank. The control sources were manually tuned to be directly out of phase with the primary tone. Sound pressure was measured in a straight line up to 8 metres from the transformer tank. It was noted that in the near field the sound pressure actually increases over that of the primary tone only. However, further away the sound pressure drops by up to 20dB below that of the primary tone only (see Figure 6.5). As is to be expected, no automatic control system was used; everything was done manually. Ross (1978), as with Conover (1956) earlier, positioned control sources close to two in situ transformers near office buildings, and by manually adjusting the gain and phase of the signal from far field pressure error sensors achieved appreciable reductions in the sound pressure levels at particular frequencies inside one of the buildings. Work by Angevine (1981) applied active control to a model transformer in an anechoic chamber with multiple acoustic "tripole" control sources and a single error microphone for each tripole behind the tripole. Each tripole was arranged in a cardioidal radiation pattern. Angevine found that increasing the number of control sources from 10 to 30 increased the sound pressure attenuation from 9dB to 19dB. Berge et al. (1987) and Berge et al. (1988) reported on active control of noise from an in situ transformer building (described previously). Control speakers were located on the transformer building (near ventilation holes) and located on the transformer. Error sensors were positioned in the far field. This work appears to be the first attempt to employ a real control system which automatically updated the control speaker output by minimising an error microphone signal, taking from 12 seconds to 4 minutes to do so. The system was tested under varying environmental conditions. The results were mixed, as noted by Conover (1956) the performance varied under differing environmental conditions. The performance was worse when 12 second updates were used over the longer update period of 4 minutes. Angevine (1990, 1992, 1993, 1994, 1995) have reported some success achieving significant noise reductions of between 15 and 20dB over an arc of up to $40^o$.

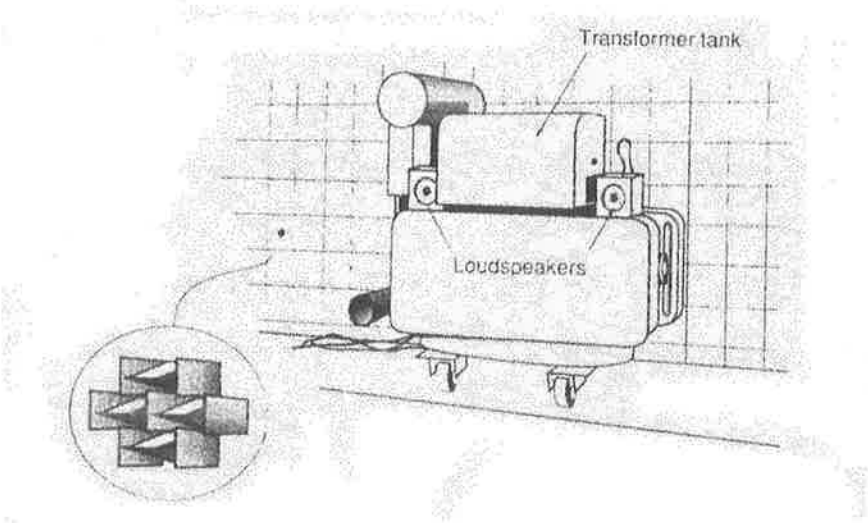


*(a) Transformer tank tested by Hesselmann*

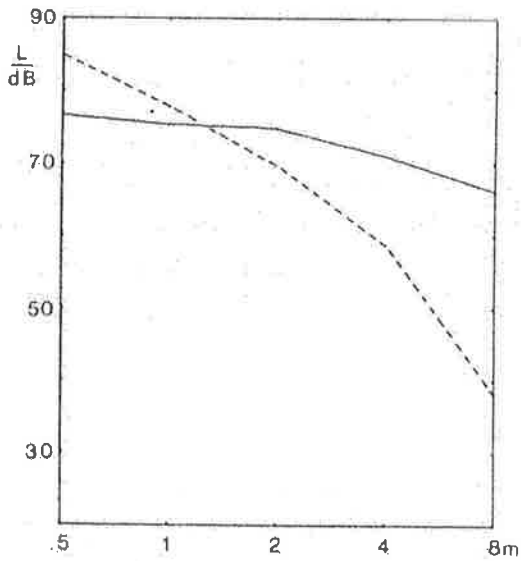


*(b) Sound pressure level measured away from the tank*

*Figure 6.5: Results after Hesselmann (1976, 1978).*

When active noise control is to be applied outdoors, ordinary acoustic sources are impractical as damage from rain, hail and snow can result. Li et al. (1997) have investigated curved panel enclosures, excited by PVDF films bonded to the inside as alternate control sources, which are effectively weatherproof. However, the radiation efficiency of these sources is limited. Burgemeister (1996) examined the use of a perforated panel (of low internal impedance) which was driven by vibration control actuators to minimise the sound at far field error microphones. The perforated panel is unaffected by exposure to the elements. In work on the commercial product Quietpower (ADTP (1997)), Brungardt et al. (1997) developed weatherproofed error microphones and control speakers.

Over the last decade experimental work on active transformer noise control has seen more advanced control systems being employed as a direct result of the availability of low cost digital signal processors (DSPs) (Smith (1997)). Cheuk et al. (1994) reported tests on an enclosed transformer, employing 8 control sources in a circular array 2 metres in diameter around the transformer with a single near field error sensor. Appreciable attenuation was reported. McLoughlin et al. (1994) tested another means of controlling the sound radiated by transformers. Their approach was to apply force actuators on the transformer tank. A control system then was designed to minimise those structural modes of the transformer tank which contribute most to the sound radiation. Difficulty in generating sufficiently large forces with practical vibration actuators was reported, as the transformer tank has a high internal impedance.

A review by Hansen et al. (1997) details studies directed at "how to" tackle a active noise and vibration control on a practical in situ transformer. Their approach suggested a hybrid of acoustic and vibration control sources.

Martin and Roure (1997), Martin and Roure (1998) have published work on the optimisation of source and sensor locations in the active control of transformer noise in an anechoic chamber. This approach involved using a search algorithm to find the optimal source and sensor locations. The results with only a few sources and sensors were significant, achieving reductions

of the order of 10dB.

There are a variety of reasons why near field error sensors would be advantageous in a transformer active noise control system; being able to attribute sound to the target transformer in a multiple transformer substation, immunity from environmental conditions, signal to noise ratio, etc. However, Hesselmann's results (see Figure 6.5) indicate that pressure levels in the near field may *increase* when global control is achieved. This suggests the potential for improved near field sensing strategies based upon intensity, as opposed to pressure.

Work by Li (2000) evaluated multiple active intensity sensors used to control transformer noise. For the study, the acoustic control sources were collocated on the transformer tank. Transfer function measurements were made between the control speakers and error microphones/intensity probes located 1 metre from the tank, and also impulse responses between a point force applied with a sledge hammer and the error microphone/intensity probe. The simulated results showed that unless many more intensity error sensors are employed, traditional pressure sensors perform better. It was also determined that vibration sources would be more effective at reducing the sound field. The aim of the work here is to further investigate this conclusion, in consideration of the studies detailed in the previous chapters.

## 6.3 Transformer

The experimental transformer used in these experiments is shown in Figure 6.6. The transformer is approximately $0.5 \times 1 \times 1$ metres in size, mounted on a trolley with heavy duty rubber wheels and was moved into the anechoic chamber along two C-section steel railings. Due to the difficulty in removing the transformer from the railings once in the chamber, it was decided to keep it sitting on the trolley and railing. In order to adequately support the weight of the transformer, the floor of the anechoic chamber (whose dimensions and cutoff frequency were described in Chapter 3) was covered in 20mm thick MDF board, similar to that used for

the baffle used in Chapters 4 and 5. The floor covering was found to have minimal effect on the experiments, and in fact it more accurately simulates a real in situ transformer on hard ground.

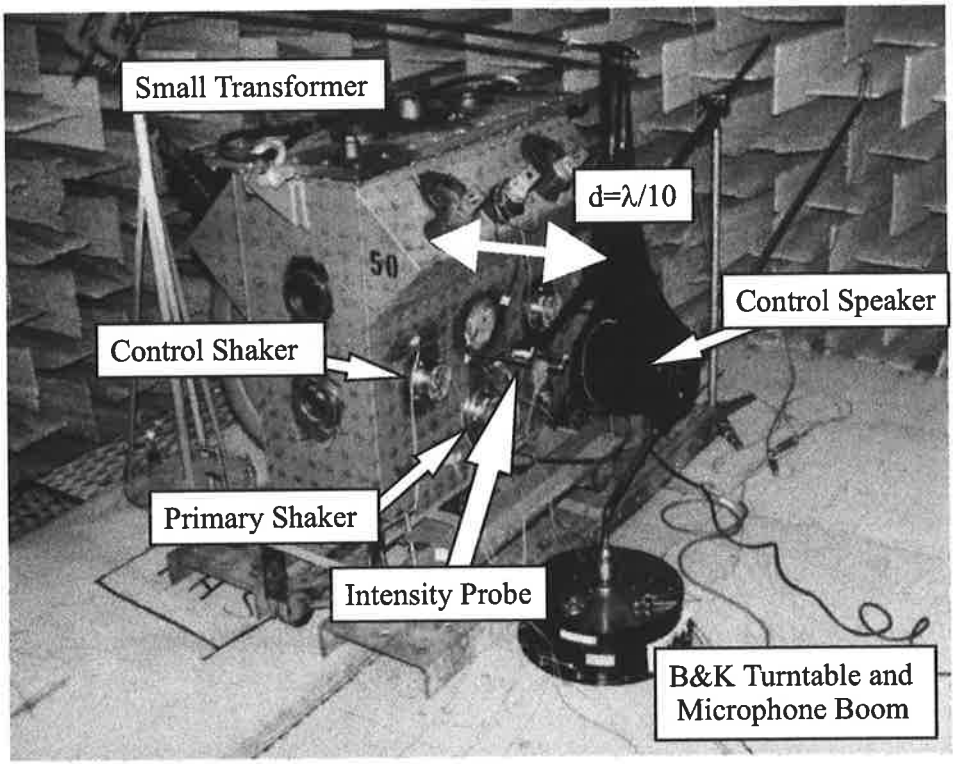


*Figure 6.6: Small transformer used in experiments, sitting on a rubber wheeled trolley on two C-section steel railings on an MDF boarded floor located in an anechoic chamber.*

The transformer was excited with AURA electrodynamic shakers (Cazzolato (1999a)) shown in Figure 6.7, which were found to produce adequate force to act as a primary excitation on the transformer tank and act as a control source. The shakers were mounted onto the transformer via a mounting shown in Figure 6.8. Work by Li (2000) found that these AURA shakers produced an insignificant bending moment and adequately modelled a point force excitation.

### 6.3.1 Acoustic control

Figure 6.10 shows the experimental setup for acoustic control with an enclosed speaker as used previously in this thesis. The control speaker was hung off a cantilever beam situated over the transformer as shown in Figure 6.6 by a pair of stockings for vibration isolation. The

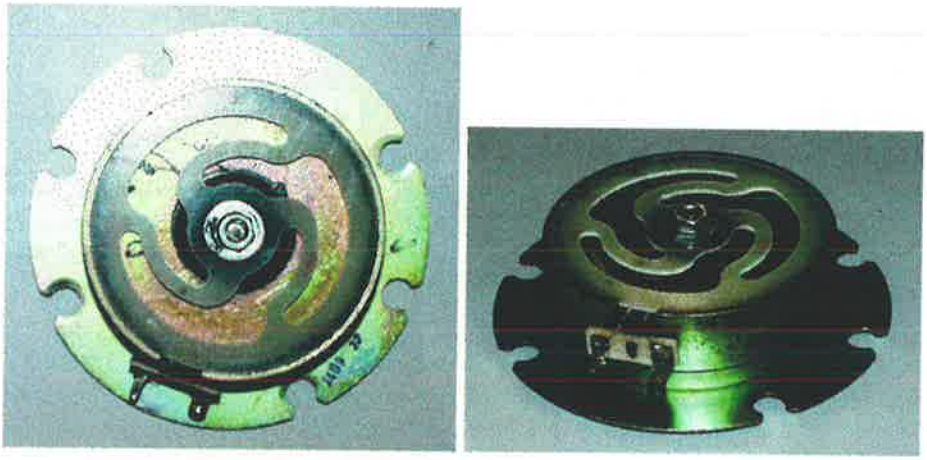

(a) Top view. (b) Angled view.

Figure 6.7: AURA shakers used as the primary exciter and vibration control sources.

Figure 6.8: Mounting plate used to affix the AURA shaker onto the transformer.

cantilever beam shown in Figure 6.6 is supported by a stand which is isolated by a rubber mat from the floor of the chamber in order to reduce the possible effects of floor panel vibrations. The primary AURA shaker was centrally mounted on the front face of the transformer.

In order to assess the power attenuation achieved when minimising an active intensity cost function as opposed to that minimising the squared pressure, the radiated sound pressure was measured with a microphone attached to a boom and turntable through an arc $180^o$, before and after control is applied. The control source was separated by a distance of $\lambda/10$ from the transformer tank. This separation distance was found in Chapters 4 to 5, for planar type radiators to yield in excess of 20dB of sound power attenuation. A B&K Type 4131 condenser microphone fed through a B&K Type 2604 Microphone Amplifier which is 1/3 octave band pass filtered in the 100Hz 1/3 octave band was used to measure the residual sound pressure. The B&K Type 4131 condenser microphone was attached to a microphone boom which was located just in in front of the transformer tank and extended 1.8 metres out (see Figure 6.6).

As in previous work, the signal from the B&K Type 4131 condenser microphone was sent to B&K Type 2307 Level Recorder which plotted the results on polar paper. The results were then scanned into a computer using Corel Trace™ and placed on a half circle polar graph. The B&K Type 4131 condenser microphone was not calibrated, since we are only interested in the pressure reduction. The same control system setup described in Appendix D was used in these experiments. A portable B&K Type 2144 Dual Channel Real-Time Frequency Analyser was used to measure the active intensity and pressure amplitude at 100Hz from the intensity probe. A HP Oscilloscope was used to check the actual amplitude reduction of the primary noise source. The control signal was observed to be reduced by between 30 and 40dB.

Figure 6.9 displays the location of the error sensors tested in these experiments.

Figure 6.11 and 6.12 show that the radial active intensity sensor performs worse than the pressure sensor, with 3~4dB less attenuation in the far field pressure when the intensity sensor is minimised. Global attenuation is evident with both intensity and pressure sensors, of the

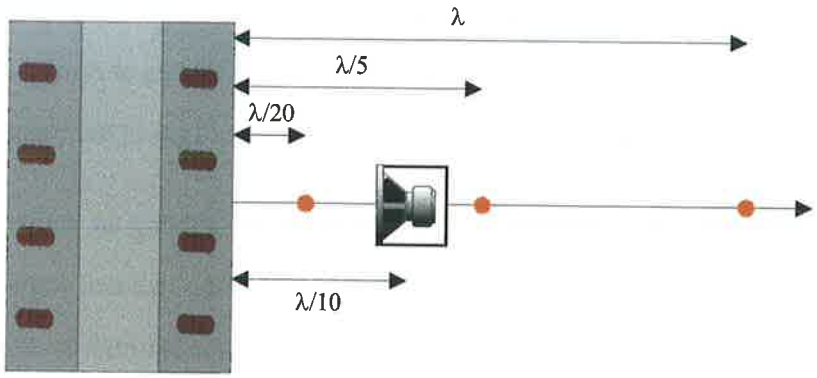


*Figure 6.9: Aerial view of transformer showing the three sensor locations considered. The red dots indicate the error sensor locations.*

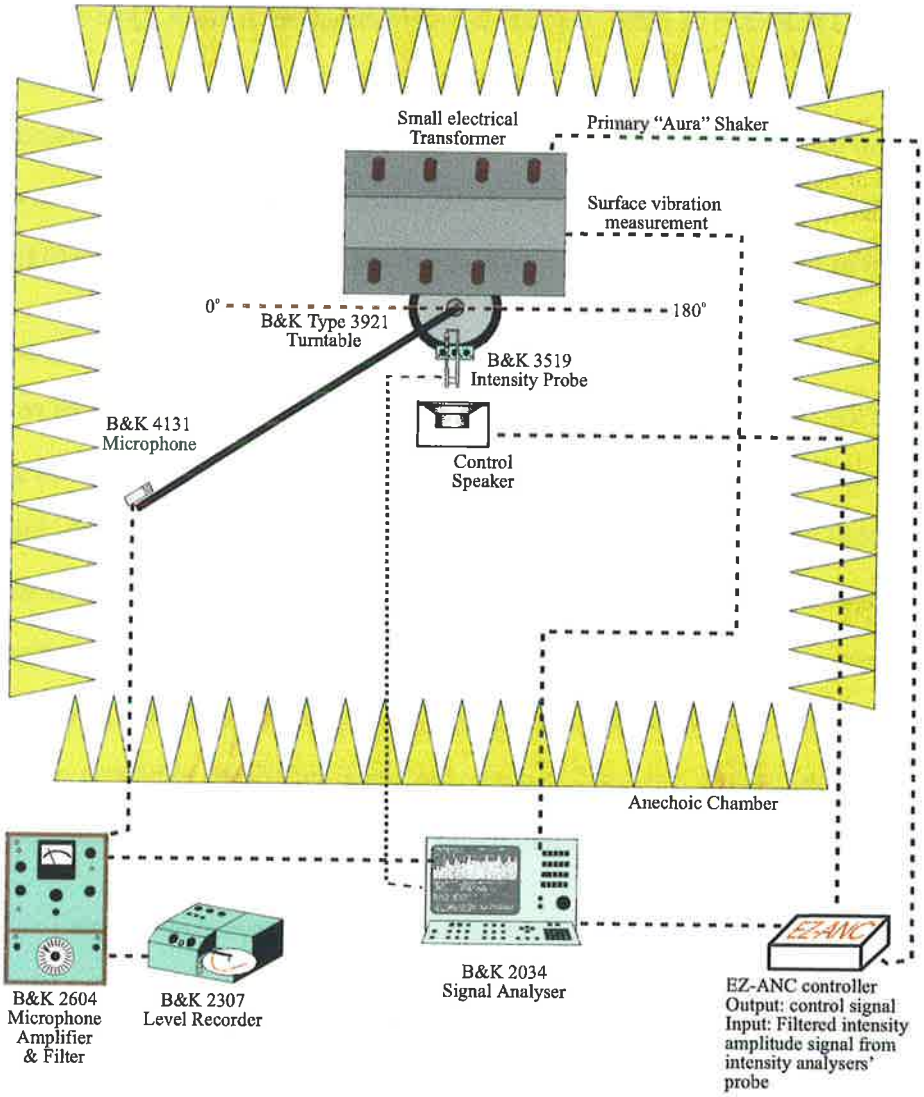


*Figure 6.10: Experimental setup of acoustic control of the small transformer in anechoic chamber.*

order of 5dB with intensity and 9dB with pressure.

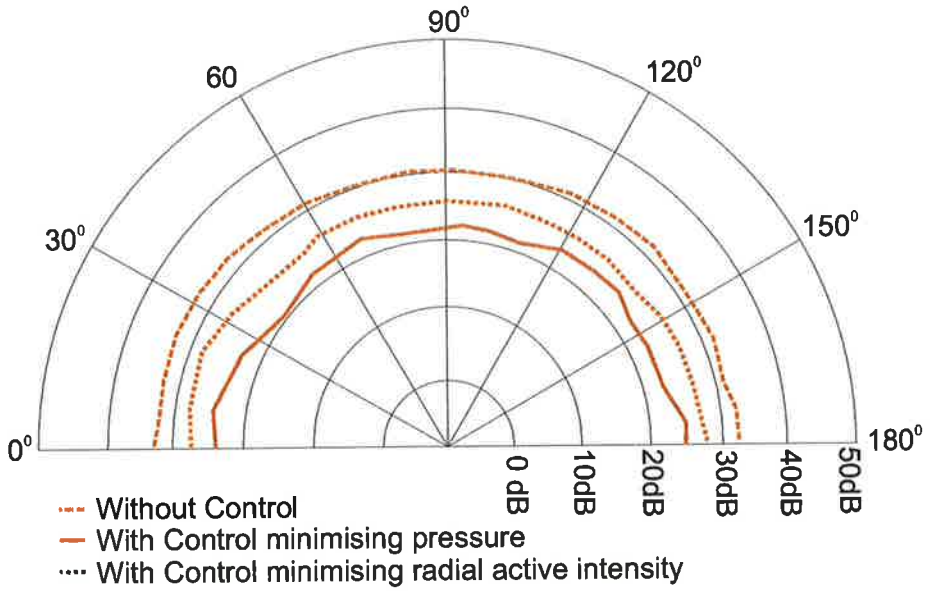


*Figure 6.11: Far field pressure before and after control when employing a single acoustic pressure or radial active intensity error sensor at λ from the front face of the transformer tank to control a 100Hz tone induced by a single AURA shaker in the approximate centre of the front face of the transformer, with a single monopole control source.*

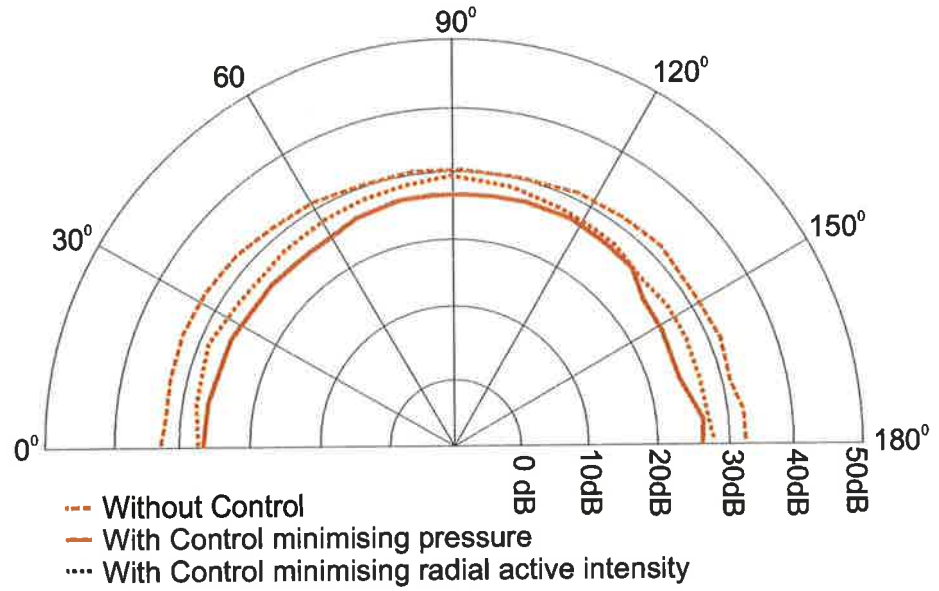


*Figure 6.12: Far field pressure before and after control when employing a single acoustic pressure or radial active intensity error sensor at λ/5 from the front face of the transformer tank to control a 100Hz tone induced by a single AURA shaker in the approximate centre of the front face of the transformer, with a single monopole control source.*

Figure 6.13 shows the results of minimising the radial active intensity and squared pressure at a sensor location half way between the transformer tank and the control source. This location exhibits the characteristic poor performance of active intensity minimised in this spatial configuration. The pressure when minimising the squared pressure was attenuated by in places more than 10dB and the active intensity lead to pressure increases of the order of 5dB.

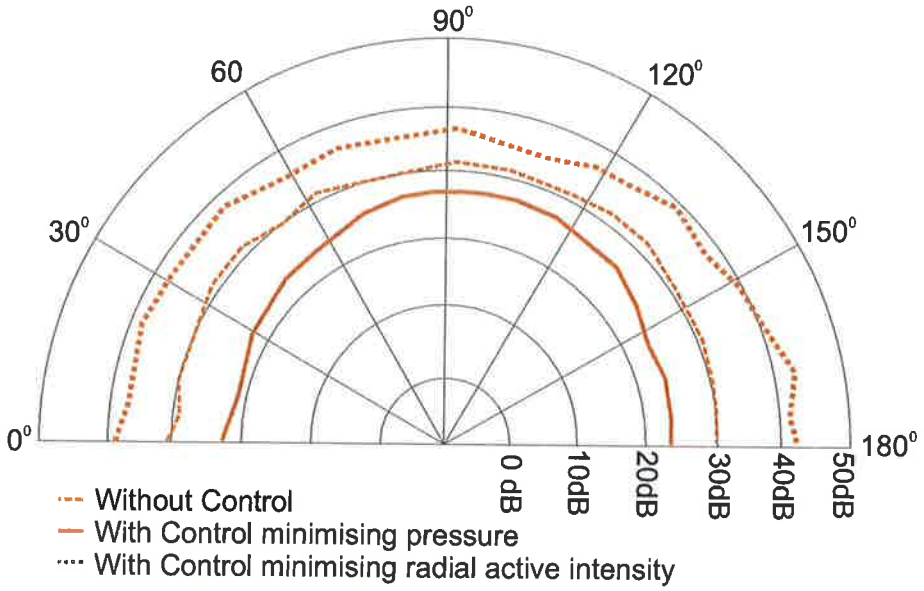


*Figure 6.13: Far field pressure before and after control when employing a single acoustic pressure or radial active intensity error sensor at $\lambda/20$ from the front face of the transformer tank to control a 100Hz tone induced by a single AURA shaker in the approximate centre of the front face of the transformer, with a single monopole control source.*

### 6.3.2 Vibration control

Figure 6.14 shows the experimental setup for vibration control of the small transformer tank. Again, the primary AURA shaker was approximately centrally mounted on the front face of the transformer. The control AURA shaker was mounted off-centre and near the top left corner of the front face of the transformer tank. The remainder of the experimental apparatus is as described in the previous section.

A Crossbow accelerometer was attached with double sided tape to seven locations on the front

face of the transformer tank and the average velocity attenuation (dB) was measured on the front face.

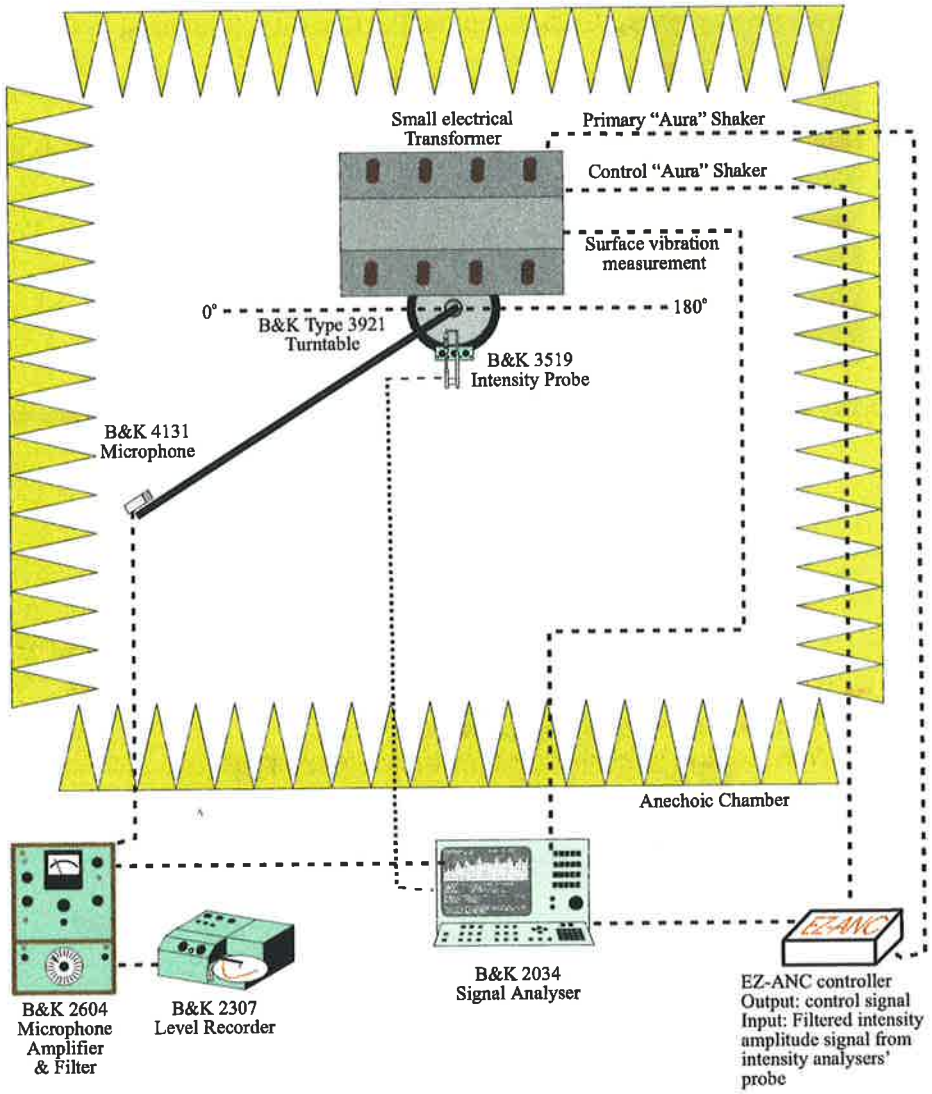


*Figure 6.14: Experimental setup of vibration control of the small transformer in anechoic chamber.*

Figure 6.15 displays the location of the error sensors tested in these experiments. Figure 6.16, 6.17 and 6.18 show that the radial active intensity sensor and the pressure sensor have approximately equal performance exhibiting pressure attenuation of 12~15dB. At the three error sensor locations tested the velocity attenuation of the front face of the transformer tank was found to be between 3 and 4 dB, indicating that the control mechanism was not modal control and possibly modal rearrangement.

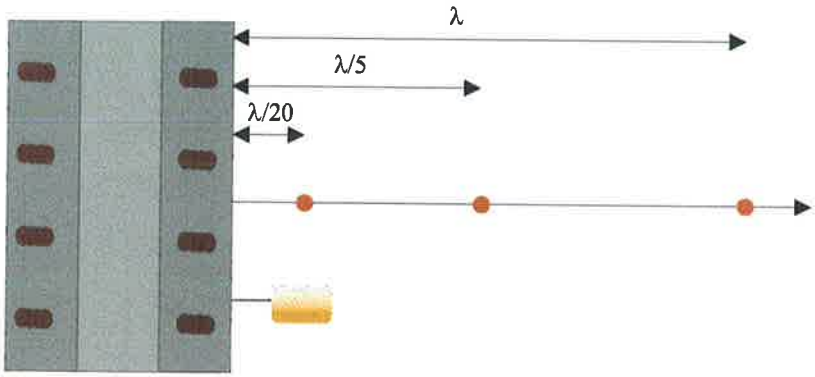


*Figure 6.15: The three sensor locations considered. The red dots indicate the error sensor location.*

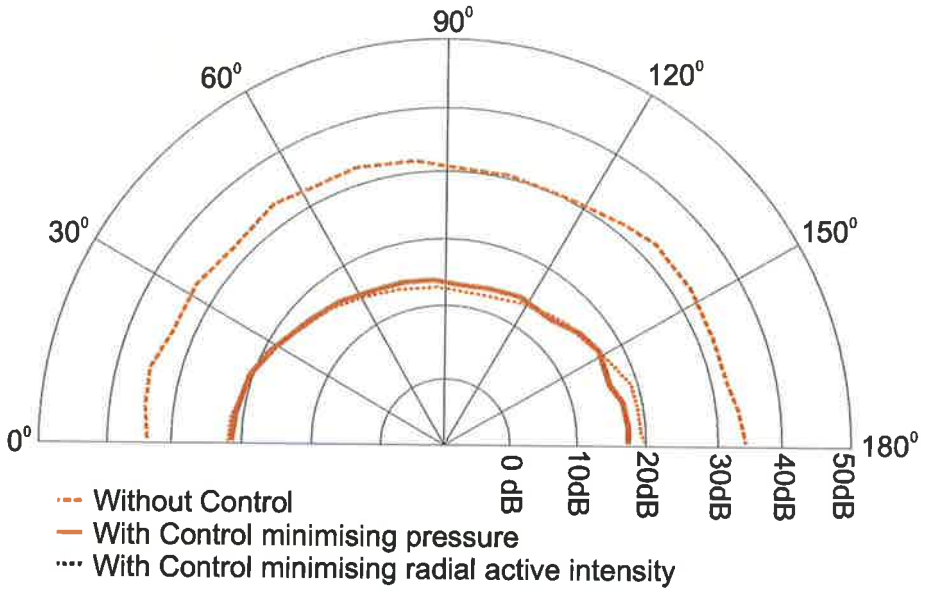


*Figure 6.16: Far field pressure before and after control when employing a single acoustic pressure or radial active intensity error sensor at λ from the front face of the transformer tank to control a 100Hz tone induced by a single AURA shaker in the approximate centre of the front face of the transformer, with a single AURA control shaker near the top left corner of the front face of the transformer.*

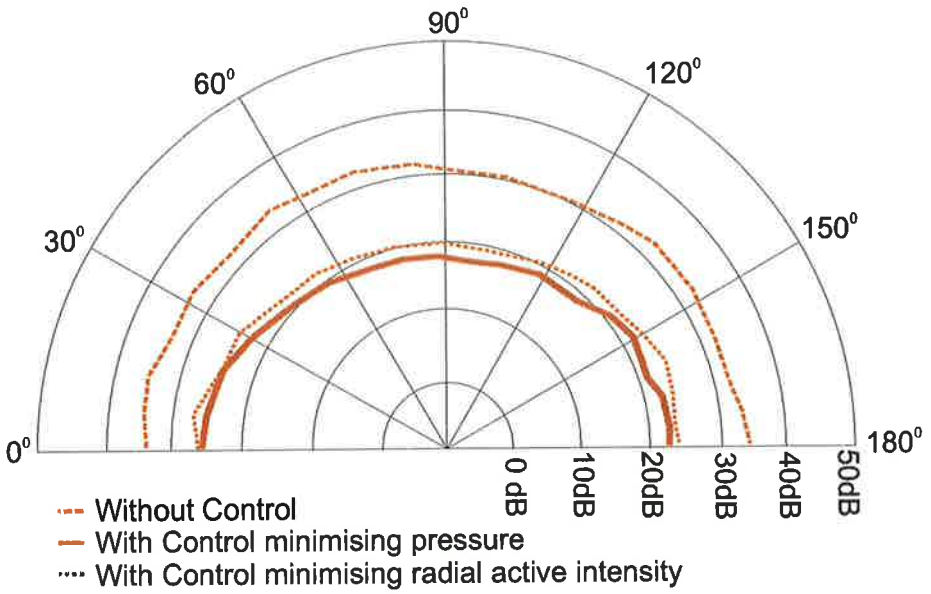


*Figure 6.17: Far field pressure before and after control when employing a single acoustic pressure or radial active intensity error sensor at $\lambda/5$ from the front face of the transformer tank to control a 100Hz tone induced by a single AURA shaker in the approximate centre of the front face of the transformer, with a single AURA control shaker near the top left corner of the front face of the transformer.*

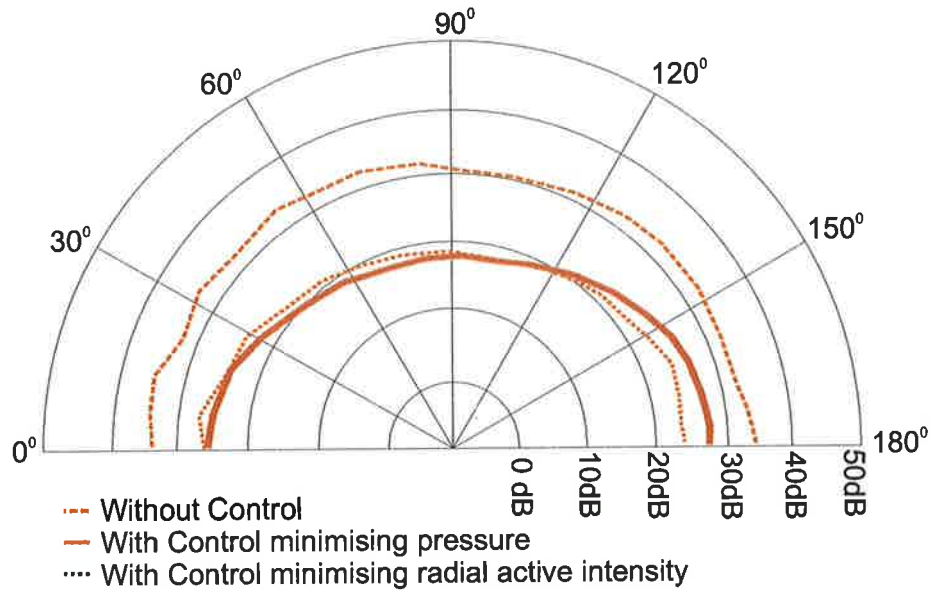


*Figure 6.18: Far field pressure before and after control when employing a single acoustic pressure or radial active intensity error sensor at $\lambda/20$ from the front face of the transformer tank to control a 100Hz tone induced by a single AURA shaker in the approximate centre of the front face of the transformer, with a single monopole control source.*

## 6.4 Conclusion

The transformer appears to be radiating as a monopole at the excitation frequency of 100Hz. Indications are that pressure error sensors lead to greater global attenuation than active intensity error sensors in the active control of a test transformer via a single acoustic monopole control source. When the active intensity error sensor is located very close to the transformer tank, between the transformer tank and the monopole control source, an increase in the sound field is observed (see Figure 6.13). Table 6.1 demonstrates what has been shown in Chapters 3 to 5, to be the poor performance of active intensity sensors between the primary and control sources, and approximately equal to the good attenuation performance achieved by pressure error sensors, at far field locations. When a single vibration control source is employed (as was shown in Chapter 5), active intensity and pressure error sensing yield similar levels of attenuation, no increases in sound levels are observed when the active intensity error sensor is moved very close ($\lambda/20$ from the transformer tank) to the transformer tank (see Table 6.2).

| Sensor Type | Location | far field Attenuation | Relevant Figures | Comments |
|---|---|---|---|---|
| Pressure | $\lambda/20$ | very good | 6.13 | between 5-10dB attenuation |
| Intensity | $\lambda/20$ | very bad (increase) | 6.13 | ~5-12dB increase in sound pressure |
| Pressure | $\lambda/5$ | good | 6.12 | between 3-8dB attenuation |
| Intensity | $\lambda/5$ | good | 6.12 | between 1-6dB attenuation |
| Pressure | $\lambda$ | very good | 6.11 | ~9-12dB attenuation |
| Intensity | $\lambda$ | very good | 6.11 | ~5-7dB attenuation |

*Table 6.1: Transformer results summary table for acoustic control.*

| Sensor Type | Location | far field Attenuation | Relevant Figures | Comments |
|---|---|---|---|---|
| Pressure | $\lambda/20$ | very good | 6.18 | ~5-12dB attenuation |
| Intensity | $\lambda/20$ | very good | 6.18 | ~7-11dB attenuation |
| Pressure | $\lambda/5$ | very good | 6.17 | ~9-12dB attenuation |
| Intensity | $\lambda/5$ | very good | 6.17 | ~8-10dB attenuation |
| Pressure | $\lambda$ | very good | 6.16 | ~11-15dB attenuation |
| Intensity | $\lambda$ | very good | 6.16 | ~11-16dB attenuation |

*Table 6.2: Transformer results summary table for vibration control.*

# Chapter 7

# Conclusions and future work

## 7.1 Introduction


*Figure 7.1: Thesis Flow chart.*

This chapter draws global conclusions using the specific results of the detailed study into the performance of active intensity error sensors in the active control of free space sound radiation. Suggestions are also made for future investigations.

## 7.2 Conclusions

The literature review established that active intensity error sensing in the active control of free space sound radiation, may be able to improve upon the attenuation performance produced through the use of traditional pressure sensors. Previous work has been based around only limited studies on very simple noise sources; specifically a monopole, and single structural modes of a baffled plate. Previous work had also been limited in the error sensor locations that

were considered. In this thesis, the use of single active intensity sensors situated on radial lines with respect to the primary source, were tested for a number of primary sources and configurations (see Figure 7.2), and for a set of three critical regions of error sensor location (see also Figure 7.2). A control strategy which used a traditional filtered-X LMS algorithm modified by a heterodyning technique was implemented. The use of traditional pressure error sensors in all of the above mentioned work was used as a benchmark, for evaluating the attenuation performance of active intensity error sensors. It was found that at error sensor locations behind and towards the far field of the control source, an active intensity error sensing strategy would (usually) only slightly improve the global sound attenuation that is achievable through pressure error sensing very close and just behind the control source ($\lambda/5$ along a radial line passing through the primary and control sources, and from the primary source). In the practical case of the active control of the sound radiation from a small transformer in an anechoic chamber, the level of attenuation observed at the error sensor location ($\lambda/5$) when employing an active intensity sensor is worse than that achieved by a pressure error sensor (see Table 7.1). It should be noted, however, that the performance of active intensity and pressure error sensors in this location are sub-optimal in terms of sound power attenuation. If the error sensor was moved further away, say to a distance of $\lambda$ from the primary source, then an active intensity error sensor produced significant (approaching the maximum sound power attenuation set by the location of the control sources) and very similar levels of attenuation to pressure error sensors. This can be explained by the fact the far field intensity is directly proportional to the squared pressure, and hence minimising far field intensity would also minimise the squared pressure.

If the active intensity error sensor is positioned between the primary and control source, (as shown in Figures 3.7, 4.7 and 5.14) then the active intensity cost function becomes negative indefinite (inverted paraboloid shape, as shown in Figures 3.16, 4.15 and 5.22). This characteristic of active intensity in such locations yields a unique maximum value of the cost function. As such, the far field sound levels are in fact increased, over their values before control was attempted.

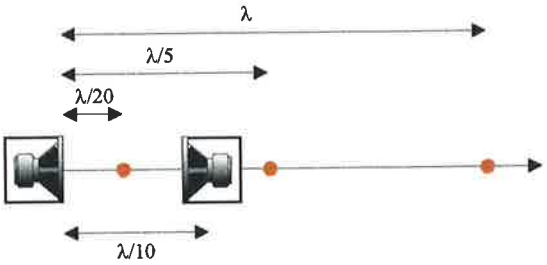


(a) Monopole primary source

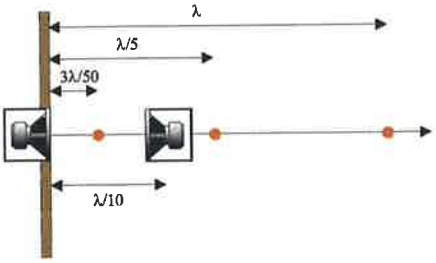


(b) Baffled monopole primary source

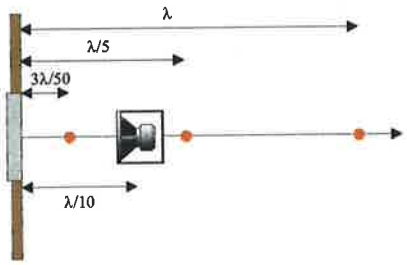


(c) Baffled plate primary source

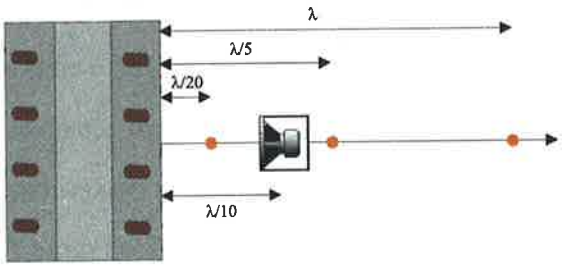


(d) transformer primary source

*Figure 7.2: The three sensor locations considered when applying acoustic control with a single monopole control source. The red dots indicate the error sensor location.*

To summarise, the effectiveness of an active intensity error sensing strategy in the active control of free space sound radiation, can:

(i.) match the performance of pressure error sensors in the far field.

(ii.) perform slightly better than pressure sensors, behind the control source.

(iii.) lead to an increase in far field sound levels when intensity is minimised between the primary and control sources.

Active intensity and pressure error sensing strategies approach the optimal sound power attenuation, when the error sensors are located in the far field. Pressure error sensors (see Figures 3.9, 4.9 and 5.16) can also approach the optimal sound power attenuation when located approximately half distance between the primary disturbance and the control source. However, there are many practical problems with near field pressure sensing, relating to the existence of the evanescent sound field. Far field error sensing, as discussed previously, also has practical difficulties. However due to the directional characteristics of far field active intensity error sensors, they could offer benefits over conventional pressure error sensors, by largely filtering out sound radiation not emitted by disturbances on axis.

The use of structural control sources, was reported extensively in the literature review. Optimising such active structural acoustic control systems usually requires knowledge of the modal characteristics of the primary disturbing structure. However, a control implementation can be made very compact by the deployment of vibration control actuators. This thesis has considered the use of active intensity error sensors in ASAC, for two primary disturbances; a plate in an infinite baffle and a small transformer on a hard floor (see Figure 7.3). Again pressure error sensors were used as a benchmark. It was found (see Table 7.2) that the choice of acoustic error sensing strategy plays little role in achieving a level of far field sound attenuation. It was shown that active intensity error sensing at locations very close to the primary source (as described in Figure 7.3 for the sensor locations $\lambda/20$ and $3\lambda/50$) do not lead to increases in

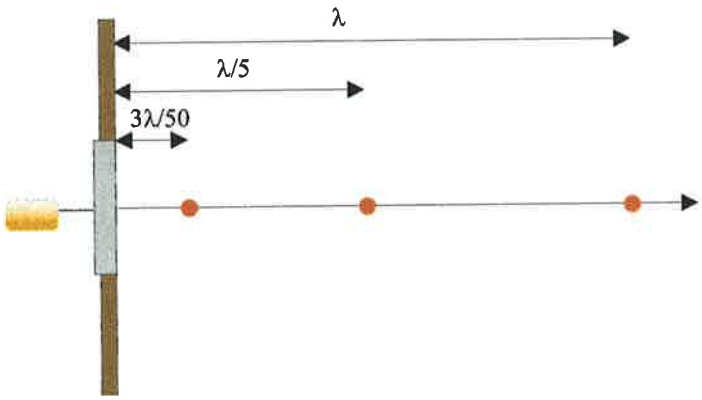


(a) Baffled plate primary source

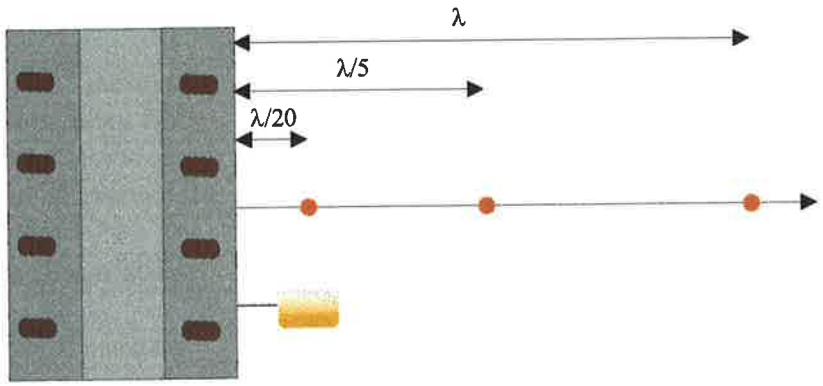


(b) transformer primary source

*Figure 7.3: The three sensor locations considered when applying vibration control with a single vibration control source located at* $\mathbf{x}_{control} = (-70,0)$mm*, and the primary source is excited at location* $\mathbf{x}_{primary} = (0,0)$mm *(centre of the structure). The red dots indicate the error sensor location.*

the far field sound levels as is the case for acoustic control. It was also shown that substantially greater levels of global sound attenuation can be achieved with vibration control sources, as previously described in the literature.

| Sensor Type | Location | far field Attenuation | Relevant Figures | Comments |
|---|---|---|---|---|
| Monopole (Chapter 3) | | | | |
| Pressure | $\lambda/20$ | good | 3.35 | between 9-10dB attenuation |
| Intensity | $\lambda/20$ | very bad (increase) | 3.35 | 6-7dB increase in sound pressure |
| Pressure | $\lambda/5$ | good | 3.34 | between 8-10dB attenuation |
| Intensity | $\lambda/5$ | good | 3.34 | approximately equal to pressure |
| Pressure | $\lambda$ | very good | 3.33 | ~10dB attenuation |
| Intensity | $\lambda$ | very good | 3.33 | slightly worse than pressure |
| Baffled Monopole (Chapter 4) | | | | |
| Pressure | $3\lambda/50$ | very good | 4.45 | between 12-16dB attenuation |
| Intensity | $3\lambda/50$ | very bad (increase) | 4.45 | 7-8dB increase in sound pressure |
| Pressure | $\lambda/5$ | good | 4.44 | between 5-8dB attenuation |
| Intensity | $\lambda/5$ | good | 4.44 | between 7-9dB attenuation |
| Pressure | $\lambda$ | very good | 4.43 | ~15dB attenuation |
| Intensity | $\lambda$ | very good | 4.43 | approximately equal to pressure |
| Baffled Plate (Chapter 5) | | | | |
| Pressure | $3\lambda/50$ | very good | 5.29 | between 15-20dB attenuation |
| Intensity | $3\lambda/50$ | very bad (increase) | 5.29 | ~5dB increase in sound pressure |
| Pressure | $\lambda/5$ | good | 5.28 | between 5-8dB attenuation |
| Intensity | $\lambda/5$ | good | 5.28 | between 7-9dB attenuation |
| Pressure | $\lambda$ | very good | 5.27 | ~12-14dB attenuation |
| Intensity | $\lambda$ | very good | 5.27 | approximately equal to pressure |
| Transformer (Chapter 6) | | | | |
| Pressure | $\lambda/20$ | very good | 6.13 | between 5-10dB attenuation |
| Intensity | $\lambda/20$ | very bad (increase) | 6.13 | ~5-12dB increase in sound pressure |
| Pressure | $\lambda/5$ | good | 6.12 | between 3-8dB attenuation |
| Intensity | $\lambda/5$ | good | 6.12 | between 1-6dB attenuation |
| Pressure | $\lambda$ | very good | 6.11 | ~9-12dB attenuation |
| Intensity | $\lambda$ | very good | 6.11 | ~5-7dB attenuation |

*Table 7.1: Results summary for acoustic control via a single monopole separated from the primary disturbance by* $\lambda/10$.

| Sensor Type | Location | far field Attenuation | Relevant Figures | Comments |
|---|---|---|---|---|
| Baffled Plate (Chapter 5) | | | | |
| Pressure | $3\lambda/50$ | very good | 5.50 | ~21dB attenuation, less than theory predicted |
| Intensity | $3\lambda/50$ | very good | 5.50 | ~21dB attenuation, less than theory predicted |
| Pressure | $\lambda/5$ | very good | 5.48 | ~21dB attenuation, less than theory predicted |
| Intensity | $\lambda/5$ | very good | 5.48 | ~21dB attenuation, less than theory predicted |
| Pressure | $\lambda$ | very good | 5.46 | ~21dB attenuation, less than theory predicted |
| Intensity | $\lambda$ | very good | 5.46 | ~21dB attenuation, less than theory predicted |
| Transformer (Chapter 6) | | | | |
| Pressure | $\lambda/20$ | very good | 6.18 | ~5-12dB attenuation |
| Intensity | $\lambda/20$ | very good | 6.18 | ~7-11dB attenuation |
| Pressure | $\lambda/5$ | very good | 6.17 | ~9-12dB attenuation |
| Intensity | $\lambda/5$ | very good | 6.17 | ~8-10dB attenuation |
| Pressure | $\lambda$ | very good | 6.16 | ~11-15dB attenuation |
| Intensity | $\lambda$ | very good | 6.16 | ~11-16dB attenuation |

*Table 7.2: Results summary for vibration control via a single point vibration control source at location* $\mathbf{x}_{control} = (-70,0)$*mm, and the primary source is excited at location* $\mathbf{x}_{primary} = (0,0)$*mm (centre of the structure).*

## 7.3 Future work

Further research is needed, building on those areas that did work, including

- far field intensity error sensing
- acoustic error sensing and vibration control actuation

As mentioned previously, there are positive benefits to using active intensity sensors. Due to their directional nature, they can filter out noise from other sources not radiated directly from the object the sensor is lined up with. Also active control of vibration using acoustic error sensors could show significant promise. If intensity sensors could be located close to the vibrating structure then a good signal to noise ratio could be maintained and simultaneously large levels of control are theoretically achievable.

The control system developed in this work needs to be expanded to multiple frequencies and multiple sensors. It has been shown that global sound attenuation of a range of sources whose dimensions are smaller than the wavelength of sound to be cancelled, can be achieved via a single control source, such as control of the fundamental frequency on one face of a transformer. Significantly less global attenuation would be achievable at higher frequencies, as the sound power attenuation for a fixed separation distance $d$ and higher wavenumber $k$ is much less. It is not known whether modal spillover is simultaneously occurring, as the analyses in this thesis were restricted to a single frequency. The effect on performance of multiple sensors is presumably (Qiu et al. (1998) and Berry et al. (1999)) to further improve performance. However an optimal number and location of sensors is as yet undetermined.

It is also worth trying more large scale studies around a large transformer (see Figure 6.2), with far field intensity sensors to improve the signal to noise ratio.

Further work is needed to analyse sources which are larger as compared to wavelength of the sound to be cancelled. Unlike the cases analysed in this thesis such sources would not behave like monopoles.

## 7.4 Reviewer's Comments

The reviewers found a few minor points which they felt needed to be addressed. Associate Prof. J. Pan, identified typographical errors and suggested the combination of the chapter introductions into a single description of the thesis layout in an introductory chapter, as they were repetitive. The author felt the need to retain these introductions as they give a brief overview of where the reader is up to in the body of work. The author is grateful for Assoctiate Prof. J. Pan's thorough comments all of which were positive.

The second anonymous reviewer, made two points concerning the explanation of the use of active intensity (time-averaged intensity) error sensors in a tradtional filtered-X LMS algorithm and the broader applicability of a loci of infinitely many minima of active intensity amplitude. Firstly, the LMS algorithm attempts to converge to the Wiener solution, i.e. an average solution. This occurs by adapting over time. From a theoretical position, the intensity will be no different to pressure in this regard. As outlined in Appendix D, the active intensity is a time-invariant quantity, which ordinarily would prohibit its use with a traditional filtered-X LMS algorithm. However, as also described in Appendix D, by applying the heterodyning technique, this problem is overcome and the filtered-X LMS algorithm can be used. Secondly the author can not guarantee that when there exists a loci of infinitely many minima of active intensity, that the control system will converge to the solution which also minimises the sound pressure. This is also described in the conclusions in Chapters 3, 4, 5, 6. The author is grateful for the positive comments of the second anonymous reviewer.

This page intentionally contains only this sentence.

# Bibliography

P.R. Adby and M.A.H. Dempster. *Introduction to Optimisation Methods*. Chapman Hall, London, 1974.

ADTP. Quiet power: The atq 100. Advanced Digital Technologies for Power, 1997.

O.L. Angevine. Active acoustic attenuation of electric transformer noise. In *Proceedings of Internoise 81*, pages 303–306, 1981.

O.L. Angevine. Active cancellation of the hum of a simulated electric transformer. In *Proceedings of Internoise 90*, pages 789–791, 1990.

O.L. Angevine. Active cancellation of the hum of large electric transformers. In *Proceedings of Internoise 92*, pages 313–316, 1992.

O.L. Angevine. Active control of hum from large power transformers - the real world. In *Proceedings of the second conference on recent advances in active control of sound and vibration, Blacksberg USA*, pages 279–290, 1993.

O.L. Angevine. The prediction of transformer noise. *Sound and Vibration*, pages 16–18, October 1994.

O.L. Angevine. Active systems for attenuating noise. *International Journal of Active Control*, 1(1):65–78, 1995.

AS2107. Acoustics: Recommended design sound levels and reverberation times for building interiors. Australian Standards, 1987.

P. Audrain, P. Masson, and A. Berry. Investigation of active structural intensity control in finite beams: theory and experiment. *Journal of the Acoustical Society of America*, 108(2): 612–622, 2000.

K.H. Baek. *Genetic algorithms for choosing source locations in active noise control systems*. PhD thesis, University of Southampton, England, 1993.

K.H. Baek and S.J. Elliott. Genetic algorithms for choosing source locations in active control system. *Proceedings of the Institute of Acoustic*, 15(3):437–445, 1993.

K.H. Baek and S.J. Elliott. Natural algorithms for choosing source locations in active control systems. *Journal of Sound and Vibration*, 186(2):245–267, 1995.

K.H. Baek and S.J. Elliott. The effects of plant and disturbance uncertainties in active control systems on the placement of transducers. *Journal of Sound and Vibration*, 230(2):261–289, 2000.

H. Baruh and K. Chloe. Sensor placement in structural control. *Journal Guidance, Control and Dynamics*, 13:524–533, 1990.

T.A. Beauvilain, J.S. Bolton, and B.K. Gardner. Sound cancellation by the use of secondary multipoles. *Journal of the Acoustical Society of America*, 107(3):1189–1202, 2000.

R. Bellman. *Introduction to Matrix Analysis*. McGraw-Hill, New York, 1960.

E. Benzaria and V. Martin. Secondary source locations in active noise control: selection or optimization? *Journal of Sound and Vibration*, 173(1):137–144, 1994.

L.L. Beranek. *Noise and Vibration Control*. Institute of Noise Control Engineering, Washington, DC., 1988.

L.L. Beranek. *Acoustics*. Book. Reprinted for the American Acoustical Society of America by the American Institute of Physics, New York, 1996.

T. Berge, O.Kr.O Pettersen, and S. Sorsdal. Active noise cancellation of transformer noise. In *Proceedings of Internoise 87*, pages 537–541, 1987.

T. Berge, O.Kr.O Pettersen, and S. Sorsdal. Active cancellation of transformer noise: field measurments. *Applied Acoustics*, pages 309–320, 1988.

A.P. Berkhoff. Sensor scheme design for active structural acoustic control. *Journal of the Acoustical Society of America*, 108(3):1037–1045, 2000.

E.F. Berkman and E.K. Bender. Perspectives on active noise and vibration control. *Sound and Vibration 30th Anniversary Edition*, pages 80–94, 1997.

A. Berry. Advanced sensing strategies for the active control of vibration and structural radiation. In *Proceedings of Active 99*, pages 73–90, 1999.

A. Berry, X. Qiu, and C.H. Hansen. Near-field sensing strategies for the active control of sound radiation from a plate. *Journal of the Acoustical Society of America*, 106(6):3394–3406, 1999.

D.A. Bies and C.H. Hansen. *Engineering Noise Control*. Unwin Hyman, London, 1996.

J.S. Bolton, B.K. Gardner, and T.A. Beauvilain. Sound cancellation by the use of secondary multipoles. *Journal of the Acoustical Society of America*, 98(4):2343–2362, 1995.

M.J. Brennan, J. Garcia-Bonito, S.J. Elliott, A. David, and R.J. Pinnington. Experimental investigation of different actuator technologies for active vibration control. *Smart materials and structures*, 8:145–153, 1999.

Bruel and Kjaer. *Sound Intensity Analysing System Type 3360 Instruction Manual*. Bruel and Kjaer, 1983.

Bruel and Kjaer. *Sound intensity*. Bruel and Kjaer, 1993.

K. Brungardt, J. Vierengel, and K. Weissman. Active structural acoustic control of noise from power transformers. *Noise-con 97*, pages 173–182, 1997.

A.J. Bullmore, P.A. Nelson, A.R.D. Curtis, and S.J. Elliott. The active minimisation of harmonic enclosed sound fields, part II: A computer simulation. *Journal of Sound and Vibration*, 117(1):15–33, 1987.

A.J. Bullmore, P.A. Nelson, and S.J. Elliott. Theoretical studies of the active control of propeller-induced cabin noise. *Journal of Sound and Vibration*, 140(2):191–217, 1990.

K.A. Burgemeister. *Novel methods of transduction for the active control of harmonic sound radiated by vibrating surfaces*. PhD thesis, Adelaide University, 1996.

B.S. Cazzolato. Aura shaker specifications. Technical report, ANVC Group Internal Report University of Adelaide, 1999a.

B.S. Cazzolato. *Sensing systems for active control of sound transmission into cavities*. PhD thesis, University of Adelaide, Australia, 1999b.

B.S. Cazzolato and C.H. Hansen. Active control of sound transmission using structural error sensing. *Journal of the Acoustical Society of America*, 104(5):2878–2889, 1998.

B.S. Cazzolato and C.H. Hansen. Errors arising from three-dimensional energy density sensing in one-dimensional sound fields. *Sound and vibration*, 236(3):375–400, 2000a.

B.S. Cazzolato and C.H. Hansen. Errors in the measurement of acoustic energy density in one-dimensional sound fields. *Sound and vibration*, 236(5):801–831, 2000b.

Y. Champoux, B. Gosselin, and J. Nicolas. Application of the intensity technique to the characterisation of transformer noise. *IEEE Transactions on Power Delivery*, 3(4):1802–1808, 1988.

F. Charette, A. Berry, and C. Guigou. Active control of sound radiation from a plate using a polyvinylidene flouride volume displacement sensor. *Journal of the Acoustical Society of America*, 103(3):1493–1503, 1998.

K.P. Cheuk, K.F. Man, Y.C. Ho, and K.S. Tang. Active noise control for power transformer. In *Proceedings of Internoise 94*, 1994.

J.Y. Chung. Cross-spectral method of measuring acoustic intensity without error caused by instrument phase mismatch. *Journal of the Acoustical Society of America*, 64:1613–1616, 1978.

C.F. Clapp and F.A. Firestone. The acoustic watt meter - an instrument for measuring sound energy flow. *Journal of the Acoustical Society of America*, pages 124–136, 1941.

R.L. Clark. Adaptive feedforward modal space control. *Journal of the Acoustical Society of America*, 98(5):2639–2650, 1995.

R.L. Clark and C.R. Fuller. Control of sound radiation with adaptive structures. *Journal of intelligent material systems and structures*, 2:431–452, 1991.

R.L. Clark and C.R. Fuller. Active structural acoustic control with adaptive structures including wavenumber considerations. *Journal of intelligent material systems and structures*, 3: 296–315, 1992a.

R.L. Clark and C.R. Fuller. Experiments on active control of structurally radiated sound using multiple piezoceramic actuators. *Journal of the Acoustical Society of America*, 91(6): 3313–3320, 1992b.

R.L. Clark and C.R. Fuller. Modal sensing of efficient acoustic radiators with polyvinylidene fluride distributed sensors in active structural control approaches. *Journal of the Acoustical Society of America*, 91(6):3321–3329, 1992c.

R.L. Clark and C.R. Fuller. Optimal displacement of piezoelectric actuators and polyvinylidene fluride error sensors in active structural acoustic control approaches. *Journal of the Acoustical Society of America*, 92(3):1521–1533, 1992d.

R.L. Clark and C.R. Fuller. Design approach for shaping polyvinylidene fluride sensors in active structural acoustic control (asac). *Journal of intelligent material systems and structures*, 3:354–365, 1993.

H. Coanda. Procede et dispositif de proctection contre les bruits. Patent, 1934. Number 762121, French Patent Office.

W.B. Conover. Fighting noise with noise. *Noise Control*, pages 78–92, March 1956.

E.W. Constans and G.H. Belegundu, A.D.and Koopmann. Design approach for minimizing sound power from vibrating shell structures. *AIAA Journal*, 36:134–139, 1998.

L. Cremer, M. Heckel, and E.E. Ungar. *Structure-borne sound.* Springer-Verlag, 1973.

K.A. Cunefare and G.H. Koopmann. A boundary element approach to optimization of active noise control sources on three-dimensional structures. *Journal of Vibration and Acoustics*, 113:387–394, 1991a.

K.A. Cunefare and G.H. Koopmann. Global optimum active noise control: Surface and far-field effects. *Journal of the acoustical society of America*, 90:365–373, 1991b.

A.R.D. Curtis, P.A. Nelson, and S.J. Elliott. Active reduction of one-dimensional enclosed souond field: An experimental investigation of three control strategies. *Journal of the Acoustical Society of America*, 88(5):2265–2268, 1990.

P. de Heering. Comments on "on the invention of active control by paul lueg"[j. acoust. soc. am. 87, 2251-2254(1990)]. *Journal of the Acoustical Society of America*, 93:2989, 1993.

C. Deffayet and P.A. Nelson. Active control of low-frequency harmonic sound radiated by a finite panel. *Journal of the acoustical society of America*, 84:2192–2199, 1988.

E.K. Dimitriadis, C.R. Fuller, and C.A. Rogers. Piezoelectric actuators for distributed vibration excitation of thin plates. *Transaction of the ASME*, 113:100–107, 1991.

N.J. Doelman. Active control of sound fields in an enclosure of low modal density. *Proceedings of Inter Noise*, pages 451–454, 1989.

C.M. Dorling, B.P. Eatwell, S.M. Hutchins, C.F. Ross, and S.G.C. Sutcliffe. A demonstraton of active noise reduction in an aircraft cabin. *Journal of Sound and Vibration*, 128(2):358–360, 1989.

G.P. Eatwell. A survey of active control in aircraft cabins. *Proceedings of Inter Noise*, pages 817–820, 1990.

K. Eghtesadi and H.G. Leventhall. Active attenuation of noise - the monopole system. *Journal of the Acoustical Society of America*, 71(3):608–611, 1982.

S.J. Elliott. Errors in acoustic intensity measurements. *Journal of Sound and Vibration*, 78 (3):439–445, 1981.

S.J. Elliott. Down with noise. *IEEE Spectrum*, June:54–61, 1999.

S.J. Elliott, A.R.D. Curtis, A.J. Bullmore, and P.A. Nelson. The active minimisation of harmonic enclosed sound fields, Part III: Experimental verification. *Journal of Sound and Vibration*, 117(1):35–58, 1987.

S.J. Elliott and M.E. Johnson. Radiation modes and the active control of sound power. *Journal of the Acoustical Society of America*, 94(4):2194–2204, 1993.

S.J. Elliott, P. Joseph, A.J. Bullmore, and P.A. Nelson. Active cancellation at a point in a pure tone diffuse sound field. *Journal of Sound and Vibration*, 120(1):183–189, 1988.

S.J. Elliott, P. Joseph, P.A. Nelson, and M.E. Johnson. power ouput minimization and power absorption in the active control of sound. *Journal of the acoustical society of America*, 90: 2501–2512, 1991.

S.J. Elliott and P.A. Nelson. The active control of enclosed sound fields. In *Proceedings of Noise-Con 87*, pages 359–364, 1987.

S.J. Elliott and P.A. Nelson. Active noise control. *IEEE Signal processing magazine*, pages Dec–35, Oct. 1993.

S.J. Elliott, P.A. Nelson, I.M. Stothers, and C.C. Boucher. Preliminary results of in-flight experiments on the active control of propeller-induced cabin noise. *Journal of Sound and Vibration*, 128(2):355–357, 1989.

S.J. Elliott, P.A. Nelson, I.M. Stothers, and C.C. Boucher. In-flight experiments on the active control of propeller-induced cabin noise. *Journal of Sound and Vibration*, 140(2):219–238, 1990.

F. Fahy. *Sound Intensity*. E&FN Spon, London, 2nd edition, 1995.

F.J. Fahy. Measurement of acoustic intensity using the cross-spectral density of two microphone signals. *Journal of the Acoustical Society of America*, 62:1057–1059, 1977.

F.J. Fahy. *Sound and structural vibration: Radiation, transmission and response.* Academic Press, London, 1985.

J.E. Ffowcs Williams. Anti-sound. *Proceedings of the Royal Society London*, A395:63–88, 1984.

S.L. Foster and E. Reiplinger. Characteristics and control of transformer sound. *IEEE Transactions on Power Apparatus and Systems PAS-100*, pages 1072–1077, 1981.

C.R. Fuller. Active control of sound transmission/radiation from elastic plates by vibration inputs: 1. analysis. *Journal of Sound and Vibration*, 136(1):1–15, 1990.

C.R. Fuller. Active control of cabin noise - lessons learned ? In *5th International congress on sound and vibration*, Adelaide, Australia., December 1997. The University of Adelaide.

C.R. Fuller and S.J. Elliot. *Active control of vibration*. Book. Academic Press, New York, 1996.

C.R. Fuller, C.H. Hansen, and S.D. Snyder. Experiments on active control of sound radiation from a panel using a piezoceramic actuator. *Sound and vibration*, 150(2):179–190, 1991.

S. Gade. Sound intensity (part 1 theory). *Bruel & Kjaer Technical Review*, 3(3-39), 1982a.

S. Gade. Sound intensity (part 2 instrumentation and applications). *Bruel & Kjaer Technical Review*, 4:3–32, 1982b.

S. Gade. Sound intensity and its application in noise control. *Sound and Vibration*, pages 14–26, 1985.

J. Garcia-Bonito, M.J. Brennan, S.J. Elliott, A. David, and R.J. Pinnington. A novel high-displacement piezoelectric actuator for active vibration control. *Smart Materials and Structures*, 7:31–42, 1998.

J. Garcia-Bonito and S.J. Elliott. Local active control of diffracted diffuse sound fields. *Journal of the Acoustical Society of America*, 98(2):1017–1024, 1995a.

J. Garcia-Bonito and S.J. Elliott. Strategies for local active control in diffuse sound fields. In *Proceedings of Active 95*, pages 561–572, 1995b.

J. Garcia-Bonito, S.J. Elliott, and C.C. Boucher. Generation of zones of quiet using a virtual microphone arrangement. *Journal of the Acoustical Society of America*, 101(6):3498–3516, 1997.

G.P. Gibbs, R.L. Clark, D.E. Cox, and J.S. Vipperman. Radiation modal expansion: Application to structural acoustic control. *Journal of the Acoustical Society of America*, 107(1): 332–339, 2000.

J.A. Giordano. An experiment on optimisation of active noise control on a three-dimensional extended radiator. *Journal of Vibration and Acoustics*, 115:53–58, 1993.

C.G. Gordon. A method for prediciting the audible noise emissions from large outdoors power transformers. *IEEE Transactions on Power Apparatus and Systems*, PAS-98(3):1109–1112, 1979.

B. Gosselin, J.C. Fortin, and A. L'Esperance. Measurement of noise emitted by electrical substations - part 1: Measurement method. In *Proceedings of Internoise 92*, pages 771–774, 1992.

D. Guicking. On the invention of active noise control by paul lueg. *Journal of the Acoustical Society of America*, 87:2251–2254, 1990.

D. Guicking. Acitve noise control a review based on patent specifications. In *Proceedings of Internoise 93*, pages 153–159, 1993.

C. Guigou and C.R. Fuller. Adaptive feedforward and feedback methods for active/passive sound radiation control using smart foam. *Journal of the Acoustical Society of America*, 104 (1):226–230, 1998.

J. Hald. A power controlled active noise cancellation technique. In *International Symposium on Active Control of Sound and Vibration*, pages 285–290, 1991.

C.H. Hansen. Active noise control from laboratory to industrial implementation. In *Proceedings of Noise-Con 97*, pages 3–38, 1997.

C.H. Hansen, X. Qiu, and X. Li. Feasibility study on acoustic noise control of power transformers. Technical report, Technical research report for Electricity Supply Association of Australia Ltd, Contract No. 97007, 1997.

C.H. Hansen, M.T. Simpson, and B.S. Cazzolato. Genetic algorithms for active sound and vibration control. In *Proceedings of IEE Inter-Active 99*, page http://www.iee.org.uk/Control/active.htm, 1999.

C.H. Hansen and S.D. Snyder. *Active control of noise and vibration.* E&FN Spon, London, 1997.

S. Haykin. *Adaptive filter theory*. Prentice Hall, Englewood Cliffs, New Jersey, 1986.

E. Henriksen. Adaptive active control of structural vibration by minimisation of total supplied power. In *Internoise 96*, pages 1615–1618. International Congress on Noise Control Engineering, 1996.

N. Hesselmann. *Ueber die Kompensation von Schallfeldern durch sekundaere Schallquellen.* Ph.D. Dissertation, Rheinisch-Westfaelischen Technischen Hochschule, Aachen, Germany, 1976.

N. Hesselmann. Investigation of noise reduction on a 100kva transformer tank by means of active methods. *Journal of Applied Acoustics*, 11:27–34, 1978.

R. Heydt, R. Pelrine, J. Joseph, J. Eckerle, and R. Kornbluh. Acoustical performance of an electrostrictive polymer film loudspeaker. *Journal of the Acoustical Society of America*, 107 (2):833–839, 2000.

C.Q. Howard. *Active isolation of machinery vibration from flexible structures*. Ph.D. Dissertation, University of Adelaide, Australia, 1999.

Z. Hu. The use of reciprocity theory in the transformer noise identification. In *Proceedings of Internoise 95*, pages 1153–1156, 1995.

Y.D. Huang and C.T. Chen. A derivation of the normal equation in fir wiener filters. *IEEE Transactions on Acoustics, Speech and Signal Processing*, ASSP-37:759–760, 1989.

INCE. Technical assesment of upper limits of noise in the workplace. *Noise News International*, 5(4):203–216, 1987.

ISO-1999. Acoustics: Determination of occupational noise exposure and estimation of noise-induced hearing impairment. International Standards Organisation, 1990.

M.J.M.' Jessel. Some evidences for a general theory of active sound absorption. In *Proceedings of Internoise 79*, pages 169–174, September 1979.

M.J.M. Jessel and O.L. Angevine. Active noise attenuation of a complex noise source. In *Proceedings of Internoise 80*, pages 689–694, December 1980.

S. Johanson and M. Winberg. A new active headset for helicopter applications. In *5th International congress on sound and vibration.* The University of Adelaide, 1997.

B.D. Johnson and C.R. Fuller. Broadband control of plate radiation using a piezoelectric double-amplifier active-skin and structural acoustic sensing. *Journal of the Acoustical Society of America*, 107(2):876–884, 2000.

M.E. Johnson. *Active control of sound transmission.* Ph.D. Dissertation, The University of Southampton, 1996.

M.E. Johnson and S.J. Elliot. Active control of sound radiation from vibrating surfaces using arrays of discrete actuators. *Sound and Vibration*, 207(5):743–759, 1997.

D.C. Kammer and L. Yao. Enhancment of on-orbit modal identification of large space structures through sensor placement. *Sound and Vibration*, 171:119–139, 1994.

S. Kang and Y. Kim. Active control noise control by sound power. In *Proceedings of Active 95*, pages 465–476, 1995.

S.W. Kang and Y.H. Kim. Active intensity control for the reduction of radiated duct noise. *Sound and Vibration*, 201(5):595–611, 1997.

S.K. Katsikas, D.T. Tsahalis, D.A. Manolas, and S. Xanthakis. Genetic algorithms for active noise control. In *Proceedings of Internoise 93*, pages 167–170, 1993.

A.J. Kempton. The ambiguity of acoustic sources - a possibility for active control? *Journal of Sound and Vibration*, 48:475–483, 1976.

C.D. Kestell. *Active control of sound in a small single engine aircraft with virtual error sensors.* Ph.D. Dissertation, University of Adelaide, 2000.

C.D. Kestell and C.H. Hansen. An overview of active noise control. In *did this print*, melborne, Australia, 1998. Safety in Action.

C.D. Kestell, C.H. Hansen, and B.S. Cazzolato. Active noise control with virtual sensors in a narrow duct. *International Journal of Acoustics and Vibration*, 5(2):1–14, 2000.

K. Kido and S. Onoda. Automatic control of acoustic noise emitted from power transformer by synthesising directivity. Series b: Technology. part 1: Reports of the institute of electrical communication (riec), Research Institutes Tohoku University, Sendai, Japan, 1972.

S.J. Kim and J.D. Jones. Optimal design of piezoactuators for active noise and vibration control. *AIAA Journal*, 29(12):2047–2053, 1991.

S.M. Kim and M.J. Brennan. Active control of harmonic sound transmission into an acoustic enclosure using both structural and acoustic radiators. *Journal of the Acoustical Society of America*, 107(5):2523–2534, 2000.

A. Kinoshite and H. Aoki. Active noise control system for automotive vehicle. Patent, 1993. Patent No. 5,245,664.00.

A.S. Knyasev and B.D. Tartakovskii. Abatement of radiation from flexurally vibrating plates by means of actiev local dampers. *Soviet Physics*, 13(1):115–117, 1967.

G.H. Koopmann, L. Song, and J.B. Fahnline. A method for computing acoustic fields based on the principle of wave superposition. *Journal of the acoustical society of America*, 86(6): 2433–2438, 1989.

G. Krishnappa and J.M. McDougall. Sound intensity distribution and energy flow in the near-field of a clamped circular plate. *Journal of Vibration, Acoustics, Stress, and Reliability in Design*, 111:465–471, 1989.

U.R. Kristiansen. A numerical study of the acoustic intensity distribution close to a vibration membrane. *Sound and Vibration*, 76(2):305–309, 1981.

S.M. Kuo and D.R Morgan. *Active Noise Control Systems: Algorithm and DSP Implementations*. Wiley, 1996.

A.V. Lambert. Geraeuschdaempfung an transformeren. *Electrical Engineering*, page 1105, 1951.

C. Laroche, J.M. Rouffet, B. Gosselin, and J. Fortin. Measurement of noise emitted by electrical substations - part 2: Measurement system. In *Proceedings of Internoise 92*, pages 775–778, 1992.

C.K. Lee and F.C. Moon. Modal sensors/actuators. *ASME Journal of Applied Mechanics*, 57:434–441, 1990.

A. Leissa. *Vibration of Plates*. Acoustical Society of America, 1993.

X. Li. *Physical systems for the active control of transformer noise*. Ph.D. Dissertation, The University of Adelaide, 2000.

X. Li, C.H. Hansen, and X. Qiu. Design of curved panel sources for active control of sound radiated by transformers. In *Fifth international congress on sound and vibration*, 1997.

X. Li, X. Qiu, R. Gu, R. Koehler, and C.H. Hansen. Active control of large electrical transformer noise using near-field error sensing. In *AAS Conference 99*, 1999a.

X. Li, X. Qiu, and C.H. Hansen. Active control of sound radiated from structures using near-field error sensing. In *Active 99, Fort Lauderdale*, pages 399–410, 1999b.

T.W. Lim. Actuator/sensor placement of modal parameter identification of flexible structures. *Modal Analysis: The International Journal of Analytical and Experimental Modal Analysis*, 8:1–13, 1993.

C. Liu and F.A. Tasker. Sensor placement for multi-input multi-output dynamic identification. In *Proceedings of AIAA/ASME/ASCE/AHS Structures, Structural Dynamics & Materials Conference*, pages 3327–3337, 1995.

P. Lueg. Process of silencing sound oscillations. Patent, 1936. Number 2043416, US Patent Office.

G. Magiante. Active sound absorption. *Journal of the Acoustical Society of America*, 61(6): 1516–1523, 1977.

G. Magiante and J.P. Vian. Application du principe de huygens aux absorbeurs acoustiques actifs. - ii. - approximations du principie de huygens. *Acustica*, 37(3), 1977.

J.P. Maillard and C.R. Fuller. Comparison of two structural sensing approaches for active structural acoustic control. *Journal of the Acoustical Society of America*, 103(1):396–400, 1998.

D.A. Manolas, T. Gialamas, and D.T. Tsahalis. A genetic algorithm for the simultaneous optimization of the sensor and actuator positions for an active noise and/or vibration control system. In *Proceedings of Internoise 96*, pages 1187–1191, 1996.

T. Martin and A. Roure. Optimization of an active noise control system using spherical harmonics expansion of the primary field. *Journal of Sound and Vibration*, 201(5):577–593, 1997.

T. Martin and A. Roure. Active noise control of acoustic sources using sperical harmonics expansion and a genetic algorithm: Simulation and experiment. *Journal of Sound and Vibration*, 212(3):511–523, 1998.

P. Masson, A. Berry, and P. Micheau. A wavelet approach to the active structural acoustic control. *Journal of the Acoustical Society of America*, 104:1453–1465, 1998.

P. Masson, A. Berry, and J. Nicolas. Active structural acoustic control using strain sensing. *Journal of the acoustical society of America*, 102:1588–1599, 1997.

M. McLoughlin, S. Hildebrand, and Z. Hu. A novel active transformer quieting system. In *Proceedings of Internoise 94*, pages 1323–1326, 1994.

L. Meirovitch and H. Baruh. The implementation of modal filters for control of structures. *Journal of Guidance, Control and Dynamics*, 8:707–716, 1985.

V.L. Metcalf, C.R. Fuller, R.J. Silcox, and D.E. Brown. Active control of sound transmission/radiation from elastic plates by vibration inputs, 2. experiments. *Sound and Vibration*, 153(3):387–402, 1992.

R.S. Ming, J. Pan, M.P. Norton, S. Wende, and H. Huang. The sound-field characterisation of a power transformer. *Journal of Applied Acoustics*, 56:257–272, 1999.

D.R. Morgan. An adaptive modal-based active control system. *Journal of the acoustical society of America*, 89:248–256, 1991.

M.M. Morse and K.U. Ingard. *Theoretical Acoustics*. McGraw-Hill, 1968.

K. Naghshineh, L.P. Heck, J.A. Olkin, and J.W. Kamman. Evaluation of an actuator placement method for active noise control applications. *Journal of Vibrations and Acoustics*, 120: 875–879, 1998.

K. Naghshineh and G.H. Koopermann. A design method for achieveing weak radiator structures using active vibration control. *Journal of the acoustical society of America*, 92(2): 856–869, 1992.

K. Naghshineh and G.H. Koopermann. Active control of sound power using acoustic basis functions as surface velocity filters. *Journal of the acoustical society of America*, 93(3): 2740–2752, 1993.

M. Nam, S.I. Hayek, and S.D. Sommerfeldt. Active control of structural intensity in connected structures. In *Active 95*, pages 209–220. Institute of Noise Control Engineering, 1995.

P.J. Nashif and S.D. Sommerfeldt. An active control strategy for minimising the energy density in enclosures. In *Proceedings of Internoise 92*, pages 357–361, 1992.

P.A. Nelson, A.R.D. Curtis, S.J. Elliott, and A.J. Bullmore. The active minimization of harmonic enclose sound fields part 1: Theory, part 2: A computer simulation part 3,: Experimental verification. *Journal of Sound and Vibration*, 117(1):1–13, 15–33, 35–58, 1987a.

P.A. Nelson, A.R.D. Curtis, S.J. Elliott, and A.J. Bullmore. The active minimization of harmonic enclosed sound fields, part I: Theory. *Journal of Sound and Vibration*, 117(1): 1–13, 1987b.

P.A. Nelson, A.R.D. Curtis, S.J. Elliott, and A.J. Bullmore. The minimum power output of free field point sources and the active control of sound. *Journal of Sound and Vibration*, 116 (3):397–414, 1987c.

P.A. Nelson and S.J. Elliott. The minimum power output of a pair of free field monopole sources. *Journal of Sound and Vibration*, 105(1):173–178, 1986.

P.A. Nelson and S.J. Elliott. *Active Control of Sound.* Academic Press, London, 1992.

B. Noble. *Applied linear algebra.* Prentice Hall, Englewood Cliffs, New Jersey, 1969.

S. Obinata, G.m Kizawa and H. Doki. Sensor placement and model reduction in stabililzation of flexible structures. *Transactions of the Japanese Society of Mechanical Engineering, Series C*, 59:75–80, 1993.

H.F. Olson. System responsive to the energy flow of sound waves. Patent, 1932. Number 1,892,644, US Patent Office.

H.F. Olson. Electronic control of noise, vibration and reverberation. *Journal of the Acoustical Society of America*, 28:966–972, September 1956.

H.F. Olson and E.G. May. Electronic sound absorber. *Journal of the Acoustical Society of America*, 25:1130–1136, 1953.

J. Pan, S.D. Snyder, C.H. Hansen, and C.R. Fuller. Active control of far-field sound radiated by a rectangular panel. *Journal of the acoustical society of America*, 91:2056–2066, 1992.

Y.C. Park and S.D. Sommerfeldt. Active control of broadband random noise in rectangular enclosures. In *Proceedings of Internoise 96*, 1996.

Y.C. Park and S.D. Sommerfeldt. Global attenuation of broadband noise fields using energy density control. *Journal of the Acoustical Society of America*, 101(1):350–359, 1997.

J.W. Parkins, S.D. Sommerfeldt, and J. Tichy. Error analysis of a practical energy density sensor. *Journal of the Acoustical Society of America*, 108(1):211–222, 2000a.

J.W. Parkins, S.D. Sommerfeldt, and J. Tichy. Narrowband and broadband active control in an enclosure using acoustic energy density. *Journal of the Acoustical Society of America*, 108 (1):192–202, 2000b.

A.D. Pierce. *Acoustics: An introduction to its physical principles and applications*. Acoustical Society of America, 1989 edition, 1989.

L.D. Pope. On prediction of propeller tone sound levels and gradients in an airplane cabin. *Journal of the Acoustical Society of America*, 88(6):2755–2765, 1990a.

L.D. Pope. On the prediction of propeller tone sound levels and gradients in an airplane cabin. *Journal of the Acoustical Society of America*, 88(6):2755–2765, 1990b.

L.D. Pope, E.G. Wilby, and J.F. Wilby. Propeller aircraft interior noise model, part i: Analytical model. *Journal of Sound and Vibration*, 118(3):449–467, 1987a.

L.D. Pope, E.G. Wilby, C.M. Willis, and W.H. Mayes. Aircraft interior noise models: Sidewall trim, stiffened structures, and cabin acoustics with floor partition. *Journal of Sound and Vibration*, 89(3):371–417, 1983.

L.D. Pope, C.M. Willis, and W.H. Mayes. Propeller aircraft interior noise model, part ii: Scale-model and flight-test comparisons. *Journal of Sound and Vibration*, 118(3):469–493, 1987b.

S. Pottie and D. Botteldooren. Optimal placement of secondary sources for active noise control using a genetic algorithm. In *Proceedings of internoise 96*, 1996.

X. Qiu and C.H. Hansen. An adaptive sound intensity control algorithm for active control of transformer noise. In *Proceedings of the Fifth International Congress on Sound and Vibration*, 1997.

X. Qiu and C.H. Hansen. Secondary acoustic source types for active noise control in free field: monopoles or multipoles? *Sound and Vibration*, 232(5):1005–1009, 2000.

X. Qiu, C.H. Hansen, and X. Li. A comparison of near-field acoustic error sensing strategies for the active control of harmonic free field sound radiation. *Sound and Vibration*, 215(1): 81–103, 1998.

X. Qiu, X. Li, and C.H. Hansen. A decomposition of the sound field radiated by a large transformer. In *Proceedings of Internoise 99*, pages 1793–1796, 1999.

J. W. S. Rayleigh. *Theory of Sound: Volumes I and II.* reprinted by Dover, New York, 1937, 1887.

K.M. Reichard, D.C. Swanson, and S.M. Hirsch. Control of acoustic intensity using a frequency domain filtered-x algorithm. In *Active 95*, pages 395–406. Institute of Noise Control Engineering, 1995.

E. Reiplinger. The effects of magnetostrictive on generation of noise by transformers. *CIGRE*, 126, 1978.

E. Reiplinger, M. Schwarzkopf, and A. Stetler. Investigation for the determination of sound radiation from network transformers. *Deutsche Arbeitsgemeinschaft fuer Akustik*, 1978.

C.F. Ross. Experiments on the active control of transformer noise. *Journal of Sound and Vibrations*, 61(4):473–480, 1978.

C.F. Ross. An algorithm for designing a broadband active sound control system. *Journal of sound and vibration*, 80(3):373–380, 1982.

D.J. Rossetti and M.A. Norris. A comparison of actuation and sensing techniques for aircraft cabin noise control. *Noise Control Engineering Journal*, 44(1):53–58, 1996.

L.H. Royster, J.D. Royster, and W.G. Thomas. Representative hearing levels by race and sex in north carolina industry. *Journal of the Acoustical Society of America*, 68:551, 1980.

C.E. Ruckman and C.R. Fuller. Optimizing actuator locations in feedforward active control systems using subset selection. In Ruckmanetal, editor, *Recent Advances in Active Control of Sound and Vibration*, volume 2nd, pages S122–S133, 1993.

C.E. Ruckman and C.R. Fuller. Optimizing actuator locations in active noise control systems using subset selection. *Sound and Vibration*, 186(3):395–406, 1995.

A. Sakuta, J. Kowalewski, and M. Colbert. Assessment thechnique for controlling trasnformer noise. In *Proceedings of Internoise 92*, pages 783–790, 1992.

A.J. Sallowayetal and C.E. Millar. Active vibration and noise control. *GEC Review.*, 11(3): 138–145, 1996.

J. Savard. The application of multi-spectrum technology to transformer noise identification. In *Proceedings of Internoise 92*, pages 787–790, 1992.

W.M. Schuller. Transformer noise. *Noise Control Engineering*, 18(3):111–116, 1982.

M.W. Schultz and R.J. Ringlee. Some characteristics of audible noise of power transformers and their relationship to audibility criteria and noise ordinances. *AIEE*, 60-175, 1960.

T.J. Schultz. Acoustic wattmeter. *Journal of the Acoustical Society of America*, 28:693–699, 1956.

L. Schwartz. *Cours d' Analyse*, volume 2. Hermann, 1967.

A.E. Schwenk, S.D. Sommerfeldt, and S.I. Hayek. Adaptive control of structural intensity associated with bending waves in a beam. *Journal of the Acoustical Society of America*, 96: 2826–2835, 1994.

P. Sergent and D. Duhamel. Optimal placement with the minimax criterion for active control of a one-dimensional sound field. *Sound and Vibration*, 207(4):537–566, 1997.

J.J Shynk. Frequency-domain and multirate adaptive filtering. *IEEE Signal Processing Magazine*, 1:14–37, January 1992.

M.T. Simpson and C.H. Hansen. Use of genetic algorithms to optimize vibration actuator placement for active control of harmonic interior noise in a cylinder. *Noise Control Engineering Journal*, 44(4):169–184, 1996.

R.H. Small. Closed-box loudspeaker systems-part 1: Analysis. *Journal of the Audio Engineering Society*, 20(10):798, 1972a.

R.H. Small. Simplified loudspeaker measurements at low frequencies. *Journal of the Audio Engineering Society*, 20(1):28, 1972b.

R.H. Small. Closed-box loudspeaker systems-part 2: Synthesis. *Journal of the Audio Engineering Society*, 21(1):11, 1973.

S.W. Smith. *The Scientist and Engineer's Guide to Digital Signal Processing*. California Technical Publishing, 1997.

S.D. Snyder, , and C.H. Hansen. Mechanisms of active noise control by vibration sources. *Sound and vibration*, 147(3):519–525, 1991a.

S.D. Snyder, , and C.H. Hansen. Using multiple regression to optimize active noise control system design. *Sound and vibration*, 148(4):537–542, 1991b.

S.D. Snyder. *The active noise control primer*. Springer Verlag, 1999.

S.D. Snyder, N.C. Burgan, and N. Tanaka. An acoustic-based modal filtering approach to sensing system design for active control of structural acoustic radiation: theoretical development. *submitted to Journal of Mechanical Systems and Signal Processing*, 2001.

S.D. Snyder and C.H. Hansen. The design of systems to actively control periodic sound transmission into enclosed spaces, part 1: Analytical models. *Journal of Sound and Vibration*, 170(4):433–449, 1994a.

S.D. Snyder and C.H. Hansen. The design of systems to actively control periodic sound transmission into enclosed spaces, part 2: Mechanisms and trends. *Journal of Sound and Vibration*, 170(4):451–472, 1994b.

S.D. Snyder, C.H. Hansen, and N. Tanaka. Shaped vibration sensors for feedforward control of structural radiation. In *Proceedings of the Second Conference on Recent Advances in Active Control of Sound and Vibration, Blacksburg, USA*, pages 177–188, 1993.

S.D. Snyder and N. Tanaka. On feedforward active control of sound and vibration using vibration error signals. *Journal of the Acoustical Society of America*, 94:2181–2193, 1993a.

S.D. Snyder and N. Tanaka. To absorb or not to absorb: Control source power output in active noise control systems. *Journal of the acoustical society of America*, 94:185–195, 1993b.

S.D. Snyder, N. Tanaka, K. Burgemeister, and C.H. Hansen. Direct-sensing of global error criteria for active noise control. In *Proceedings of Active 95*, pages 849–859, 1995a.

S.D. Snyder, N. Tanaka, and Y. Kikushima. The use of optimally shaped piezo-electric film sensors in the active control of free field structural radiation, part 1: Feedforward control. *Journal of Vibrations and Acoustics*, 117:311–322, July 1995b.

S.D. Snyder, N. Tanaka, and Y. Kikushima. The use of optimally shaped piezo-electric film sensors in the active control of free field structural radiation, part 2: Feedback control. *Journal of Vibration and Acoustics*, 118:112–121, January 1996.

S.D. Sommerfeldt and P.J. Nashif. A comparision of control strategies for minimising the sound field in enclosures. In *Proceedings of Noise-Con 91*, pages 299–306, 1991.

S.D. Sommerfeldt and P.J. Nashif. Energy based control of the sound field in enclosures. In *The Second International Congress on Recent Developments is Air- and Structure-Borne Sound and Vibration*, pages 361–368, 1992.

S.D. Sommerfeldt and P.J. Nashif. An adaptive filtered-x algorithm for energy based active control. *Journal of the Acoustical Society of America*, 96(1):300–306, 1994.

S.D. Sommerfeldt and J. Parkins. Active control of energy density in three dimensional enclosures. *Journal of the Acoustical Society of America*, 95(5):2989, 1994.

S.D. Sommerfeldt, J.W. Parkins, and Y.C. Park. Global active noise control in rectangular enclosures. In *Proceedings of Active 95*, pages 477–488, 1995.

L. Song, G.H. Koopmann, and J.B. Fahnline. Active control of the acoustic radiation of a vibrating structure using a superposition formulation. *Journal of the acoustical society of America*, 89(6):2786–2792, 1991a.

L. Song, G.H. Koopmann, and J.B. Fahnline. Numerical errors associated with the method of superposition for computing acoustic fields. *Journal of the acoustical society of America*, 89(6):2625–2633, 1991b.

J.Q. Sun, S.M. Hirsch, and V. Jayachandran. Sensor systems for global vibration and noise control. *Journal of the acoustical society of America*, 103(3):1504–1509, 1998.

C. Sung and C.T. Jan. Active control of structurally radiated sound from plates. *Journal of the acoustical society of America*, 102:370–381, 1997.

W. Svensson and P.A. Wilberg. Optimising the placement of microphones and loudspeakers in an aeroplane mounted active noise control system using stochastic search methods. In *Noise-Con 98*, pages 283–288, 1998.

D. Swanson. Active control of acoustic intensity using a frequency domain filtered-x algorithm. In *Proceedings of Internoise 94*, pages 1253–1258, 1994.

C.C. Tan and C.I. Hird. Active control of the sound field of a constrained panel by an electromagnetic actuator - an experimental study. *Journal of Applied Acoustics*, 52(1):31–51, 1997.

N. Tanaka and Y. Kikushima. Active modal control and its robustness using point sensors and point actuators. *JSME International Journal, series C*, 42(1):54–61, 1999a.

N. Tanaka and Y. Kikushima. Active vibration control of a distributed-parameter structure (proposition of cluster control). *JSME International Journal, series C*, 42(1):10–17, 1999b.

N. Tanaka, Y. Kikushima, M. Kuroda, and S.D. Snyder. Active control of acoustic power radiated from a vibrating planar structure using smart sensors (acoustic power suppression using adaptive feedforward control). *JSME International Journal, series C*, 39(1):49–57, 1996a.

N. Tanaka, S.D. Snyder, and C.H. Hansen. Distributed parameter modal filtering using smart sensors. *Journal of Vibrations and Acoustics*, 118:630–640, October 1996b.

A.M. Teplitzky. Electric utility noise abatement. In *Proceedings of Internoise 95*, pages 165–168, 1995.

H.M. Thornton. *Active power minimisation in the free field using a finite number of error sensors*. PhD thesis, University of Southampton, England, 1988.

M.O. Tokhi. Tutorial on active noise control. In *Proceedings of Fifth International Congress on Sound and Vibration*, 1997.

M.O Tokhi and R.R. Leitch. *Active Noise Control*. Clarendon Press, 1992.

D.T. Tsahalis, S.K. Katsikas, and D.A. Manolas. A genetic algorithm for optimal positioning of actuators in active noise control: results from the asanca project. In *Proceedings of Internoise 93*, pages 83–88, 1993.

G.O. Usry, P. Saha, J. Hadden, and A. Pierce. Prediction of far field sound radiation from transformers. *IEEE Transactions on Power Apparatus and Systems*, PAS-99(1):358–364, 1980.

A.I. Vyalyshev, A.I. Dubinin, and B.D. Tartakovshii. Active acoustic reduction of a plate. *Soviet Physics*, 32(2):96–98, 1986.

B. Wang. Applications of genetic algorithms to the optimum design of active control system. *Proceedings of Internoise 93*, pages 231–236, 1993.

B. Wang. Optimal placement of microphones and piezoelectric transducer actuators for far-field sound radiation control. *Journal of the Acoustical Society of America*, 99(5):2975–2984, 1996.

B. Wang, R.A. Burdisso, and C.R. Fuller. Optimal placement of piezoelectric actuators for active structural acoustic control. *Journal of Intelligent Material, Systems and Structures*, 5: 67–77, 1994.

B. Wang and C.R. Fuller. Near-field pressure, intensity, and wave-number distributions for active structural acoustic control of plate radiation: theoretical analysis. *Journal of the Acoustical Society of America*, 92:1489–1498, 1991.

B. Wang, C.R. Fuller, and E.K. Dimitriadis. Active control of noise transmission through rectangular plates using multiple piezoelectric or point actuators. *Journal of the Acoustical Society of America*, 90:2820–2830, 1991a.

B. Wang, C.R. Fuller, and E.K. Dimitriadis. Active control of structurally radiated noise using multiple piezoelectric actuators. *AIAA Journal*, 29(2):1802–1809, 1991b.

G.E. Warnaka. Active attenuation of noise - the state of the art. *Noise Control Engineering*, 18:100–110, 1982.

B. Widrow and S.D. Stearns. *Adaptive Signal Processing*. Prentice-Hall, 1985.

E.G. Williams. A series expansion of the acoustic power radiated from planar sources. *Journal of the Acoustical Society of America*, 73:1520–1524, 1983.

L. Yao, W.A. Sethares, and D.C. Kammer. Sensor placement for on-orbit modal identification via a genetic algorithm. *Journal of AIAA*, 31:1922–1928, 1993.

J.M. Zalas and J. Tichy. Active attenuation of propeller blade pass noise. Technical Report CR-172386, NASA, 1984.

A.C. Zander. *Influence of sensor and source on active noise control systems*. Ph.D. Dissertation, University of Adelaide, Australia, 1994.

A.C. Zander and C.H. Hansen. A comparison of error sensing strategies for the active control of duct noise. *Journal of the Acoustical Society of America*, 94:841–848, 1993.

D.C. Zimmermann. A darwinian approach to the actuator number and placement problem with non-negligible actuator mass. *Mechanical Systems and Signal Processing*, 7(4):363–374, 1993.

# Appendix A

# Intensity definitions

## A.1 Introduction

This thesis has focused on the potential of a move away from pressure sensing and to cost functions based on energy for free space active noise control.

For more than 20 years research into enclosed sound field error sensing strategies based on energy (potential or kinetic energy) or energy flow (power and intensity) have been investigated and shown in some cases to produce a greater level of control over a greater region than simple pressure sensors. More recently, driven in part by the need for remedial noise control on installed large electrical transformers, research has been undertaken to investigate energy based error sensing strategies in the active control of free field noise problems. Problems arising in far field sensing, such as poor controller stability due to a poor signal to noise ratio, have lead to some research into near field sensing strategies. However, the use of traditional pressure error sensors does guarantee that far field pressure reductions accompany near field error signal minimisation.It is thought that intensity error sensing may provide a viable alternative.

## A.2 Definition

Sound intensity is a vector quantity defined as (Bies and Hansen (1996)) the product of the sound pressure and the component of the particle velocity in the direction of the intensity vector. It is a measure of the rate at which work is done on an acoustic medium by an advancing sound wave. The direction of the intensity vector is arbitrary, and selected to suit the problem. The instantaneous intensity vector $\mathbf{I}_d(\mathbf{r},t)$ at position $\mathbf{r}$ and time $t$ in the desired direction of the unit vector $\hat{\mathbf{I}}_d$ as shown in Figure A.1 is given by

$$\mathbf{I}_d(\mathbf{r},t) = p(\mathbf{r},t)\mathbf{u}_d(\mathbf{r},t) \tag{A.1}$$

where $p(\mathbf{r},t)$ is the sound pressure at position $\mathbf{r}$ and time $t$ and $\mathbf{u}_d(\mathbf{r},t)$ is the component of the particle velocity in the desired direction $\hat{\mathbf{I}}_d$ where $\mathbf{u}_d$ is the projection of the radial particle velocity $\mathbf{u}$ onto $\mathbf{I}_d$ given by

$$\mathbf{u}_d(\mathbf{r},t) = proj_{\mathbf{I}_d}\mathbf{u}(\mathbf{r},t) = (\mathbf{u} \bullet \mathbf{I}_d)\mathbf{I}_d \tag{A.2}$$

and $\mathbf{u}(\mathbf{r},t)$ is the particle velocity and $cos\theta = \frac{|\mathbf{I}_d|}{|\mathbf{I}|}$. Or alternatively the radial (with respect to the source) instantaneous intensity vector is given by

$$\mathbf{I}(\mathbf{r},t) = p(\mathbf{r},t)\mathbf{u}(\mathbf{r},t) \tag{A.3}$$

and hence the instantaneous intensity vector $\mathbf{I}_d(\mathbf{r},t)$ at position $\mathbf{r}$ and time $t$ in the desired direction of the unit vector $\hat{\mathbf{I}}_d$ is given by the projection of $\mathbf{I}$ onto $\mathbf{I}_d$ as

$$\mathbf{I}_d(\mathbf{r},t) = proj_{\mathbf{I}}\mathbf{I}_d = (\mathbf{I}_d \bullet \mathbf{I})\mathbf{I} \tag{A.4}$$

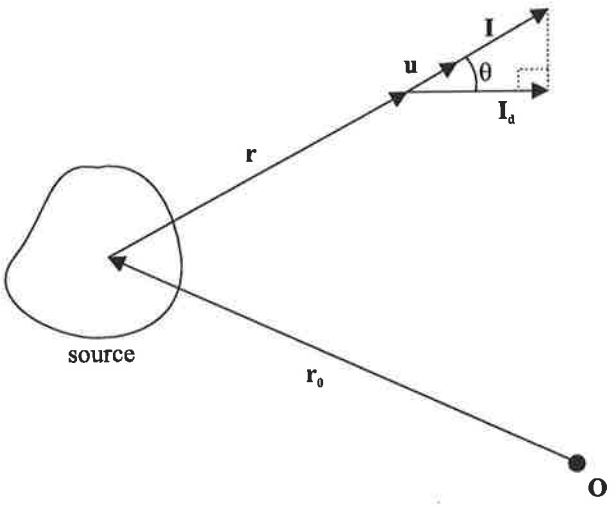


*Figure A.1: Intensity at location* $\mathbf{r}$ *in the direction of* $\mathbf{I}_d$ *due to the action of an acoustic source.*

## A.3 Active and reactive intensity

Consider the case of single frequency sound. The sound pressure at position $\mathbf{r}$ from the source centre (as shown in Figure A.1) and time $t$ can be expressed as the real part of a complex exponential as

$$p(\mathbf{r},t) = P(\mathbf{r})\mathbf{Re}\left\{e^{jk(ct+\mathbf{r}+\theta/k)}\right\} \tag{A.5}$$

where the angular frequency $\omega = kc$, $P(\mathbf{r})$ is the real pressure amplitude and $\theta$ is the phase. The complex notation is used here to simplify the appearance of the formula. By rewriting the phase to include the $k\mathbf{r}$ as $\theta_p(\mathbf{r}) = k\mathbf{r} + \theta$ equation (A.5) can be written as

$$p(\mathbf{r},t) = P(\mathbf{r})\mathbf{Re}\left\{e^{j(\omega t+\theta_p(\mathbf{r}))}\right\} \tag{A.6}$$

Similarly, the particle velocity can be expressed as

$$\mathbf{u}(\mathbf{r},t) = \mathbf{U}(\mathbf{r})\mathbf{Re}\left\{e^{jk(ct+\mathbf{r}+\phi/k)}\right\} \tag{A.7}$$

where $\mathbf{U}(\mathbf{r})$ is the real particle velocity amplitude vector in the normal direction and $\phi$ is the phase. As with equation (A.6), equation (A.7) can be rewritten as

$$\mathbf{u}(\mathbf{r},t) = \mathbf{U}(\mathbf{r})\mathbf{Re}\left\{e^{j(\omega t+\theta_u(\mathbf{r}))}\right\} \tag{A.8}$$

where $\theta_u(\mathbf{r}) = k\mathbf{r}+\phi$. Applying the definition of the particle velocity in the normal direction and introducing the unit normal vector $\hat{\mathbf{n}} = \frac{\mathbf{r}}{r}$ where $r = |\mathbf{r}|$

$$\mathbf{u}(\mathbf{r},t) = \frac{-\hat{\mathbf{n}}}{j\omega\rho}\frac{\partial p(\mathbf{r},t)}{\partial r} \tag{A.9}$$

gives

$$\mathbf{u}(\mathbf{r},t) = \frac{\hat{\mathbf{n}}}{\omega\rho}\mathbf{Re}\left\{\left[-P\frac{\partial\theta_p}{\partial r}+j\frac{\partial P}{\partial r}\right]e^{j(\omega t+\theta_p)}\right\} \tag{A.10}$$

substituting equation (A.10) and (A.6) into (A.3) gives

$$\mathbf{I}(\mathbf{r},t) = \frac{-\hat{\mathbf{n}}}{\omega\rho}\left[P^2\frac{\partial\theta_p}{\partial r}cos^2(\omega t+\theta_p)+P\frac{\partial P}{\partial r}cos(\omega t+\theta_p)sin(\omega t+\theta_p)\right] \tag{A.11}$$

In equation (A.11) the first term is the product of the sound pressure and the in-phase component of the particle velocity and is defined as the active intensity. The second term is the product of sound pressure and the in-quadrature component of the particle velocity and is defined as the reactive intensity. The active intensity describes the acoustic energy that is transmitted to the far field. The reactive intensity is a measure of the energy stored in the sound field during each cycle, but not transmitted.

By applying standard trigonometric identities: the half-angle formula $cos^2\theta = \frac{1}{2}(1+cos2\theta)$ and double-angle formula $sin2\theta = 2sin\theta cos\theta$ equation (A.11) becomes

$$\mathbf{I}(\mathbf{r},t) = \frac{-\hat{\mathbf{n}}}{2\omega\rho}\left[P^2\frac{\partial\theta_p}{\partial r}(1+cos2(\omega t+\theta_p))+P\frac{\partial P}{\partial r}sin2(\omega t+\theta_p)\right] \tag{A.12}$$

It should be noted that the instantaneous intensity described in equation (A.12) is not linearly correlated with the original sound pressure. Equation (A.12) contains a sinusoid at double the original frequency $2\omega$. This has serious implications for the use of intensity error sensors in the time domain (Swanson (1994)). If a reference signal with good coherence with the error signal can not be found then a feedforward control system will not converge to the minimum error signal. Many authors have published on active vibration control using structural intensity error sensing strategies or active noise control using acoustic intensity error sensing (Hald (1991), Schwenk et al. (1994), Reichard et al. (1995), Sommerfeldt and Nashif (1994), Nam et al. (1995), Henriksen (1996), Kang and Kim (1997)), but to date no practical control system using intensity error sensing has been built. In the time domain coherence problems mentioned by Swanson (1994), have led to development of work-arounds such as the so called heterodyning technique (Howard (1999)) which allows for single frequency intensity control in the time domain. This technique uses a low-pass filter to filter out the $2\omega$ frequency component in the intensity signal, so that the resultant signal is linearly correlated with the reference signal.

Alternatively, substituting equations (A.6) and (A.8) into (A.3) gives the instantaneous intensity in the radial direction as

$$\mathbf{I}(\mathbf{r},t) = P\mathbf{U}cos(\omega t+\theta_p)cos(\omega t+\theta_u) \tag{A.13}$$

using trigonometric identities equation (A.13) can be written as

$$\mathbf{I}(\mathbf{r},t) = \frac{P\mathbf{U}}{2}[(1+cos2(\omega t+\theta_p))cos(\theta_p-\theta_u)+sin2(\omega t+\theta_p)sin(\theta_p-\theta_u)] \tag{A.14}$$

Taking the time-average or mean value of $\mathbf{I}(\mathbf{r},t)$ where the time-average of a function $F(t)$ is

given by

$$\langle F(t)\rangle = \lim_{T\to\infty}\frac{1}{T}\int_0^T F(t)dt \tag{A.15}$$

gives

$$\mathbf{I}(\mathbf{r}) = \frac{PU}{2}cos(\theta_p - \theta_u) \tag{A.16}$$

which also is the amplitude of the active intensity. The amplitude of the reactive intensity is given by equation (A.14) as

$$\mathbf{I}_r(\mathbf{r}) = \frac{PU}{2}sin(\theta_p - \theta_u) \tag{A.17}$$

If the complex notation for the sound pressure and particle velocity is kept, that is the sound pressure is given by $p(\mathbf{r},t) = Ae^{j\omega t}$ where $A$ is the complex pressure amplitude and the particle velocity is given by $\mathbf{u}(\mathbf{r},t) = Be^{j\omega t}$ where $B$ is the complex particle velocity amplitude, then the active intensity (or time-average intensity) can be written as

$$\mathbf{I}(\mathbf{r}) = \mathbf{Re}\{AB^*\} \tag{A.18}$$

and the reactive intensity amplitude is given by

$$\mathbf{I}_r(\mathbf{r}) = \mathbf{Im}\{AB^*\} \tag{A.19}$$

# Appendix B

# Derivation of pressure, velocity, intensity and power of a monopole source

## B.1 Acoustic pressure and particle velocity of a monopole source

Consider a small sphere with surface velocity amplitude $U = U_0 e^{j\omega t}$, oscillating at an angular frequency of ω rad/s, at the location defined by $r = |\mathbf{r}| = |\mathbf{r}_e - \mathbf{r}_q|$.

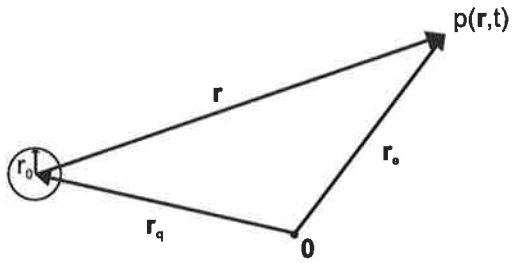


*Figure B.1: Small spherical source, with constant surface velocity amplitude.*

The spherical wave equation gives the expression for the acoustic pressure at a single tone of frequency $f$ Hz or angular frequency ω rad/s as (Bies and Hansen (1996))

$$p(\mathbf{r},t) = \frac{j\omega A\rho}{r} e^{j(\omega t - kr)} \tag{B.1}$$

and using the following equation (Morse and Ingard (1968))

$$\mathbf{u}(\mathbf{r},t) = -\frac{\partial}{\partial r}\frac{1}{\rho}\int p(\mathbf{r},t)dt \tag{B.2}$$

the particle velocity in the radial direction from the source at a single tone of frequency $f$ Hz or angular frequency $\omega$ rad/s as

$$\mathbf{u}(\mathbf{r},t) = \hat{n}\{\frac{A}{j\omega\rho r^2} e^{-j(\omega t - kr)} + \frac{A}{\rho c r} e^{j(\omega t - kr)}\} \tag{B.3}$$

where $\hat{n} = \mathbf{r}/r$ is the radial unit vector.

On the surface of the sphere the particle velocity equates to the surface velocity, at $r = r_0$,

$$\mathbf{u}(\mathbf{r}_0,t) = \hat{n} U_0 e^{j\omega t} \tag{B.4}$$

substituting equation (B.4) into (B.3) gives

$$U_0 = \frac{A}{j r_0 \rho \omega}\left(\frac{1}{r_0} + kj\right) e^{-jkr_0}$$

rearranging and taking the limit as $kr_0 \to 0$, such that the size of the sphere tends to a point and hence represents a point source,

the pressure amplitude is now given by

$$A = j\omega r_0^2 \rho U_0 \tag{B.5}$$

The volume velocity is given by product of the surface area and the r.m.s. time-averaged surface velocity amplitude (Bies and Hansen (1996)) as

$$Q = 4\pi r_0^2 \sqrt{\langle U^2 \rangle} \tag{B.6}$$

where

$$\langle U^2 \rangle = \lim_{T \to \infty} \frac{1}{T} \int_0^T U^2 dt \tag{B.7}$$

substituting $U = Re\{U_0 e^{j\omega t}\} = U_0 cos\omega t$, and $T = 2\pi/\omega$ gives

$$\langle U^2 \rangle = \frac{U_0^2}{2}$$

and hence the r.m.s. volume velocity or source strength is given by

$$Q = 4\pi r_0^2 \frac{U_0}{\sqrt{2}} \tag{B.8}$$

and hence the volume velocity is given by

$$q = Q\sqrt{2} \tag{B.9}$$

substituting (B.8) and (B.9) and (B.5) into (B.1) and (B.3) and ignoring the temporal components gives

$$p(r) = \frac{j\omega\rho q}{4\pi r} e^{-jkr} \tag{B.10}$$

and

$$\mathbf{u}(r) = \frac{q}{4\pi}\left(\frac{1}{r^2} + \frac{jk}{r}\right)e^{-jkr} \tag{B.11}$$

which describe the spatial pressure and particle velocity distributions of a monopole point source.

Now define an acoustic transfer impedance which is the complex number relating the complex pressure to the complex source strength of a point source (Nelson and Elliott (1992)) such that

$$p(r) = qZ(r) \tag{B.12}$$

For free field point sources

$$Z(r) = \frac{j\omega\rho e^{-jkr}}{4\pi r} \tag{B.13}$$

and define the velocity transfer impedance which is the complex number relating the complex particle velocity to the complex source strength of a point source as

$$\mathbf{u} = q\mathbf{H}(r) \tag{B.14}$$

For free field point sources

$$\mathbf{H}(r) = \frac{1}{4\pi}\left(\frac{1}{r^2} + \frac{jk}{r}\right)e^{-jkr} \tag{B.15}$$

## B.2 Active intensity and sound power

The active intensity of a monopole source in the direction of the particle velocity is given by

$$\mathbf{I} = \frac{1}{2} Re\{p^* \mathbf{u}\} \tag{B.16}$$

The sound power is defined as the amount of acoustic energy a source radiates per unit time. Its definition can be re-expressed in terms of the definition of sound intensity. Since the reactive intensity does not contribute to the far field radiated acoustic energy, the sound power can be expressed in terms of the active intensity alone as follows

$$W = \int_S (\frac{1}{2} Re\{p^* \mathbf{u}\}) \cdot \hat{n} dS \tag{B.17}$$

where the integral is over any surface $S$ that encloses the source or sources.

If the surface $S$ is taken to be the radius of the small sphere described in Figure B.1, and the limit as the radius of the sphere tends to zero is taken the sound power of a monopole source reduces to

$$W = \frac{1}{2} Re\{p^* q\} \tag{B.18}$$

where $p$ is the pressure at the surface and $q$ is the complex source strength.

Substituting (B.12) into (B.18) gives

$$W = \frac{1}{2} |q|^2 Re\{Z(r \to 0)\} \tag{B.19}$$

where

$$Z(r) = \frac{\omega^2 \rho}{4\pi c}\left(\frac{je^{-jkr}}{kr}\right) \tag{B.20}$$

$$= \frac{\omega^2 \rho}{4\pi c}\left(\frac{sinkr}{kr} + j\frac{coskr}{kr}\right) \tag{B.21}$$

as $kr \to 0$, $\frac{sinkr}{kr} \to 1$ and $\frac{coskr}{kr} \to 0$, hence

$$Z(r) = \frac{\omega^2 \rho}{4\pi c} \tag{B.22}$$

Therefore the sound power radiated by a monopole source can be expressed as

$$W = \frac{1}{2}|q|^2 \frac{\omega^2 \rho}{4\pi c} \tag{B.23}$$

# Appendix C

# Intensity measurement

## C.1 B&K Type 3360 sound intensity analysing system

### C.1.1 Introduction

Intensity measurement has a long history stretching back to the 1930's; see Olson (1932), Clapp and Firestone (1941) and Schultz (1956) as part of attempts to measure the sound power from a source. See Gade (1982a), Gade (1982b), Gade (1985) and Bruel and Kjaer (1993) for a review of intensity measurement and its application to noise control. The B&K Sound Intensity Analysing System Type 3360 consists of the sound intensity probe Type 3519, Sound Intensity Analyzer Type 2134 and Display Unit Type 4715. This system was used in manual control (see Chapter 3) and real control system (see Chapters 4, 5 and 6, which is described in detail in Appendix D). In the case of manual control of a single monopole in a free field, the sound intensity probe was positioned at the error sensor location and the single monopole control source gain and phase manually adjusted until the Display Unit showed a minimised sound intensity amplitude. When a real control system was employed a DC intensity signal from the sound intensity analyser was passed through a multiplier circuit where it was converted to

an AC signal by multiplication by a sine wave reference signal. This AC intensity signal was minimised by the control system.

### C.1.2 Measurement process

The B&K Type 3360 Sound Intensity Analysing System uses two closely spaced microphones and a finite difference approximation to calculate the time-averaged sound intensity $I_{av}$ in the direction $\overrightarrow{AB}$ (from $A$ to $B$) as

$$I_{av} = pv \tag{C.1}$$

where the $p$ is the average rms pressure between the two microphones given by

$$p = \frac{p_A + p_B}{2} \tag{C.2}$$

and $v$ is the particle velocity in the direction of $\overrightarrow{AB}$ can be approximated by integrating over time the difference in sound pressure of microphone $B$ to microphone $A$, separated by a distance $\Delta r$ (shown in Figure C.2) and is given by

$$v = -\frac{1}{\rho}\int \frac{p_B - p_A}{\Delta r} dt \tag{C.3}$$

where $\rho$ is the density of the acoustic medium (air) and $p_B - p_A$ is the pressure difference.

Figure C.1 shows the process of converting the sound pressure inputs at microphone $A$ and $B$ to the time-averaged sound intensity. The microphone signals are first put through a preamplifier, then an analogue to digital converter (ADC). At this point the signals are already separated into 1/3-octave bands by a 1/3-octave digital filter bank. The average of the two pressure

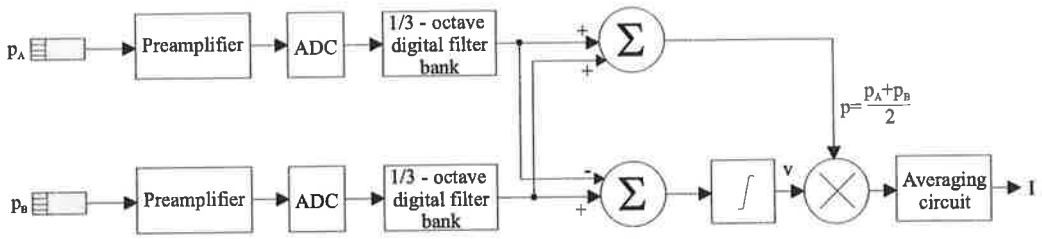


*Figure C.1: Method of calculating the time average sound intensity.*

signals is computed and their difference computed. The pressure difference is passed through an integrator to extract the estimation of the particle velocity. Then the average pressure is multiplied by the integrated pressure difference to give the quasi-instantaneous sound intensity. Finally the intensity signal is put through an averaging circuit, to give the time-averaged sound intensity. In the experiments described here, the analyser was set to exponentially average the instantaneous intensity in increments of 30 milliseconds. Which was the limit of the analyser and managed to provide a smoothly varying signal for the control system to process and remain stable.

### C.1.3 Calibration

The B&K Type 2134 Sound Intensity Analyzer was calibrated one microphone at a time using a standard pistonphone (Type 4220). Hence both microphone $A$ and $B$ were calibrated to $124dB$ with an accuracy of $\pm 0.15dB$ at the pistonphone operating frequency which was 250Hz. Temperature and barometric variations were neglected and the sound intensity signal was not corrected for these effects. Unlike newer analysers the Type 2134 does not use a purpose built calibrator (B&K Sound Intensity Calibrator Type 3541), which calibrates out phase mismatches in the pressure signal and also calibrates the pressure gradient. As such this method of measuring the sound intensity is not as accurate, however still useful to demonstrate the validity of the theoretical simulations presented.

### C.1.4 Measurement errors

By using a two microphone technique to measure the sound intensity a number of systematic errors are introduced, which limit the frequency range at which it can be used. The principal systematic error of the two microphone technique is the finite difference approximation used to estimate the particle velocity through the pressure gradient. This bias error $L_{\Delta r}$ (in dB) can

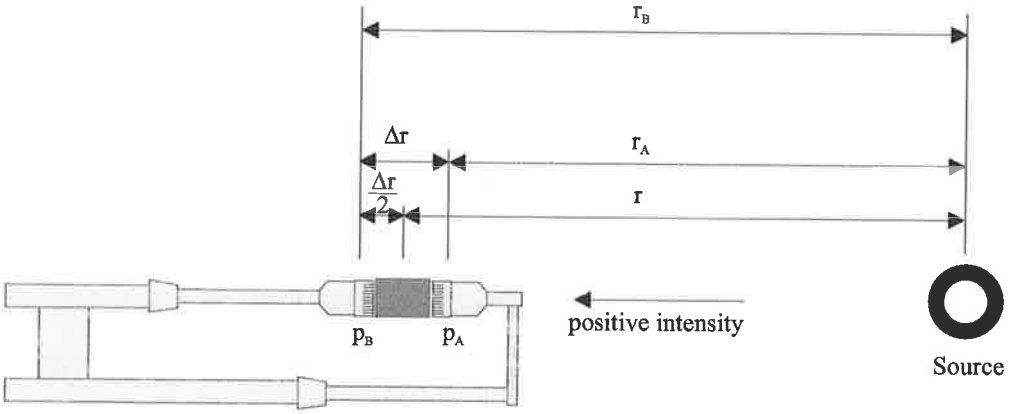


*Figure C.2: Configuration of the B&K Type 3519 Sound Intensity Probe.*

be calculated for ideal multipole sources (Bruel and Kjaer (1983)) as

$$L_{\Delta r} = 10log_{10}\left(\frac{sin k\Delta r}{k\Delta r}\frac{r^2}{r_A r_B}\right) \tag{C.4}$$

where $k$ is the wavenumber, $\Delta r = r_B - r_A$ is the microphone spacing and $r = r_B - \frac{\Delta r}{2}$ as shown in Figure C.2. An arbitrary positive direction can be assigned to the intensity signal. Arbitrary in the sense that it does not matter whether positive intensity is defined to be acoustic energy flow to or from the source or sources. Furthermore the B&K Type 3519 Intensity probe exhibits directional sensitivity. The most accurate measurements are produced by pointing the probe in direction of the source or sources. When $\Delta r \ll r$ equation (C.4) reduces to

$$L_{\Delta r} = 10log_{10}\left(\frac{sin k\Delta r}{k\Delta r}\right) \tag{C.5}$$

and hence the finite difference approximation underestimates the sound intensity at high frequencies. If the microphone spacing could be made as small as possible then the bias error by equation (C.5) would reduce. However a further problem exists. Phase mismatch between the two microphones increases the bias error at small microphone spacings. The influence on the bias error of the phase mismatch (Bruel and Kjaer (1983)) is given by

$$L_{\Delta r} = 10log_{10}\left(\frac{sin(k\Delta r - \varphi)}{k\Delta r}\right) \tag{C.6}$$

Phase mismatch also increases the bias error particularly at low frequencies. In the experiments described here the B&K Type 3519 Sound Intensity Probe used 1/2 inch B&K microphones at a fixed spacing of 50mm. The excitation frequency of all sources investigated (monopoles, plate and transformer) was 100Hz, hence from equation (C.6) the bias error due to a phase mismatch of $0.3^o$ at a microphone spacing of $\Delta r = 50mm$ and at the excitation frequency is less than 0.5dB. For a comprehensive error analysis of intensity measurements see Elliott (1981) and Fahy (1985).

## C.2 Frequency-domain intensity measurement

Swanson (1994) suggested an alternative control algorithm to the time-domain filtered-x LMS algorithm discussed in Appendix A, namely a frequency-domain filtered-X LMS algorithm (see Shynk (1992) for a complete description of this algorithm). This algorithm has been formulated to control acoustic intensity by Reichard et al. (1995) in ducts. This algorithm requires a different form of the acoustic intensity than the time-domain form presented in Appendix A, which has been approximated by the measurement procedure in Section C.1.2. For modern formulations of this technique see Chung (1978), Fahy (1977) and Fahy (1985).

The average sound pressure between the two microphones in the intensity probe (described in Section C.1.2) in the frequency-domain at location $\mathbf{r}$ and a frequency $\omega$ is given by

$$P(\mathbf{r},\omega) = \Gamma\{\frac{p_A(\mathbf{r},t)+p_B(\mathbf{r},t)}{2}\} = \frac{1}{2}\int_{-\infty}^{\infty}[p_A(\mathbf{r},t)+p_B(\mathbf{r},t)]e^{-j\omega t}dt = \frac{1}{2}[P_A(\mathbf{r},\omega)+P_B(\mathbf{r},\omega)] \tag{C.7}$$

where the Fourier transform is defined by

$$\Gamma\{f(t)\} = \int_{-\infty}^{\infty} f(t)e^{-j\omega t}dt \tag{C.8}$$

The particle velocity as measured by a two microphone intensity probe is given by

$$\mathbf{U}(\mathbf{r},\omega) = \Gamma\{\frac{-1}{j\omega\rho\Delta r}[p_B(\mathbf{r},t)-p_A(\mathbf{r},t)]\} = \frac{-[P_B(\mathbf{r},\omega)-P_A(\mathbf{r},\omega)]}{j\rho\omega\Delta r} = \frac{-1}{j\omega\rho\Delta r}\int_{-\infty}^{\infty}[p_B(\mathbf{r},t)-p_A(\mathbf{r},t)]e^{-j\omega t}dt \tag{C.9}$$

In the frequency-domain the active or time-averaged intensity is given by Fahy (1995) as

$$\mathbf{I}(\mathbf{r},\omega) = \mathbf{Re}\{G_{pu}(\mathbf{r},\omega)\} \tag{C.10}$$

where $G_{pu}(\mathbf{r},\omega)$ is the cross-spectrum of the pressure and particle velocity given by equations (C.7) and (C.9) and **Re** is the real part of $G_{pu}(\mathbf{r},\omega)$. The cross-spectrum of the pressure and particle velocity is defined by

$$G_{pu}(\mathbf{r},\omega) = \langle P^*(\mathbf{r},\omega)\mathbf{U}(\mathbf{r},\omega)\rangle \tag{C.11}$$

Equation (C.10) is the frequency-domain version of equation (A.18) and can be rewritten (Fahy (1995)) as

$$\mathbf{I}(\mathbf{r},\omega) = \frac{1}{\rho\omega\Delta r}\mathbf{Im}\{G_{p_A p_B}(\mathbf{r},\omega)\} \tag{C.12}$$

where $G_{p_A p_B}(\mathbf{r},\omega)$ is the cross-spectrum between microphone $A$ and $B$ and **Im** is the imaginary part of $G_{p_A p_B}(\mathbf{r},\omega)$. Equation (C.12) can also be written as

$$\mathbf{I}(\mathbf{r},\omega) = \frac{1}{\rho\omega\Delta r}\mathbf{Im}\{P_A(\mathbf{r},\omega)P_B^*(\mathbf{r},\omega)\} \tag{C.13}$$

Despite the frequency domain algorithm being around for almost a decade, no such control system has ever been built. In light of this it was decided to focus the experimental work on the time-domain intensity measurement technique.

This page intentionally contains only this sentence.

# Appendix D

# Controller

## D.1 Active intensity as an error signal

This section describes a method of generating a signal which is proportional to the total active intensity at the excitation frequency and is suitable for use as an error signal with an existing feedforward active noise controller, using a filtered-X LMS adaptive algorithm. Sound pressure is a time varying quantity and hence can be directly used as an error signal in a traditional filtered-X LMS algorithm. The total active intensity (time-averaged intensity) can be measured by several techniques (Fahy (1995)), the most common technique involves a phase-matched microphone pair. This technique requires post processing of the microphone signals (see Appendix C) to combine them into a single measure. The measured time-averaged intensity which is a DC (time invariant) signal can not be used in a traditonal filtered-X LMS algorithm. To use active intensity as an error signal this DC signal must be modified to be a time dependent. The proposed method involves the heterodyning (Howard (1999)) of the active (time-averaged) intensity amplitude (absolute value of the active intensity) DC signal (multiplied by a reference signal) with a reference signal. The resulting signal has a frequency which is the same as the reference signal and an amplitude proportional to the (time-averaged) intensity. Another problem with using total active intensity as a cost function with a typical

LMS type active controller is that the calculation of the total active intensity by the two microphone technique in the time-domain results in a signal which is twice the frequency of the reference signal. Thus the error signal is uncorrelated with the reference signal, which means that the LMS algorithm will not perform the required cost function optimisation.

## D.2 Control system

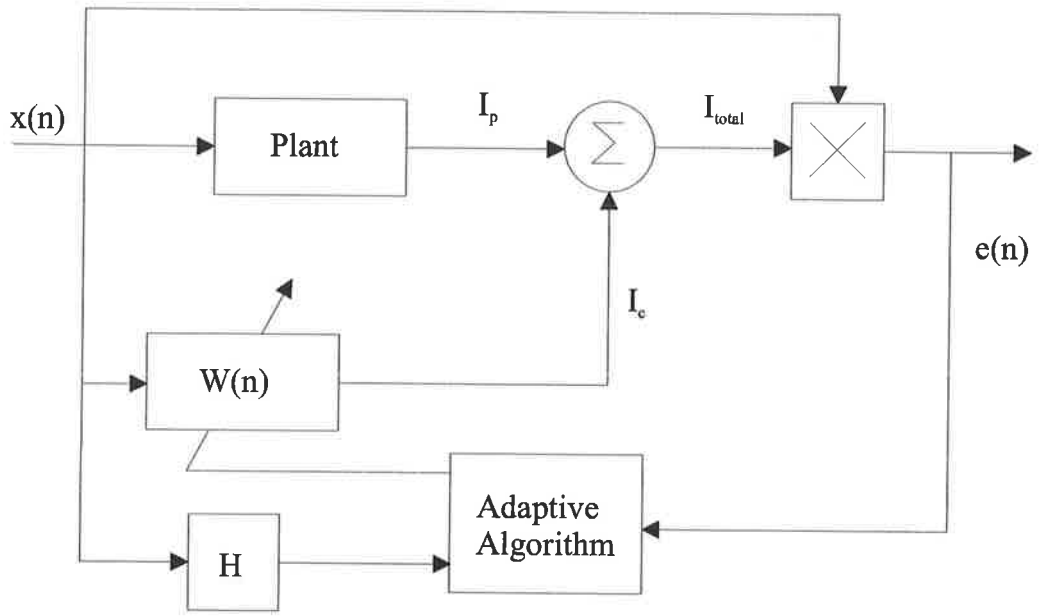


*Figure D.1: Control block diagram of a filtered-X LMS implementation using active intensity amplitude as an error signal.*

The multiplication method used to derive an error signal can be used in a conventional filtered-X LMS algorithm. A control block diagram is shown in Figure D.1. A reference signal $\mathbf{x}(n)$ is at the $n$th sample is supplied to a plant (which is the free-field radiation system which in this case refers to the baffled monopole and monopole control source, but could also refer to a simply supported rectangular steel plate in a baffle (Chapter 5), or a small transformer (Chapter 6)) which causes a primary active intensity response $\mathbf{I}_p(n)$ at the error sensor location. The reference signal is also provided to an adaptive controller which adapts slowly compared to the rate of change of the reference signal $\mathbf{x}(n)$. The adaptive controller filters the reference signal

to derive a control signal $\mathbf{I}_c(n)$ given by

$$\mathbf{I}_c(n) = \mathbf{W}(n) * \mathbf{X}(n) \tag{D.1}$$

where $\mathbf{W}(n)$ is a vector of the filter coefficients $w_i(n)$ and $*$ is the convolution and $\mathbf{X}(n)$ is a vector of past reference signal values $\mathbf{x}(n)$. This control signal can be supplied to a control speaker of control shaker which applies a control sound field or control force on the structure. The control signal passes through the cancellation path which can be modelled by a transfer function $\mathbf{H}$. The response of the control speaker or control shaker, the power amplifiers and error sensor is included in the cancellation path transfer function (CPTF). The CPTF can be computed on-line whilst control is on, or it can be done off-line before using the controller. The control signals and the primary signals are additive such that the total active intensity $\mathbf{I}_{total}(n)$ is given by

$$\mathbf{I}_{total}(n) = \mathbf{I}_p(n) - \mathbf{I}_c(n) \tag{D.2}$$

$$= \mathbf{I}_p(n) - \mathbf{W}(n) * \mathbf{X}(n) \tag{D.3}$$

The total active intensity $\mathbf{I}_{total}(n)$ signal measured by the B&K Sound Intensity Analyser is a DC signal, and when it is multiplied by the reference signal to obtain the error signal at the reference frequency (now it is coherent with the reference signal)

$$\mathbf{e}(n) = \mathbf{I}_{total}(n) * \mathbf{x}(n) \tag{D.4}$$

of which the time averaged (expectation value) is proportional to the total active intensity amplitude (absolute value of the total active intensity) in the direction of the intensity probe.

Combining equations (D.3) and (D.4), the error signal can be written as

$$\mathbf{e}(n) = (\mathbf{I}_p(n) - \mathbf{W}(n) * \mathbf{X}(n)) * \mathbf{x}(n) \tag{D.5}$$

where

$$Z = \mathbf{I}_p(n) - \mathbf{W}(n) * \mathbf{X}(n) \tag{D.6}$$

The cost function used by the conventional filtered-X LMS algorithm is given by $J = \mathbf{E}(\mathbf{e}(n)^2)$, where $\mathbf{E}\{\}$is the statistical expectation operator. Substituting (D.5) into the cost function gives

$$J = \mathbf{E}\{(Z * \mathbf{x}(n))(Z * \mathbf{x}(n))^T\} \tag{D.7}$$

where the superscript $T$ is the vector transpose. Equation (D.7) is a quadratic function of the filter weights. The error surface is a paraboloid (bowl) shape. The total active intensity amplitude $\mathbf{I}_{total} * \mathbf{x}$ is a positive definite cost function. As shown previously the total active intensity can at certain error sensor locations become negative and hence only have a maximum, hence the total active intensity amplitude will at those locations have a locus of infinitely many minima, not all of which will be close to minimising the sound power. Figures D.2 and D.3 show the experimental setup used.

The signal generator of a Hewlett Packard 35665A Digital Signal Analyser was used to generate a 100Hz sinusoidal signal which was used as a reference signal and fed to the EZ-ANC™ and also as the input signal to primary noise source. This 100Hz signal was put through a variable gain amplifier and fed to either the primary enclosed speaker, baffled speaker or electrodynamic shaker on the plate or to the transformer.

The signal from the B&K Type 3519 Intensity probe is connected to the B&K Type 2134 Sound Intensity Analyzer. The Sound Intensity Analyzer has a DC output which is proportional to the intensity amplitude (strictly positive) and this signal is fed to a multiplier circuit

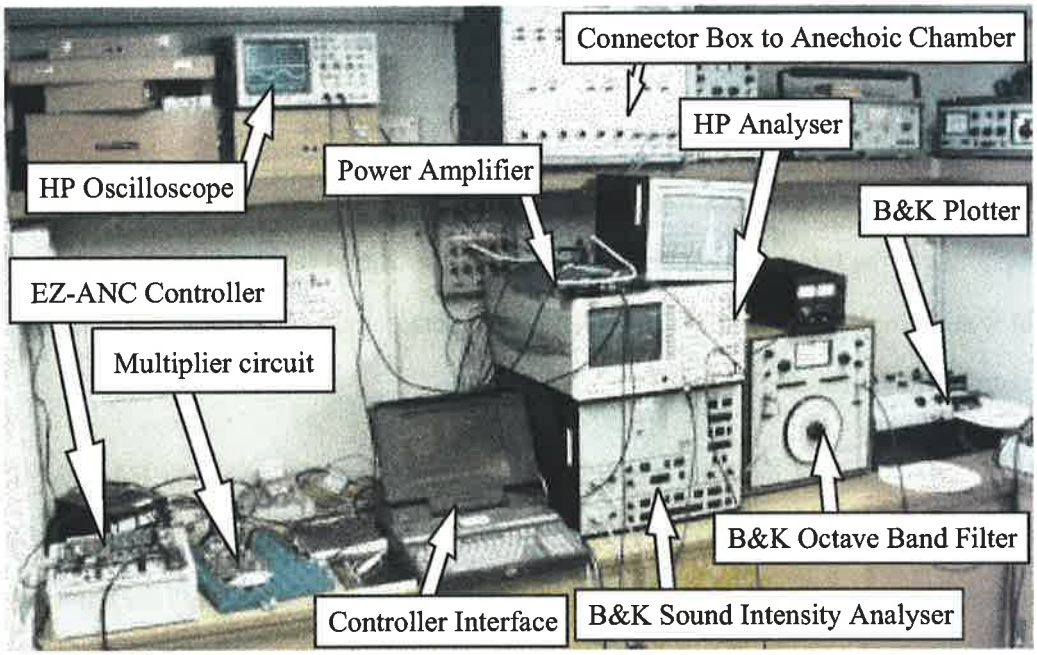


*Figure D.2: Photograph of the control system setup.*

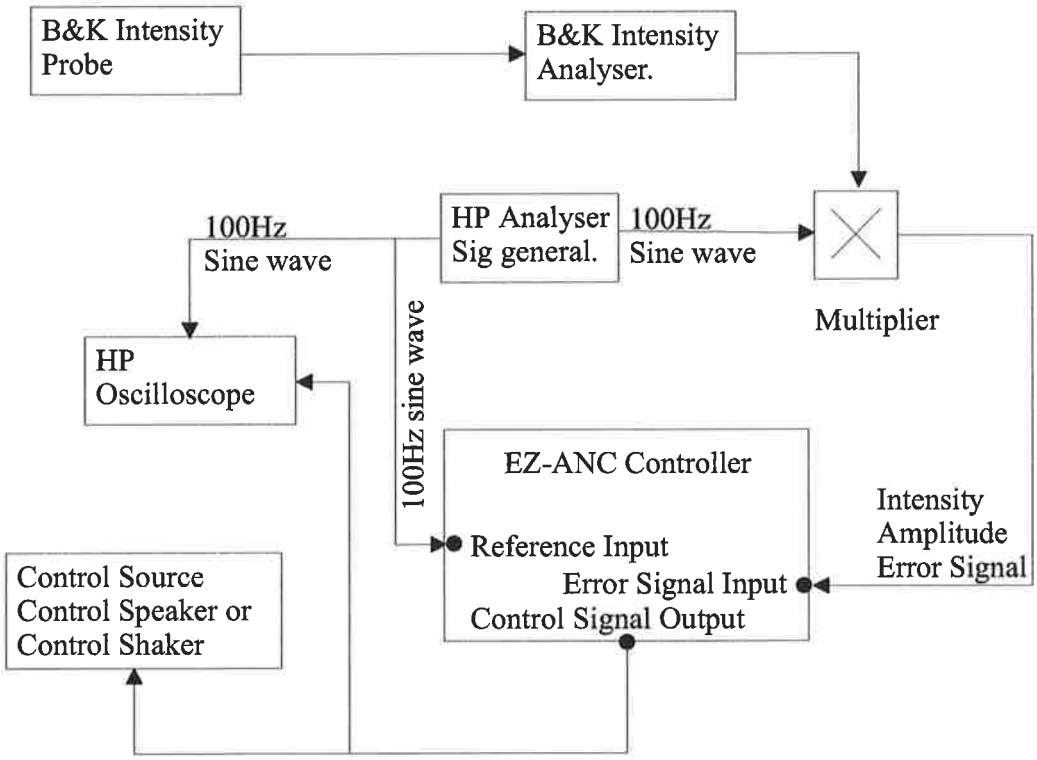


*Figure D.3: Block diagram of the control system.*

(Howard (1999)) shown in Figure D.4. The mulitplier circuit, multiplies the intensity amplitude by the AC (100Hz sinusoid signal) reference signal, to obtain a time signal which is proportional to the intensity amplitude and is linearly correlated with the reference signal.

When a squared pressure cost function was desired, the average pressure between the two microphones in the Intensity probe was output from the Sound Intensity Analyser and this DC signal was multiplied by the reference signal to generate a pressure error signal also linearly correlated with the reference signal.

The error signal (active intensity amplitude or pressure) is then fed to the EZ-ANC™. The CPTF is modelled off-line and once the EZ-ANC™ is tuned, the approriate control signal minimising the error signal is output and connected to a power amplifier and the control source (enclosed speaker or electrodynamic shaker).

A HP Oscilloscope was used to check the actual amplitude reduction of the primary noise source. The control signal was on average reduced by between 30 and 40dB.

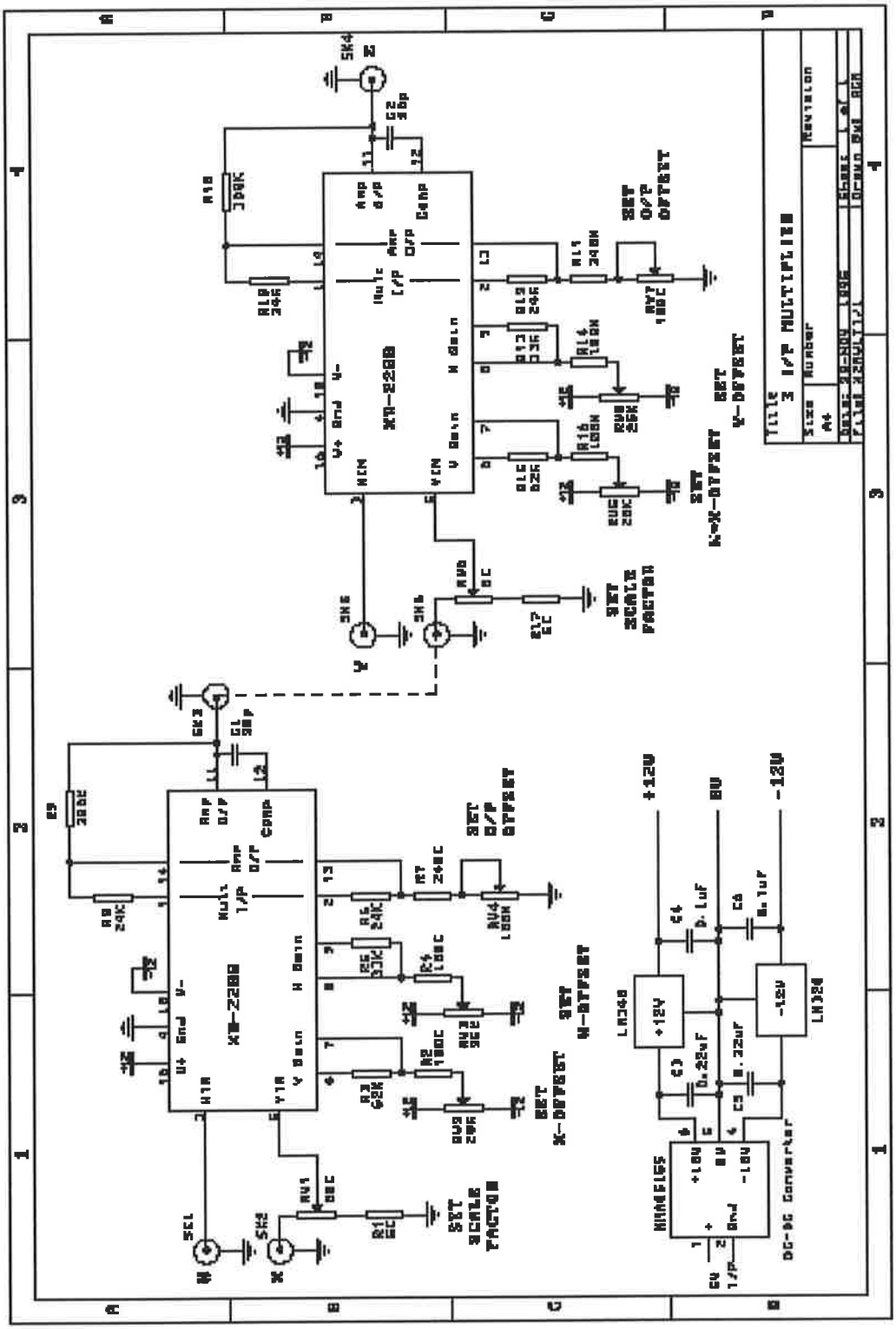


*Figure D.4: Multiplier circuit used in heterodyning (Howard (1999)).*

This page intentionally contains only this sentence.

# Appendix E

# Quadratic optimisation

*Definition:* A quadratic form $J$ is defined as a real function of a complex variable $q$ of the form

$$J = q^*Aq + b^*q + bq^* + c \tag{E.1}$$

where $A$, $c$ are both real numbers and $b$ is a complex number.

*Definition:* A quadratic form is said to be positive definite if and only if $J > 0$ for all complex values of $q$ .

*Theorem:* If a quadratic form is positive definite then it is guaranteed to have a unique minimum.

*Proof:* Let $J > 0$ for some complex number $q$.

Consider the complex value $q$ given by

$$q = x + jy \tag{E.2}$$

where $x, y$ are real, $j = \sqrt{-1}$ and we can write the real part of $q$ as

$$x = \frac{1}{2}(q + q^*) \tag{E.3}$$

and the imaginary part of $q$ as

$$y = \frac{1}{2j}(q - q^*) \tag{E.4}$$

We can define the complex derivatives in terms of real derivatives (Schwartz (1967)) as

$$\frac{\partial}{\partial q} = \frac{1}{2}(\frac{\partial}{\partial x} - j\frac{\partial}{\partial y}) \tag{E.5}$$

and

$$\frac{\partial}{\partial q^*} = \frac{1}{2}(\frac{\partial}{\partial x} + j\frac{\partial}{\partial y}) \tag{E.6}$$

Now define we the complex gradient (Haykin (1986)) as

$$\nabla J = \frac{\partial J}{\partial x} + j\frac{\partial J}{\partial y} \tag{E.7}$$

where we can use equation (E.6) to write (E.7) as

$$\nabla J = 2\frac{\partial J}{\partial q^*} \tag{E.8}$$

The extremum of $J$ is evaluated by equating $\nabla J = 0$, the optimal value $q_{opt}$ is then the complex number that ensures $\nabla J = 0$

Writing $b = b_r + jb_i$ where $b_r$ is the real part and $b_i$ is the imaginary part of $b$ and remembering that $|q|^2 = q^*q$, $J$ can be written as

$$J = (x - jy)A(x + jy) + (b_r - jb_i)(x + jy) + (b_r + jb_i)(x - jy) + c \tag{E.9}$$

which reduces to

$$J = Ax^2 + Ay^2 + 2b_r x + 2b_i y + c \tag{E.10}$$

Now evaluating the gradient as

$$\nabla J = 2Ax + 2b_r + j(2Ay + 2b_i) \tag{E.11}$$

which gives

$$\nabla J = 2A(x + jy) + 2(b_r + jb_i) \tag{E.12}$$

which reduces to

$$\nabla J = 2Aq + 2b \tag{E.13}$$

setting the gradient of $J$ equal to zero gives

$$\nabla J = Aq + b = 0 \tag{E.14}$$

which has an extreme value of $q = q_{opt}$ given by

$$q_{opt} = -b/A \tag{E.15}$$

*Definition:* Suppose that $J$ has continuous second-order partial derivatives and that $\nabla J = 0$. Set

$$\begin{aligned} \alpha &= \frac{\partial^2 J(q_{opt})}{\partial x^2} \\ \beta &= \frac{\partial^2 J(q_{opt})}{\partial y \partial x} \\ \gamma &= \frac{\partial^2 J(q_{opt})}{\partial y^2} \end{aligned} \tag{E.16}$$

and form the discriminant $\delta = \beta^2 - \alpha\gamma$.

If $\delta > 0$, then $q_{opt}$ is a saddle point.

If $\delta < 0$, then $J$ has

1. A local minimum at $q_{opt}$ if $\alpha > 0$ and $\gamma > 0$.
2. A local maximum at $q_{opt}$ if $\alpha < 0$ and $\gamma < 0$.

Evaluating the second-order partial derivatives gives

$$\begin{aligned} \alpha &= \frac{\partial^2 J(q_{opt})}{\partial x^2} = 2A \\ \beta &= \frac{\partial^2 J(q_{opt})}{\partial y \partial x} = 0 \\ \gamma &= \frac{\partial^2 J(q_{opt})}{\partial y^2} = 2A \end{aligned} \tag{E.17}$$

Hence if $A > 0$ then $\alpha > 0$ and $\gamma > 0$ and hence $\delta < 0$ .

Therefore

$$q_{opt} = -b/A \tag{E.18}$$

describes a minimum value of the quadratic form $J$. Q.E.D.

Consider cost functions shown in Figures E.1 and E.2, they have unique minima. Both cost functions are positive quadratics, Figure E.1 is positive definite and Figure E.2 is shifted down so that the minimum is a negative value.

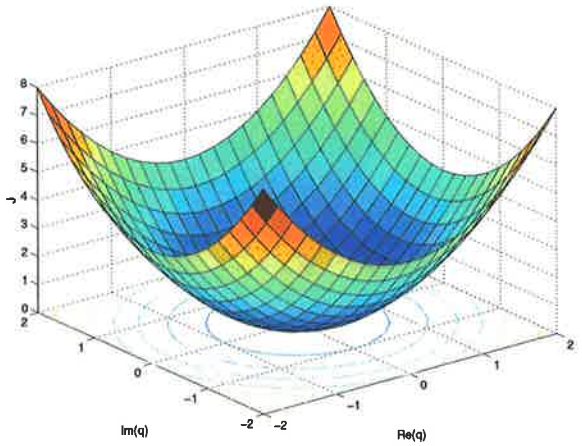


*Figure E.1: A plot of a quadratic cost function J versus the real and imaginary parts of the variable q. J is positive definite and is always greater than zero. A unique minimum exists.*

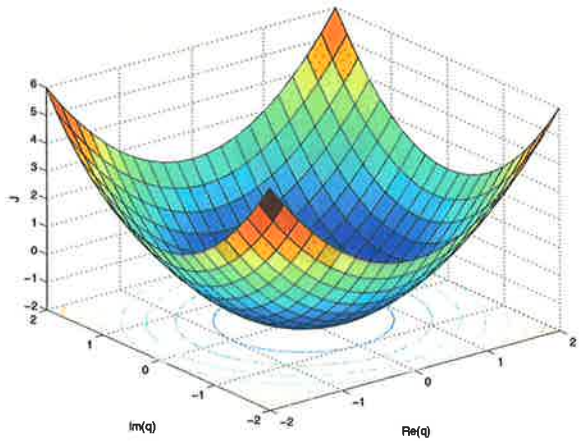


*Figure E.2: A plot of a quadratic cost function J versus the real and imaginary parts of the variable q. J is positive indefinite and is not always greater than zero. A unique minimum exists, but the cost function J is negative at the optimal value of q.*

There do exist cost functions whose extremum is a maximum. Consider cost functions shown in Figures E.3 and E.4, they have unique maxima. Both cost functions are negative quadratics, Figure E.3 is negative definite and Figure E.4 is shifted down so that the minimum is a positive value.

Consider the case where $A < 0$, and therefore $\alpha < 0$ and $\gamma < 0$. In this case the optimal value $q_{opt}$ will be a maximum, as for example is shown in Figures E.3 and E.4.

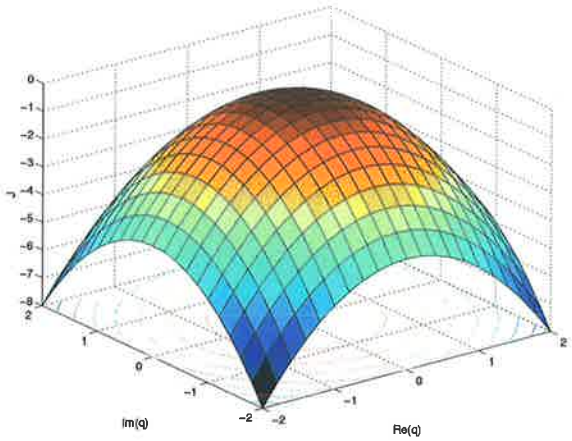


*Figure E.3: A plot of a quadratic cost function J versus the real and imaginary parts of the variable q. J is negative definite and is always less than zero. A unique maximum exists.*

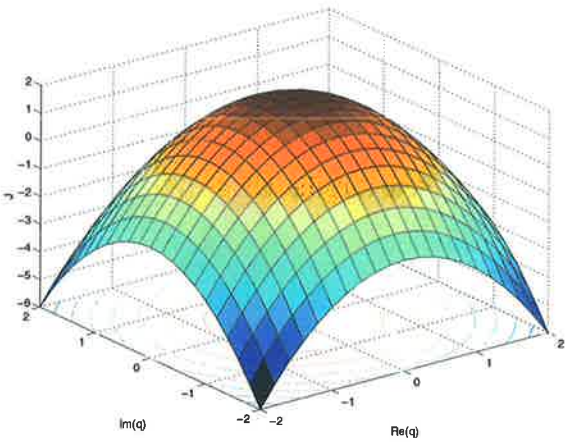


*Figure E.4: A plot of a quadratic cost function J versus the real and imaginary parts of the variable q. J is negative indefinite and is not always greater than zero. A unique maximum exists, but the cost function J is positive at the optimal value of q.*

# Appendix F

# Presentations and publications originating from this thesis

This sections lists the publications and international presentations that have directly resulted from the work undertaken to complete this thesis.

## F.1 International journals

1. Near field intensity error sensing in the active control of a free field acoustic monopole source, *Robert Koehler and Scott D. Snyder, submitted to* Journal of Sound and Vibration, 2000

2. Near field intensity error sensing in the active control of a free field acoustic monopole source in an infinite baffle, *Robert Koehler and Scott D. Snyder, accepted as a Technical Note* in the International Journal of Acoustics and Vibration, April, 2001

## F.2 Conference papers

1. Real-time intensity error sensing in active noise control. *Robert Koehler and Scott D. Snyder* Proceedings of Internoise 98, Christchurch, New Zealand. 1998

2. Active control of large electrical transformer noise using near field error sensing. *Xun Li, Xiaojun Qiu, Rongrong Gu, Robert Koehler and Colin Hansen* Proceedings of AAS Annual Meeting, Melbourne, Australia. 1999

# Appendix G

# Glossary

| | |
|---|---|
| $p(\mathbf{r},t)$ | acoustic pressure (Pascals) |
| $\omega$ | angular frequency (radians/second) |
| $f$ | frequency (Hertz) |
| $\lambda$ | wavelength (metres) |
| $\rho$ | density of acoustic medium ($kg/m^3$) |
| $k$ | wave number ($m^{-1}$) |
| $c$ | speed of sound in acoustic medium (m/s) |
| $t$ | time (s) |
| $r$ | radial displacement from source to observation point (m) |
| $\mathbf{r}_e$ | displacement from origin to observation point (m) |
| $\mathbf{r}_q$ | displacement from origin to source point (m) |
| $A$ | pressure amplitude (Pa) |

| | |
|---|---|
| $\mathbf{u}(r,t)$ | particle velocity (m/s) |
| $U_0$ | surface velocity amplitude (m/s) |
| $r_0$ | radius of spherical source (m) |
| $q$ | volume velocity or source strength ($m^3/s$) |
| $\langle U^2 \rangle$ | time-averaged surface velocity amplitude squared ($m^2/s^2$) |
| $T$ | period of oscillation (s) |
| $Re\{.\}$ | real part of $\{.\}$ |
| $Im\{.\}$ | imaginary part of $\{.\}$ |
| $X^*$ | conjugate of $X$ |
| $X^T$ | transpose of $X$ |
| $X^H$ | conjugate transpose of $X$ (hermitian) |
| $\|X\|$ | amplitude of, magnitude of $X$ |
| $Q$ | root mean squared volume velocity ($m^3/s$) |
| $Z(r)$ | acoustic transfer impedance ($kg/m^4s$) |
| $H(r)$ | velocity transfer impedance ($kg/m^4s$) |
| $\mathbf{I}$ | active intensity ($W/m^2$) |
| $W$ | sound power (W) |
| $S$ | surface area of surface enclosing a source or sources ($m^2$) |
| $\hat{n}$ | normal unit vector (dimensionless) |
| $p_{pp}$ | acoustic pressure at the position of the primary source due to the primary source (Pa) |

| | |
|---|---|
| $p_{cp}$ | acoustic pressure due to the control source at the position of the primary source (Pa) |
| $p_{cc}$ | acoustic pressure at the position of the control source due to the control source (Pa) |
| $p_{pc}$ | acoustic pressure at the position of the control source due to the primary source (Pa) |
| $d$ | separation distance between primary source and control source (m) |
| $q_p$ | primary source strength $(m^3/s)$ |
| $q_c$ | control source strength $(m^3/s)$ |
| $p_p$ | acoustic pressure due to the primary source (Pa) |
| $p_c$ | acoustic pressure due to the control source (Pa) |
| $Z_p$ | acoustic transfer impedance due to the primary source at the observation point $(kg/m^4s)$ |
| $Z_c$ | acoustic transfer impedance due to the control source at the observation point $(kg/m^4s)$ |
| $L_x$ | width of the plate (m) |
| $L_z$ | height of the plate (m) |
| $h$ | thickness of the plate (m) |
| $E$ | Youngs Modulus for steel (Pa) |
| $\rho_s$ | Density of steel $(kg/m^3)$ |
| $\nu$ | Poissons Ratio |
| $\zeta$ | Damping Ratio |

| | |
|---|---|
| $\rho$ | Density of Air ($kg/m^3$) |
| $A$ | Area of plate ($m^2$) |
| $v_p$ | velocity amplitude of plate (m/s) |
| $Z_{mono}$ | acoustic transfer impedance due to control and image source at observation point ($kg/m^4s$) |
| $H_{mono}$ | acoustic velocity transfer impedance due to control and image source at observation point ($kg/m^4s$) |
| $Z_{rad}$ | acoustic transfer impedance due to the plate primary source at observation point ($kg/m^4s$) |
| $H_{rad}$ | acoustic velocity transfer impedance due to the plate primary source at observation point ($kg/m^4s$) |
| $\mathbf{u}_p$ | particle velocity of the primary source (m/s) |
| $\mathbf{u}_c$ | particle velocity of the control source (m/s) |
| $r_p$ | distance from the primary source to the observation point (error sensor location) (m) |
| $r_c$ | distance from the control source to the observation point (error sensor location) (m) |
| $r_i$ | distance from the mirror image source to the observation point (error sensor location) (m) |
| $r_e$ | distance from the origin to the observation point (error sensor location) (m) |